EMERGING INFECTIOUS DISEASES®

U.S. CENTERS FOR DISEASE CONTROL AND PREVENTION

Environmental Pathogens

January 2026

Raffaello Sanzio da Urbino (Raphael), *Self-Portrait*, ca. 1504–1506. Oil on poplar. 47.3 cm × 34.8 cm (18.6 in × 13.7 in). The Uffizi, Florence, Italy.

Pages 1–168

EMERGING INFECTIOUS DISEASES

A Peer-Reviewed Journal Tracking and Analyzing Disease Trends

Emerging Infectious Diseases is published monthly by the Centers for Disease Control and Prevention, 1600 Clifton Rd NE, Mailstop H16-2, Atlanta, GA 30329-4018, USA. Telephone 404-639-1960; email eideditor@cdc.gov

EMERGING INFECTIOUS DISEASES®

Environmental Pathogens **January 2026**

On the Cover

Raffaello Sanzio da Urbino (Raphael), *Self-Portrait*, ca. 1504–1506. Oil on poplar. 47.3 cm × 34.8 cm (18.6 in × 13.7 in). The Uffizi, Florence, Italy.

About the Cover p. 162

Perspective

Synopses

Research

Dispatches

EMERGING INFECTIOUS DISEASES®
January 2026

Research Letters

EMERGING INFECTIOUS DISEASES®
January 2026

About the Cover

Online Report

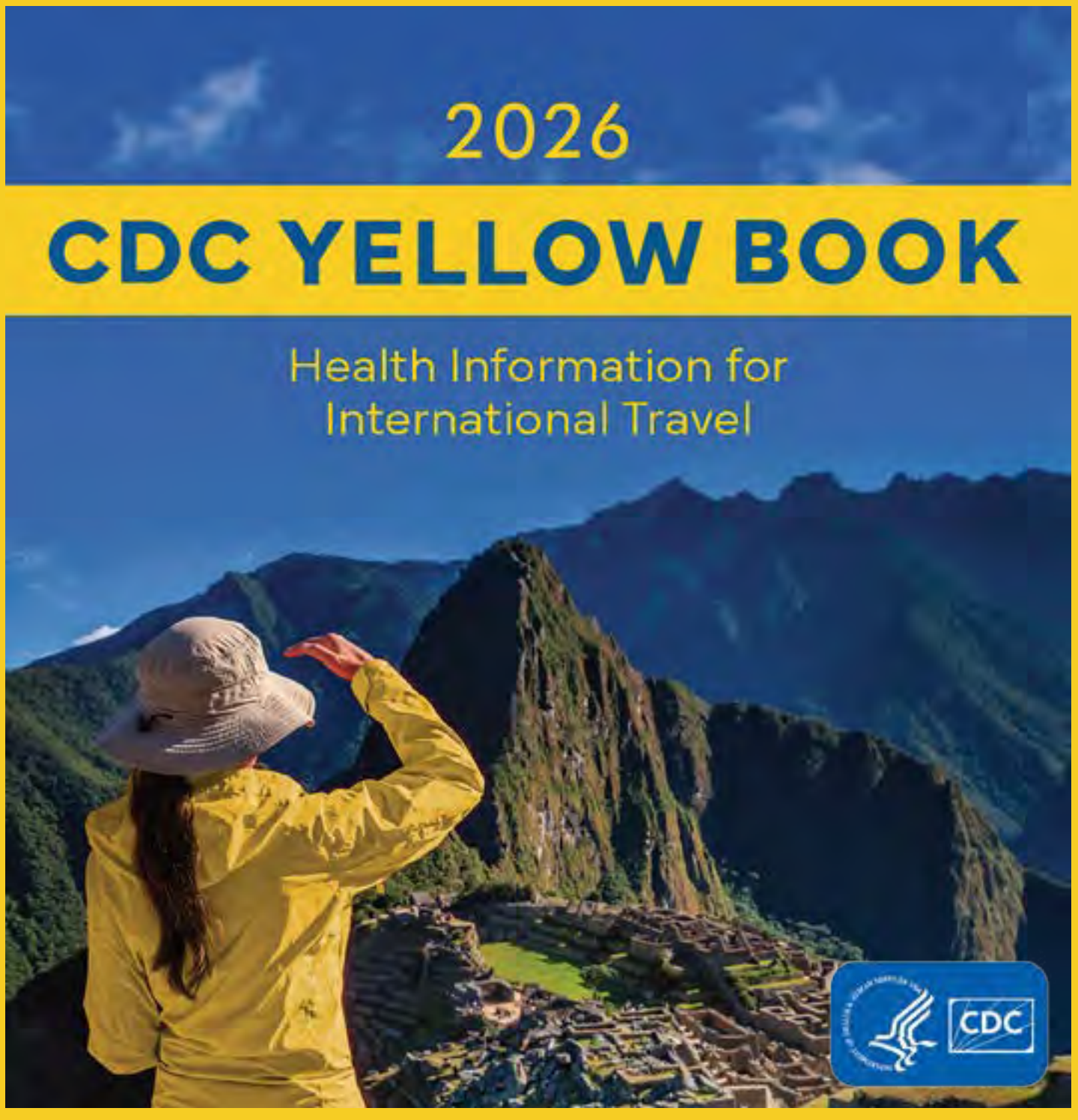

Launch of CDC Yellow Book 2026– A Trusted Travel Medicine Resource

CDC is pleased to announce the launch of the **CDC Yellow Book 2026**. The CDC Yellow Book is a resource containing the U.S. government's travel medicine recommendations and has been trusted by the travel medicine community for over 50 years. Healthcare professionals can use the print and digital versions to find the most up-to-date travel medicine information to better serve their patients' healthcare needs.

The CDC Yellow Book is available online now at www.cdc.gov/yellowbook and in print starting in June 2025 through Oxford University Press and other major online booksellers.

Emerging Respiratory Virus Threats from Influenza D and Canine Coronavirus HuPn-2018

Gregory C. Gray, Anastasia N. Vlasova, John A. Lednicky, Thang Nguyen-Tien, Ismaila Shittu, Feng Li

In 2009 and again in 2019, public health warnings were confirmed by the emergence, rapid widespread transmission, and lethality of novel influenza and coronaviruses. The world continues to suffer disease from these respiratory viruses. Two newly recognized emergent respiratory viruses, influenza D and canine coronavirus HuPn-2018, have been shown to have considerable potential for causing future human epidemics, but diagnostics and surveillance for the viruses are lacking. We reviewed data regarding influenza D virus and coronavirus canine coronavirus HuPn-2018. Those data strongly indicate that these viruses are major newly recognized threats. However, little is being done to respond to or prevent disease associated with these viruses, warranting the question of whether we will learn from previous pandemics.

Although science has developed effective countermeasures for most bacterial and vector-borne emerging pathogens, novel respiratory viruses continue to cause largescale human epidemics. Particularly problematic are pathogens that are of zoonotic origin. Viruses causing epidemics seem especially common among the Orthomyxoviridae and Coronaviridae viral families (*1*–*6*; https://www.who.int/emergencies/disease-outbreak-news/item/2025-DON560; https://data.who.int/dashboards/covid19/deaths?n=o) (Table). Those epidemics have routinely caught medical professionals off-guard and caused largescale disease and death. Two recently discovered viruses, influenza D and canine coronavirus HuPn-2018 (CCoV-HuPn-2018), seem especially worthy of closer public health attention.

Author affiliations: University of Texas, Galveston, Texas, USA (G.C. Gray, T. Nguyen-Tien, I. Shittu); The Ohio State University, Wooster, Ohio, USA (A.N. Vlasova); University of Florida, Gainesville, Florida, USA (J.A. Lednicky); University of Kentucky, Lexington, Kentucky, USA (F. Li)

DOI: https://doi.org/10.3201/eid3201.251764

Influenza D Virus

First detected and characterized in pigs with signs of respiratory illness in 2011, much has been learned about influenza D virus (IDV) since its first recognition (*7*,*8*). Like influenza A, B, and C viruses, IDVs are enveloped RNA viruses having segmented genomes that can change through reassortment, recombination, and mutation. IDVs belong to the genus *Deltainfluenzavirus* of the virus family Orthomyxoviridae. They share ≈50% amino acid identity with influenza C viruses (ICVs) across their genomes, but IDVs are much more prevalent in animal species. Initially thought to be enzootic in pigs and cattle, IDVs have now been detected in many livestock and wildlife species, including camels, deer, giraffes, kangaroos, llamas, wallabies, and wildebeests (*9*–*14*) (Figure 1). We have recently found evidence for IDV infections in poultry (*12*). A growing list of susceptible hosts for this new virus seems to be similar to those observed in the infection ecology of highly pathogenic avian influenza A(H5N1) viruses.

Like ICVs, a ubiquitous pathogen that causes minor influenza in humans, IDVs rely upon a hemagglutinin-esterase-fusion glycoprotein for cell binding and entry. Multiple recognized IDV strains or clades are chiefly classified by their hemagglutinin-esterase-fusion sequence circulating in animals. The genes of different IDV clades can reassort when they infect the same cell, and this mixing of genetic material leads to the generation of novel progeny viruses. Although science has had much more time to describe the ecology of ICVs, which were discovered in 1947, IDVs may reassort and recombine with other IDVs, suggesting that they are rapidly evolving (*15*). Although IDV prevalence is often high in cattle (G.C. Gray, unpub. data, 2025 Dec 11) compared with ICVs (*16*), IDVs may have more opportunity to gain characteristics that would threaten humans.

Although not all pig or cattle herds worldwide are affected by IDVs (*17*–*19*), many animal species

Table. Recent epidemics or pandemics from respiratory viruses thought to be zoonotic*

Period	Virus	Virus family	Deaths	Scope
1918–1920	Influenza A(H1N1)	Orthomyxoviridae	20–100 million (*1*)	Worldwide
1957–1958	Influenza A(H2N2)	Orthomyxoviridae	1–4 million (*2*)	Worldwide
1968–1969	Influenza A(H3N2)	Orthomyxoviridae	1–4 million (*3*)	Worldwide
2002–2004	SARS-CoV-1	Coronaviridae	774 (*4*)	29 countries (*5*)
2009–2010	Influenza A(H1N1)	Orthomyxoviridae	151,700–575,400 (*6*)	Worldwide
2012–present	MERS-CoV	Coronaviridae	2,627†	27 countries†
2019–present	SARS-CoV-2	Coronaviridae	7.1 million‡	Worldwide

*MERS-CoV, Middle East respiratory syndrome coronavirus; SARS-CoV, severe acute respiratory syndrome coronavirus.
†Per World Health Organization (https://www.who.int/emergencies/disease-outbreak-news/item/2025-DON560).
‡Per World Health Organization as of October 2025 (https://data.who.int/dashboards/covid19/deaths?n=o).

clearly have infections periodically. The largest animal reservoir seems to be cattle, despite the first IDV being isolated from a diseased pig. The full spectrum of IDV illness in cattle is not known, but IDV is now recognized to contribute to one of the largest disease problems in cattle, bovine respiratory disease complex, which is estimated to cost the US cattle industry >$1 billion annually (*20*). As a measure of IDV endemicity, in our recent studies of 12 beef and dairy cattle farms in the United States and Mexico, we have detected (and often isolated) IDV >50 times among >500 nasal swab specimens obtained from sick or healthy cattle (G.C. Gray, unpub. data, 2025 Dec 11).

Although no viable (i.e., infectious) IDV has thus far been isolated from humans, mounting evidence indicates that the virus is zoonotic. Several human studies suggest that IDV causes subclinical infections in humans, especially among persons with occupational exposure to animals. In 2016, we reported a seroepidemiologic study of cattle workers in Florida, USA, where we found that >97% of cattle workers had neutralizing antibody to IDV, compared with 18% among a non–cattle exposed control population (*13*). In 2023, we reported a study of dairy workers in Colorado, where we found that 67% of 31 workers had molecular evidence of IDV in their nasal washes during a 5-day period (*21*).

Recently, a scientific team in China has reported compelling animal model, aerosol, and seroepidemiologic data that provide even stronger evidence that IDV is causing subclinical infections in humans (*14*). The team found that 73% of 612 study participants (97% among those with respiratory symptoms) in northeast China had serologic evidence of infection (*14*). They documented viral transmission in the air between ferrets, replication in primary human epithelial cells, infection in mice and dog models, and concluded that IDV has acquired the capacity for human-to-human transmission and that IDV strains already pose a potential panzootic threat (*14*). Of note, that study provides the first serologic evidence of widespread IDV in a general human population. The IDV strain in China that was used in the study, D/HY11, was isolated in 2023 from cattle and seems to

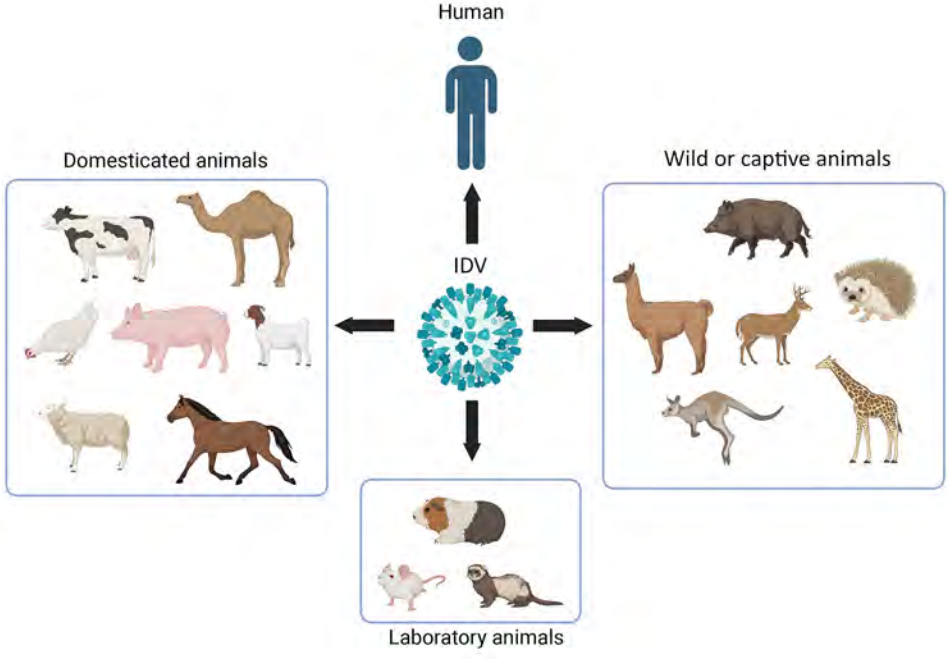

Figure 1. Schematic illustration of the host range of IDV. Natural infections have been confirmed through the detection of virus genomic RNA, virus isolation, or the presence of IDV antibodies in domestic animals, wild animals, captive animals, and humans (*9*–*13*). Clinically apparent infections have been observed in laboratory animals, including ferrets, guinea pigs, and mice, that have been exposed to IDV in laboratory experiments (*14*). Figure created in BioRender (https://biorender.com/uxr6kea). IDV, influenza D virus.

be more efficient for airborne transmission in ferrets than strains used in previous studies. The observed increase in aerosol transmission is probably associated with mutations identified in this new strain, especially in the polymerase P3 gene, but more studies are needed to understand the underlying mechanisms behind these findings. Nevertheless, IDV replication and transmission in ferrets, 1 surrogate model for humans in influenza studies, and efficient replication in human primary airway epithelial cells observed in that work and another study (*22*) provide a theoretical framework that the virus will adapt and evolve for effective growth and human-to-human spread.

CCoV-HuPn-2018

In 2021, we first reported the cell culture isolation and characterization of a novel canine–feline recombinant alphacoronavirus, CCoV-HuPn-2018, from a nasopharyngeal swab sample from a child hospitalized with pneumonia in Sarawak State, Malaysia (*23*). The virus shared ≈97% nucleotide identity in most structural genes with canine coronavirus II, but its spike gene contained segments from feline coronavirus and transmissible gastroenteritis virus, which are specific for the canine coronavirus IIb subtype, suggesting a complex recombinant origin. A subsequent virus culture and characterization in urine specimens from persons visiting Haiti (*24*) indicated a 99.4% identity, confirming the circulation of CCoV-HuPn-2018 in different geographic regions. In addition, similar animal alphacoronaviruses have been detected among humans with respiratory illness living in Bangkok, Thailand (*25*), and in the US state of Arkansas (*26*). Recently, we detected CCoV-HuPN-2018 among 18 of 200 pneumonia patients hospitalized in the area of Hanoi, Vietnam, suggesting that this virus may have a wide geographic distribution and variable (and possibly increasing) prevalence (*27*) (Figure 2**)**. The virus is entirely missed by common clinical diagnostics tests for the detection of respiratory viruses.

Although these findings do not yet prove that CCoV-HuPn-2018 is a frequent, worldwide cause of severe respiratory disease, they suggest that CCoV-HuPn-2018 (or very similar viruses) merit our closer study. Recent studies of the spike protein of CCoV-HuPN-2018 have shed light on its interaction with the aminopeptidase N from canines, felines, and porcines, but not humans, as functional receptors for cell entry (*28*–*30*). Nevertheless, CCoV-HuPn-2018 spike protein pseudotyped virus infects multiple human cancer cell lines in a human aminopeptidase N–independent manner. Earlier clades of CCoV-HuPn-2018 might have not yet evolved to be an efficient human pathogen, but they may be evolving now, as evidenced by the increased number of patients affected by the virus in the study by our surveillance team in Vietnam (*27*).

Other Viruses

Of course, in addition to IDV and CCoV-HuPn-2018, public health professionals should seek to detect other animal respiratory viruses as they spill over to infect humans. When possible, such surveillance should be

Figure 2. Locations of canine coronavirus HuPn-2018 or similar virus detections among humans with respiratory illness (*23*–*27*). Figure created in R version 4.4.1 (https://cran.rstudio.com).

strategically focused at the human–animal nexus where we recognize the risk is high (*31*). For instance, the risk for novel swine viruses spilling over from swine to infect swine workers is exceedingly high compared with the similar risk for avian influenza viruses spilling over from poultry to infect poultry workers (*32*–*37*). Similarly, we are aware of the zoonotic threat of other animal coronaviruses infecting persons directly or indirectly exposed to their animal hosts (*38*,*39*). In addition, we posit that evidence of animal adenoviruses spilling over to infect humans is mounting (*40*). In recent years, molecular evidence has shown that a vampire bat–like adenovirus in Malaysia (*41*) and a bovine adenovirus in Pakistan (J.R.E. Ansari et al., unpub. data, https://doi.org/10.21203/rs.3.rs-5811360/v1) were associated with human respiratory disease. Because of those and other observations, we argue that periodic surveillance with targeted and panspecies diagnostics would be prudent when addressing emerging respiratory virus threats for viruses in 6 viral families (Adenoviridae, Coronaviridae, Orthomyxoviridae, Paramyxoviridae, Picornaviridae, and Pneumoviridae) (*42*). Conducting such surveillance in concert with occasional agnostic next-generation sequencing of specimens associated with unusual illnesses can help us better prepare for future pandemic threats at more sustainable costs than previous strategies that sought to detect novel pathogens in many wildlife hosts (*43*).

Conclusions

The novelist Stephen King adapted a classical English language quip to illustrate our tendency to ignore our previous mistakes: "Fool me once, shame on you. Fool me twice, shame on me. Fool me three times, shame on both of us" (*44*). As we prepare for the next pandemic, we would be wise to heed his advice.

Currently, we know of no human or veterinary laboratory-approved molecular or serologic assays for IDV or CCoV-HuPN-2018. Hence, our knowledge about the viruses' epidemiology and clinical manifestations are limited to a modest number of research studies. Even so, the limited data regarding these novel, newly detected viruses indicate that that they are a major threat to public health. If we wish to avoid being fooled again by a novel virus suddenly gaining efficient human-to-human transmissibility and causing large human epidemics, we would be wise to develop better surveillance systems and new countermeasures for these and similar viruses. Potential actions include the development of commercial real-time reverse transcription PCR diagnostic tests specifically targeting IDV and CCoV-HuPN-2018 viruses. Conducting periodic assessments for novel respiratory viruses could detect what might be cryptic causes of hospitalizations or animal epizootics in geographic areas recognized to be sites of increased presence of emerging pathogens (*42*,*45*). As we have shown, this surveillance can easily be performed with panspecies and next-generation sequencing diagnostics (*42*,*46*,*47*). Clinicians should consider IDV and CCoV-HuPN-2018 in their workup of pneumonia patients when a primary battery of diagnostic tests fail to identify a pathogen. Scientists should begin evaluating antiviral drugs as effective therapy for the treatment of IDV and CCoV-HuPN-2018 infections. If further epidemiologic study indicates that the investment is warranted, human vaccine development should be considered for both IDV and CCoV-HuPN-2018. Furthermore, with respect to detecting new respiratory virus threats, when specific novel animal spillover risks are identified, they may often be mitigated with targeted interventions such as those recently reviewed by Vora et al. (*48*) and Plowright et al. (*49*).

This project was supported financially by an Agriculture and Food Research Initiative competitive grant from the American Rescue Plan Act through the US Department of Agriculture's Animal and Plant Health Inspection Service (grant no. 2023-70432-39558), the American Lung Association (grant no. Covid-862514), the US Department of Agriculture's Agricultural Research Service (agreement no. 58-3022-4-048), and startup funding from the University of Texas Medical Branch (all awarded to G.C.G. as principal investigator).

About the Author

Dr. Gray is a public health physician, infectious disease epidemiologist, and director of the One Health Research and Training Laboratory at the University of Texas Medical Branch. His research interests include emerging pathogens, especially those that are zoonotic and cause respiratory disease.

References

1. Murray CJ, Lopez AD, Chin B, Feehan D, Hill KH. Estimation of potential global pandemic influenza mortality on the basis of vital registry data from the 1918-20 pandemic: a quantitative analysis. Lancet. 2006;368:2211–8. https://doi.org/10.1016/S0140-6736(06)69895-4
2. Viboud C, Simonsen L, Fuentes R, Flores J, Miller MA, Chowell G. Global mortality impact of the 1957–1959 influenza pandemic. J Infect Dis. 2016;213:738–45. https://doi.org/10.1093/infdis/jiv534
3. Honigsbaum M. Revisiting the 1957 and 1968 influenza pandemics. Lancet. 2020;395:1824–6. https://doi.org/10.1016/S0140-6736(20)31201-0
4. Cherry JD. The chronology of the 2002–2003 SARS mini pandemic. Paediatr Respir Rev. 2004;5:262–9. https://doi.org/10.1016/j.prrv.2004.07.009

5. Cherry JD, Krogstad P. SARS: the first pandemic of the 21st century. Pediatr Res. 2004;56:1–5. https://doi.org/10.1203/01.PDR.0000129184.87042.FC
6. Dawood FS, Iuliano AD, Reed C, Meltzer MI, Shay DK, Cheng PY, et al. Estimated global mortality associated with the first 12 months of 2009 pandemic influenza A H1N1 virus circulation: a modelling study. Lancet Infect Dis. 2012;12:687–95. https://doi.org/10.1016/S1473-3099(12)70121-4
7. Hause BM, Collin EA, Liu R, Huang B, Sheng Z, Lu W, et al. Characterization of a novel influenza virus in cattle and swine: proposal for a new genus in the Orthomyxoviridae family. MBio. 2014;5:e00031–14. https://doi.org/10.1128/mBio.00031-14
8. Hause BM, Ducatez M, Collin EA, Ran Z, Liu R, Sheng Z, et al. Isolation of a novel swine influenza virus from Oklahoma in 2011 which is distantly related to human influenza C viruses. PLoS Pathog. 2013;9:e1003176. https://doi.org/10.1371/journal.ppat.1003176
9. Liu R, Sheng Z, Huang C, Wang D, Li F. Influenza D virus. Curr Opin Virol. 2020;44:154–61. https://doi.org/10.1016/j.coviro.2020.08.004
10. Sreenivasan CC, Sheng Z, Wang D, Li F. Host range, biology, and species specificity of seven-segmented influenza viruses—a comparative review on influenza C and D. Pathogens. 2021;10:1583. https://doi.org/10.3390/pathogens10121583
11. Kwasnik M, Rola J, Rozek W. Influenza D in domestic and wild animals. Viruses. 2023;15:2433. https://doi.org/10.3390/v15122433
12. Bailey ES, Fieldhouse JK, Alarja NA, Chen DD, Kovalik ME, Zemke JN, et al. First sequence of influenza D virus identified in poultry farm bioaerosols in Sarawak, Malaysia. Trop Dis Travel Med Vaccines. 2020;6:5. https://doi.org/10.1186/s40794-020-0105-9
13. White SK, Ma W, McDaniel CJ, Gray GC, Lednicky JA. Serologic evidence of exposure to influenza D virus among persons with occupational contact with cattle. J Clin Virol. 2016;81:31–3. https://doi.org/10.1016/j.jcv.2016.05.017
14. Gao H, Sun W, Lu P, Dong Z, Wu J, Li Y, et al. Efficient airborne transmission of influenza D virus in ferret models and serological evidence of human exposure in Northeast China. Emerg Microbes Infect. 2025;14:2564308. https://doi.org/10.1080/22221751.2025.2564308
15. Limaye S, Lohar T, Dube H, Ramasamy S, Kale M, Kulkarni-Kale U, et al. Rapid evolution leads to extensive genetic diversification of cattle flu influenza D virus. Commun Biol. 2024;7:1276. https://doi.org/10.1038/s42003-024-06954-4
16. Guerra FM Jr, Edgar EM, Oguzie JU, Marushchak LV, Pattillo M, Gray GC. Sparse evidence of influenza C on US dairy and beef cattle farms. Influenza Other Respir Viruses. 2025;19:e70167. https://doi.org/10.1111/irv.70167
17. Umar S, Ma MJ, Gray GC. Influenza D virus was not detected among prospectively studied swine farm in multiple provinces of China. Influenza Other Respir Viruses. 2023;17:e13223. https://doi.org/10.1111/irv.13223
18. Farrell AS, Bui VN, Dao TD, Hoang TD, Gray GC. No influenza D virus detected among pigs, northern Vietnam. Influenza Other Respir Viruses. 2021;15:315–7. https://doi.org/10.1111/irv.12812
19. Pulscher LA, Maruschak LV, Shittu I, Alsharif H, Gray GC. No evidence of novel respiratory viruses on two Texas dairy farms before the H5N1 avian influenza virus epizootic. Influenza Other Respir Viruses. 2025;19:e70146. https://doi.org/10.1111/irv.70146
20. O'Donoghue S, Waters SM, Morris DW, Earley B. A comprehensive review: bovine respiratory disease, current insights into epidemiology, diagnostic challenges, and vaccination. Vet Sci. 2025;12:778. https://doi.org/10.3390/vetsci12080778
21. Leibler JH, Abdelgadir A, Seidel J, White RF, Johnson WE, Reynolds SJ, et al. Influenza D virus exposure among US cattle workers: a call for surveillance. Zoonoses Public Health. 2023;70:166–70. https://doi.org/10.1111/zph.13008
22. Holwerda M, Kelly J, Laloli L, Stürmer I, Portmann J, Stalder H, et al. Determining the replication kinetics and cellular tropism of influenza D virus on primary well-differentiated human airway epithelial cells. Viruses. 2019;11:377. https://doi.org/10.3390/v11040377
23. Vlasova AN, Diaz A, Damtie D, Xiu L, Toh TH, Lee JS, et al. Novel canine coronavirus isolated from a hospitalized patient with pneumonia in east Malaysia. Clin Infect Dis. 2022;74:446–54. https://doi.org/10.1093/cid/ciab456
24. Lednicky JA, Tagliamonte MS, White SK, Blohm GM, Alam MM, Iovine NM, et al. Isolation of a novel recombinant canine coronavirus from a visitor to Haiti: further evidence of transmission of coronaviruses of zoonotic origin to humans. Clin Infect Dis. 2022;75:e1184–7. https://doi.org/10.1093/cid/ciab924
25. Theamboonlers A, Samransamruajkit R, Thongme C, Amonsin A, Chongsrisawat V, Poovorawan Y. Human coronavirus infection among children with acute lower respiratory tract infection in Thailand. Intervirology. 2007;50:71–7. https://doi.org/10.1159/000097392
26. Silva CS, Mullis LB, Pereira O, Saif LJ, Vlasova A, Zhang X, et al. Human respiratory coronaviruses detected in patients with influenza-like illness in Arkansas, USA. Virol Mycol. 2014;2014(Suppl 2).
27. Phan PT, Wijayaratne G, Bodinayake CK, Oguzie JU, Nguyen-Tien T, Marushchak LV, et al. Diverse respiratory viruses detected among hospitalized patients with pneumonia in Sri Lanka and Vietnam. IJID Reg. 2025;17:100757. https://doi.org/10.1016/j.ijregi.2025.100757
28. Tortorici MA, Walls AC, Joshi A, Park YJ, Eguia RT, Miranda MC, et al. Structure, receptor recognition, and antigenicity of the human coronavirus CCoV-HuPn-2018 spike glycoprotein. Cell. 2022;185:2279–2291.e17. https://doi.org/10.1016/j.cell.2022.05.019
29. Liu Y, Chen D, Wang Y, Li X, Qiu Y, Zheng M, et al. Characterization of CCoV-HuPn-2018 spike protein-mediated viral entry. J Virol. 2023;97:e0060123. https://doi.org/10.1128/jvi.00601-23
30. Wang F, Yang G, Yan L. Crystal structures of fusion cores from CCoV-HuPn-2018 and SADS-CoV. Viruses. 2024;16:272. https://doi.org/10.3390/v16020272
31. Holmes EC. The ecology of viral emergence. Annu Rev Virol. 2022;9:173–92. https://doi.org/10.1146/annurev-virology-100120-015057
32. Borkenhagen LK, Wang GL, Simmons RA, Bi ZQ, Lu B, Wang XJ, et al. High risk of influenza virus infection among swine workers: examining a dynamic cohort in China. Clin Infect Dis. 2020;71:622–9. https://doi.org/10.1093/cid/ciz865
33. Ma M, Anderson BD, Wang T, Chen Y, Zhang D, Gray GC, et al. Serological evidence and risk factors for swine influenza infections among Chinese swine workers in Guangdong Province. PLoS One. 2015;10:e0128479. https://doi.org/10.1371/journal.pone.0128479
34. Myers KP, Olsen CW, Setterquist SF, Capuano AW, Donham KJ, Thacker EL, et al. Are swine workers in the United States at increased risk of infection with zoonotic influenza virus? Clin Infect Dis. 2006;42:14–20. https://doi.org/10.1086/498977
35. Khuntirat BP, Yoon IK, Blair PJ, Krueger WS, Chittaganpitch M, Putnam SD, et al. Evidence for subclinical avian influenza

virus infections among rural Thai villagers. Clin Infect Dis. 2011;53:e107–16. https://doi.org/10.1093/cid/cir525
36. Kayali G, Ortiz EJ, Chorazy ML, Gray GC. Evidence of previous avian influenza infection among US turkey workers. Zoonoses Public Health. 2010;57:265–72. https://doi.org/10.1111/j.1863-2378.2009.01231.x
37. Borkenhagen LK, Salman MD, Ma MJ, Gray GC. Animal influenza virus infections in humans: a commentary. Int J Infect Dis. 2019;88:113–9. https://doi.org/10.1016/j.ijid.2019.08.002
38. Sánchez CA, Li H, Phelps KL, Zambrana-Torrelio C, Wang LF, Zhou P, et al. A strategy to assess spillover risk of bat SARS-related coronaviruses in Southeast Asia. Nat Commun. 2022;13:4380. https://doi.org/10.1038/s41467-022-31860-w
39. Vlasova AN, Toh TH, Lee JS, Poovorawan Y, Davis P, Azevedo MSP, et al. Animal alphacoronaviruses found in human patients with acute respiratory illness in different countries. Emerg Microbes Infect. 2022;11:699–702. https://doi.org/10.1080/22221751.2022.2040341
40. Borkenhagen LK, Fieldhouse JK, Seto D, Gray GC. Are adenoviruses zoonotic? A systematic review of the evidence. Emerg Microbes Infect. 2019;8:1679–87. https://doi.org/10.1080/22221751.2019.1690953
41. Fieldhouse JK, Bailey ES, Toh TH, Hii KC, Mallinson KA, Ting J, et al. Panspecies molecular assays detect viral pathogens missed by real-time PCR/reverse-transcriptase PCR among pneumonia patients, Sarawak, Malaysia. Trop Dis Travel Med Vaccines. 2020;6:13. https://doi.org/10.1186/s40794-020-00114-2
42. Gray GC, Robie ER, Studstill CJ, Nunn CL. Mitigating future respiratory virus pandemics: new threats and approaches to consider. Viruses. 2021;13:637. https://doi.org/10.3390/v13040637
43. Aatresh AV, Lipsitch M. What is the relationship between viral prospecting in animals and medical countermeasure development? MBio. 2025;16:e0203325. https://doi.org/10.1128/mbio.02033-25
44. King S. On writing: a memoir of the craft. New York: Scribner; 2000.
45. Gray GC, Abdelgadir A. While we endure this pandemic, what new respiratory virus threats are we missing? Open Forum Infect Dis. 2021;8:ofab078. https://doi.org/10.1093/ofid/ofab078
46. Shittu I, Oguzie JU, Hernández-Vidal G, Moreno-Degollado G, Silva DB, Marushchak LV, et al. Novel rodent coronavirus-like virus detected among beef cattle with respiratory disease in Mexico. Viruses. 2025;17:433. https://doi.org/10.3390/v17030433
47. Oguzie JU, Hernandez-Vidal G, Moreno-Degollado G, Gray GC. First detection of boosepivirus B1 in a sick yearling's nasal swab, Mexico. Influenza Other Respir Viruses. 2025;19:e70165. https://doi.org/10.1111/irv.70165
48. Vora NM, Hannah L, Walzer C, Vale MM, Lieberman S, Emerson A, et al. Interventions to reduce risk for pathogen spillover and early disease spread to prevent outbreaks, epidemics, and pandemics. Emerg Infect Dis. 2023;29:1–9. https://doi.org/10.3201/eid2903.221079
49. Plowright RK, Ahmed AN, Coulson T, Crowther TW, Ejotre I, Faust CL, et al. Ecological countermeasures to prevent pathogen spillover and subsequent pandemics. Nat Commun. 2024;15:2577. https://doi.org/10.1038/s41467-024-46151-9

Address for correspondence: Gregory C. Gray, University of Texas Medical Branch, 301 University Blvd, Rte 0435, Galveston, TX 77555-0435, USA; email: gcgray@utmb.edu

Pulmonary Histoplasmosis, Taiwan, 1997–2024

Ting-Wei Kao, Shang-Chen Yang, Hsiang-Wei Hu, Yu-Tsung Huang, Chin-Chung Shu, Wang-Huei Sheng

Pulmonary histoplasmosis has traditionally been considered geographically restricted to disease-endemic regions. Taiwan, historically nonendemic, has recently witnessed rising infections. We conducted a retrospective study by reviewing adult patients in Taiwan who had pathologically confirmed pulmonary histoplasmosis during June 1997–December 2024. We analyzed 14 cases with lung involvement. Eight case-patients were male and 6 female; mean age was 56.6 years. Of note, 11 case-patients (78.6%) had no history of travel to histoplasmosis-endemic regions; 10 (71.4%) were immunocompetent. Left upper lobe involvement was most common (n = 4 [28.6%]), with nodular lesions predominating (n = 12 [85.7%]). Most (11 [78.6%]) patients received antifungal therapy, mostly with voriconazole. Outcomes were favorable; 1 (7.1%) patient died. Two additional case-patients without lung involvement exhibited similar demographics and clinical outcomes. Case identification rate has increased since 2015. This 27-year study documents the emergence of pulmonary histoplasmosis in Taiwan, emphasizing the need for heightened clinical suspicion in nonendemic regions.

Histoplasmosis, caused by the thermally dimorphic fungus *Histoplasma capsulatum*, is a well-established disease pathogen. The clinical spectrum of histoplasmosis ranges from asymptomatic infection to life-threatening disseminated disease, depending on the extent of exposure and host immune status (*1*). In immunocompromised patients, particularly those with HIV infection or hematologic malignancies or who are receiving immunosuppressive therapy, histoplasmosis can manifest as progressive disseminated disease with high mortality rates (*2*). In immunocompetent hosts, complications rarely develop but indicate treatment once present (*3*). Common manifestations include mediastinal lymphadenitis or fibrosis and chronic pulmonary sequalae (*4*).

Traditionally, histoplasmosis has been considered a geographically restricted mycosis confined to well-defined endemic locations. The organism is found predominantly in soil enriched with bird excreta. Evolving epidemiologic reports have shown that histoplasmosis, previously confined to the endemic area of the Ohio and Mississippi River basins, can occur anywhere in the United States (*5*,*6*). Central and South America represented the other established endemic regions (*7*,*8*). Cases identified outside those regions have been predominantly attributed to travel exposure or reactivation of latent infections acquired during prior visits to endemic areas. Nevertheless, the conventional understanding of histoplasmosis as exclusively associated with endemic regions has been challenged by case reports from areas previously considered nonendemic worldwide (*9*). Those reports suggest that the environmental niche of *H. capsulatum* fungus may be more extensive than previously recognized and so might have changed environmental conditions, intensified global travel, and improved diagnostic capabilities. Furthermore, the organism's capability to establish environmental reservoirs in new geographic locations challenges traditional disease transmission patterns and epidemiologic surveillance approaches. Enabled by the ecologic preference for nitrogen-rich soil, especially soil contaminated with bird and bat guano, and the association with avian and chiropteran hosts that can disperse the fungus across regions (*10*), *Histoplasma capsulatum* has a documented capability to establish environmental reservoirs in new geographic locations. Molecular surveillance and ecologic niche

Author affiliations: National Taiwan University Hospital, Department of Internal Medicine, National Taiwan University College of Medicine, Taipei, Taiwan (T.-W. Kao, S.-C. Yang, C-.C. Shu, W.-H. Sheng); National Taiwan University Hospital, Department of Pathology, Taipei (H.-W. Hu); National Taiwan University Hospital, Department of Laboratory Medicine, National Taiwan University College of Medicine, Taipei (Y.-T. Huang); Graduate Institute of Clinical Medicine, National Taiwan University College of Medicine, Taipei (C.-C. Shu); National Taiwan University Hospital Hsinchu Branch, Department of Internal Medicine, Hsinchu, Taiwan (W.-H. Sheng)

DOI: https://doi.org/10.3201/eid3201.251091

modeling have reported that *Histoplasma* spp. can persist in both traditional endemic and newly recognized areas (*11*).

Taiwan, situated in the Western Pacific region, has traditionally been considered nonendemic for histoplasmosis based on limited historical documentation and the absence of systematic surveillance reports. A total of 17 cases in Taiwan during 1977–2022 were identified by literature review (*12*); those reports did not detail possible exposure by occupation, condition and characteristics of case-patients' lungs, or outcomes. Still, those cases have delineated an evolving epidemiologic landscape that warrants comprehensive investigation (*13*). The increasing recognition of histoplasmosis cases in Taiwan, in conjunction with the heterogeneous clinical manifestations and variable host–pathogen interactions, necessitates detailed characterization of disease burden and clinical characteristics. Therefore, our study aimed to elucidate the demographic, clinical, radiologic, and therapeutic characteristics of pulmonary histoplasmosis in Taiwan over a 27-year period.

We observed the ethical principles of Declaration of Helsinki in designing and conducting this study. The research ethics committee of National Taiwan University Hospital approved the study (no. 202506155RINB); informed consent was waived because of the retrospective nature of the study.

Materials and Methods

Study Design and Participants

We conducted a retrospective observational study at National Taiwan University Hospital, a 2,600-bed tertiary medical center in Taipei, Taiwan. We designed the study protocol to include all cases of histoplasmosis diagnosed during June 1997–December 2024. We systematically identified participants through an exhaustive search of the electronic medical record database using diagnosis coding for histoplasmosis from the International Classification of Diseases, 10th Revision. We defined the inclusion criteria as adult patients (≥20 years of age) with pathologically confirmed histoplasmosis. All tissue specimens underwent standardized processing protocols including hematoxylin and eosin staining, periodic acid-Schiff staining, and Gomori methenamine silver staining for organism detection and morphological characterization. Experienced pathologists confirmed histoplasmosis diagnosis on the basis of concomitant presence of characteristic intracellular yeast forms of *H. capsulatum* in tissue specimens, 2–4 μm in size, with narrow-based budding, and in the absence of transverse septum (Figure 1). In addition, the primary treating physician determined pulmonary involvement on the basis of clinical assessment, radiologic evidence, and microbiologic findings from respiratory tract specimens or lung tissue.

Data Extraction

For each identified case, we systematically retrieved demographic information including age at diagnosis, sex, body mass index, smoking history, occupation, pet ownership, residential distribution, and detailed travel history within 6 months preceding diagnosis. We used Centers for Disease Control and Prevention definitions for endemicity for travel destination (*14*). We also documented clinical data including cardinal manifestations of pulmonary histoplasmosis (fever, dyspnea, cough, and bodyweight loss), underlying conditions, immunosuppression factors, and antifungal medication. We defined immunosuppression as those who received immunosuppressive therapy. We systematically reviewed chest imaging studies to characterize the location, extent, and pattern of pulmonary involvement. We classified lesions by morphologic appearance and anatomic distribution by pulmonary lobe.

Statistical Analysis

We performed statistical analyses using SPSS Statistics 19.0 software (https://www.ibm.com) and compiled descriptive statistics as mean ±SD for continuous variables and frequencies with percentages for

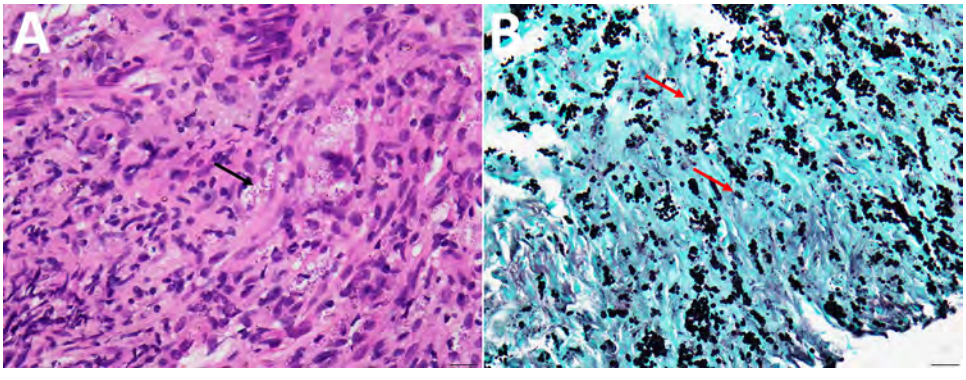

Figure 1. Representative histopathologic findings of pulmonary histoplasmosis in Taiwan, 1997–2024. A) Hematoxylin and eosin stain delineates numerous tiny ovoid yeasts within macrophages; occasional narrow-based budding indicated (black arrow). B) Grocott's methenamine silver stain shows yeasts with narrow-based budding (red arrows). Scale bars represent 20 μm.

Table 1. Characteristics of case-patients in study of pulmonary histoplasmosis in Taiwan, 1997–2024*

Case no.	Age, y/ sex	Date	Travel history	Occupation	Pet	Residence region	Involved site (details)	Immunocompromised factor	Antifungal agent
With lung involvement									
1	21/F	2001 Apr	USA (Illinois)†	Teacher	None	North	Lung (nodule)	Immunocompetent	None
2‡	86/M	2003 Feb	Indonesia,† Thailand,† Saudi Arabia, China (Shandong)	Excavator driver	None	North	Lung (nodule)	Addison's disease	Amphotericin B
3	71/M	2014 Aug	India,† Guatemala,† USA (California)	Electronics	None	North	Lung (nodule)	Immunocompetent	None
4	20/F	2016 Jul	None	Student	None	North	Lung (nodule)	Immunocompetent	Voriconazole
5	74/F	2016 Jul	None	Housewife	None	North	Lung (nodule)	Immunocompetent	Posaconazole
6	36/M	2019 Aug	None	Office worker	None	North	Lung (nodule)	Immunocompetent	Voriconazole
7	32/M	2019 Dec	None	Unknown	None	Middle	Lung (nodule)	Immunocompetent	Posaconazole
8	66/M	2020 May	None	Unknown	None	North	Disseminated (involving skin, lymph node, and GI tract)	Kidney transplant	Voriconazole
9	54/M	Mar 2021	None	Electronic engineering	None	North	Lung (nodule)	Immunocompetent	Itraconazole
10	53/M	Oct 2021	None	Cement worker	None	Middle	Lung (nodule)	Immunocompetent	None
11	83/F	Dec 2021	None	None	None	North	Lung (consolidation)	Rheumatoid arthritis	Voriconazole
12	63/F	Sep 2023	None	Housewife	None	Middle	Lung (nodule)	Immunocompetent	Fluconazole
13	60/F	2023 Sep	None	Indoor decoration	Duck	North	Lung (ill-defined opacity), bone marrow	Myelodysplasic syndrome	Ambisome
14§	74/M	2024 Sep	None	Cement worker	None	Middle	Lung (nodule)	Immunocompetent	Voriconazole
Without lung involvement									
15	27/M	1997 Jun	Malaysia,† Thailand,† Singapore†	Unknown	None	North	Disseminated (involving lung, bone marrow, GI tract, and lymph node)	HIV	Amphotericin B
16	78/M	2003 Oct	None	Farmer	None	East	Mediastinal lymph node	None	Amphotericin B

*GI, gastrointestinal.
†These areas likely to be hyperendemic, cases likely to occur regularly, and locally acquired cases to be reported.
‡Patient died of respiratory failure.
§Patient survived with Evans syndrome.

categorical variables. Because the sample size was relatively small for this rare disease, we compared groups using nonparametric tests: Mann-Whitney U test for continuous variables and Fisher exact test for binary categorical variables. We defined statistical significance as a 2-sided p value <0.05.

Results

A total of 14 persons with pathologically confirmed histoplasmosis and lung involvement comprised the primary cohort for analysis. We identified 2 additional patients without lung involvement for comparison (Table 1). The population was predominantly male (8 [57.1%] vs. 6 [42.9%] female); mean age was 56.6 years. Most patients were never smokers (12 [85.7%]); the remaining 2 had a history of former smoking. Regarding geographic distribution, 10 (71.4%) patients resided in northern Taiwan, and 4 (28.6%) patients were from the middle Taiwan regions. Of note, occupational exposure to dust or soil environments was present in 3 (21.4%) patients; 1 (7.1%) was a pet owner. Three (21.4%)

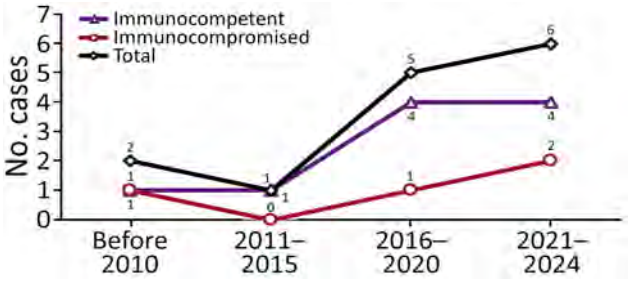

Figure 2. Epidemiologic trend of pulmonary histoplasmosis in Taiwan, stratified by host immunity, 1997–2024. Numbers above data points indicate numbers of cases.

patients had a history of travel to recognized disease-endemic areas.

Clinical manifestations varied across the cohort. When assessed individually, each cardinal symptom was present in 21.4%–35.7% of the study population. However, up to 64.3% of the patients manifested a constellation of these symptoms. Underlying conditions were notable within the study population. Two (14.3%) patients had a history of tuberculosis; 1 experienced remote infection, and 1 had a concurrent case of pulmonary histoplasmosis. Four (28.6%) patients were receiving immunosuppressive therapies: 2 patients for autoimmune diseases, 1 patient for active hematologic malignancy, and 1 patient for solid organ transplantation. Diagnostic confirmation of histoplasmosis was achieved primarily through histopathologic examination, whereas microbiologic confirmation through positive fungal culture was achieved in 2 (14.3%) patients.

We observed temporal distribution of cases during 2016–2024 (Figure 2). Throughout the study, the number of immunocompetent patients consistently exceeded their immunocompromised counterparts. We noted anatomic involvement in radiographic images consistent with typical manifestations of pulmonary histoplasmosis described in endemic regions (Figure 3). The predominant pattern was nodular lesions (12 [85.7%] patients); the 2 exceptions appeared as consolidation and ill-defined opacity. Most (11 [78.6%]) patients received appropriate antifungal treatment (Figure 4). Voriconazole was the most commonly administered therapeutic agent, followed by amphotericin B, posaconazole, fluconazole, and itraconazole.

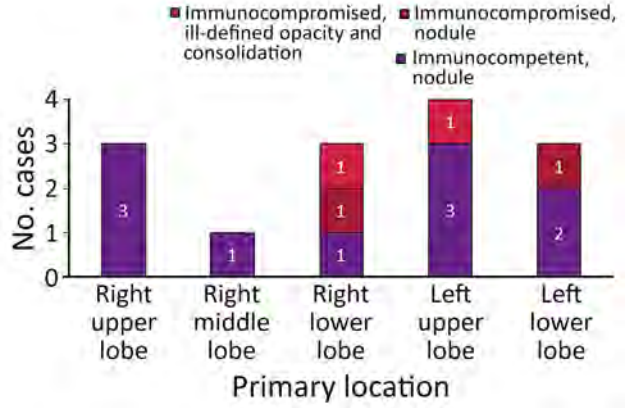

Figure 3. Locations and characteristics of primary lung lesions in patients with pulmonary histoplasmosis in Taiwan, 1997–2024.

Comparative analysis by host immunity revealed no statistically significant differences in symptom presentation, underlying conditions, absolute neutrophil count, and C-reactive protein level between the immunocompetent and immunocompromised groups. However, immunosuppressed patients were numerically but not significantly older (73.8 vs. 49.8 years of age; $p = 0.07$). In addition, the elderly patients demonstrated a higher tendency to exhibit cardinal symptoms (83.3% vs. 50.0%; $p = 0.30$). Conversely, younger patients manifested slightly lower absolute neutrophil counts (3.2 vs. 5.3 k/μL; $p = 0.15$).

The overall prognosis was favorable. One patient (patient 2), who was immunosuppressed from steroid use for Addison's disease, eventually experienced severe pneumonia with hypoxemic respiratory failure despite treatment with amphotericin B (1 mg/kg/d) and died in the hospital (*15*). Patient 14 experienced consequent immune system dysregulation by manifesting idiopathic thrombocytopenic purpura and autoimmune hemolytic anemic (Evans syndrome); that patient survived till the study endpoint (*16*).

We identified 2 patients during the study period who had histoplasmosis without thoracic involvement; they experienced multiorgan involvement including the gastrointestinal tract, skin, colon, lymph nodes, and bone marrow. One patient had concurrent HIV infection with Kaposi sarcoma; the other was considered immunocompetent. Comparative analysis revealed no significant demographic or clinical parameter differences between pulmonary and nonpulmonary cases (Tables 2–4).

Discussion

This comprehensive, longitudinal analysis of histoplasmosis cases in Taiwan over a 27-year period fundamentally challenges the established paradigm that histoplasmosis remains confined to traditionally recognized endemic geographic regions. Our findings demonstrate the emergence of histoplasmosis in Taiwan and underscore the importance of considering a histoplasmosis diagnosis even in geographic locations previously classified as nonendemic or in immunocompetent patients.

Our results extend previous observations documenting 17 histoplasmosis cases from Taiwan over 4 decades (*12*). Local *Talaromyces marneffei*, another dimorphism fungus with similar morphology, has been identified in Taiwan; *H. capsulatum* can be distinguished histologically by its pathognomonic feature of the central septum (*17*). The marked increase in diagnosed histoplasmosis cases since 2016 exemplifies enhanced case recognition, a likely result of improved diagnostic modalities (*18*). The absence of culture or molecular typing can prevent definite diagnosis, as reflected in therapeutics. Even though itraconazole had been endorsed as standard treatment (*19*), only 6% of the patients in our cohort were treated with it. Voriconazole was the most frequently prescribed alternative instead, perhaps because of its lower adverse effect on gastrointestinal tract and liver function, as well as its broader antifungal spectrum when diagnosis remains indefinite.

A notable finding of our study is the limited travel history among affected patients. National health insurance data indicated a local incidence of histoplasmosis at 0.24/100,000 population annually (*20*); our study suggested that local acquisition of histoplasmosis in Taiwan may be more common than previously recognized. Whether those cases can be attributed to indigenous transmission or imported disease remained unknown; however, our study provides more definitive evidence for local acquisition by demonstrating the high proportion of patients without relevant travel history.

We hypothesized that the environmental niche of *H. capsulatum* is geographically more widespread than previously considered (*21*). Several factors contributed to fungal growth and spore production in previously nonendemic areas, including climate change, urbanization, construction activities, soil transportation, and changes in bird population distribution. Climate change creates favorable environmental conditions for *H. capsulatum* fungus survival and proliferation in regions previously considered unsuitable. The increasing urbanization and construction activities disturbed soil containing dormant fungal spores, resulting in aerosolization and subsequent human exposure. In addition, global trade and transportation of soil materials, agricultural products, and construction materials likely enable the introduction and establishment of *H. capsulatum* in novel geographic locations. Approximately 30% of cement clinker used for construction in Taiwan is imported, which might provide a route of transmission for *H. capsulatum* and subsequently serve as an exposure source.

Figure 4. Distribution of antifungal agents used in cases of pulmonary histoplasmosis in Taiwan, 1997–2024.

The emergence of histoplasmosis in immunocompetent persons represents another concerning epidemiologic trend. Previous studies have reported cases of immunocompetent hosts with disseminated histoplasmosis, although most had obvious exposure through construction work (*22*). In our series, not all cases could be identified with specific exposure sources either through occupation or travel history. A similar case report from South Korea also described a patient with pulmonary histoplasmosis who was neither immunocompromised nor had travel history (*23*). Although immunosuppression has been well established as an important predisposing factor for severe histoplasmosis, our study

Table 2. Key parameters in study of pulmonary histoplasmosis by host immunity status, Taiwan, 1997–2024*

Characteristic	All, N = 14	Immunocompetent, n = 10	Immunocompromised, n = 4	p value
Mean age, y, ± SD	56.6 ± 21.8	49.8 ± 21.2	73.8 ± 12.7	0.07
Sex				
M	8 (57.1)	6 (60.0)	2 (50.0)	1.00
F	6 (42.9)	4 (40.0)	2 (50.0)	
Any cardinal symptoms	9 (64.3)	5 (50.0)	4 (100.0)	0.22
Tuberculosis	2 (14.3)	1 (10.0)	1 (25.0)	0.49
HIV	0	0	0	NA
Travel history	3 (21.4)	2 (20.0)	1 (25.0)	1.00
Immunosuppression	4 (28.6)			
ANC ± SD	4.1 ± 2.1	4.2 ± 1.7	3.9 ± 3.4	1.00
CRP ± SD	4.2 ± 3.8	3.1 ± 4.0	5.2 ± 4.2	0.40
In-hospital death	1 (7.1)	0	1 (25.0)	0.29
Complication	2 (14.3)	1 (10.0)	1 (25.0)	0.51

*Values are no. (%) except as indicated. ANC, absolute neutrophil count; CRP, C-reactive protein; NA, not applicable.

Table 3. Key parameters in study of pulmonary histoplasmosis, by lung involvement, Taiwan, 1997–2024*

Characteristic	Yes, n = 14	No, n = 2†	p value
Mean age, y, ± SD	56.6 ± 21.8	52.5 ± 25.5	1.00
Sex			
M	8 (57.1)	2 (100)	0.26
F	6 (42.9)	0 (0)	
Any cardinal symptoms	9 (64.3)	2 (100)	0.32
Tuberculosis	2 (14.3)	0	0.58
HIV	0	1 (50.0)	**0.008**
Travel history	3 (21.4)	1 (50.0)	0.40
Immunosuppression	4 (28.6)	1 (50.0)	0.55
ANC ± SD	4.1 ± 2.1	NA	NA
CRP ± SD	4.2 ± 3.8	NA	NA
In-hospital death	1 (7.1)	0	0.71
Complication	2 (14.3)	0	0.58

*Values are no. (%) except as indicated. Values in bold text are statistically significant. ANC, absolute neutrophil count; CRP, C-reactive protein; NA, not applicable.
†These 2 additional cases were used as controls.

demonstrates that most patients were immunocompetent at the time of diagnosis. In addition to heterogeneous clinical manifestations observed in our cohort, those cases suggested that traditional risk stratification approaches might need revision and that environmental factors or genetic susceptibility play pivotal roles. Genetic polymorphisms in immune response genes may influence individual susceptibility to histoplasmosis infection and disease severity (*24*). Environmental factors, such as the intensity and duration of exposure, coexisting respiratory conditions, or concurrent infections, could also modulate disease manifestation in immunocompetent hosts. The occurrence of disseminated disease in the additional cases we describe exemplifies the potential severity of histoplasmosis even in presumably low-risk populations. The development of Evans syndrome in 1 patient further demonstrates the potential for complex immunological complications after histoplasmosis infection. Despite those complications, the favorable outcomes achieved with appropriate antifungal therapy demonstrate the efficacies of early recognition and treatment.

Of radiology results, nodular lesions remained the most prevalent pattern we observed at >80%, which closely matches previous reports (*25*). However, some studies have described additional specific patterns including cavitary lesions (*26*), halo (*27*) or reverse halo (*28*) signs, and spindle cell lesions (*29*). Because of those imaging findings, pulmonary histoplasmosis can be easily confused with primary lung malignancy or metastatic lesions, thereby mandating tissue-based diagnostic procedures. The exceptionally low yield of fungal cultures in our study emphasizes the inherent diagnostic difficulties associated with histoplasmosis; histopathologic examination remained the primary diagnostic modality. The integration of molecular diagnostic methodologies, including PCR-based assays, monoclonal antibody–based assays (*30*), and next-generation sequencing approaches (*31*), could enhance detection rates and support pathological findings. Those advanced diagnostic modalities could be particularly valuable in nonendemic settings where clinical suspicion may be lower and traditional diagnostic methods may be less reliable. Moreover, antigen detection assays, particularly

Table 4. Comparisons of key parameters in study of pulmonary histoplasmosis by disease manifestation in lungs, Taiwan, 1997–2024*

Characteristic	All, N = 14	Nodule, n = 12	Other, n = 2†	p value
Mean age, y, ± SD	56.6 ± 21.8	54.2 ± 22.1	71.5 ± 16.3	0.36
Sex				
M	8 (57.1)	8 (66.7)	0	0.09
F	6 (42.9)	4 (33.3)	2 (100)	
Any cardinal symptoms	9 (64.3)	7 (58.3)	2 (100)	0.27
Tuberculosis	2 (14.3)	2 (16.7)	0	0.55
HIV	0	0	0	NA
Travel history	3 (21.4)	3 (25.0)	0	0.44
Immunosuppression	4 (28.6)	2 (16.7)	2 (100)	**0.02**
ANC ± SD	4.1 ± 2.1	4.2 ± 1.6	3.5 ± 4.7	0.83
CRP ± SD	4.2 ± 3.8	4.7 ± 4.6	3.0 ± 2.3	1.00
In-hospital death	1 (7.1)	1 (8.3)	0	0.68
Complication	2 (14.3)	2 (16.7)	0	0.55

*Values are no. (%) except as indicated. Values in bold text are statistically significant. ANC, absolute neutrophil count; CRP, C-reactive protein; NA, not applicable.
†These 2 additional cases were used as controls.

urinary *Histoplasma* antigen testing, have shown promise in endemic areas to enable diagnosis in nonendemic regions, especially for disseminated cases.

Our findings underscore the critical need for heightened clinical suspicion of histoplasmosis even in previously considered nonendemic settings, particularly given the varied manifestations observed in both immunocompromised and immunocompetent patients. Future research should prioritize systematic environmental reservoir identification, genetic determinants of host susceptibility, and optimization of diagnostic approaches specific to nonendemic settings. Previous studies have applied PCR to identify local acquisition in wildlife and environment samples (*32*,*33*); we expect the molecular approach to demonstrate that epidemiology of infectious disease evolves in response to changing environmental and demographic factors, emphasizing the need for adaptive surveillance and clinical preparedness strategies.

A limitation of this study is that its retrospective nature inherently limited data completeness and potentially introduced selection bias toward more severe patients requiring invasive investigation. Potential study participants were identified by International Classification of Diseases coding and confirmed as having histoplasmosis after pathology review; most lacked positive culture of *H. capsulatum*, which would provide a definite diagnosis. A second limitation is that we documented only recent travel history in our study. Reactivation of *H. capsulatum* that was acquired from remote travel cannot be totally excluded. Third, the small sample size confined statistical power for subgroup analyses and obscured subtle but clinically important differences between different patient phenotypes; we acknowledge that the small sample reflected the rarity of the disease. Fourth, we identified the patients in our study relying on histopathologic diagnosis; we lacked culture data for validation. We might have underestimated genuine incidence of histoplasmosis because mild or asymptomatic case records might not indicate tissue sampling. Finally, we did not address the identification of local fungal reservoirs and transmission sources.

In conclusion, this 27-year case series provides evidence for the emergence of histoplasmosis in Taiwan, potentially challenging traditional geographic boundaries of such infections. The high proportion of patients without travel history to endemic regions is suggestive of local acquisition and possible *H. capsulatum* reservoirs in the environment. The predominance of immunocompetent hosts among our cases indicates evolving epidemiologic patterns that require further clinical recognition and risk assessment strategies. We recommend high clinical suspicion for histoplasmosis in patients with compatible clinical and radiologic findings, even in the absence of travel history or obvious immunocompromising conditions.

Acknowledgments

We thank the Medical Information Management Office of National Taiwan University Hospital.

About the Author

Dr. Kao is a fellow in the department of pulmonary and critical care medicine of National Taiwan University Hospital, Taipei. He actively participated in both primary care and research of pulmonary fungal infection.

References

1. Barros N, Wheat JL, Hage C. Pulmonary histoplasmosis: a clinical update. J Fungi (Basel). 2023;9:236. https://doi.org/10.3390/jof9020236
2. Furcolow ML. Comparison of treated and untreated severe histoplasmosis: a communicable disease center cooperative mycoses study. JAMA. 1963;183:823–9.
3. Arnold SR, Spec A, Baddley JW, Pappas P, Lentz RJ, Wolf J, et al. 2025 clinical practice guideline update by the Infectious Diseases Society of America on histoplasmosis: treatment of asymptomatic histoplasma pulmonary nodules (histoplasmomas) and mild or moderate acute pulmonary histoplasmosis in adults, children, and pregnant people. Clin Infect Dis. 2025;2025:ciaf256. https://doi.org/10.1093/cid/ciaf256
4. Galgiani JN, Kauffman CA. Coccidioidomycosis and histoplasmosis in immunocompetent persons. N Engl J Med. 2024;390:536–47. https://doi.org/10.1056/NEJMra2306821
5. Benedict K, Toda M, Jackson BR. Revising conventional wisdom about histoplasmosis in the United States. Open Forum Infect Dis. 2021;8:ofab306. https://doi.org/10.1093/ofid/ofab306
6. Ashraf N, Kubat RC, Poplin V, Adenis AA, Denning DW, Wright L, et al. Re-drawing the maps for endemic mycoses. Mycopathologia. 2020;185:843–65. https://doi.org/10.1007/s11046-020-00431-2
7. Kauffman CA. Histoplasmosis: a clinical and laboratory update. Clin Microbiol Rev. 2007;20:115–32. https://doi.org/10.1128/CMR.00027-06
8. Thompson GR III, Le T, Chindamporn A, Kauffman CA, Alastruey-Izquierdo A, Ampel NM, et al. Global guideline for the diagnosis and management of the endemic mycoses: an initiative of the European Confederation of Medical Mycology in cooperation with the International Society for Human and Animal Mycology. Lancet Infect Dis. 2021;21:e364–74. https://doi.org/10.1016/S1473-3099(21)00191-2
9. Liu X, Zhao Z, Zong Z. Precise geographical distribution and call for accurate identification of histoplasmosis cases in China. Lancet Microbe. 2024;5:100943. https://doi.org/10.1016/j.lanmic.2024.07.006
10. Rodrigues AM, Beale MA, Hagen F, Fisher MC, Terra PPD, de Hoog S, et al. The global epidemiology of emerging *Histoplasma* species in recent years. Stud Mycol. 2020;97:100095. https://doi.org/10.1016/j.simyco.2020.02.001
11. Bernardes JPRA, Tenório BG, Lucas J Jr, Paternina CEM, da Silva RKM, Erazo FAH, et al. Mapping *Histoplasma* spp.

in bats and cave ecosystems: evidence from midwestern Brazil. Appl Environ Microbiol. 2025;91:e0033525. https://doi.org/10.1128/aem.00335-25
12. Hsu JC, Chang PH, Tai CH, Chen YC. Histoplasmosis in Taiwan: case summary and literature review. Life (Basel). 2024;14:738. https://doi.org/10.3390/life14060738
13. Gandhi P, Hebert B, Yun A, Bradley J, Moldoveanu B. Histoplasmosis around the world: a global perspective on the presentation, virulence factors, and treatment of histoplasmosis. Am J Med Sci. 2024;368:287–99. https://doi.org/10.1016/j.amjms.2024.06.011
14. Centers for Disease Control and Prevention. Areas with histoplasmosis. 2024 [cited 2025 Jul 20]. https://www.cdc.gov/histoplasmosis/data-research/maps/index.html
15. Tseng TC, Liaw SJ, Hsiao CH, Wang CY, Lee LN, Huang TS, et al. Molecular evidence of recurrent histoplasmosis with 9-year latency in a patient with Addison's disease. J Clin Microbiol. 2005;43:4911–3. https://doi.org/10.1128/JCM.43.9.4911-4913.2005
16. Kao TW, Tsai MT, Pan SC, Shu CC, Liao WY, Jerng JS. Concurrent pulmonary TB and histoplasmosis in an HIV-negative patient with Evans syndrome. IJTLD Open. 2025;2:176–8. https://doi.org/10.5588/ijtldopen.24.0607
17. Qin L, Zhao L, Tan C, Chen XU, Yang Z, Mo W. A novel method of combining Periodic Acid Schiff staining with Wright-Giemsa staining to identify the pathogens *Penicillium marneffei*, *Histoplasma capsulatum*, *Mucor* and *Leishmania donovani* in bone marrow smears. Exp Ther Med. 2015;9:1950–4. https://doi.org/10.3892/etm.2015.2357
18. Azar MM, Hage CA. Laboratory diagnostics for histoplasmosis. J Clin Microbiol. 2017;55:1612–20. https://doi.org/10.1128/JCM.02430-16
19. Wheat J, Sarosi G, McKinsey D, Hamill R, Bradsher R, Johnson P, et al.; Infectious Diseases Society of America. Practice guidelines for the management of patients with histoplasmosis. Clin Infect Dis. 2000;30:688–95. https://doi.org/10.1086/313752
20. Huang YS, Denning DW, Shih SM, Hsiung CA, Wu UI, Sun HY, et al. Fungal diseases in Taiwan—national insurance data and estimation. J Fungi (Basel). 2019;5:78. https://doi.org/10.3390/jof5030078
21. Tai CH, Sun PL, Chien CC, Chiu CH, Chen YC. Indigenous case of disseminated histoplasmosis: a possible underdiagnosed disease in Taiwan. J Microbiol Immunol Infect. 2022;55:1334–6. https://doi.org/10.1016/j.jmii.2022.09.008
22. Klein M, Khan M, Salinas JL, Sanchez R. Disseminated pulmonary histoplasmosis in immunocompetent patients: a common epidemiological exposure. BMJ Case Rep. 2019;12:e227994. https://doi.org/10.1136/bcr-2018-227994
23. Jung EJ, Park DW, Choi JW, Choi WS. Chronic cavitary pulmonary histoplasmosis in a non-HIV and immunocompromised patient without overseas travel history. Yonsei Med J. 2015;56:871–4. https://doi.org/10.3349/ymj.2015.56.3.871
24. Carvalho A, Cunha C, Pasqualotto AC, Pitzurra L, Denning DW, Romani L. Genetic variability of innate immunity impacts human susceptibility to fungal diseases. Int J Infect Dis. 2010;14:e460–8. https://doi.org/10.1016/j.ijid.2009.06.028
25. Chen Q, Guo W, Guo W, Mu X, Guo J. Pulmonary histoplasmosis on the Chinese mainland: two case reports and literature review. J Infect Dev Ctries. 2024;18:318–25. https://doi.org/10.3855/jidc.17934
26. Lee YJ, Kang HR, Song JH, Sin S, Lee SM. Pulmonary histoplasmosis identified by video-assisted thoracic surgery (VATS) biopsy: a case report. J Korean Med Sci. 2018;33:e15. https://doi.org/10.3346/jkms.2018.33.e15
27. Pereira GH, Almeida LY, Okubo RS, Marchiori E. Pulmonary histoplasmosis presenting with a halo sign on CT in an immunocompetent patient. J Bras Pneumol. 2013;39:523–4. https://doi.org/10.1590/S1806-37132013000400019
28. Marchiori E, Melo SMD, Vianna FG, Melo BSD, Melo SSD, Zanetti G. Pulmonary histoplasmosis presenting with the reversed halo sign on high-resolution CT scan. Chest. 2011;140:789–91. https://doi.org/10.1378/chest.11-0055
29. Gravdahl DJ, Gardetto JS, Hurley JR, Tazelaar HD, Koontz PW, Leslie KO. Pulmonary histoplasmosis producing a spindle cell "pseudotumor." Am J Clin Pathol. 2011;136:410–5. https://doi.org/10.1309/AJCP13KZDDJCICAT
30. Zhang X, Gibson B Jr, Daly TM. Evaluation of commercially available reagents for diagnosis of histoplasmosis infection in immunocompromised patients. J Clin Microbiol. 2013;51:4095–101. https://doi.org/10.1128/JCM.02298-13
31. Xie C, Yang Y, Wu X, Chen Z, Zhu N, Song Y, et al. A case of pulmonary histoplasmosis treated with voriconazole. J Infect Dev Ctries. 2022;16:570–4. https://doi.org/10.3855/jidc.15297
32. Hernández-Alomía F, Brito J, Pilatasig AL, Reyes-Barriga D, Carrión-Olmedo JC, Jarrín-V P, et al. *Histoplasma capsulatum* in wild mammals from Ecuador. PLoS Negl Trop Dis. 2025;19:e0013410. https://doi.org/10.1371/journal.pntd.0013410
33. Gómez LF, Gade L, Litvintseva AP, McEwen JG, Peláez CA, Arango M, et al. Comparison between two molecular techniques: nested and real-time polymerase chain reaction targeting 100-kDa Hc protein for detection of *Histoplasma capsulatum* in environmental samples. Am J Trop Med Hyg. 2022;106:1329–32. https://doi.org/10.4269/ajtmh.20-1396

Address for correspondence: Chin-Chung Shu, Division of Pulmonary and Critical Care Medicine, Department of Internal Medicine, National Taiwan University Hospital, No. 7, Chung-Shan South Rd, Taipei, Taiwan; email: ccshu@ntu.edu.tw

Retrospective Case Series of Ocular Lyme Disease, 1988–2025

Jenna Bellafiore, Abdallah Mahrous, Vaishnavi Gurumurthy, Eugene Capitle, Steven E. Schutzer

Medscape CME Activity

In support of improving patient care, this activity has been planned and implemented by Medscape, LLC and Emerging Infectious Diseases. Medscape, LLC is jointly accredited with commendation by the Accreditation Council for Continuing Medical Education (ACCME), the Accreditation Council for Pharmacy Education (ACPE), and the American Nurses Credentialing Center (ANCC), to provide continuing education for the healthcare team.

Medscape, LLC designates this Journal-based CME activity for a maximum of 1.00 ***AMA PRA Category 1 Credit(s)™***. Physicians should claim only the credit commensurate with the extent of their participation in the activity.

Successful completion of this CME activity, which includes participation in the evaluation component, enables the participant to earn up to 1.0 MOC points in the American Board of Internal Medicine's (ABIM) Maintenance of Certification (MOC) program. Participants will earn MOC points equivalent to the amount of CME credits claimed for the activity. It is the CME activity provider's responsibility to submit participant completion information to ACCME for the purpose of granting ABIM MOC credit.

All other clinicians completing this activity will be issued a certificate of participation. To participate in this journal CME activity: (1) review the learning objectives and author disclosures; (2) study the education content; (3) take the post-test with a 75% minimum passing score and complete the evaluation at http://www.medscape.org/journal/eid; and (4) view/print certificate. For CME questions, see page 166.

NOTE: It is the policy of Medscape Education to avoid the mention of brand names or specific manufacturers in accredited educational activities. However, trade and manufacturer names in this activity are provided in an effort to provide clarity. The use of brand or manufacturer names should not be viewed as an endorsement by Medscape of any specific product or manufacturer.

Release date: January 29, 2026; Expiration date: January 29, 2027

Learning Objectives

Upon completion of this activity, participants will be able to:

- Analyze ocular complications of Lyme disease
- Assess the proportion of microbiologically proven cases of Lyme disease with ocular complications

CME Editor

Jude Rutledge, BA, Technical Writer/Editor, Emerging Infectious Diseases. *Disclosure: Jude Rutledge, BA, has no relevant financial relationships.*

CME Author

Charles P. Vega, MD, Health Sciences Clinical Professor of Family Medicine, University of California, Irvine School of Medicine, Irvine, California. *Disclosure: Charles P. Vega, MD, has the following relevant financial relationships: consultant or advisor for Boehringer Ingelheim; Exact Sciences.*

Authors

Jenna Bellafiore, DO; Abdallah Mahrous, MD; Vaishnavi Gurumurthy, MD; Eugene Capitle, MD; Steven E. Schutzer, MD.

Reports of ocular manifestations of Lyme disease (LD) are uncommon, and signs and symptoms may be overlooked by physicians. We conducted a retrospective case series of ocular LD reported during 1988–2025. Among 27 published reports in PubMed, we noted that, in 38 cases, the most common ocular manifestation was uveitis, representing 45% of cases, followed by optic neuritis and cranial nerve palsies (including trochlear and abducens). Not all cases met Centers for Disease Control and Prevention surveillance guidelines for LD, given that some case reports were published before the current guidelines. Cases that provided microbiologic proof were 2 anterior uveitis cases, 1 case of anterior uveitis with abducens's nerve palsy, 1 case of intermediate uveitis, and 1 case of intranuclear ophthalmoplegia. Ocular LD can have a broad variety of manifestations; therefore, physicians should be aware of those manifestations and obtain microbiologic proof for a more definitive diagnosis and epidemiologic value when possible.

Lyme disease (LD), caused by *Borrelia burgdorferi*, is the leading vectorborne disease in the United States (*1*,*2*), transmitted by *Ixodes* ticks (*3*). LD has been described conceptually in stages, although manifestations of what was described as later stages can occur at the initial stage of infection. The initial stage often manifests with a characteristic skin rash, erythema migrans, described as a centrifugally expanding erythematous annular skin lesion with a clear center, or the bull's-eye lesion, at the site of the tick bite (*4*). However, the classic form of erythema migrans does not occur in many cases, even those with microbiologic proof of the infection (*5*,*6*). The second stage of disease, occurring weeks to months later, and third stage of disease, occurring months later, are known to have a wide variety of manifestations, including neurologic, cardiac, and musculoskeletal signs and symptoms (*1*,*4*). Arthralgias are common in early LD, whereas arthritis, when it occurs, appears in later stages (*7*). In addition, various ocular etiologies have been observed during the second and third stages of LD.

Although reports of ocular LD are rare, it can manifest in various ways, including, but not limited to, uveitis; optic neuritis; cranial nerve III, IV, and VII palsies; papilledema; and retinal vasculitis. We reviewed previously described case reports of ocular LD, summarizing the clinical manifestations to further clarify the possible manifestations of ocular LD to help guide physicians regarding when to consider this diagnosis. A caveat is that many of the early published cases did not necessarily follow the Centers for Disease Control and Prevention (CDC) case definitions at the time they were reported. Those definitions are for surveillance and not meant as clinical criteria for individual diagnosis and treatment (*8*,*9*).

Author affiliations: Rutgers New Jersey Medical School, Newark, New Jersey, USA (J. Bellafiore, V. Gurumurthy, E. Capitle, S.E. Schutzer); Weill Cornell Medical College, New York, New York, USA (A. Mahrous)

DOI: https://doi.org/10.3201/eid3201.250769

Methods

This retrospective case series aimed to evaluate ocular manifestations of LD by reviewing cases identified in the PubMed database that were published during 1988–2025. We included published articles in PubMed up until March 15, 2025, that described clinical manifestations of various forms of ocular LD. We conducted the literature search in PubMed by using the search terms "ocular Lyme" and "ocular and variations, with *B. burgdorferi*." Inclusion criteria included articles that discussed ≥1 case report of ocular manifestations of LD. Exclusion criteria included inability to obtain full text, text in language other than English, and studies that did not discuss clinical manifestations of a specific case. We noted a paucity of articles that met CDC criteria at the time the cases were reported. Despite those limitations, we were able to illustrate the specific variety of ocular conditions by screening 176 articles; among the reviewed full texts, 29 were eligible for sufficient analysis. We excluded 2 texts because no English versions of the texts were available. We reviewed 27 publications (Table; Appendix Table, https://wwwnc.cdc.gov/EID/article/32/1/25-0769-App1.pdf). In order of decreasing assurance that the patient had LD were microbiologic evidence (e.g., DNA) or culture-positive test results for *B. burgdorferi*, meeting CDC criteria for LD with serologic conversion, CDC criteria otherwise being met, and CDC criteria not being met.

Results

The reviewed literature (Table; Appendix Table) highlights diverse ocular manifestations of LD and the basis for their diagnosis and method for treatment. Of the 38 cases we analyzed, 5 cases had microbiologic proof of LD (*10*–*14*) (Table). Cases that had microbiologic proof were 2 cases of anterior uveitis, 1 case of intermediate uveitis, 1 case of abducens nerve palsy with anterior uveitis, and 1 case of intranuclear ophthalmoplegia.

Ocular LD Cases with Microbiologic Proof

One case occurred in a 67-year-old man who had bilateral, progressive, asymmetric crystalline keratopa-

thy. The patient had been taking methotrexate and systemic steroids for several years for recurrent iridocyclitis and arthritis of unknown cause. The patient had a penetrating keratoplasty of the right eye because of decreased visual acuity and had recurrence of the crystalline keratopathy 6 months later. Another 6 months later, he experienced acute vision loss accompanied by massive crystalline deposits. Another keratoplasty was performed, and a corneal specimen had spirochete-like bodies detected by light and electron microscopic examination and broadrange (16S rDNA) PCR tests that were positive for *B. burgdorferi* sensu lato DNA. The patient was then treated with intravenous ceftriaxone for 2 weeks and was continued on his immunosuppression agents; he also received tetracycline eyedrops and steroid eyedrops, which were continued for over 2 years. The corneal findings remained unchanged.

Another case occurred in a 26-year-old woman with unilateral intermediate uveitis, specifically pars planitis. Her vitreous fluid tested PCR-positive for *B. burgdorferi*. She was treated with oral doxycycline (100 mg 2×/d) and 2 months later had onset of keratitis and inflammation in the other eye. She was then started on intravenous ceftriaxone and experienced substantial improvement in her symptoms. However, 10 days later, after she had onset of severe thrombocytopenia, ceftriaxone was discontinued, and she was started on oral nitrofurantoin therapy for 2 months. She had continual visual deterioration, and a vitrectomy was performed. The vitreous fluid was found to be PCR-positive for a 232-bp segment specific for *B. burgdorferi*.

Another case with microbiologic proof occurred in a 45-year-old women who initially had systemic symptoms of fever, chills, headache, light headed-

Table. Published case reports of ocular Lyme disease that indicate microbiologic proof of Lyme disease, 1988–2025*

Article authors	Year†	Evidence	Age/sex	Ocular manifestations, diagnosis, and additional symptoms	Treatment and resolution time in article
Dietrich et al. (*10*)	2008	Corneal specimen: spirochete-like bodies and fragments detected by light and electron-microscopic examination. PCR: positive for *Borrelia burgdorferi* sensu lato DNA. IFA: borderline. Western blot: weak reaction.	67/M	History of recurrent iridocyclitis and arthritis (unknown etiology) treated with methotrexate and steroids; developed progressive asymmetric keratopathy	Penetrating keratoplasty 2 times. IV ceftriaxone for 2 wks, and systemic immunosuppression (prednisone and methotrexate) continued. Tetracycline eyedrops and steroid eyedrops continued for >2 y without recurrence.
Hilton et al. (*11*)	1996	Vitreous fluid: positive PCR test result for 232-bp segment specific for *B. burgdorferi*; ELISA-negative (repeat test 4 mo later positive); Western blot negative, with faint reactivity to 4 IgG bands (repeat test 4 mo later positive).	26/F	Diagnosed with pars planitis	Doxycycline 100 mg 2×/d with improvement but recurrence. Treated with IV ceftriaxone 2 g/d for 10 d, followed by 2 mo oral macrolides. Visual deterioration requiring vitrectomy.
Kauffmann and Wormser (*12*)	1990	IFA: positive IgM and IgG. Vitreous debris examination showed occasional intact spirochetes compatible with Lyme disease. FTA-ABS and VRDL negative for *Treponema pallidum*.	45/F	Painful red eye with decreased vision and periorbital edema; diagnosed with iritis and posterior synechiae; additional symptoms: headache, lightheadedness, fevers, nausea, vomiting, EM-like rash	Prior treatment with steroids with development of sudden rise in ocular pressure with proptosis, conjunctival purulent discharge, and rapid-onset dense cataract. Started on nafcillin and gentamicin for possible orbital cellulitis. Without improvement, had vitrectomy 2 times.
Sauer et al. (*13*)	2009	ELISA: positive. Western blot: positive; aqueous humor: *Borrelia* spp. DNA noted.	39/F	Acute diplopia, pain and redness; diagnosed with abducens nerve palsy and anterior uveitis; additional symptoms: EM and arthralgia	Ceftriaxone 2 g/d for 2 wks and topical steroids with recovery.
Hardon et al. (*14*)	2002	ELISA-positive for IgG. CSF PCR positive for *Borrelia* spp. CSF antibody: negative.	31/M	Reduced eye movements; diagnosed with bilateral internuclear ophthalmoplegia	IV ceftriaxone 2 g/d for 3 wks with resolution.

*As of March 15, 2025. Year listed is the year of publication unless the year of the case is otherwise specified in the cited article. Not all cases were based on current Centers for Disease Control and Prevention case definition. CSF, cerebrospinal fluid; EM, erythema migrans; FTA-ABS, fluorescent treponemal antibody absorption test; IFA, indirect immunofluorescence assay; IV, intravenous; VDRL, Venereal Disease Research Laboratory test.

ness, and an erythema migrans–like rash. Approximately 30 days later, she had iritis with posterior synechiae. For the iritis, she received a subconjunctival injection of triamcinolone (40 mg) but then had onset of hypopyon with vitritis. She was then started on oral prednisone therapy (up to 100 mg/d), but the inflammation worsened, and she had onset of severe panophthalmitis. She then had a sudden rise in intraocular pressure with proptosis and a conjunctival purulent discharge and was started on nafcillin and gentamicin for orbital cellulitis. One week later, she had 1 lensectomy and 2 vitrectomy procedures; the specimen obtained during the second vitrectomy was stained by using the Deiterle method and showed occasional intact spirochetes on microscopic examination. A fluorescent treponemal antibody absorption test and a Venereal Disease Research Laboratory test showed that the specimen was negative for *Treponema pallidum* (the bacteria that causes syphilis).

Another case with microbiologic proof occurred in a 39-year-old woman who had a history of recent tick bite (within 3 months); a history of erythema migrans rash, arthralgia, and acute diplopia; and pain and redness in 1 eye. She was found to have abducens nerve palsy with anterior uveitis. Workup showed *Borrelia* spp. DNA in the aqueous humor specimen. She was treated with topical steroids and ceftriaxone for 2 weeks, during which time the patient recovered.

Another case in this series of cases with microbiologic proof of LD occurred in a 31-year-old man who had bilateral intranuclear ophthalmoplegia. A lumbar puncture was performed, and the result of a PCR test of the cerebrospinal fluid (CSF) was positive for *Borrelia* spp. The patient was treated with intravenous ceftriaxone for 3 weeks, and symptoms resolved. CSF from a repeat lumbar puncture after 3 months tested negative for *Borrelia* spp. by PCR.

Possible or Probable Ocular LD Cases

Although some case reports showed microbiologic proof of LD through testing of CSF or specimens from the eye, many of the cases we found in the literature were diagnosed on the basis of laboratory results or erythema migrans in the setting of a recent tick bite. We assessed all the reported cases of possible or probable ocular LD (Appendix Table). Some of the cases followed the 2-tier or modified 2-tier testing method for LD; however, not all cases followed this method for diagnosis. Of all the case reports we reviewed (Table; Appendix Table), the most common ocular manifestation noted was uveitis (reported in 17 patients). Another common manifestation was cranial nerve palsies, which affect ocular movement (7 patients had abducens nerve palsy, and 2 patients has trochlear nerve palsy). Another 8 patients were found to have optic neuritis, of whom 4 had papillitis. Two patients had retinal vasculitis, and 2 patients had optic disc edema. One patient had scleritis. Additional symptoms noted in only 1 case report each included 1 case of ocular muscle myositis, 1 case of papilledema, 1 case of optic disc edema, 1 case of interstitial keratitis, 1 case of ocular flutter, 1 case of opsoclonus, and 1 case of internuclear ophthalmoplegia. Systemic symptoms such as fatigue, arthralgia, and influenza-like illness were frequently observed, indicating the multisystemic nature of LD.

Discussion

Reports of ocular involvement in LD are relatively rare; such cases are sometimes linked to early infiltration into the eye by *B. burgdorferi* bacteria or *B. burgdorferi* remaining dormant in the eye and then manifesting with symptoms later (*4*). The reported cases we describe do not include a reaction of the eye from a tick bite occurring on or around the eye. Ocular LD demonstrates a broad spectrum of manifestations, most commonly various forms of uveitis (anterior, intermediate, posterior, and panuveitis) but also cranial nerve palsies, optic neuritis, retinal vasculitis, scleritis, and other rare ocular findings, often accompanied by systemic symptoms such as fatigue, arthralgia, and influenza-like illness, which underscore LD's multisystemic nature. Of the 38 cases we reviewed, only 5 had definitive microbiologic confirmation through PCR or culture, whereas the remainder were classified as probable or possible on the basis of clinical features and serologic testing, which varied in consistency, reflecting historical diagnostic challenges.

First reported in the 1980s, shortly after *B. burgdorferi* was identified as the causative agent, ocular LD was initially described in case reports of conjunctivitis, uveitis, optic neuritis, and cranial nerve palsies. Certain cases of uveitis may be confused with conjunctivitis (pink eye) (Figure). Although diagnostic methods advanced in the 1990s and 2000s with improved serologic assays and PCR testing, microbiologic proof for ocular LD cases has remained rare. Our findings are consistent with previous literature, which has also documented the diversity of manifestations, the predominance of uveitis, the rarity of microbiologic confirmation, and variability in adherence to diagnostic guidelines, particularly in older reports. Similar studies include systematic reviews by Lu and Zand in 2022 (*1*), which analyzed LD-associated

Figure. Anterior uveitis in a patient from a series of cases of ocular Lyme disease. Uveitis may be distinguished from the more common conjunctivitis (pink eye) by any number of features that warrant an ophthalmology examination. Uveitis is more likely to have eye pain, light sensitivity, smaller or irregular-shaped pupil, blurry vision, and floaters.

optic neuritis; Klaeger and Herbort in 2010 (*3*), which focused on retinal vascular changes; Johnson et al. in 2018 (*7*), which studied broader LD manifestations, including ocular findings; and multiple case series from the 1980s through 2000s, such as Fatterpekar et al. in 2002 (*4*) describing orbital LD (*1*,*3*,*4*,*7*).

The heterogeneity of ocular manifestations found in patients with microbiologic proof of LD highlights the importance of testing for *B. burgdorferi* in patients with otherwise unexplained ocular manifestations. In addition, very few publications provided direct microbiologic proof of LD. Ideally, to recognize the possible ocular manifestations of LD, the presence of microbiologic proof of *B. burgdorferi* in some part of the body would be necessary.

Limitations of this study include the lack of microbiologic proof in most cases, heterogeneity in diagnostic criteria, small sample size, retrospective design with reliance on published case reports susceptible to reporting bias, incomplete or inconsistent clinical data, and temporal variability, given that many cases were published decades ago before modern diagnostic tools and treatment protocols. Those factors limit generalizability of case report findings to current clinical practice.

This comprehensive but limited analysis of published cases highlights clinical symptoms of possible or probable cases of LD. The successful outcomes in most cases, despite some requiring prolonged or repeated treatment, underscore the necessity of a multidisciplinary approach. Going forward, more comprehensive descriptions of ocular involvement should be published. This retrospective case series highlights the importance of further studies that can provide direct microbiologic proof for diagnosis of LD and guide the treatment of ocular manifestations in LD. Those measures will help us determine if ocular LD is an emerging condition.

In summary, LD can have, albeit rarely, a wide variety of ocular manifestations, most commonly uveitis, cranial nerve palsies, and optic neuritis. When evaluating a patient who lives or travels in an area of high LD prevalence, keeping LD in the differential diagnosis is important. A patient may seek primary care and clinicians in variety of subspecialties such as rheumatology, ophthalmology, infectious diseases, and neurology because of the various clinical manifestations of the illness. Therefore, all physicians need to be aware of the possibility of LD and be knowledgeable of how to test for it (or be ready to refer the patient to a colleague with expertise in LD) and report such cases to public health officials (*6*).

Funding for this work came in part from the Wieden Family Public Foundation.

About the Author

Dr. Bellafiore is a senior rheumatology fellow at Rutgers New Jersey Medical School. Her research interests include autoimmune diseases and infectious mimickers of autoimmune diseases.

References

1. Lu Y, Zand R. Characteristics of Lyme optic neuritis: a case report of Lyme associated bilateral optic neuritis and systematic review of the literature. BMC Neurol. 2022;22:113. https://doi.org/10.1186/s12883-022-02627-z
2. Lantos PM, Rumbaugh J, Bockenstedt LK, Falck-Ytter YT, Aguero-Rosenfeld ME, Auwaerter PG, et al. Clinical practice guidelines by the Infectious Diseases Society of America (IDSA), American Academy of Neurology (AAN), and American College of Rheumatology (ACR): 2020 guidelines for the prevention, diagnosis and treatment of Lyme disease. Clin Infect Dis. 2021;72:e1–48. https://doi.org/10.1093/cid/ciaa1215
3. Klaeger AJ, Herbort CP. Cotton wool spots as possible indicators of retinal vascular pathology in ocular lyme borreliosis. Int Ophthalmol. 2010;30:599–602. https://doi.org/10.1007/s10792-008-9268-5
4. Fatterpekar GM, Gottesman RI, Sacher M, Som PM. Orbital Lyme disease: MR imaging before and after treatment: case report. AJNR Am J Neuroradiol. 2002;23:657–9.
5. Schutzer SE, Berger BW, Krueger JG, Eshoo MW, Ecker DJ, Aucott JN. Atypical erythema migrans in patients with PCR-positive Lyme disease. Emerg Infect Dis. 2013;19:815–7. https://doi.org/10.3201/eid1905.120796
6. Schutzer SE, Coyle PK. How do I approach the evaluation and treatment of early Lyme disease? NEJM Evid. 2024;3: EVIDccon2300131.
7. Johnson KO, Nelder MP, Russell C, Li Y, Badiani T, Sander B, et al. Clinical manifestations of reported Lyme disease cases

in Ontario, Canada: 2005–2014. PLoS One. 2018;13:e0198509. https://doi.org/10.1371/journal.pone.0198509
8. Kugeler KJ, Earley A, Mead PS, Hinckley AF. Surveillance for Lyme disease after implementation of a revised case definition—United States, 2022. MMWR Morb Mortal Wkly Rep. 2024;73:118–23. https://doi.org/10.15585/mmwr.mm7306a1
9. Kugeler KJ, Schwartz AM, Delorey MJ, Mead PS, Hinckley AF. Estimating the frequency of Lyme disease diagnoses, United States, 2010–2018. Emerg Infect Dis. 2021;27:616–9. https://doi.org/10.3201/eid2702.202731
10. Dietrich T, Geissdörfer W, Schlötzer-Schrehardt U, Holbach L, Schoerner C, Seitz B. *Borrelia*-associated crystalline keratopathy with intracorneal detection of *Borrelia garinii* by electron microscopy and polymerase chain reaction. Cornea. 2008;27:498–500. https://doi.org/10.1097/ICO.0b013e318162a8f5
11. Hilton E, Smith C, Sood S. Ocular Lyme borreliosis diagnosed by polymerase chain reaction on vitreous fluid. Ann Intern Med. 1996;125:424–5. https://doi.org/10.7326/0003-4819-125-5-199609010-00028
12. Kauffmann DJ, Wormser GP. Ocular Lyme disease: case report and review of the literature. Br J Ophthalmol. 1990;74:325–7. https://doi.org/10.1136/bjo.74.6.325
13. Sauer A, Hansmann Y, Jaulhac B, Bourcier T, Speeg-Schatz C. Five cases of paralytic strabismus as a rare feature of Lyme disease. Clin Infect Dis. 2009;48:756–9. https://doi.org/10.1086/597041
14. Hardon WJ, Bernsen HJ, van Nouhuys-Leenders J, Mulder B. Internuclear ophthalmoplegia as the first sign of neuroborreliosis. J Neurol. 2002;249:1119–20. https://doi.org/10.1007/s00415-002-0747-8

Address for correspondence: Steven E. Schutzer, Rutgers New Jersey Medical School, 185 S Orange Ave, Newark, NJ 07103, USA; email: schutzer@gmail.com

Two Cases of Q Fever in Pregnancy, including Management of the Newborn, Australia

Robyn Silcock, Robert Horvath, Su May Chew, Clare Nourse

Optimal management of the birthing parent with Q fever in pregnancy and of the infant has not been established. *Coxiella burnetii* expresses a tropism for the placenta; resulting infection can potentially lead to spontaneous abortion and fetal demise. Although evidence around preventing transmission and infection in the peripartum and postpartum period is lacking, reports of healthy babies born to mothers with acute or chronic Q fever in pregnancy are increasing. Historically, many clinicians have recommended against breastfeeding in this setting because of a theoretical risk for bacterial transmission through breastmilk. We discuss 2 women in Australia who had Q fever in pregnancy, focusing on the peripartum period and infant management. Breastfeeding was encouraged in both cases. Both infants were born healthy and at term and have demonstrated no serologic or clinical evidence of Q fever infection in the first year of life.

Optimal management of the birthing parent with Q fever in pregnancy and of the newborn infant has not been established. *Coxiella burnetii*, the causative bacteria for Q fever, has a tropism for the placenta in humans and other mammals (*1*); infection can result in spontaneous abortion and fetal demise. However, several studies have reported healthy, unaffected infants born to mothers with a diagnosis of acute or chronic Q fever in pregnancy (*2*–*7*). Published evidence is lacking to guide best practices for managing such infants. Evidence is currently best gleaned from the occasional published case report of Q fever in pregnancy, despite most having no, or minimal, discussion of infant management. Many experts recommend against breastfeeding (*8*,*9*), although the evidence base for that recommendation remains theoretical (*1*).

In this article, we discuss 2 women in Australia in whom Q fever was diagnosed in pregnancy, with particular focus on the peripartum period and management of the infant. Breastfeeding was encouraged for both newborn infants. Written and verbal parental consent for the publication of this case report was obtained. This study was approved by the Children's Health Queensland Hospital and Health Service Human Research Ethics Committee.

Case 1

A 28-year-old primiparous, previously healthy woman was admitted to hospital with fevers and headaches at 10 weeks' gestation. She was prescribed 14 days of empiric doxycycline (safe for use during the first trimester); however, diagnosis of Q fever was not made until seroconversion was noted at 24 weeks' gestation. Retrospective testing of a blood sample from 10 weeks' gestation detected *C. burnetii* DNA through PCR; results of serologic testing were initially nonreactive (Table 1).

The woman lived in an urban suburb of Brisbane, Queensland, Australia, with her sister, brother-in-law, 3 nephews, a dog, and a pet lizard. She had not traveled overseas nor had any contact with cattle or sheep farms. A few months before conception, she had commenced work in a pet food cannery. Although Q fever vaccination had been recommended given occupational risk (livestock exposure through pet food), she had not yet been immunized.

Upon retrospective diagnosis of Q fever, trimethoprim/sulfamethoxazole (cotrimoxazole) was prescribed for the period of 25–32 weeks' gestation, according to local and international recommendations (*10*,*11*). Her routine fetal ultrasound scan at 20 weeks'

Author affiliations: Pathology Queensland, Herston, Queensland, Australia (R. Silcock, R. Horvath); Queensland Children's Hospital, Brisbane, Queensland, Australia (R. Silcock, C. Nourse); University of Queensland, Brisbane (R. Silcock, C. Nourse); Q Fever Interest Group, Brisbane (R. Silcock, R. Horvath, S.M. Chew, C. Nourse); Prince Charles Hospital, Brisbane (R. Horvath); Toowoomba Hospital, Toowoomba, Queensland, Australia (S.M. Chew)

DOI: https://doi.org/10.3201/eid3201.251048

gestation found no morphologic abnormalities. A third trimester scan reported mild femur length shortening but was otherwise unremarkable. Third trimester blood tests confirmed the mother's seroconversion to Q fever (Table 1).

The woman gave birth to a healthy baby boy at 39 weeks, 6 days of gestation by spontaneous vaginal delivery. Birth weight was 2,560 g (3rd percentile). The infant required a 24-hour admission to the special care nursery for hypoglycemia. Of note, at the time of delivery, results of PCR testing of the mother's blood for *C. burnetii* were positive, and serologic titers in the postpartum period increased.

Placental histopathology revealed acute chorionitis and chorionic vasculitis, noting some unusual features and multinucleate giant cells in the inflammatory infiltrate and focal but prominent necrosis of subchorionic inflammatory infiltrate. Focal changes of chronic villitis were also seen. There was no necrotizing villitis nor placental abscess formation, which differed from previous cases of Q fever placentitis seen in Queensland (L. Taege, pers. comm., pathology report, 2023 Jun 30). *C. burnetii* was detected by PCR from the placenta but was not detected from either cord blood or breastmilk.

Breastfeeding was encouraged in the setting of regular clinical review and serologic and PCR testing of mother, infant, and breastmilk (Table 1). The infant was exclusively breastfed until 6 months of age and continued breastfeeding into the second year of life after introduction of solids. The baby has remained well, with growth parameters tracking on the 80th percentile, and has shown no clinical signs of Q fever infection. Although the infant showed high IgG titers at 6 weeks postpartum, which might represent infection, the titers waned over time, more in keeping with transplacental transfer of maternal IgG. Furthermore, at birth, phase 2 results of IgM serologic testing were nonreactive and remained nonreactive when tested on 4 occasions in the first 12 months of life.

The mother's echocardiogram 3 months postpartum was normal. Because results of Q fever serologic testing remained strongly positive with a chronic infection profile (Table 1), treatment with doxycycline was recommended. The patient, however, elected not to begin therapy postpartum. Further imaging evaluations, such as fludeoxyglucose-18 positron emission tomography or computer tomography, were not conducted. The mother was advised to contact her infectious diseases physicians before future pregnancies because of the risk for repeat placental infections.

Case 2

A 30-year-old woman, gravida 6, para 4, tested positive for Q fever on serologic tests and PCR of blood taken at 8 weeks' gestation, discovered as part of a public health investigation. Two months earlier, she had aided in the delivery of a calf, where known Q fever exposure had occurred. The woman lived on a dairy farm with her children and partner. Pathologic testing at that time revealed reactive phase 2 and phase 1 IgG and IgM (Table 2). Retrospective review of available serologic tests found similar results from 4 months earlier (Table 2). Of note, Q fever DNA was detected in both blood samples by PCR, although a dedicated blood tube was not obtained in either case. Q fever serology from 10 years earlier was negative. It was thus deemed that the patient, at the time of diagnosis, had chronic/persistent focalized Q fever infection in pregnancy, although the exact timing of infection was unclear. The patient was started on doxycycline during the first trimester until 13 weeks, then took cotrimoxazole with folic acid supplementation from 14 to 34 weeks' gestation. Serologic tests for Q fever remained positive throughout her pregnancy, but PCR of blood did not detect Q fever on 3 other occasions.

The pregnancy was otherwise uncomplicated, and no morphologic abnormalities were identified by ultrasound. A healthy baby boy was born by induced vaginal delivery at 37 weeks' gestation with a birth weight of 2,510 g (2nd percentile). Q fever was not detected from the placenta or breastmilk by PCR. Placental histology showed no signs of acute or chronic infection. Breastfeeding was encouraged.

Table 1. Serologic and PCR monitoring for case 1 during pregnancy, at delivery, and during the first 12 months postpartum in study of Q fever in pregnancy, including management of the newborn, Australia*

Time	Maternal phase 2 IgM	Maternal phase 2 IgG (IFA)	Maternal phase 1 IgG (IFA)	Infant phase 2 IgM (EIA)	Infant phase 2 IgG (IFA)	Infant phase 1 IgG (IFA)	Infant blood PCR	Maternal blood PCR	Breastmilk PCR
10 weeks' gestation	Neg	<10	–	–	–	–	–	Detected	–
29 weeks' gestation	320	5,120	2,560	–	–	–	–	ND	–
At delivery	160	2,560	1,280	Neg	NA	NA	ND	Detected	ND
6 weeks postpartum	320	10,240	10,240	Neg	≥1,280	640	ND	ND	ND
4 months postpartum	80	10,240	10,240	Neg	≥1,280	320	ND	ND	ND
7 months postpartum	80	20,480	5,120	Neg	160	40	ND	ND	ND
12 months postpartum	80	20,480	5,120	Neg	80	<10	ND	ND	ND

*EIA, enzyme immunoassay; IFA, immunofluorescence assay; NA, not available (not tested); ND, not detected; neg, negative; –, not applicable.

Table 2. Serologic and PCR monitoring for case 2 during pregnancy, at delivery, and during the first 9 months postpartum in study of Q fever in pregnancy, including management of the newborn, Australia*

Time	Maternal phase 2 IgM	Maternal phase 2 IgG (IFA)	Maternal phase 1 IgG (IFA)	Infant phase 2 IgM (EIA)	Infant phase 2 IgG	Infant phase 1 IgG	Infant blood PCR	Maternal blood PCR	Breastmilk PCR
3 months preconception	320	320	40	–	–	–	–	Detected	–
8 weeks' gestation	80	160	160	–	–	–	–	Detected	–
14 weeks' gestation	160	320	640	–	–	–	–	ND	–
20 weeks' gestation	160	≥1,280	≥1,280	–	–	–	–	ND	–
32 weeks' gestation	80	320	640	–	–	–	–	ND	–
At delivery	80	80	320	Neg	320 (IFA)	80 (IFA)	ND	ND	ND
6 weeks postpartum	40	80	160	NA	NA	NA	NA	ND	ND
4 months postpartum	80	80	80	Neg	EIA neg	EIA neg	ND	ND	ND
6 months postpartum	80	80	160	Neg	EIA neg	EIA neg	ND	ND	ND
9 months postpartum	80	80	320	NA	NA	NA	NA	NA	NA

*EIA, enzyme immunoassay; IFA, immunofluorescence assay; NA, not available (not tested); ND, not detected; neg; negative; –, not applicable.

In the 9 months postpartum that were documented, the mother's phase IgG has remained elevated, 1:320 at most recent testing (Table 2). The baby has remained well; growth parameters have tracked on the 10th to 25th percentile, and no serologic evidence of Q fever acquisition has been noted (IgM nonreactive, IgG nonreactive by 6 months of age [Table 2]). *C. burnetii* PCR of breastmilk was negative on 4 occasions from birth until 6 months postpartum. The mother chose to cease breastfeeding at 8 months postpartum.

Literature Review

C. burnetii is found in all areas of the world except New Zealand and Antarctica (*12*). At least half of Q fever infections are asymptomatic (*13*). Rarely, a persistent focalized infection (also known as chronic Q fever) develops (*12*,*13*). Persistent or chronic infection is more common during pregnancy because of the bacteria's ongoing replication within the placenta (*14*). Population-based seroprevalence studies have shown mixed results when evaluating the effects of Q fever infection on obstetric outcome (*15*).

The management of Q fever perinatally is beset by lack of evidence and difference of opinion. No consensus guidelines exist for the management of Q fever in pregnant women or newborns, although some national guidelines comment specifically on the treatment of Q fever in pregnancy (*10*,*14*). Several case series and case reports of Q fever in pregnancy have been published. The largest case series of 53 patients from France over a 15-year period found obstetric complications in 37 (69.8%) women, most commonly intrauterine growth retardation, intrauterine fetal death, and premature delivery (*16*). Another large series from France involving 29 women reported obstetric complications in 66% of women (*9*). Both series reported improved obstetric outcomes in those women prescribed antimicrobial therapy (cotrimoxazole or roxithromycin) for at least 5 to 10 weeks before delivery. However, a marked selection bias is present in those studies because Q fever is often only diagnosed at the time of fetal demise or other obstetric complication, especially in persons who did not receive antimicrobial therapy (*9*,*16*).

Case series from the Netherlands and Germany during Q fever outbreaks present a more optimistic picture. Munster et al. (*17*) compared 183 seropositive women to 1,046 seronegative women during a large outbreak in the Netherlands and found no difference in preterm delivery, birth weight, size for gestational age, or perinatal mortality between the groups. A smaller series from Germany involved 11 women during 2 distinct outbreaks. Infected women were offered a variety of treatment (cotrimoxazole, macrolide, sulfadiazine, and pyrimethamine or a combination thereof), and 2 women received no treatment (*2*). Of those 11 pregnancies, 1 maternal death occurred (reported as unrelated), 1 child was born with syndactyly (whose mother had received clarithromycin), and 1 late preterm delivery at 35 weeks occurred. The other 8 infants were born at term and healthy (*2*).

Antimicrobial treatment in women with Q fever infection in pregnancy is complicated by concerns about potential maternal and neonatal toxicity. For both reported women, treatment was initiated upon diagnosis. Because of concern about congenital anomalies and miscarriage, trimethoprim/sulfamethoxazole was avoided in the first trimester, and in both cases doxycycline was prescribed. Doxycycline is considered safe in pregnancy until 18 weeks' gestation. Beyond that time, doxycycline is not recommended because of concerns around bone growth inhibition and discoloration of deciduous teeth of the newborn, complications that were observed with the use of earlier tetracyclines. However, despite concerns, evidence is lacking that doxycycline causes tooth discoloration or bone growth inhibition, and doxycycline

is increasingly used in children (*18*,*19*). With regard to cotrimoxazole in pregnancy, concerns persist that it could be linked to hemolytic anemia and jaundice in the newborn after maternal treatment close to delivery, but evidence does not support that link (*20*). Although current US Centers for Disease Control and Prevention guidelines recommend that physicians consider ceasing cotrimoxazole at 32 weeks' gestation, many physicians, including ourselves, recommend continuing to 36 weeks (*15*) or until delivery (*14*). Of note, the cessation of cotrimoxazole at 32 weeks in case 1 might have contributed to blood PCR positivity at the time of birth and subsequent higher maternal serologic titers. Although doxycycline has been shown to have superior anti-*Coxiella* activity than cotrimoxazole (*21*), until further safety data are available on doxycycline's use during the second and third trimesters, we recommend doxycycline until week 16 followed by cotrimoxazole until delivery.

Several other case reports have been published after Q fever infection in pregnancy (Table 3). In the absence of universal or prospective Q fever testing, published case series and case reports might have a selection bias, because relatively asymptomatic Q fever infection in an uncomplicated pregnancy is unlikely to be assessed for Q fever infection.

Acknowledging the limitations of seroprevalence studies and the selection bias of case reports and series, we have not found any evidence of congenital Q fever syndrome. Although fetal demise can occur and there have been 2 documented cases of Q fever detection in aborted fetuses confirming placental transmission (*32*,*33*), babies born alive after Q fever infection in pregnancy show no signs or sequelae of in utero infection.

Similarly, no definitive case of neonatal or infant Q fever has ever been reported. Four cases of infant Q fever have been described internationally; however, all of those reports have a likely alternative diagnosis or represent transplacental transfer of antibodies (*34*–*37*). Of note, no infant cases of Q fever were reported in the large, well-documented outbreaks in the Netherlands (*38*,*39*).

Despite the lack of reports of confirmed Q fever in neonates or infants, concerns around Q fever transmission through breastmilk are often cited (*6*,*8*). *C. burnetii* DNA has been detected by PCR in dairy milk, although transmission through ingestion of unpasteurized dairy products has not been conclusively demonstrated (*12*,*40*). *C. burnetii* has also been identified in human milk. A 1981 paper from India reported 5 of 97 samples of human milk tested were found to be positive for *C. burnetii* or its antibody (*41*). A further study from India in 1986 reported 22 of 153 human milk samples demonstrated *C. burnetii* antibodies; 4 of the positive samples then demonstrated the presence of the bacteria by specific seroconversion in guinea pigs (*42*). On the basis of those reports, in 1990, Langley concluded, "*C. burnetii* can be excreted in human milk" (*1*). This review went on to describe 1 previously published case of a 9-month-old baby in Scotland who died of sudden infant death syndrome in 1983. In the postmortem examination, high Q fever antibodies were identified, and acquisition of Q fever through breastmilk was speculated but not confirmed (*36*). The theoretical risk for breastmilk transmission of Q fever has subsequently been used to recommend that women who have had Q fever during pregnancy do not breastfeed (*8*).

Infant feeding practices are often not discussed in case reports of perinatal Q fever. Among the numerous published case series and studies of Q fever in pregnancy (Table 3), only 5 commented on infant feeding practices (*4*,*7*,*23*,*27*,*43*); breastfeeding was permitted in just 1 recent case in Australia (*7*). The authors report the baby was healthy and asymptomatic at the time of writing (4 months of age) (*7*). A case series from Limoges, France, references "women who breastfed against recommendations" (*9*), and a series from Germany alludes to cessation of breastfeeding upon detection of C. *burnetii* by PCR in breastmilk (*2*). Neither report specifically commented on follow-up of the breastfed infant(s) (*2*,*9*).

The benefits of breastfeeding to both mother and baby have become more evident in recent decades (*44*–*46*). Breastfeeding in mothers living with other infectious diseases, such as HIV, is becoming more widely accepted and supported in many countries (*47*). Given the paucity of evidence to recommend against breastfeeding in Q fever infection, in both of the cases reported in this study, breastfeeding was encouraged in accordance with the mothers' preferences. No transmission of Q fever occurred; both infants have tested negative by blood PCR on multiple occasions and have shown no signs of seroconversion. Results of PCR testing of breastmilk for *C. burnetii* were negative on every occasion (Tables 1, 2).

Infection control precautions at the time of delivery to prevent potential mother-to-child transmission or nosocomial transmission to staff and other patients are key (*32*,*48*). *C. burnetii* is aerosolized, and the placenta carries high bacterial loads even after antenatal treatment. Airborne precautions in the delivery suite and operating theater are recommended. In both cases described, the use of interventions such as scalp electrodes was permitted as

clinically indicated, the mother and infant were not separated, and the infant was washed after delivery and then managed with standard precautions. *C. burnetii* is highly resistant to inactivation by standard disinfectants. The US Centers for Disease Control and Prevention recommends cleaning with Micro-Chem Plus (a dual-quaternary ammonium/detergent compound) (National Chemical Laboratories, https://www.nclonline.com), a 1:100 dilution of household bleach, or 1% Virkon S treatment (*14*).

After the birth of an infant to a parent with Q fever in pregnancy, we recommend histologic examination and PCR testing of the placenta; clinical, serologic, and PCR monitoring of mother and infant for a period of 6 months to 1 year; and, if feasible, serial PCR testing of breastmilk. Our second case also dem-

Table 3. Published cases of Q fever infection in pregnancy reviewed for study of Q fever in pregnancy, including management of the newborn, Australia*

Mother's age, country (reference)	Gestation	Treatment	Outcome
42 y, the Netherlands (*22*)	Shortly before conception; steep increase in IgG phase I and IgG phase II and PCR serum positive at 25 weeks'	Cotrimoxazole (allergy so changed to erythromycin)	Induction of labor at 38 weeks; healthy baby, birth weight 3,850 g; amniotic fluid and placenta PCR positive; newborn blood PCR negative
29 y, Slovenia (*3*)	Seroconversion found at 9 weeks; febrile illness 10 days before conception	Azithromycin for 6 d at 9 weeks' gestation	Spontaneous vaginal delivery at term; birth weight 3,500 g; amniotic fluid and placenta PCR negative
39 y, Australia (*4*)	Fever at 7 weeks; seroconversion at 9 weeks	Cotrimoxazole from 9 to 36 weeks' gestation	Spontaneous vaginal delivery at term; birth weight 3,600 g; placenta, blood, breastmilk PCR negative
27 y, Germany (*23*)	Acute Q fever at 7 weeks; retrospective diagnosis at 19 weeks	Erythromycin from 25 to 26 weeks' gestation; rifampin + clarithromycin from 26 weeks through delivery	Delivery at 30 weeks; birth weight 3,900 g
28 y, Spain (*5*)	14 weeks	No treatment	Delivery at 36 weeks; healthy baby, birth weight 2,125 g
26 y, United Kingdom (*24*)	14 weeks	No treatment	Intrauterine fetal demise at 25 weeks; *C. burnetii* detected on placental stains
28 y, Israel (*25*)	22 weeks' gestation; fever since 16 weeks; acute Q fever on serology	Erythromycin and rifampin from 22 to 30 weeks' gestation	Premature labor at 30 weeks; birth weight 1,300 g; baby treated for 14 d with rifampin + erythromycin; complete recovery
29 y, Israel (*26*)	21 weeks' gestation; fevers since 17 weeks; chronic Q fever on serology	Erythromycin at 21 weeks' gestation, then tetracycline from 22 weeks gestation until induction at 28 weeks	Induced at 28 weeks; birth weight 1,000 g; placenta necrotic; *C. burnetii* isolated; baby not infected; yellow teeth
34 y, Spain (*27*)	21 weeks' gestation; febrile; acute Q fever on serology	Cotrimoxazole from 21 weeks' gestation until term	Delivery at 40 weeks; healthy baby, birth weight 2,930 g; formula fed
18 y, Spain (*28*)	Fevers at 19 weeks' gestation; seropositive 1 month later	Clarithromycin commenced at 20 weeks' gestation; duration not specified	Delivery at 40 weeks; healthy baby
34 y, Israel (*29*)	Pyrexia of unknown origin at 24 weeks' gestation; 26 weeks abruption	No treatment	Viable baby delivered; birth weight 967 g; PCR Q fever positive
27 y, Israel (*30*)	26 weeks' gestation; 3-week history of fevers	Doxycycline commenced at 26 weeks' gestation, continued until IUFD at 27 weeks	Intrauterine fetal demise at 27 weeks
29 y, Australia (*7*)	29 weeks' gestation	Cotrimoxazole from 29 to 30 weeks' gestation; clarithromycin from 31 weeks until term (rash with cotrimoxazole)	Medical induction at 39 weeks; healthy baby; amniotic fluid, fetal blood, and placenta PCR negative
26 y, United Kingdom (*31*)	28 weeks' gestation (acute Q fever seroconversion between 16 and 29 weeks)	Ciprofloxacin from 29 weeks' gestation until induction at 32 weeks	Induced at 32 weeks; healthy baby
34 y, Israel (*29*)	Fevers at 29 weeks' gestation	No treatment	Placental abruption; delivered at 31 weeks; healthy baby; birth weight 1,514 g; placenta PCR positive
22 y, Australia (*6*)	Fevers at 28 weeks' gestation; acute Q fever on serology	Cotrimoxazole from 29 weeks' gestation until term	Spontaneous vaginal delivery at 40 weeks; *C. burnetti* detected on PCR of placenta, not detected in breastmilk; patient well

*Cotrimoxazole, trimethoprim/sulfamethoxazole.

onstrates the potential for Q fever to develop chronicity or recrudescence after preconception acute infection, likely reflecting *Coxiella burnetii*'s tropism for uterine tissue. This phenomenon has been previously described in 1 woman during the outbreak in the Netherlands (Table 3) (*22*). As such, close observation for Q fever in pregnancy should also be recommended for any cases of acute Q fever in the period 3–6 months before conception. Reactivation of Q fever in subsequent pregnancies has also been described (*33*).

In conclusion, we report 2 women with Q fever in pregnancy, 1 infected in the first trimester and 1 likely infected 3–6 months before conception with persistent focal disease evident through pregnancy. Both women received antimicrobial therapy (doxycycline and cotrimoxazole) until 32–34 weeks' gestation. In both cases, healthy, albeit small, infants were born at term with no evidence of long-term sequelae or in utero infection. Both infants were breastfed for ≥6 months without transmission of Q fever. Although transmission precautions at the time of delivery remain key, our experience, as well as review of the literature, provides reassurance for women who wish to breastfeed after Q fever infection during pregnancy. Given the rarity and paucity of strong scientific evidence, we would advocate that all pregnant persons with Q fever infection be referred to an expert group.

About the Author

Dr. Silcock is a pediatric infectious diseases physician and general pediatrician at the Queensland Children's Hospital. She has a strong clinical and research interest in perinatal infections.

References

1. Langley JM. Perinatal Q fever: is *Coxiella burnetii* a human perinatal pathogen? In: Marrie TJ, editor. Q fever, volume 1: the disease. Boca Raton (FL): CRC Press; 1990. p. 201–12.
2. Boden K, Brueckmann A, Wagner-Wiening C, Hermann B, Henning K, Junghanss T, et al. Maternofetal consequences of *Coxiella burnetii* infection in pregnancy: a case series of two outbreaks. BMC Infect Dis. 2012;12:359.
3. Cerar D, Karner P, Avsic-Zupanc T, Strle F. Azithromycin for acute Q fever in pregnancy. Wien Klin Wochenschr. 2009;121:469–72.
4. Marks S, Olenski M. Q fever in the first trimester: a case report from northern rural New South Wales. Trop Med Infect Dis. 2019;4:90.
5. Téllez A, Sanz Moreno J, Valkova D, Domingo C, Anda P, de Ory F, et al. Q fever in pregnancy: case report after a 2-year follow-up. J Infect. 1998;37:79–81.
6. Denman J, Woods M. Acute Q fever in pregnancy: report and literature review. Intern Med J. 2009;39:479–81.
7. Braddick M, Woods ML, Prabhaharan S. Acute Q fever in third trimester pregnancy. BMJ Case Rep. 2021;14:e242558.
8. Raoult D, Fenollar F, Stein A. Q fever during pregnancy: diagnosis, treatment, and follow-up. Arch Intern Med. 2002;162:701–4.
9. Coste Mazeau P, Hantz S, Eyraud JL, Donadel L, Lacorre A, Rogez S, et al. Q fever and pregnancy: experience from the Limoges Regional University Hospital. Arch Gynecol Obstet. 2016;294:233–8.
10. Antibiotic Expert Groups. Therapeutic guidelines: antibiotic. Version 16. Melbourne: Therapeutic Guidelines Limited; 2019.
11. Centers for Disease Control and Prevention. Clinical guidance for Q fever [cited 2025 Sep 17]. https://www.cdc.gov/q-fever/hcp/clinical-guidance/index.html
12. Maurin M, Raoult D. Q fever. Clin Microbiol Rev. 1999;12:518–53.
13. Parker NR, Barralet JH, Bell AM. Q fever. Lancet. 2006;367:679–88.
14. Anderson A, Bijlmer H, Fournier P-E, Graves S, Hartzell J, Kersh GJ, et al. Diagnosis and management of Q fever—United States, 2013: recommendations from CDC and the Q Fever Working Group. MMWR Recomm Rep. 2013;62:1–30.
15. Ghanem-Zoubi N, Paul M. Q fever during pregnancy: a narrative review. Clin Microbiol Infect. 2020;26:864–70.
16. Carcopino X, Raoult D, Bretelle F, Boubli L, Stein A. Managing Q fever during pregnancy: the benefits of long-term cotrimoxazole therapy. Clin Infect Dis. 2007;45:548–55.
17. Munster JM, Leenders AC, Hamilton CJ, Meekelenkamp JC, Schneeberger PM, van der Hoek W, et al. Routine screening for *Coxiella burnetii* infection during pregnancy: a clustered randomised controlled trial during an outbreak, the Netherlands, 2010. Euro Surveill. 2013;18:20504.
18. Boast A, Curtis N, Gwee A. QUESTION 1: teething issues: can doxycycline be safely used in young children? Arch Dis Child. 2016;101:772–4.
19. Pöyhönen H, Nurmi M, Peltola V, Alaluusua S, Ruuskanen O, Lähdesmäki T. Dental staining after doxycycline use in children. J Antimicrob Chemother. 2017;72:2887–90.
20. Yu PA, Tran EL, Parker CM, Kim HJ, Yee EL, Smith PW, et al. Safety of antimicrobials during pregnancy: a systematic review of antimicrobials considered for treatment and postexposure prophylaxis of plague. Clin Infect Dis. 2020;70(Suppl 1):S37–50.
21. Clay, K.A., et al., Evaluation of the efficacy of doxycycline, ciprofloxacin, levofloxacin, and co-trimoxazole using in vitro and in vivo models of Q fever. Antimicrob Agents Chemother. 2021;65:e0067321.
22. Munster JM. Q fever during pregnancy: lessons from the Dutch epidemic [dissertation]. Groningen: University of Groningen; 2012.
23. Hellmeyer L, Schmitz-Ziegler G, Slenczka W, Schmidt S. Q fever in pregnancy: a case report and review of the literature [in German]. Z Geburtshilfe Neonatol. 2002;206:193–8.
24. Friedland JS, Jeffrey I, Griffin GE, Booker M, Courtenay-Evans R. Q fever and intrauterine death. Lancet. 1994;343:288.
25. Bental T, Fejgin M, Keysary A, Rzotkiewicz S, Oron C, Nachum R, et al. Chronic Q fever of pregnancy presenting as *Coxiella burnetii* placentitis: successful outcome following therapy with erythromycin and rifampin. Clin Infect Dis. 1995;21:1318–21.
26. Riechman N, Raz R, Keysary A, Goldwasser R, Flatau E. Chronic Q fever and severe thrombocytopenia in a pregnant woman. Am J Med. 1988;85:253–4.
27. García Lavandeira S, Blanco Pérez S, Varillas del Río C. Q fever and pregnancy [in Spanish]. Clin Invest Ginecol Obstet. 2013;40:127–30.

28. Jover-Díaz F, Robert-Gates J, Andreu-Gimenez L, Merino-Sanchez J. Q fever during pregnancy: an emerging cause of prematurity and abortion. Infect Dis Obstet Gynecol. 2001;9:47–9.
29. Shinar S, Skornick-Rapaport A, Rimon E. Placental abruption remote from term associated with Q fever infection. Obstet Gynecol. 2012;120:503–5.
30. Levin G, Herzberg S, Attari R, Abu Khatab A, Gil M, Rottenstreich A. Q fever first presenting as a septic shock resulting in intrauterine fetal death. Eur J Obstet Gynecol Reprod Biol. 2018;229:204–5.
31. Ludlam H, Wreghitt TG, Thornton S, Thomson BJ, Bishop NJ, Coomber S, et al. Q fever in pregnancy. J Infect. 1997;34:75–8.
32. Racult D, Stein A. Q fever during pregnancy—a risk for women, fetuses, and obstetricians. N Engl J Med. 1994;330:371.
33. Stein A, Raoult D. Q fever during pregnancy: a public health problem in southern France. Clin Infect Dis. 1998;27:592–6.
34. Gaburro D. Epidemiological and clinical consideration on a *Coxiella burnetii* infection in three premature twin girls [in Italian]. G Mal Infett Parassit. 1956;8:384–9.
35. Derrick EH. The course of infection with *Coxiella burnetii*. Med J Aust. 1973;1:1051–7.
36. Ellis ME, Smith CC, Moffat MA. Chronic or fatal Q-fever infection: a review of 16 patients seen in North-East Scotland (1967–80). Q J Med. 1983;52:54–66.
37. Richardus JH, Dumas AM, Huisman J, Schaap GJ. Q fever in infancy: a review of 18 cases. Pediatr Infect Dis. 1985;4:369–73.
38. van der Hoek W, Meekelenkamp JC, Leenders AC, Wijers N, Notermans DW, Hukkelhoven CW. Antibodies against *Coxiella burnetii* and pregnancy outcome during the 2007–2008 Q fever outbreaks in the Netherlands. BMC Infect Dis. 2011;11:44.
39. de Lange MM, Hukkelhoven CW, Munster JM, Schneeberger PM, van der Hoek W. Nationwide registry-based ecological analysis of Q fever incidence and pregnancy outcome during an outbreak in the Netherlands. BMJ Open. 2015;5:e006821.
40. Signs KA, Stobierski MG, Gandhi TN. Q fever cluster among raw milk drinkers in Michigan, 2011. Clin Infect Dis. 2012;55:1387–9.
41. Kumar A, Yadav MP, Kakkar S. Human milk as a source of Q-fever infection in breast-fed babies. Indian J Med Res. 1981;73:510–2.
42. Prasad BN, Chandiramani NK, Wagle A. Isolation of *Coxiella burnetii* from human sources. Int J Zoonoses. 1986;13:112–7.
43. Munster JM, Hamilton CJ, Leenders AC, Lestrade PJ. Chronic Q fever during pregnancy [in Dutch]. Ned Tijdschr Geneeskd. 2011;155:A2781.
44. Horta BL, Rollins N, Dias MS, Garcez V, Pérez-Escamilla R. Systematic review and meta-analysis of breastfeeding and later overweight or obesity expands on previous study for World Health Organization. Acta Paediatr. 2023;112:34–41.
45. Pérez-Escamilla R, Tomori C, Hernández-Cordero S, Baker P, Barros AJD, Bégin F, et al.; 2023 Lancet Breastfeeding Series Group. Breastfeeding: crucially important, but increasingly challenged in a market-driven world. Lancet. 2023;401:472–85.
46. Victora CG, Horta BL, Loret de Mola C, Quevedo L, Pinheiro RT, Gigante DP, et al. Association between breastfeeding and intelligence, educational attainment, and income at 30 years of age: a prospective birth cohort study from Brazil. Lancet Glob Health. 2015;3:e199–205.
47. Waitt C, Low N, Van de Perre P, Lyons F, Loutfy M, Aebi-Popp K. Does U=U for breastfeeding mothers and infants? Breastfeeding by mothers on effective treatment for HIV infection in high-income settings. Lancet HIV. 2018;5:e531–6.
48. Amit S, Shinar S, Halutz O, Atiya-Nasagi Y, Giladi M. Suspected person-to-person transmission of Q fever among hospitalized pregnant women. Clin Infect Dis. 2014;58:e146–7.

Address for correspondence: Robyn Silcock, Department of Infectious Diseases, Level 12, Queensland Children's Hospital, 501 Raymond Terrace, South Brisbane, QLD 4101, Australia; email: robyn.silcock@gmail.com

Case Series of Bacteremia Associated with Probiotic Use in Children after Cardiac Surgery, China

Xiaofeng Wang,[1] Shuo Li,[1] Da Huo,[1] Chenyu Li,[1] Qian Zhang, Xu Wang

We examined probiotic-associated bacteremia in a cohort of postoperative pediatric cardiac surgery patients in China. Among 16,436 children who underwent cardiac surgery during 2019–2024, a total of 5,034 received probiotics; 6 developed bacteremia with probiotic strains (*Bacillus subtilis*, *Bacillus licheniformis*, *Lacticaseibacillus rhamnosus*). Three cases occurred in children who had not directly received probiotics, suggesting potential cross-contamination or catheter-related transmission. All 6 patients had complex congenital heart disease and central venous catheters; 5 underwent palliative surgery. Fever, elevated C-reactive protein and leukocytes, and use of respiratory support were common. Antibiotic therapy achieved blood-culture clearance in all; 1 death occurred because of underlying cardiac disease, not infection. Our findings conclude probiotic-associated bacteremia is rare and usually resolves with antibiotics; outcomes correlate more with cardiac complexity than bacteremia itself. Maintaining perioperative probiotic use and enhancing infection-control measures, specifically regarding central line care, are recommended to minimize the risk for probiotic-associated bacteremia in pediatric cardiosurgical patients.

Probiotics are preparations containing live microorganisms that confer health benefits on the host when administered in adequate amounts (*1*). They are widely used in humans for preventing and treating various conditions, such as gastrointestinal, neonatal, allergic, and recurrent respiratory infectious diseases (*2*–*5*). However, the increasing application of probiotics has brought associated infections into focus (*6*). Some case reports indicate that the use of probiotics can lead to safety issues such as systemic infections. For instance, patients with impaired immune function can develop *Lactobacillus*-related bacteremia and endocarditis (*7*). In 2021, a systematic review analyzed 1,537 studies over a period of nearly 25 years and found 49 cases of invasive infections associated with the use of probiotics in children. Most of those infections were in children who were <2 years of age and had underlying conditions that encouraged invasive infections to develop, such as prematurity and the use of central venous catheter (CVC) (*8*).

In recent years, given progress in research on the gut microbiota of patients with congenital heart disease, the application of probiotics in patients after heart surgery has also attracted widespread attention. In a 2024 randomized controlled trial involving 112 adult congenital heart disease patients, of whom 57 were given the probiotic *Lactobacillus plantarum 24-7* and 55 were given a placebo, results showed probiotic supplementation could improve symptoms such as bloating and hard stools, and no adverse events related to probiotics were recorded (*9*). In neonatal congenital heart disease patients, a randomized controlled trial involving 100 patients, in which 50 were given the probiotic *Bifidobacterium lactis* plus inulin and 50 a placebo, the incidence of nosocomial sepsis, necrotizing enterocolitis, and death was significantly reduced in the probiotic treatment group (*10*). A randomized controlled trial involving 82 pediatric patients, 41 in the probiotics group and 41 in the placebo group, analyzed the microbiota in

Author affiliations: National Center for Cardiovascular Disease and Fuwai Hospital, Chinese Academy of Medical Sciences, Peking Union Medical College, Beijing, China (X. Wang, C. Li, Q. Zhang, X. Wang); Peking University First Hospital, Beijing (S. Li); Institute for Infectious Disease and Endemic Disease Control, Beijing Center for Disease Prevention and Control, Beijing (D. Huo); Capital Medical University School of Public Health, Beijing (D. Huo)

DOI: https://doi.org/10.3201/eid3201.250298

[1]These authors contributed equally to this article.

feces and blood, organic acid concentrations in feces, plasma intestinal fatty acid binding protein, and immunological responses (*11*). The total number of obligate anaerobes was higher in the intervention group than in the control group after postoperative day 7, and the team concluded that probiotics might alleviate intestinal damage induced by cardiopulmonary bypass in children (*11*).

As use of probiotics increases, however, cases of probiotic-associated bacteremia in children after heart surgery have been reported. For example, a 2019 study (*12*) reported the case of a 15-month-old child with dilated cardiomyopathy and severe mitral regurgitation who underwent mechanical valve replacement surgery. After surgery, the child was given probiotics to prevent antibiotic-associated diarrhea and subsequently developed fever and increased C-reactive protein (CRP) and leukocytes; blood cultures were positive for *Bifidobacterium* spp. After discontinuing probiotics and adjusting antibiotics, cultures tested negative and clinical symptoms improved (*12*). Another case was reported involving a neonate with coarctation of aorta and marginal hypoplastic left heart syndrome who underwent aortic repair and pulmonary banding operation (*13*). The neonate was given probiotics postoperatively to improve feeding intolerance and prevent necrotizing enterocolitis. The child developed increased CRP and leukocytes and thrombocytopenia; blood cultures tested positive for *Lactobacillus* (now *Lacticaseibacillus*) *rhamnosus*. Although the blood cultures became negative and acute phase reactants normalized after discontinuing probiotics and adjusting antibiotics, the child still had fever, somnolence, and hemodynamic instability and eventually died (*13*).

Such limited case reports are far from sufficient to address concerns regarding the safety of those probiotics in pediatric patients after cardiac surgery. The main obstacle to conducting clinical research is the low incidence of probiotic-associated bacteremia, which results in insufficient sample sizes to carry out high-level clinical studies. This case series study focuses on probiotic-associated bacteremia in postoperative pediatric cardiac surgery patients at a hospital in China.

Methods

This study was conducted retrospectively and included all children who underwent cardiac surgery during 2019–2024 at the National Center for Cardiovascular Disease and Fuwai Hospital in Beijing, China. We retrieved clinical data from medical records, including demographic and surgery-related characteristics, such as age, sex, weight, cardiac malformations, surgical procedures, residual deformities after surgery (palliative surgery, arrhythmia, heart failure, pulmonary hypertension), main postoperative treatments, reasons for probiotic use, reasons for blood culture testing, respiratory and circulatory support, CRP and leukocyte levels at the time of infection, concurrent infections, antibiotic use before infection, probiotic species, possible routes of infection (probiotic use, CVC insertion), comorbidities, antibiotic therapy, and outcomes.

This hospital applies 3 different types of probiotics. The first contains *Bacillus subtilis*, *Enterococcus faecium*, and multivitamins (Beijing Hanmei Pharmaceutical Co., Ltd., https://www.bjhanmi.com.cn); the second contains *Bacillus licheniformis* and lactose (Northeast Pharmaceutical Group Shenyang First Pharmaceutical Co., Ltd., http://www.nepharm.com); and the third contains *L. rhamnosus* and *Bifidobacterium* (Nestle People's Republic of China Co., Ltd., https://www.nestle.com). The probiotic species used in this study are closely related to strains previously reported in the literature (*1*). Although the probiotic preparations used at this hospital contain *Enterococcus faecium* and *Bifidobacterium*, those bacteria are also part of the normal gut flora. Therefore, patients with bacteremia caused by those 2 pathogens are not attributed to probiotic-associated bacteremia.

At the hospital, probiotic administration is considered in specific high-risk scenarios, such as cardiopulmonary bypass time of >120 minutes, cyanotic congenital heart disease, complex congenital heart diseases or those complicated by cardiac insufficiency, antibiotic use lasting >7 days, and the presence of intestinal dysfunction (e.g., abdominal distension and diarrhea). Conversely, probiotics are contraindicated in patients receiving immunosuppressants after organ transplantation and in those with acute intestinal diseases, such as necrotizing enterocolitis or intestinal perforation.

Catheter-related bloodstream infection was defined in accordance with the Clinical Practice Guidelines for the Diagnosis and Management of Intravascular Catheter-Related Infection: 2009 Update by the Infectious Diseases Society of America (*14*). A diagnosis requires either isolation of the same organism from ≥1 percutaneous blood culture and from the catheter tip (>15 CFU/mL on semiquantitative culture of a 5-cm segment) or paired blood cultures (1 from the catheter hub and 1 from a peripheral vein) that satisfy the differential-time-to-positivity criterion (e.g., microbial growth detected in the hub sample ≥2 hours earlier than in the peripheral sample).

This study was approved by the hospital's ethics committee (identification no. 2024-2319). Because of the study's retrospective nature, the requirement for informed consent was waived. The ethical principles of the 1975 Declaration of Helsinki were followed in this study.

Results

Among 16,436 postoperative patients, 5,034 received probiotic treatment. Probiotic-associated bacteremia was documented in 6 patients, 3 of whom had not directly received probiotics. In the 3 treated patients, the causative organisms matched the administered probiotic preparations.

The ages of the 6 patients ranged from 8 months to 13 years (Table 1). Five of them received palliative surgery because of complex heart diseases. All patients had postoperative residual deformities. Three patients had a direct history of probiotic use. CVCs were inserted in all patients when the probiotic infections occurred. Fever with increased leukocyte count and CRP were the main manifestations of probiotic infection. After administration of antibiotic medications and discontinuing probiotics, 5 patients recovered (1 of whom had a cerebral embolism, manifesting in convulsions and hemiplegia), whereas 1 patient died of severe cardiac disease. In the deceased case-patient, the patient's blood culture turned negative after a 6-day course of antibiotic therapy, indicating that the bacteremia was effectively controlled (Table 2). Nevertheless, the patient, who had a single-ventricle cardiac malformation and had undergone a Glenn procedure, subsequently developed a pulmonary embolism, which led to an increase in pulmonary vascular resistance, resulting in circulatory failure and eventual death. Therefore, the patient's death was not directly attributable to the infection.

Discussion

In this study, we investigated probiotic-associated bacteremia in children after cardiac surgery. The incidence we observed is similar to the result of a recent literature report (5 blood culture–positive *Clostridium butyricum* bacteremia cases from a total of 6,576 persons who had blood cultures positive for any bacteria) (*15*). Probiotic-associated bacteremia in pediatrics was mainly reported in premature infants, most likely attributable to severe underlying diseases and compromised immune function (*16*). Patients undergoing cardiac surgery are susceptible to a dysregulated inflammatory response because of surgical stress. That response can lead to systemic complications such as immunosuppression and impaired intestinal epithelial barrier function, thereby increasing the risk for various infections, including probiotic-associated bacteremia (*17*).

Of note, probiotics possess distinct characteristics that differentiate them from common pathogenic microorganisms. The highly acidic environment of human gastric juice is lethal to most common pathogens. Probiotics, however, possess substantial acid tolerance, enabling them to survive such bactericidal activity, reach the intestines intact, and subsequently colonize to exert their beneficial effects (*18*,*19*). If reduced immune function combined with impaired intestinal epithelial barrier function occurs in

Table 1. Demographic characteristics and surgical parameters of 6 patients in study of bacteremia associated with probiotic use in children after cardiac surgery*

	Patient number					
Category	1	2	3	4	5	6
Age/sex	6 y/F	8 mo/M	8 mo/M	1.5 y/M	9 mo/F	13 y/F
Body weight, kg	21.5	5.4	5.1	11	7.2	57
Height, cm	111	63	62	85	70	150
SpO_2, %	80	86	92	91	100	78
Cardiac disease	Single ventricle	Swiss-cheese VSD	PAA/TECD/MAPCAs	mL-TGA; TR	Dilated cardiomyopathy	DORV; complications of previous Glenn procedure; TR
Cardiac procedure	Fontan	PA-banding	RV-PA connection	DSO; tricuspid valvuloplasty	PA-banding	Tricuspid valve replacement
Palliative surgery	Yes	Yes	Yes	No	Yes	Yes
Residual deformities	Pulmonary hypertension	Increased pulmonary blood flow	Pulmonary dysplasia; MAPCAs	Cardiac dysfunction	Cardiac dysfunction	COVID-19; pulmonary embolism
Maximum VIS	29	9	14	26	8	11
Vasopressin use	Yes	No	Yes	Yes	No	Yes
Maximum CVP, mm Hg	19	4	9	13	8	12

*Patient 6 died of severe cardiac disease, not attributable to probiotic use. CVP, central venous pressure; DORV, double outlet right ventricle; DSO, double switch operation; MAPCAs, major aortopulmonary collateral arteries; mL-TGA, congenitally corrected transposition of the great arteries; PAA, pulmonary artery atresia; PA, pulmonary artery; RV, right ventricle; TECD, total endocardial cushion defect; TR, tricuspid regurgitation; VIS, vasoactive inotropic score; VSD, ventricular septal defect.

Table 2. Infection-related data of 6 patients in study of bacteremia associated with probiotic use in children after cardiac surgery*

Category	Patient number					
	1	2	3	4	5	6
Symptoms of onset	Fever	Fever	Fever	Fever	Fever	Fever + shock
Pathogen	*Bacillus licheniformis*	*Bacillis subtilis*	*B. subtilis*	*B. licheniformis*	*B. subtilis*	*Lacticaseibacillus rhamnosus*
Prior antibiotic exposure	Yes	Yes	Yes	Yes	Yes	Yes
Concurrent infection	No	No	*Burkholderia cepacia* (sputum)	*Acinetobacter baumanii* (blood)	No	No
Leukocyte count, × 10^9 cells/L	16.91	27.34	13.31	41.3	5.89	26.69
Neutrophils, %	79.1	84.9	90.1	76.6	80.2	77.2
CRP, mg/L	74.9	55.1	23.8	99.9	155	305
CRBSI	No	No	No	No	Yes	No
Probiotic use	No	Yes	No	Yes	No	Yes
Probiotic duration, d	No	6	No	10	No	6
Abdominal distension/diarrhea	No	Yes	No	Yes	No	Yes
Respiratory support during infection	Mechanical ventilation	High-flow nasal cannula	Mechanical ventilation	Mechanical ventilation	No	Mechanical ventilation
VIS during infection	14	No	6	10	No	4
CVC insertion	Yes	Yes	Yes	Yes	Yes	Yes
Antibiotic	Imipenem/ cilastatin; vancomycin	Linezolid; cefoperazone/ sulbactam	Meropenem	Meropenem vancomycin	Piperacillin/ tazobactam	Meropenem
Antibiotic duration, d	10	12	10	10	7	12
Outcomes	Discharged at 65 dpo	Cerebral embolism, discharged at 136 dpo	Discharged at 71 dpo	Discharged at 153 dpo	Discharged at 42 dpo	Died 12 d after infection

*CRBSI, catheter-related bloodstream infection; CRP, C-reactive protein; CVC, central venous catheter; dpo, days postoperative; VIS, vasoactive inotropic score.

children after cardiac surgery, enterogenous bacteremia can occur.

In this study, 5 of the 6 children underwent palliative surgeries because of complex cardiac diseases. Their cardiopulmonary functions were not corrected after the operations. They still had many problems, such as residual hypoxemia, heart failure, and pulmonary hypertension (patients nos. 1, 3, and 6 received vasopressin treatment). Another child (patient no. 4), although having undergone corrective surgery, had left ventricular dysfunction because of preoperative atrioventricular valve regurgitation. The child also required a long period of extracorporeal membrane oxygenation support after the surgery. This constellation of severe, unresolved cardiopulmonary impairments provided a plausible pathological foundation for probiotic-associated bacteremia. The presence of those high-risk factors collectively pointed to bacterial translocation as a key underlying mechanism. Consequently, their infections are more likely attributable to their critical underlying conditions than to a direct pathogenic effect of the probiotics.

Moreover, those patients often require the insertion of CVCs postoperatively, which further increases the risk for infections (*20*). Patient no. 5 serves as a pertinent example of this scenario, because the infection occurred without documented probiotic use and yet in the absence of other recognized translocation risks. In this patient, after the isolation of *B. subtilis* from a percutaneous blood culture, the same organism was isolated from the catheter tip, with semiquantitative culture yielding >15 CFUs. Those findings confirmed a diagnosis of catheter-related bloodstream infection. Similar routes of transmission have been reported in previous literature, but without discussion on infection control recommendations. This case prompted a detailed investigation into potential transmission routes. After detailed investigation and analysis, we found that, in probiotic preparations, some spore-forming organisms are not sensitive to common disinfectants (such as alcohol); the alcohol-based hand rub is less reliable than soap-and-water hand hygiene and sporicidal environmental cleaning (*21*). Those precautions, however, should not be generalized to non–spore-forming probiotics, because *Clostridioides difficile*–like precautions are intended specifically for cases of suspected spore transmission.

In 2 specific cases, the patients had no history of probiotic intake and no positive CVC cultures, so the route of transmission remained undetermined. We hypothesized that this missing information could be related to the preparation of probiotic medications, which at the time were not handled separately from other oral drugs in the hospital, creating a risk for cross-contamination. This notion was supported by the occasional detection of *B. subtilis* in routine environmental surveillance.

Because this hospital does not routinely perform antimicrobial susceptibility testing on probiotic strains, such data are unavailable to guide therapy. In clinical practice, therapeutic strategy is based on the identified pathogens from blood culture, supplemented by a review of the relevant literature (*22*–*24*). This process allows for the empirical selection of appropriate antibacterial agents to eliminate the bacteremia. Treatment efficacy is subsequently evaluated through clinical indicators, such as body temperature, leukocyte, CRP, and follow-up blood culture results. Although this process constitutes an empirical approach, the resolution of bacteremia (as confirmed by negative blood cultures in all patients) demonstrates its clinical acceptability. Given the rarity of probiotic-associated bacteremia and its successful resolution with antibiotic therapy without direct adverse outcomes, we do not recommend altering the current use of probiotics in post–cardiac surgery patients.

The first limitation of this study is that, because a means of genetic strain testing (e.g., whole-genome sequencing) was not available, we cannot definitively confirm that the bacteremia originated from the administered probiotic preparations. Second, because of the small number of cases, we were unable to adequately control for potential confounders such as disease severity, immunosuppression, central venous catheter use, prolonged intensive care unit stay, or prior antibiotic exposure, which might have influenced the development of probiotic-associated bacteremia. Therefore, the findings can only suggest an association rather than establish causality. Finally, in 2 patients, other pathogens (*Burkholderia cepacia* and *Acinetobacter baumanii*) were concurrently isolated from blood or sputum, making it impossible to determine which bacterium was responsible for clinical deterioration.

In conclusion, this single-center case series found probiotic-associated bacteremia to be a rare occurrence. Among the identified cases, clinical outcomes were more closely linked to patients' underlying complex cardiac conditions than to the bacteremia itself. On the basis of those findings, probiotics appear to be generally safe for use in pediatric patients undergoing cardiac surgery. In addition to the gastrointestinal tract, CVCs might also serve as potential routes of transmission. Therefore, enhanced infection prevention and control measures, specifically regarding central line care, are warranted in pediatric cardiosurgical patients to minimize the risk for probiotic-associated bacteremia.

This study was supported by the National High Level Hospital Clinical Research Funding (grant nos. 2025-GSP-QN-7, 2025-GSP-QN-40 and 2025-GSP-GG-19).

About the Author

Dr. Wang is a pediatric intensive care unit physician at Fuwai Hospital, Beijing, China. He specializes in perioperative infection prevention and control for congenital heart disease.

References

1. Depoorter L, Vandenplas Y. Probiotics in pediatrics. A review and practical guide. Nutrients. 2021;13:2176. https://doi.org/10.3390/nu13072176
2. Lukasik J, Dierikx T, Besseling-van der Vaart I, de Meij T, Szajewska H, van der Schoor SRD, et al.; Multispecies Probiotic in AAD Study Group. Multispecies probiotic for the prevention of antibiotic-associated diarrhea in children: a randomized clinical trial. JAMA Pediatr. 2022;176:860–6. https://doi.org/10.1001/jamapediatrics.2022.1973
3. van den Akker CHP, van Goudoever JB, Shamir R, Domellöf M, Embleton ND, Hojsak I, et al. Probiotics and preterm infants: a position paper by the European Society for Paediatric Gastroenterology Hepatology and Nutrition Committee on Nutrition and the European Society for Paediatric Gastroenterology Hepatology and Nutrition Working Group for Probiotics and Prebiotics. J Pediatr Gastroenterol Nutr. 2020;70:664–80. https://doi.org/10.1097/MPG.0000000000002655
4. Carucci L, Nocerino R, Paparo L, De Filippis F, Coppola S, Giglio V, et al. Therapeutic effects elicited by the probiotic *Lacticaseibacillus rhamnosus* GG in children with atopic dermatitis. The results of the ProPAD trial. Pediatr Allergy Immunol. 2022;33:e13836. https://doi.org/10.1111/pai.13836
5. Li KL, Wang BZ, Li ZP, Li YL, Liang JJ. Alterations of intestinal flora and the effects of probiotics in children with recurrent respiratory tract infection. World J Pediatr. 2019;15:255–61. https://doi.org/10.1007/s12519-019-00248-0
6. Doron S, Snydman DR. Risk and safety of probiotics. Clin Infect Dis. 2015;60(Suppl 2):S129–34. https://doi.org/10.1093/cid/civ085
7. Ambesh P, Stroud S, Franzova E, Gotesman J, Sharma K, Wolf L, et al. Recurrent *Lactobacillus* bacteremia in a patient with leukemia. J Investig Med High Impact Case Rep. 2017;5:2324709617744233. https://doi.org/10.1177/2324709617744233
8. D'Agostin M, Squillaci D, Lazzerini M, Barbi E, Wijers L, Da Lozzo P. Invasive infections associated with the use of probiotics in children: a systematic review. Children (Basel). 2021;8:924. https://doi.org/10.3390/children8100924
9. Yang H, Lan W, Luo C, Huang Q, Zhong Z, Yang J, et al. *Lactobacillus plantarum 24-7* improves postoperative bloating and hard stools by modulating intestinal microbiota in patients with congenital heart disease: a randomized controlled trial. Food Funct. 2024;15:2090–102. https://doi.org/10.1039/D3FO05452G
10. Dilli D, Aydin B, Zenciroğlu A, Özyazici E, Beken S, Okumuş N. Treatment outcomes of infants with cyanotic congenital heart disease treated with synbiotics. Pediatrics. 2013;132:e932–8. https://doi.org/10.1542/peds.2013-1262

11. Toritsuka D, Aoki M, Higashida A, Fukahara K, Nishida N, Hirono K, et al. Probiotics may alleviate intestinal damage induced by cardiopulmonary bypass in children. Eur J Cardiothorac Surg. 2024;65:ezae152. https://doi.org/10.1093/ejcts/ezae152
12. Pruccoli G, Silvestro E, Pace Napoleone C, Aidala E, Garazzino S, Scolfaro C. Are probiotics safe? Bifidobacterium bacteremia in a child with severe heart failure. Infez Med. 2019;27:175–8.
13. Aydoğan S, Dilli D, Özyazici A, Aydin N, Şimşek H, Orun UA, et al. *Lactobacillus rhamnosus* sepsis associated with probiotic therapy in a term infant with congenital heart disease. Fetal Pediatr Pathol. 2022;41:823–7. https://doi.org/10.1080/15513815.2021.1966144
14. Mermel LA, Allon M, Bouza E, Craven DE, Flynn P, O'Grady NP, et al. Clinical practice guidelines for the diagnosis and management of intravascular catheter-related infection: 2009 Update by the Infectious Diseases Society of America. Clin Infect Dis. 2009;49:1–45. https://doi.org/10.1086/599376
15. Sada RM, Matsuo H, Motooka D, Kutsuna S, Hamaguchi S, Yamamoto G, et al. *Clostridium butyricum* bacteremia associated with probiotic use, Japan. Emerg Infect Dis. 2024;30:665–71. https://doi.org/10.3201/eid3004.231633
16. Zbinden A, Zbinden R, Berger C, Arlettaz R. Case series of *Bifidobacterium longum* bacteremia in three preterm infants on probiotic therapy. Neonatology. 2015;107:56–9. https://doi.org/10.1159/000367985
17. Owens J, Qiu H, Knoblich C, Gerjevic L, Izard J, Xu L, et al. Feeding intolerance after pediatric cardiac surgery is associated with dysbiosis, barrier dysfunction, and reduced short-chain fatty acids. Am J Physiol Gastrointest Liver Physiol. 2024;327:G685–96. https://doi.org/10.1152/ajpgi.00151.2024
18. Valle-Vargas MF, Rojas-Muñoz YV, Ruiz-Pardo RY, Villamil-Díaz L, Quintanilla-Carvajal MX. Improving the survival under gastric conditions of a potential multistrain probiotic produced in co-culture. AMB Express. 2025;15:20. https://doi.org/10.1186/s13568-024-01810-4
19. El-Hosseny MF, Seadawy MG, Abdel-Monem MO, Hassan MG. Complete genome sequencing and probiotic characterization of promising lactic acid bacterial strains isolated from dairy products in Egyptian markets. BMC Microbiol. 2025;25:67. https://doi.org/10.1186/s12866-025-03757-3
20. Yu X, Chen M, Liu X, Chen Y, Hao Z, Zhang H, et al. Risk factors of nosocomial infection after cardiac surgery in children with congenital heart disease. BMC Infect Dis. 2020;20:64. https://doi.org/10.1186/s12879-020-4769-6
21. Oh E, Shin H, Han S, Do SJ, Shin Y, Pi JH, et al. Enhanced biocidal efficacy of alcohol based disinfectants with salt additives. Sci Rep. 2025;15:3950. https://doi.org/10.1038/s41598-025-87811-0
22. Idelevich EA, Pogoda CA, Ballhausen B, Wüllenweber J, Eckardt L, Baumgartner H, et al. Pacemaker lead infection and related bacteraemia caused by normal and small colony variant phenotypes of Bacillus licheniformis. J Med Microbiol. 2013;62:940–4. https://doi.org/10.1099/jmm.0.051987-0
23. Hashimoto T, Yahiro T, Khan S, Kimitsuki K, Hiramatsu K, Nishizono A. *Bacillus subtilis* bacteremia from gastrointestinal perforation after natto ingestion, Japan. Emerg Infect Dis. 2023;29:2171–2. https://doi.org/10.3201/eid2910.230084
24. Salminen MK, Rautelin H, Tynkkynen S, Poussa T, Saxelin M, Valtonen V, et al. Lactobacillus bacteremia, species identification, and antimicrobial susceptibility of 85 blood isolates. Clin Infect Dis. 2006;42:e35–44. https://doi.org/10.1086/500214

Address for correspondence: Xu Wang, National Center for Cardiovascular Disease and Fuwai Hospital, No. 167 N Lishi Rd, Xicheng District, Beijing, 100037, China; email: fwpicu@163.com

Group A *Streptococcus* Meningitis, United States, 1997–2022

Paulina A. Hawkins, Sopio Chochua, Namrata Prasad, Jennifer O. Okaro, Yuan Li, Tasha Martin, Ann Thomas, Bridget J. Anderson, Kari E. Burzlaff, Lee Harrison, Shannon Seopaul, Nisha Alden, Rachel Herlihy, William Schaffner, H. Keipp Talbot, Ruth Lynfield, Kathy Como-Sabetti, Maria Rosales, Shua Chai, Sam Sefton, Jessica R. Howard-Anderson, Sarah Khanlian, Jessica Houston, Susan Petit, Adam L. Cohen, Christopher J. Gregory

Medscape CME Activity

In support of improving patient care, this activity has been planned and implemented by Medscape, LLC and Emerging Infectious Diseases. Medscape, LLC is jointly accredited with commendation by the Accreditation Council for Continuing Medical Education (ACCME), the Accreditation Council for Pharmacy Education (ACPE), and the American Nurses Credentialing Center (ANCC), to provide continuing education for the healthcare team.

Medscape, LLC designates this Journal-based CME activity for a maximum of 1.00 ***AMA PRA Category 1 Credit(s)™***. Physicians should claim only the credit commensurate with the extent of their participation in the activity.

Successful completion of this CME activity, which includes participation in the evaluation component, enables the participant to earn up to 1.0 MOC points in the American Board of Internal Medicine's (ABIM) Maintenance of Certification (MOC) program. Participants will earn MOC points equivalent to the amount of CME credits claimed for the activity. It is the CME activity provider's responsibility to submit participant completion information to ACCME for the purpose of granting ABIM MOC credit.

All other clinicians completing this activity will be issued a certificate of participation. To participate in this journal CME activity: (1) review the learning objectives and author disclosures; (2) study the education content; (3) take the post-test with a 75% minimum passing score and complete the evaluation at https://www.medscape.org/qna/processor/76466?showStandAlone=true&src=prt_jcme_eid_mscpedu; and (4) view/print certificate. For CME questions, see page 167.

NOTE: It is the policy of Medscape Education to avoid the mention of brand names or specific manufacturers in accredited educational activities. However, trade and manufacturer names in this activity are provided in an effort to provide clarity. The use of brand or manufacturer names should not be viewed as an endorsement by Medscape of any specific product or manufacturer.

Release date: January 26, 2026; Expiration date: January 26, 2027

Learning Objectives

Upon completion of this activity, participants will be able to:

- Assess demographic variables associated with group A streptococcal (GAS) meningitis
- Analyze rate of comorbid illness among children and adults with GAS meningitis
- Evaluate other GAS syndromes among patients with GAS meningitis
- Distinguish rate of antimicrobial resistance among patients with GAS meningitis

CME Editor

Amy J. Guinn, MA, Technical Writer/Editor, Emerging Infectious Diseases. *Disclosure: Amy J. Guinn, BA, MA, has no relevant financial relationships.*

CME Author

Charles P. Vega, MD, Health Sciences Clinical Professor of Family Medicine, University of California, Irvine School of Medicine, Irvine, California. *Disclosure: Charles P. Vega, MD, has the following relevant financial relationships: consultant or advisor for Boehringer Ingelheim; Exact Sciences.*

Authors

Paulina A. Hawkins, MPH; Sopio Chochua, MD, PhD; Namrata Prasad, PhD; Jennifer O. Okaro, MPH; Yuan Li, PhD; Tasha Martin, MPH; Ann Thomas, MD, MPH; Bridget J. Anderson, PhD; Kari E. Burzlaff, MPH; Lee Harrison, MD; Shannon Seopaul, MPH; Nisha Alden, MPH; Rachel Herlihy, MD, MPH; William Schaffner, MD; H. Keipp Talbot, MD, MPH; Ruth Lynfield, MD; Kathy Como-Sabetti, MPH; Maria Rosales; Shua Chai, MD, MPH; Sam Sefton, MPH; Jessica R. Howard-Anderson, MD, MSc; Sarah Khanlian, MPH; Jessica Houston, MPH; Susan Petit, MPH; Adam L. Cohen, MD, MPH; Christopher J. Gregory, MD, MPH.

Group A *Streptococcus* (GAS) causes a variety of diseases in humans but is not widely appreciated as a cause of meningitis. During 1997–2022, ten sites participating in the Active Bacterial Core Surveillance network in the United States identified GAS meningitis cases. We calculated annual incidence and case-fatality rates (CFRs) for 320 of those cases and determined antimicrobial resistance by whole-genome sequencing. Annual incidence of GAS meningitis ranged from 0.02 to 0.07 cases/100,000 persons. Children <1 year of age had the highest average annual incidence, 0.23 cases/100,000 children. GAS meningitis had a higher CFR (19.4%) than meningitis caused by group B *Streptococcus*, *Streptococcus pneumoniae*, *Neisseria meningitidis*, or *Haemophilus influenzae*. Clindamycin resistance among GAS meningitis isolates increased from 3.2% during 1997–2002 to 17.7% during 2018–2022. Clinicians should be aware that meningitis is an uncommon but severe manifestation of invasive GAS and has a higher CFR than more established meningitis etiologies.

Group A *Streptococcus* (GAS) infections include invasive GAS (iGAS) infections, which are associated with high case-fatality rates (CFRs) (*1*). Clinical manifestations of iGAS disease include cellulitis, bacteremia, pneumonia, necrotizing fasciitis, and streptococcal toxic shock syndrome (STSS) (*1*,*2*). Treatment for iGAS infection includes supportive care and antimicrobial treatment, including combination therapy with penicillin and clindamycin in severe infections (*3*). GAS vaccine candidates in development include a 30-valent M protein–based vaccine (*4*).

Meningitis is an uncommonly reported but severe manifestation of iGAS infection (*1*). Among 91 pediatric intracranial GAS infections in the United States during 1997–2014, meningitis was the most common illness and was associated with the highest CFR (*5*). Meningitis was responsible for 2% of severe GAS disease cases in Europe during 2003–2004 (*6*), and GAS was responsible for 2% of community-acquired bacterial meningitis cases in the Netherlands during 2006–2013 (*7*). Analyses from several countries have identified recent increases in GAS meningitis, potentially associated with changes in strain characteristics (*8*,*9*).

In contrast to other bacterial pathogens such as *Streptococcus pneumoniae* (pneumococcus), group B *Streptococcus* (GBS), *Haemophilus influenzae*, *Neisseria meningitidis* (meningococcus), and *Listeria monocytogenes* (*10*), GAS has not been widely recognized as a cause of meningitis. Thus, GAS infection has not been included in clinical practice guidelines for central nervous system infections (*11*) or recent reviews of bacterial meningitis (*12*). Trends in incidence rates and clinical and microbiological characteristics of GAS meningitis cases in the United States have not been as thoroughly described as other meningitis etiologies (*10*). We used active laboratory- and population-based GAS surveillance to describe incidence, demographic and clinical characteristics, and associated *emm* types and antimicrobial resistance profiles for GAS meningitis in the United States during 1997–2022. We compared those findings to other manifestations of GAS disease and other bacterial meningitis etiologies to more thoroughly describe epidemiology of GAS-related meningitis.

Materials and Methods

Surveillance

The Active Bacterial Core surveillance (ABCs) system (*13*), within the Emerging Infections Program Network of the Centers for Disease Control and Prevention, identifies GAS meningitis cases and other invasive bacterial infections. From 1997 to 2015, areas covered under the ABCs system expanded (Appendix Table, https://wwwnc.cdc.gov/EID/article/32/1/25-0871-App1.pdf). By 2022, ABCs areas included ≈34.9 million residents in 10 states.

ABCs defines iGAS as GAS isolated from a normally sterile site, or from a wound culture if accompanied by a diagnosis of necrotizing fasciitis or STSS, in a resident of a surveillance area (*13*). Consistent with previous ABCs reports, we defined a meningitis case as an ABCs pathogen (*S. pneumoniae*, GAS, GBS, *H. influenzae*, *N. meningitidis*) isolated from

Author affiliations: Centers for Disease Control and Prevention, Atlanta, Georgia, USA (P.A. Hawkins, S. Chochua, N. Prasad, J.O. Okaro, Y. Li, S. Chai, A.L. Cohen, C.J. Gregory); Oregon Health Authority, Portland, Oregon, USA (T. Martin, A. Thomas); New York State Department of Health, Albany, New York, USA (B.J. Anderson, K.E. Burzlaff); Bloomberg School of Public Health, Johns Hopkins University, Baltimore, Maryland, USA (L. Harrison, S. Seopaul); Colorado Department of Public Health and the Environment, Denver, Colorado, USA (N. Alden, R. Herlihy); Vanderbilt University School of Medicine, Nashville, Tennessee, USA (W. Schaffner, H.K. Talbot); Minnesota Department of Health, St. Paul, Minnesota, USA (R. Lynfield, K. Como-Sabetti); California Emerging Infections Program, Oakland, California, USA (M. Rosales, S. Chai); Emory University School of Medicine, Atlanta (S. Sefton, J.R. Howard-Anderson); New Mexico Department of Health, Santa Fe, New Mexico, USA (S. Khanlian, J. Houston); Connecticut Department of Public Health, Hartford, Connecticut, USA (S. Petit)

DOI: https://doi.org/10.3201/eid3201.250871

cerebrospinal fluid in any patient or from another sterile site in a patient with a clinical diagnosis of meningitis in the medical record (*10*). For this study, we included all ABCs cases identified during January 1, 1997–December 31, 2022.

Laboratory Testing

We performed whole-genome sequencing (WGS) on all available isolates from GAS meningitis cases, as previously described (*14*,*15*). We analyzed sequences by using a previously validated bioinformatics pipeline to identify *emm* type and multilocus sequence type (ST), predict antimicrobial resistance, and determine the presence of select virulence factors (*14*,*15*).

Before 2015, we performed antimicrobial susceptibility testing by using broth microdilution, as previously described (*14*). Starting in 2015, we predicted susceptibility by WGS, on the basis of detection of resistance determinants (*14*,*15*), or by using a penicillin-binding protein 2× typing scheme for β-lactams (*14*). Those methods are comparable, as previously reported (*15*).

Statistical Analyses

We calculated annual GAS meningitis incidence, expressed as the number of cases per 100,000 persons, stratified by age (<18 years and ≥18 years), by using US Census annual population estimates for ABCs catchment areas. We also calculated average annual incidence of meningitis caused by each ABCs pathogen, stratified by age group (0–11 months, 1–4 years, 5–17 years, 18–64 years, ≥65 years), during 3 time periods: before the meningococcal conjugate vaccine (MCV4) was introduced (1997–2005); after MCV4 was introduced, and during introduction of pneumococcal conjugate vaccine (PCV) 7, but before introduction the meningococcal B (MenB) vaccine (2006–2015); and after introduction of both meningococcal vaccines and 2 pneumococcal vaccines (PCV7, PCV13) (2016–2022). All time periods occurred after introduction of the *H. influenza* type b (Hib) vaccine. For that comparison, we limited catchment areas to the areas common to all ABCs pathogens. To estimate the national burden of GAS meningitis in the United States, we applied age- and race-specific observed incidence of GAS meningitis from the ABCs data to the total US population.

We calculated CFR on the basis of outcome at discharge. We compared categorical variables by using Fisher exact test or χ^2 test and considered $p<0.05$ statistically significant. We examined linear trends by using linear regression and a *t*-test or by using the Cochran-Armitage test for binomial proportions.

We defined an isolate as covered by the 30-valent vaccine when its *emm* types were included in the vaccine, that is, *emm* types 1, 2, 3, 4, 5, 6, 11, 12, 14, 18, 19, 22, 24, 28, 29, 44, 49, 58, 73, 75, 77, 78, 81, 82, 83, 87, 89, 92, 114, and 118 (*4*). We calculated changes in the percentage of clindamycin-resistant isolates and distribution of *emm* types over 5 time periods of similar length: 1997–2002, 2003–2007, 2008–2012, 2013–2017, and 2018–2022.

Results

Demographic and Clinical Characteristics of GAS Meningitis Case-Patients

During 1997–2022, we identified a total of 38,262 cases of iGAS infection through ABCs, among which 320 (0.84%) met our meningitis definition. Most (69.3%) GAS meningitis cases occurred during December–May annually (Appendix Figure 1).

Of the 320 GAS meningitis cases, 112 (35.0%) occurred in children (persons <18 years of age) (Table 1). During the same timeframe, children accounted for only 8.8% (n = 3,342) of nonmeningitis iGAS cases (n = 37,942). The median age of patients with GAS meningitis was 41 (range 0–92, IQR 8–58) years, significantly lower than the median age of 53 (range 0–107, IQR 36–68) years among nonmeningitis iGAS patients ($p<0.001$). We saw no statistically significant difference in sex, race, or ethnicity between iGAS patients with and without meningitis (Tables 1, 2).

Of 112 pediatric patients with GAS meningitis, only 6.2% had ≥1 underlying condition, compared with 15.3% of pediatric iGAS cases with nonmeningitis syndromes ($p<0.01$) (Table 1). Among adults (persons ≥18 years of age), 70.7% of GAS meningitis patients and 78.8% of nonmeningitis iGAS patients had ≥1 underlying condition (Table 2).

Across all age groups, 40.3% of patients with GAS meningitis had ≥1 additional iGAS clinical syndrome, such as otitis media, pneumonia, abscess, septic shock, cellulitis, or STSS, documented in ABCs. The most common clinical syndromes co-occurring with GAS meningitis were pneumonia (9.8%) among children and otitis media (18.3%) among adults (Tables 1, 2). The CFR in adults increased from 20.7% (43/208) to 51.6% (16/31) when meningitis was complicated by septic shock or STSS ($p<0.01$).

The overall CFR for GAS meningitis was 19.4%; CFR was 20.8% among persons <1 year of age, 24.0% among persons 1–4 years of age, 12.7% among persons 5–17 years of age, 20.9% among persons 18–64 years of age, and 20.0% among persons ≥65 years of age. We saw no statistically significant variation in CFR across

Table 1. Demographic and clinical characteristics of pediatric patients with group A *Streptococcus* meningitis versus other nonmeningitis invasive group A *Streptococcus* infections, United States, 1997–2022*

Characteristics	Meningitis, n = 112	Nonmeningitis, n = 3,342	p value
Age range			
0–11 mo	24 (21.4)	471 (14.1)	**0.04**
1–4 y	25 (22.3)	1,134 (33.9)	**0.01**
5–17 y	63 (56.3)	1,736 (52.0)	0.37
Sex			
M	56 (50)	1,943 (58.1)	0.09
F	56 (50)	1,399 (41.9)	
Race and ethnicity			
White non-Hispanic	43 (38.4)	1,109 (33.2)	0.25
Black non-Hispanic	18 (16.1)	540 (16.2)	>0.99
American Indian/Alaska Native non-Hispanic	2 (1.8)	73 (2.2)	0.85
Asian/Pacific Islander non-Hispanic	5 (4.5)	188 (5.6)	0.64
Other non-Hispanic	0 (0.0)	7 (0.2)	0.24
Hispanic	24 (21.4)	664 (19.9)	0.67
Unknown	20 (17.9)	761 (22.7)	0.22
Underlying conditions			
Chronic medical conditions†	4 (3.6)	381 (11.4)	**0.004**
Immunocompromising conditions‡	1 (0.9)	90 (2.7)	0.25
Obesity	2 (1.8)	103 (3.1)	0.47
None of the above	99 (88.4)	2,673 (80.0)	**0.004**
Unknown	6 (5.4)	157 (4.5)	
Co-occurring syndromes			
Otitis media	6 (5.4)	NA	NA
Pneumonia	11 (9.8)	NA	NA
Abscess	7 (6.8)	NA	NA
Septic shock	9 (8.0)	NA	NA
Cellulitis	9 (8.0)	NA	NA
Streptococcal toxic shock syndrome	4 (3.6)	NA	NA
None of the above	78 (69.6)	NA	NA
Outcomes			
Died (CFR)	19 (17.0)	106 (3.2)	**<0.001**
Vaccine target coverage			
emm type data available	94 (83.9)	2,616 (78.3)	
emm type in 30-valent vaccine§	86 (91.5)	2,440 (93.3)	0.49
Antimicrobial susceptibility			
Susceptibility data available	91 (81.3)	2,079 (62.2)	
Nonsusceptible			
Erythromycin	4 (4.4)	163 (7.9)	0.23
Clindamycin	4 (4.4)	103 (4.9)	0.86
Levofloxacin	1 (1.1)	16 (0.8)	0.68

*Bold font indicates statistical significance. CFR, case-fatality rate; NA, not applicable
†Chronic medical conditions included asthma, chronic obstructive pulmonary disease, diabetes, cirrhosis, alcohol abuse, atherosclerotic cardiovascular disease, congestive heart failure, burns, cerebrospinal fluid leak, and cerebrovascular accident.
‡Immunocompromising conditions included multiple myeloma, sickle cell disease, asplenia, organ transplantation, immunoglobulin deficiency, immunosuppressive therapy, human immunodeficiency virus or the acquired immunodeficiency syndrome (HIV–AIDS), leukemia, Hodgkin's disease, lupus, nephrotic syndrome, and chronic kidney disease.
§30-valent vaccine *emm* types include 1, 2, 3, 4, 5, 6, 11, 12, 14, 18, 19, 22, 24, 28, 29, 44, 49, 58, 73, 75, 77, 78, 81, 82, 83, 87, 89, 92, 114, and 118.

the years of the study in any of the age groups. Overall, 4,104 iGAS case-patients died during the study period, and 62 (1.5%) of those deaths were caused by meningitis. Of the 125 deaths among pediatric iGAS cases, 19 (15.2%) were caused by meningitis.

GAS Meningitis Incidence Trends and National Estimates

Annual GAS meningitis incidence fluctuated little across the study period, from 0.02 to 0.07 cases/100,000 persons, representing 0.3%–1.9% of iGAS infections in ABCs each year (Appendix Figure 2). In contrast, the incidence of all iGAS infections in ABCs remained stable during 1997–2013 (3.1 to 4.2 cases/100,000 persons), before beginning to rise in 2014, reaching 8.2 cases/100,000 persons in 2022.

GAS meningitis incidence was higher in younger age groups, representing 3.2% of all pediatric iGAS cases and with an annual average incidence of 0.06 cases/100,000 children. GAS meningitis represented 0.6% of adult iGAS cases and had an average annual incidence of 0.03 cases/100,000 adults (Figure 1). Children <1 year of age had the highest GAS meningitis incidence, an average annual incidence of 0.23 cases/100,000 children, representing 4.8% of iGAS cases in patients <1 year of age. Adults 18–64 years of age had the lowest GAS meningitis incidence, an average

annual incidence of 0.03 cases/100,000 persons. Extrapolating those incidences to the entire country, we estimated 3,528 cases of meningitis caused by GAS in the United States during the 26-year period of 1997–2022, ranging from 49 to 239 cases annually, including 686 fatal cases.

GAS Meningitis Incidence Compared with Other Bacterial Meningitis Etiologies

During 1997–2022, ABCs received 11,026 reported cases of bacterial meningitis caused by GAS, GBS, *S. pneumoniae*, *N. meningitidis*, or *H. influenzae*. The percentage of meningitis cases caused by GAS increased over time (p<0.001) (Appendix Figure 3).

The average annual incidence of GAS meningitis across all ages (0.04 cases/100,000 persons) was lower than that of meningitis caused by the other pathogens in the 1997–2005 and 2006–2015 periods (Table 3) but similar to the incidence of meningococcal meningitis (0.04 cases/100,000 persons) in 2016–2022. However, the overall CFR of GAS meningitis for each age group was higher (13.1%–26.1%) than that of the other pathogens, except for GBS and *S. pneumoniae* in the ≥65 years of age group (Table 3). When stratified

Table 2. Demographic and clinical characteristics of adult patients with group A *Streptococcus* meningitis versus other nonmeningitis invasive group A *Streptococcus* infections, United States, 1997–2022*

Characteristics	Meningitis, n = 208	Nonmeningitis, n = 34,600	p value
Age range, y			
18–64	153 (73.6)	23,106 (66.7)	
≥65	55 (26.4)	11,494 (33.2)	**0.04**
Sex			
M	93 (44.7)	19,193 (55.5)	**0.002**
F	115 (55.3)	15,407 (44.5)	
Race and ethnicity			
White non-Hispanic	102 (49.0)	15,432 (44.6)	0.20
Black non-Hispanic	24 (11.5)	3,943 (11.4)	0.93
American Indian/Alaska Native non-Hispanic	2 (0.9)	1,142 (0.3)	0.06
Asian/Pacific Islander non-Hispanic	3 (1.4)	702 (2.0)	0.59
Other non-Hispanic	0	12 (0.03)	0.07
Hispanic	18 (8.7)	3,495 (10.1)	0.50
Unknown	59 (28.4)	9,391 (27.2)	0.69
Underlying conditions			
Chronic medical conditions†	102 (49.0)	21,740 (62.8)	**<0.001**
Immunocompromising conditions‡	24 (11.5)	4,887 (14.1)	0.29
Obesity	50 (24.0)	9,565 (27.7)	0.25
Smoking	22 (12.9)	4,432 (16.5)	0.34
Experiencing homelessness	12 (9.8)	2,778 (12.0)	0.23
Living in long-term care facility	4 (3.3)	1,538 (6.7)	0.06
Intravenous drug use	12 (5.8)	4,225 (12.2)	**0.002**
None of the above	61 (29.3)	7,335 (21.2)	0.06
Unknown	5 (2.4)	589 (1.7)	
Co-occurring syndromes			
Otitis media	38 (18.3)	NA	NA
Pneumonia	27 (12.9)	NA	NA
Abscess	15 (8.0)	NA	NA
Septic shock	27 (13.0)	NA	NA
Cellulitis	18 (8.7)	NA	NA
Streptococcal toxic shock syndrome	6 (2.9)	NA	NA
None of the above	113 (52.9)	NA	NA
Outcome			
Died (CFR)	43 (20.7)	3,936 (11.4)	**<0.001**
Vaccine target coverage			
emm type data available	169 (81.3)	28,568 (82.6)	
emm type in 30-valent vaccine§	152 (89.9)	24,235 (84.8)	0.06
Antimicrobial susceptibility			
Susceptibility data available	167 (80.3)	25210 (72.9)	
Nonsusceptible			
Erythromycin	20 (11.9)	5,217 (20.7)	**0.004**
Clindamycin	17 (10.2)	4,571 (18.1)	**0.005**
Levofloxacin	1 (0.6)	267 (1.1)	0.64

*Bold font indicates statistical significance. CFR, case-fatality rate; NA, not applicable
†Chronic medical conditions included asthma, chronic obstructive pulmonary disease, diabetes, cirrhosis, alcohol abuse, atherosclerotic cardiovascular disease, congestive heart failure, burns, cerebrospinal fluid leak, and cerebrovascular accident.
‡Immunocompromising conditions included multiple myeloma, sickle cell disease, asplenia, organ transplantation, immunoglobulin deficiency, immunosuppressive therapy, human immunodeficiency virus or the acquired immunodeficiency syndrome (HIV–AIDS), leukemia, Hodgkin's disease, lupus, nephrotic syndrome, and chronic kidney disease.
§30-valent vaccine *emm* types include 1, 2, 3, 4, 5, 6, 11, 12, 14, 18, 19, 22, 24, 28, 29, 44, 49, 58, 73, 75, 77, 78, 81, 82, 83, 87, 89, 92, 114, and 118.

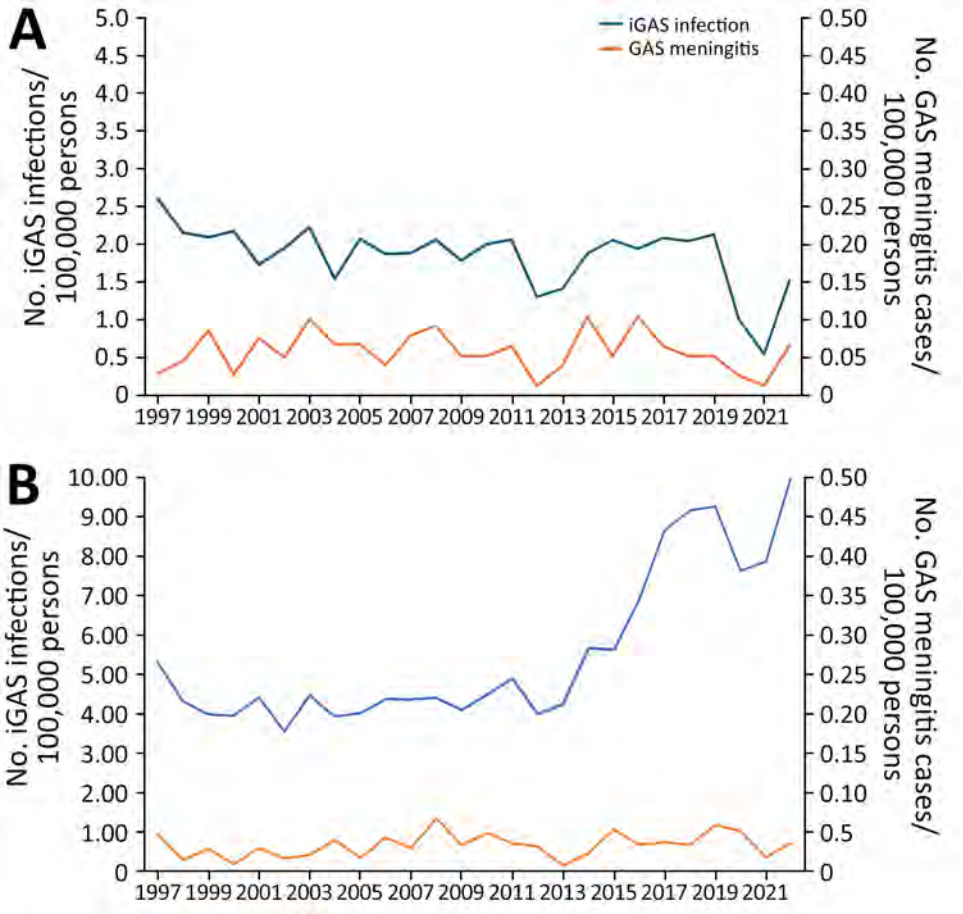

Figure 1. Incidence of iGAS meningitis versus GAS infections, by age, United States, 1997–2022. A) Patients <18 years of age; B) patients ≥18 years of age. Scales for the y-axes differ substantially to underscore patterns but do not permit direct comparisons. GAS, group A *Streptococcus*; iGAS, invasive GAS.

by age group (Appendix Figure 4), the percentage of GAS meningitis among all meningitis cases in ABCs was highest (8.7%) in the 5–17 years of age group and lowest (1.1%) in the 0–11 months of age group.

emm Types and Vaccine Targets

Among GAS meningitis cases, 263 (82.2%) had isolates available for *emm* typing; 153 (58.0%) were cultured from cerebrospinal fluid, 106 (40.1%) from blood, and 5 (1.9%) from other sources. We identified 41 *emm* types among GAS meningitis isolates; the 10 most common *emm* types covered 76.0% of isolates. Overall, nonmeningitis isolates had higher *emm* diversity than meningitis isolates; 136 different *emm* types were identified, and 64.6% of isolates were covered by the 10 most common *emm* types (Appendix Figure 5).

The 2 most common *emm* types among meningitis cases were *emm*1 (31.9%) and *emm*12 (12.2%), accounting for 48.9% of isolates from children and 41.4% from adults. *emm*6 (9.6%) was the third most common type among children and *emm*28 (5.9%) was the third most common among adults. CFR among case-patients with an *emm*1 isolate (26.2%) was significantly higher than CFR among case-patients with other *emm* types (13.3%) ($p<0.05$). Of the 84 *emm*1 GAS meningitis isolates, 2 isolates identified in 2020 belonged to the $M1_{UK}$ lineage. Among nonmeningitis cases, the most common types were *emm*1 (16.5%) and *emm*89 (7.5%).

Among children with GAS meningitis, the percentage of *emm*1 isolates ranged from 21.7% during 2008–2012 to 46.7% during 2018–2022; the percentage of isolates belonging to the 7 most common *emm* types (1, 3, 4, 6, 12, 28, and 89) increased from 37.5% (6/16) during 1997–2002 to 93.5% (14/15) during 2018–2022 (Figure 2). Among meningitis isolates from adult patients, the percentage of isolates belonging to the 7 most common *emm* types ranged from 41.3% (19/46) during 2018–2022 to 90.5% (38/42) during 2008–2012. The *emm* types included in the 30-valent vaccine candidate represented 91.5% of isolates from pediatric meningitis cases and 89.9% of isolates from adult meningitis cases.

Antimicrobial Resistance

Among meningitis cases, 259 (80.9%) had isolates available for antimicrobial drug susceptibility

testing. We determined or predicted 25 (10.0%) isolates were resistant to erythromycin, of which 21 (84.0%) were also resistant to clindamycin, 1 (4.0%) was also resistant to levofloxacin, and 1 (4.0%) was also resistant to chloramphenicol. We did not detect β-lactam, linezolid, or vancomycin resistance among available isolates. Of the 21 clindamycin-resistant isolates, 8 (38.1%) were *emm*92 and 4 (19.1%) were *emm*12 type; all *emm*92 isolates were part of the same ST82 lineage. The percentage of clindamycin-resistant isolates among GAS meningitis cases increased over time (Figure 3), from 3.2% (n = 1) during 1997–2002 to 17.7% (n = 11) during 2018–2022 ($p<0.05$), but remained lower than rates among nonmeningitis cases, from which clindamycin resistance increased from 0.6% (n = 10) during 1997–2002 to 29.0% (n = 3,088) during 2018–2022 ($p<0.05$).

Discussion

We explored trends in GAS meningitis in the United States over 26 years and demonstrated that meningeal infection is an uncommon but severe manifestation of iGAS and that GAS meningitis incidence is similar to that of more widely recognized meningitis etiologies. Although the incidence of bacterial meningitis in the United States has decreased overall since 2008 (*10*), driven largely by decreases in *S. pneumoniae* and *N. meningitidis*, the incidence of GAS meningitis remained stable across the years of the study. However, the percentage of bacterial meningitis caused by GAS in the United States has substantially increased over time. Starting in 2022, multiple countries reported increases in iGAS disease and meningitis (*2*,*8*,*9*), suggesting that GAS could further expand as a meningitis etiology. Although the overall incidence of GAS meningitis remains lower than those for meningitis

Table 3. Incidence and case-fatality rates for GAS meningitis and meningitis caused by other bacterial pathogens, United States, 1997–2022*

Rates per age group	GAS	GBS	*Streptococcus pneumoniae*	*Hemophilus influenzae*	*Neisseria meningitides*
Incidence rate†					
0–11 mo					
1997–2005	0.34	12.30	8.95	1.71	3.04
2006–2015	0.22	12.80	4.57	2.14	1.59
2016–2022	0.15	12.64	2.75	2.71	0.48
All years	0.23	12.61	5.37	2.17	1.71
1–4 y					
1997–2005	0.04	0.03	1.49	0.21	0.73
2006–2015	0.06	0.02	0.61	0.35	0.24
2016–2022	0.07	0.01	0.53	0.35	0.04
All years	0.06	0.02	0.84	0.31	0.32
5–17 y					
1997–2005	0.05	0.03	0.35	0.05	0.45
2006–2015	0.05	0.02	0.25	0.03	0.07
2016–2022	0.04	0.01	0.27	0.05	0.02
All years	0.05	0.02	0.28	0.04	0.16
18–64 y					
1997–2005	0.02	0.09	0.84	0.07	0.23
2006–2015	0.03	0.07	0.70	0.07	0.09
2016–2022	0.03	0.07	0.53	0.08	0.03
All years	0.03	0.07	0.68	0.07	0.11
≥65 y					
1997–2005	0.04	0.15	1.50	0.17	0.10
2006–2015	0.06	0.10	1.27	0.16	0.08
2016–2022	0.06	0.17	0.90	0.22	0.04
All years	0.06	0.14	1.18	0.19	0.07
All ages					
1997–2005	0.04	0.26	0.98	0.11	0.32
2006–2015	0.04	0.24	0.74	0.12	0.11
2016–2022	0.04	0.22	0.57	0.14	0.04
All years	0.04	0.24	0.75	0.12	0.14
Case-fatality rate, %‡					
0–11 mos	21.7	7.0	6.7	4.7	5.4
1–4 y	26.1	12.5	11.2	2.5	5.5
5–17 y	13.1	4.8	8.1	1.9	10.7
18–64 y	20.9	14.4	15.6	3.8	11.0
≥65 y	20.4	26.3	21.3	7.7	15.4
All ages	17.9	9.9	15.2	4.9	9.6

*GAS, group A *Streptococcus*; GBS, group B *Streptococcus*.
†Cases per 100,000 population.
‡Rate for 1997–2022.

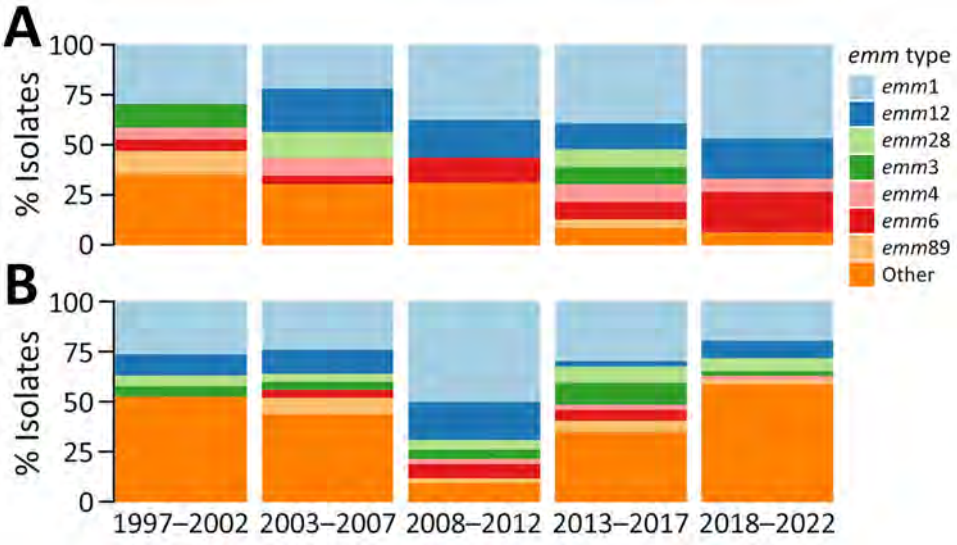

Figure 2. Distribution of *emm* types among isolates from group A *Streptococcus* meningitis cases, by age, United States, 1997–2022. A) Patients <18 years of age; B) patients ≥18 years of age.

caused by *S. pneumoniae, H. influenzae*, and GBS, the CFR was 1.5–4 times higher for GAS meningitis. In this large cohort, the 19.4% CFR for GAS meningitis closely approximates that seen in prior studies (*16*,*17*), and CFR did not decrease over time.

In our study, children <1 year of age had the highest incidence of GAS meningitis and the second highest CFR, consistent with previous reports of GAS meningitis in young children (*18*–*20*). Preliminary ABCs data for 2023 (P.A. Hawkins et al., unpub. data) showed the incidence of GAS meningitis in that age group increased from 0.15 (95% CI 0.04–0.37) cases/100,000 children during 2016–2022 to 1.06 (95% CI 0.26–2.38) cases/100,000 children, even though the overall incidence of GAS meningitis remained stable. Compared with other etiologies of bacterial meningitis in ABCs among children <1 year of age, GAS still represents a small percentage of meningitis cases, most of which are caused by GBS.

We observed a seasonal pattern of GAS meningitis cases, and a peak in winter and early spring; that same pattern has been reported for GAS pharyngitis and iGAS infections in the United States and Europe (*1*,*5*,*6*,*14*). One study proposed that the seasonal pattern might be explained by concurrently circulating viral infections during high-incidence

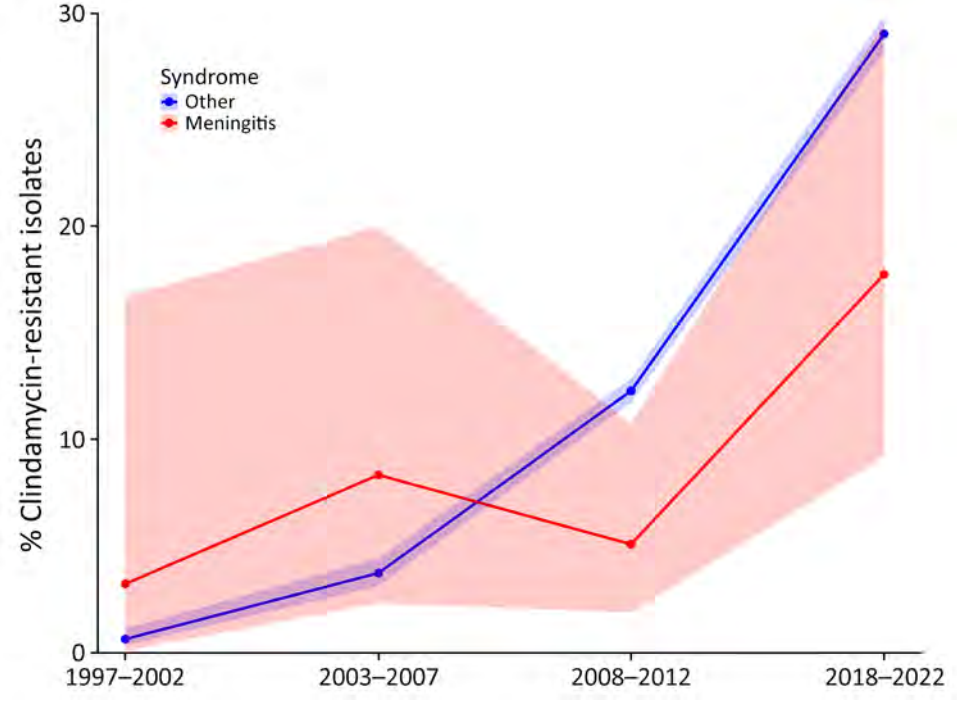

Figure 3. Clindamycin resistance among isolates from group A *Streptococcus* (GAS) meningitis and other GAS-related syndromes, United States, 1997–2022. The graph demonstrates increasing rates of clindamycin resistance among GAS isolates over time. Shading indicates 95% CIs.

periods, along with effects of crowding and close contact because of increased time spent indoors during cold months (*1*).

We also noted that the percentage of GAS meningitis patients with underlying conditions was low, particularly among pediatric patients, and that >90% of cases occurring in children without underlying medical conditions, potentially reflecting the severity of *emm*1 infections, as previously documented (*1*). Although most GAS meningitis cases in our study occurred in previously healthy children, nearly 1 in 5 pediatric GAS meningitis cases were fatal. We noted otitis media in ABCs for 13.8% of all GAS meningitis cases, consistent with previous reports that found that GAS meningitis was often preceded or accompanied by otitis media or sinusitis (*16*,*17*,*20*–*23*) and likely resulted from continuous spread of the infection rather than particular virulence factors (*24*)

The 2 most common *emm* types we identified among GAS meningitis isolates, *emm*1 and *emm*12, belonged to the *emm* pattern A-C, which has a strong preference for infection at the throat (*25*,*26*). *emm*1 and *emm*12 are among the most common *emm* types in pharyngitis isolates reported across the United States, Canada, and Europe (*15*,*27*–*30*). *emm*1 has also been documented as the predominant strain from GAS meningitis cases in small studies from several countries in Europe, which identified increases in overall iGAS and GAS meningitis incidence associated with *emm*1, particularly the $M1_{UK}$ lineage (*1*,*8*,*9*,*16*,*17*,*20*,*31*–*33*). However, despite a substantial increase in $M1_{UK}$ isolates in ABCs sites in the United States from 2015–2018 to 2019–2021 (*34*), only 2 of 263 meningitis isolates typed in our study belonged to the $M1_{UK}$ lineage. Isolates from GAS meningitis cases in this study were less diverse overall than those from other iGAS infections, highlighting the potential for vaccines in development to provide substantial protection against this disease manifestation.

The first-line antimicrobial regimen used in the empiric treatment of bacterial meningitis is typically a combination of vancomycin plus a third-generation cephalosporin, or a fluoroquinolone for patients who might have a severe allergy to β-lactams (*35*). Clindamycin combined with β-lactams has been associated with improved survival in severe iGAS infections (*36*) and is frequently used as part of combination antimicrobial therapy in intracranial GAS infections (*21*,*22*). We did not observe any β-lactam or vancomycin resistance among the 259 isolates tested and found only 1 isolate resistant to fluoroquinolones. On the other hand, clindamycin resistance among GAS meningitis isolates substantially increased across the years of this study, consistent with a reported 3-fold increase in macrolide and clindamycin resistance from 2013 to 2022 among iGAS isolates in ABCs (*2*). The poor diffusion of clindamycin over the meningeal membranes is an additional challenge and has led to recommendations to use high-dose clindamycin or linezolid as an adjunctive antibiotic (*37*,*38*).

One limitation of our study was the low incidence of GAS meningitis reported in ABCs, which made it difficult to detect patterns from year to year; however, we were able to show trends in the epidemiology of GAS meningitis in the United States over time. A limitation posed by ABCs data is the focus on invasive disease, which does not fully capture concurrent noninvasive GAS disease syndromes such as otitis media and pharyngitis; those syndromes have been reported in a high percentage of GAS meningitis cases in previous studies. Another limitation of ABCs is that it does not collect outcome data after discharge, which is necessary to assess long-term sequelae and delayed death. Neurologic sequelae occur in a large percentage of patients who survive GAS meningitis (*7*,*16*,*17*). Finally, we did not collect antibiotic use history and thus were unable to determine any correlation between antibiotic use and antimicrobial resistance or outcome in GAS meningitis cases.

In summary, we assessed 26 years of clinical, epidemiologic, and molecular data available from the well-established and robust ABCs system, which provided a large collection of GAS meningitis cases. Our findings provide insights into GAS meningitis, its epidemiology and clinical manifestations, and its contribution to the overall burden of bacterial meningitis in the United States since evolution of bacterial meningitis epidemiology after introduction and sustained use of vaccines against other pathogens causing meningitis, including *S. pneumoniae*, *N. meningitidis*, and *H. influenzae*. Our findings highlight the need for including GAS in future meningitis studies and reviews and in updated meningitis clinical practice guidelines and can help inform clinical practice, vaccine design, and public health interventions in the United States. Clinicians should be aware that meningitis is an uncommon but severe manifestation of invasive GAS and has a higher CFR than other meningitis etiologies; therefore, they should consider GAS in the differential diagnosis of meningitis.

Acknowledgments

We thank all persons in the ABCs areas involved in surveillance activities and maintenance of the ABCs system. We also thank the laboratory staff at the 10 sites

who isolate ABCs pathogens and make tracking those infections possible. We also thank the Streptococcus Laboratory of the Pneumonia & Streptococcus Laboratory Branch, Division of Bacterial Diseases, National Center for Immunization and Respiratory Diseases, Centers for Disease Control and Prevention (CDC) for isolate characterization and the Minnesota Department of Public Health laboratory for performing phenotypic antimicrobial susceptibility testing of all isolates from Minnesota.

This activity was reviewed by CDC, was deemed not research, and was conducted consistent with applicable federal law and CDC policy, including 45 C.F.R. part 46.102(l)(2), 21 C.F.R. part 56; 42 U.S.C. 241(d); 5 U.S.C. 552a; 44 U.S.C. 3501 et seq.

Funding for Active Bacterial Core surveillance is provided by the Emerging Infections Program of the CDC.

Author contributions: P.A.H. and C.J.G. conceived and designed the study. P.A.H., C.J.G., and A.L.C. analyzed and interpreted data and drafted the article. S.C. and Y.L. acquired, analyzed, and interpreted data. N.P. analyzed and interpreted data. J.O.O., T.M., A.T., B.J.A., K.E.B., L.H., Sh.S., N.A., R.H., W.S., H.K.T., R.L., K.C.-S., M.R., S.C., Sa.S., J.R.H.-A., S.K., J.H., and S.P. acquired data.

About the Author

Ms. Hawkins is a molecular epidemiologist focusing on streptococcal diseases and was an associate fellow in the National Center for Immunization and Respiratory Diseases, Centers for Disease Control and Prevention, at the time of this research. Her primary research interests include antimicrobial resistance and genomics.

References

1. Nelson GE, Pondo T, Toews KA, Farley MM, Lindegren ML, Lynfield R, et al. Epidemiology of invasive group A streptococcal infections in the United States, 2005–2012. Clin Infect Dis. 2016;63:478–86. https://doi.org/10.1093/cid/ciw248
2. Gregory CJ, Okaro JO, Reingold A, Chai S, Herlihy R, Petit S, et al. Invasive group A streptococcal infections in 10 US states. JAMA. 2025;333:1498–507. https://doi.org/10.1001/jama.2025.0910
3. Allen U, Moore D. Invasive group A streptococcal disease: management and chemoprophylaxis. Paediatr Child Health. 2010;15:295–302. https://doi.org/10.1093/pch/15.5.295
4. Pastural É, McNeil SA, MacKinnon-Cameron D, Ye L, Langley JM, Stewart R, et al. Safety and immunogenicity of a 30-valent M protein-based group a streptococcal vaccine in healthy adult volunteers: a randomized, controlled phase I study. Vaccine. 2020;38:1384–92. https://doi.org/10.1016/j.vaccine.2019.12.005
5. Link-Gelles R, Toews KA, Schaffner W, Edwards KM, Wright C, Beall B, et al. Characteristics of intracranial group A streptococcal infections in US children, 1997–2014. J Pediatric Infect Dis Soc. 2020;9:30–5. https://doi.org/10.1093/jpids/piy108
6. Lamagni TL, Darenberg J, Luca-Harari B, Siljander T, Efstratiou A, Henriques-Normark B, et al.; Strep-EURO Study Group. Epidemiology of severe *Streptococcus pyogenes* disease in Europe. J Clin Microbiol. 2008;46:2359–67. https://doi.org/10.1128/JCM.00422-08
7. Bijlsma MW, Brouwer MC, Kasanmoentalib ES, Kloek AT, Lucas MJ, Tanck MW, et al. Community-acquired bacterial meningitis in adults in the Netherlands, 2006–14: a prospective cohort study. Lancet Infect Dis. 2016;16:339–47. https://doi.org/10.1016/S1473-3099(15)00430-2
8. van der Putten BCL, Vlaminckx BJM, de Gier B, Freudenburg-de Graaf W, van Sorge NM. Group A streptococcal meningitis with the $M1_{UK}$ variant in the Netherlands. JAMA. 2023;329:1791–2. https://doi.org/10.1001/jama.2023.5927
9. Nielsen H, Storgaard M, Helweg-Larsen J, Larsen L, Jepsen MPG, Hansen BR, et al. Group A streptococcus meningitis in adults, Denmark. Emerg Infect Dis. 2023;29:1937–9. https://doi.org/10.3201/eid2909.230627
10. Prasad N, Kobayashi M, Collins JP, Rubis AB, Derado G, Delahoy MJ, et al. The epidemiology of bacterial meningitis in the United States during 2008–2023: an analysis of active, laboratory, population-based, multistate surveillance data. Lancet Reg Health Am. 2025;47:101120. https://doi.org/10.1016/j.lana.2025.101120
11. Sigfrid L, Perfect C, Rojek A, Longuere KS, Lipworth S, Harriss E, et al. A systematic review of clinical guidelines on the management of acute, community-acquired CNS infections. BMC Med. 2019;17:170. https://doi.org/10.1186/s12916-019-1387-5
12. Hasbun R. Initial therapy and prognosis of community-acquired bacterial meningitis in adults [cited 2024 Sep 19]. https://www.uptodate.com/contents/initial-therapy-and-prognosis-of-community-acquired-bacterial-meningitis-in-adults
13. Centers for Disease Control and Prevention. Active bacterial core surveillance (ABCs) [cited 2026 Jan 5]. https://www.cdc.gov/abcs/index.html
14. Chochua S, Metcalf BJ, Li Z, Rivers J, Mathis S, Jackson D, et al. Population and whole genome sequence based characterization of invasive group A streptococci recovered in the United States during 2015. MBio. 2017;8:e01422-17. https://doi.org/10.1128/mBio.01422-17
15. Li Y, Rivers J, Mathis S, Li Z, Velusamy S, Nanduri SA, et al. Genomic surveillance of *Streptococcus pyogenes* strains causing invasive disease, United States, 2016–2017. Front Microbiol. 2020;11:1547. https://doi.org/10.3389/fmicb.2020.01547
16. Lucas MJ, Brouwer MC, Bovenkerk S, Man WK, van der Ende A, van de Beek D. Group A streptococcal meningitis in adults. J Infect. 2015;71:37–42. https://doi.org/10.1016/j.jinf.2015.01.008
17. Drost EHGM, Chekrouni N, van Soest TM, Schipper K, van Sorge NM, Brouwer MC, et al. Increasing incidence of community-acquired adult group A streptococcal meningitis in the Netherlands. J Infect. 2024;88:68–70. https://doi.org/10.1016/j.jinf.2023.11.007
18. de Almeida Torres RS, Fedalto LE, de Almeida Torres RF, Steer AC, Smeesters PR. Group A streptococcus meningitis in children. Pediatr Infect Dis J. 2013;32:110–4. https://doi.org/10.1097/INF.0b013e31826fd4af
19. Shetty AK, Frankel LR, Maldonado Y, Falco DA, Lewis DB. Group A streptococcal meningitis: report of a case and review of literature since 1976. Pediatr Emerg Care. 2001;17:430–4. https://doi.org/10.1097/00006565-200112000-00007

20. Dou ZZ, Li W, Hu HL, Guo X, Hu B, Chen TM, et al. Group A streptococcal meningitis in children: a short case series and systematic review. Eur J Clin Microbiol Infect Dis. 2024;43:1517–31. https://doi.org/10.1007/s10096-024-04863-2
21. Cobo-Vázquez E, Aguilera-Alonso D, Grandioso-Vas D, Gamell A, Rello-Saltor V, Oltra-Benavent M, et al.; PedGAS-net Working Group. Central nervous system infection by group A streptococcus in children in Spain (2019–2023): a nationwide multicenter study. Pediatr Infect Dis J. 2025;159:107982. https://doi.org/10.1016/j.ijid.2025.107982
22. Hutton D, Kameda-Smith M, Afshari FT, Elawadly A, Hogg F, Mehta S, et al. Intracranial invasive group A streptococcus: a neurosurgical emergency in children. J Neurosurg Pediatr. 2023;32:478–87. https://doi.org/10.3171/2023.5.PEDS23109
23. Kjærgaard N, Bodilsen J, Justesen US, Schønheyder HC, Andersen CØ, Ellermann-Eriksen S, et al.; DASGIB Study Group. Community-acquired meningitis caused by beta-haemolytic streptococci in adults: a nationwide population-based cohort study. Eur J Clin Microbiol Infect Dis. 2019;38:2305–10. https://doi.org/10.1007/s10096-019-03678-w
24. Marquardt L, Andreoni F, Boumasmoud M, Schweizer TA, Heuberger DM, Parietti E, et al. Group A streptococcus strains causing meningitis without distinct invasive phenotype. MicrobiologyOpen. 2024;13:e1394. https://doi.org/10.1002/mbo3.1394
25. Bessen DE, Lizano S. Tissue tropisms in group A streptococcal infections. Future Microbiol. 2010;5:623–38. https://doi.org/10.2217/fmb.10.28
26. McGregor KF, Spratt BG, Kalia A, Bennett A, Bilek N, Beall B, et al. Multilocus sequence typing of *Streptococcus pyogenes* representing most known *emm* types and distinctions among subpopulation genetic structures. J Bacteriol. 2004;186:4285–94. https://doi.org/10.1128/JB.186.13.4285-4294.2004
27. Shulman ST, Tanz RR, Dale JB, Beall B, Kabat W, Kabat K, et al.; North American Streptococcal Pharyngitis Surveillance Group. Seven-year surveillance of North American pediatric group A streptococcal pharyngitis isolates. Clin Infect Dis. 2009;49:78–84. https://doi.org/10.1086/599344
28. Virolainen M, Gröndahl-Yli-Hannuksela K, Rantakokko-Jalava K, Seiskari T, Lönnqvist E, Kolari T, et al.; DICAR study group. Epidemiology and *emm* types among group A streptococcal pharyngitis in Finland: a prospective laboratory-based study. Eur J Clin Microbiol Infect Dis. 2024;43:233–41. https://doi.org/10.1007/s10096-023-04714-6
29. Sitkiewicz I, Borek A, Gryko M, Karpińska A, Kozińska A, Obszańska K, et al. Epidemiology of *Streptococcus pyogenes* upper respiratory tract infections in Poland (2003–2017). J Appl Genet. 2024;65:635–44. https://doi.org/10.1007/s13353-024-00875-y
30. Kailankangas V, Vilhonen J, Gröndahl-Yli-Hannuksela K, Rantakokko-Jalava K, Seiskari T, Auranen K, et al. Presence of *Streptococcus pyogenes* in the throat in invasive group A streptococcal disease: a prospective two-year study in two health districts, Finland. Infect Dis (Lond). 2023;55:405–14. https://doi.org/10.1080/23744235.2023. 2192287
31. Gouveia C, Bajanca-Lavado MP, Mamede R, Araújo Carvalho A, Rodrigues F, Melo-Cristino J, et al.; Portuguese Group for the Study of Streptococcal Infections, Portuguese Study Group of Pediatric Invasive Streptococcal Disease. Sustained increase of paediatric invasive *Streptococcus pyogenes* infections dominated by $M1_{UK}$ and diverse *emm*12 isolates, Portugal, September 2022 to May 2023. Euro Surveill. 2023;28:2300427. https://doi.org/10.2807/1560-7917.ES.2023.28.36.2300427
32. Vieira A, Wan Y, Ryan Y, Li HK, Guy RL, Papangeli M, et al. Rapid expansion and international spread of $M1_{UK}$ in the post-pandemic UK upsurge of Streptococcus pyogenes. Nat Commun. 2024;15:3916. https://doi.org/10.1038/s41467-024-47929-7
33. Rodriguez-Ruiz JP, Lin Q, Lammens C, Smeesters PR, van Kleef-van Koeveringe S, Matheeussen V, et al. Increase in bloodstream infections caused by *emm*1 group A *Streptococcus* correlates with emergence of toxigenic $M1_{UK}$, Belgium, May 2022 to August 2023. Euro Surveill. 2023;28:2300422. https://doi.org/10.2807/1560-7917.ES.2023.28.36.2300422
34. Li Y, Rivers J, Mathis S, Li Z, Chochua S, Metcalf BJ, et al. Expansion of invasive group A *Streptococcus* $M1_{UK}$ lineage in active bacterial core surveillance, United States, 2019 –2021. Emerg Infect Dis. 2023;29:2116–20. https://doi.org/10.3201/eid2910.230675
35. Tunkel AR, Hartman BJ, Kaplan SL, Kaufman BA, Roos KL, Scheld WM, et al. Practice guidelines for the management of bacterial meningitis. Clin Infect Dis. 2004;39:1267–84. https://doi.org/10.1086/425368
36. Babiker A, Li X, Lai YL, Strich JR, Warner S, Sarzynski S, et al. Effectiveness of adjunctive clindamycin in β-lactam antibiotic-treated patients with invasive β-haemolytic streptococcal infections in US hospitals: a retrospective multicentre cohort study. Lancet Infect Dis. 2021;21:697–710. https://doi.org/10.1016/S1473-3099(20)30523-5
37. Rezahosseini O, Roed C, Gitz Holler J, Frimodt-Møller N, Harboe ZB. Adjunctive antibiotic therapy with clindamycin or linezolid in patients with group A streptococcus (GAS) meningitis. Infect Dis (Lond). 2023;55:751–3. https://doi.org/10.1080/23744235.2023.2231073
38. Gatti G, Malena M, Casazza R, Borin M, Bassetti M, Cruciani M. Penetration of clindamycin and its metabolite N-demethylclindamycin into cerebrospinal fluid following intravenous infusion of clindamycin phosphate in patients with AIDS. Antimicrob Agents Chemother. 1998;42:3014–7. https://doi.org/10.1128/AAC.42.11.3014

Address for correspondence: Christopher J. Gregory, Centers for Disease Control and Prevention, 1600 Clifton Rd NE, Mailstop H24-8, Atlanta, GA 30329-4018, USA; email: hgk4@cdc.gov

Reduced Emergency Department Visits and Hospitalizations in Infants after Universal Respiratory Syncytial Virus Immunization, Italy, 2024–25

Simone Villa,[1] Simona Scarioni,[1] Enrico Pigozzi, Manuel Maffeo, Mauro Maistrello, Giorgio Bagarella, Francesco Scovenna, Federica Morani, Marlen Romano, Gianvincenzo Zuccotti, Massimo Agosti, Catia Borriello, Elena Pariani, Guido Bertolaso, Luigi Vezzosi, Fausto Baldanti, Mario Melazzini, Elena Azzolini, Gabriele del Castillo,[2] Danilo Cereda;[2] Regional Immunization Council[3]

During the 2024–25 winter season, a universal immunization campaign with nirsevimab was implemented in a region of Italy to prevent respiratory syncytial virus (RSV) infection among infants <12 months of age. We assessed its effects using regional syndromic surveillance data on emergency department visits (EDVs) and hospitalizations for lower respiratory tract infections and RSV infections. We estimated expected burden using an interrupted time series analysis, based on historical trends, and observed values with predictions. Children 1–5 years of age, not eligible for immunization, served as a comparison group. Among infants, EDVs for acute lower respiratory tract infections decreased by 42.7% and hospitalizations decreased by 46.5%, whereas EDVs for RSV infection decreased by 49.3% and hospitalizations decreased by 55.0%. No reductions were observed in children 1–5 years of age, confirming ongoing RSV circulation. Our findings support the effectiveness of universal nirsevimab immunization in reducing severe RSV-related outcomes among infants.

Respiratory syncytial virus (RSV) is the most common cause of acute lower respiratory tract infections (LRTI) in children and can potentially result in bronchiolitis, which often requires hospitalization. Young children, especially during their first 6 months of life, are at high risk for illness and death caused by RSV, particularly during a first infection (*1*).

Nirsevimab (Beyfortus; AstraZeneca, https://www.astrazeneca.com; Sanofi Pasteur, https://www.sanofi.com), a long-acting monoclonal antibody (mAb) against RSV, has an extended half-life of ≈71 days (*2*) and has been used in recent years to prevent severe RSV infections and outcomes in children <1 year of age. Recent clinical trials have demonstrated its efficacy in preventing RSV-associated acute LRTI, with an observed efficacy of 75% (*3*). In addition, a 62% reduction in hospitalization because of RSV-associated LRTI has been reported (*3*), which increased to 78.4% among preterm infants (*4*). A pragmatic trial conducted under near real-world conditions showed 83.2% overall effectiveness of nirsevimab and 75.7% effectiveness in reducing severe RSV-associated LRTI requiring supplemental oxygen (*5*). Other studies using real-world data have reported similar results, especially for RSV-related hospitalizations

Author affiliations: Directorate General for Health, Lombardy Region, Milan, Italy (S. Villa, S. Scarioni, E. Pigozzi, M. Maffeo, M. Maistrello, G. Bagarella, F. Scovenna, F. Morani, C. Borriello, G. Bertolaso, L. Vezzosi, M. Melazzini, G. del Castillo, D. Cereda); University of Milan, Milan (S. Villa, S. Scarioni, E. Pigozzi, F. Scovenna, G. Zuccotti, E. Pariani); Regional Company for Innovation and Purchasing Aria S.p.A., Milan (M. Romano); Buzzi Children's Hospital, Milan (G. Zuccotti); Hospital "F. Del Ponte," University of Insubria, Varese, Italy (M. Agosti); Fondazione IRCCS Policlinico San Matteo, Pavia, Italy (F. Baldanti); University of Pavia, Pavia (F. Baldanti); Humanitas University, Pieve Emanuele, Italy (E. Azzolini)

DOI: https://doi.org/10.3201/eid3201.250870

[1]These authors contributed equally to this article and share first authorship.

[2]These authors contributed equally to this article and share last authorship.

[3]Members of the Regional Immunization Council are listed at the end of this article.

and severe RSV disease (*6*–*8*). A systematic review and meta-analysis has further validated that mAb administration in infants reduces the burden of RSV-related hospital and ICU admissions (*9*).

Initial experiences with routine nirsevimab immunization in infants have been reported in several hospitals across Europe (*10*–*12*), and new population-level studies are emerging, all indicating a marked positive effect, especially in very young infants (*12*). This positive effect is further supported by evidence from settings where both maternal and infant immunization programs are implemented, suggesting potential additive benefits in reducing the burden of RSV-related illness (*13*).

During October 2024–March 2025, a large-scale immunization campaign using nirsevimab was launched in Lombardy, Italy, a region of northern Italy with nearly 10 million inhabitants, for infants <12 months of age. We conducted a study to estimate the effects of the campaign on the incidence of emergency department visits (EDVs) and hospital admissions associated with acute LRTI and RSV infection. Because studies conducted so far did not account for season-to-season variability (*6*–*9*), which could result in inaccurate estimates of the effects of RSV immunization, we performed an interrupted time series analysis that incorporated this element to estimate changes in trends before and after the program was implemented.

This project, conducted using routinely collected health data, was deemed by the Directorate General for Health of the Lombardy Region to be public health surveillance (Regional Government Resolution DGR n. XII/3010 of September 9, 2024, concerning the assessment of universal RSV immunization), not research, and was conducted according to applicable regional (Regional Law n. 33/2009, Art. 5 bis) and national law and policy (Italian Legislative Decree n. 196/2003, as amended by Legislative Decree n. 101/2018, Art. 2-sexies). Data processing complied with national and European data protection regulations (General Data Protection Regulation 2016/679).

Materials and Methods

Study Design and Population

The study used an interrupted time series design combined with a negative binomial regression model. The analysis covered the period of August 27, 2018 (ISO week 35–2018), through May 11, 2025 (ISO week 19–2025).

The primary study population for evaluating an intermediate intervention outcome consisted of infants <12 months of age residing in the Lombardy region of Italy. All analyses were based on the secondary use of anonymized datasets routinely collected by the Lombardy Region's Directorate General for Health as part of its public health mandate.

Data

The regional Emergency Department Syndromic Surveillance system is a new instrument developed by the Prevention Unit of the Lombardy Region's Directorate General for Health (*14*). Emergency department (ED) records were classified as EDVs if the patient was evaluated in the ED and not admitted; records were classified as hospitalizations if the patient was admitted. Each ED record was classified using codes from the International Classification of Diseases, 9th Revision, Clinical Modification (ICD-9-CM), providing a concise and precise description of the primary diagnosis of the visit. To analyze the performance of the immunization campaign, additional codes for acute LRTI and RSV infection were monitored (Appendix Table 1, https://wwwnc.cdc.gov/EID/article/32/1/25-0870-App1.pdf).

We obtained data on the number of births from the regional demographic registry, which collects and updates vital statistics, including births, deaths, and resident population data. We obtained data on the number of nirsevimab administrations from the regional data flow system, which systematically records individual vaccination events across healthcare settings. Using data on monthly birth cohorts and individual-level vaccination records, we linked each nirsevimab administration to the corresponding child to calculate immunization coverage for birth cohorts during January 2024–March 2025.

RSV Immunization Campaign

The 2024–25 immunization campaign against RSV infection in the Lombardy region targeted all infants born during January 1, 2024–March 31, 2025. A multicenter approach was used to ensure broad coverage; immunizations were provided through vaccination centers, general pediatricians, hospital pediatric departments, and hospital maternity units.

Beginning October 10, 2024, infants born during January–October 2024 were eligible to receive a single dose of nirsevimab (50 mg or 100 mg according to weight) at vaccination centers or from general pediatricians. Starting November 1, 2024, nirsevimab became available for direct administration at hospital maternity units. Infants who were not immunized at

birth were subsequently contacted through vaccination centers or general pediatricians to receive the RSV immunization. Maternal vaccination for RSV was not available in this region or in Italy during the 2024–25 season.

Statistical Analysis

We aggregated EDVs and hospital admissions into weekly counts and displayed them graphically by ISO week. We defined epidemic seasons as beginning in ISO week 35 of 1 year and ending in ISO week 19 of the following year, capturing the full duration of RSV activity. We stratified descriptive calculations by age group: <1 year and 1–5 years.

To evaluate the effects of the immunization campaign, we conducted interrupted time-series analyses using generalized linear models. The primary impact indicators analyzed in this study included EDVs and hospitalizations for acute LRTI and RSV infection. The intervention period ran from October 10, 2024 (ISO week 41–2024) through March 31, 2025 (ISO week 14–2025).

We trained Poisson and negative binomial regression models using historical data and used them to predict outcomes for the 2024–25 season. Because the seasonal patterns of pre-COVID seasons differ substantially from those after the first waves of COVID-19 in the region, we used data from ISO week 35–2021 to ISO week 41–2024 to train the model. Weekly counts of EDVs and hospitalizations for acute LRTI and RSV infection were used as outcome variables (Appendix). We used the model to generate counterfactual estimates (i.e., the expected number of EDVs and hospitalizations for acute LRTI and RSV infection in the absence of an RSV immunization campaign). We then compared observed cases with those estimates, which were displayed with 95% uncertainty intervals (95% UIs).

To determine whether differences between observed and expected values among infants were caused by a general reduction in RSV circulation rather than the immunization campaign, we compared EDVs and hospitalizations for acute LRTIs and RSV infection in children 1–5 years of age. Those children were not eligible for nirsevimab and served as the comparison group.

We conducted a sensitivity analysis (Appendix) to further corroborate results when excluding diagnoses that could potentially lead to misclassification of EDVs or hospitalizations. We performed all analyses using Python 3.13.0 (https://www.python.org/downloads/release/python-3130) with the pandas, numpy, matplotlib, statsmodels, and patsy packages. We cleaned and managed historical data before December 31, 2024, by using SAS 9.4 (SAS Institute Inc., https://www.sas.com).

Results

A total of 64,903 doses of nirsevimab were administered by the end of the immunization campaign on March 31, 2025, consisting of 34,913 doses at 100 mg and 29,990 doses at 50 mg. Those doses were given to 61,732 infants out of 77,983 births registered during January 1, 2024–March 31, 2025, resulting in an overall immunization coverage rate of 79.2% (Appendix Table 3).

We observed pronounced seasonal trends across both age groups in all winter seasons, except for 2020–21, when public health and social measures were widely implemented in the Lombardy Region in response to the initial waves of the COVID-19 pandemic (Figures 1, 2). Epidemic waves after this period exhibited substantially higher peaks than did pre-COVID seasons (i.e., 2018–19 and 2019–20); patterns of EDVs and hospital admissions were increasingly delayed, and most cases occurred among infants <12 months of age (Figure 1).

In the postpandemic seasons (2021–22, 2022–23, and 2023–24), peaks in EDVs for acute LRTIs and RSV infection among children <12 months of age were typically observed from ISO week 46 (2021–22 season) to ISO week 1 (2022–23 season); an average of 359 (range 354–364) visits for acute LRTIs and 78 (range 68–98) visits for RSV infections occurred (Table 1; Appendix Table 4). Seasonal peaks in both EDVs and hospital admissions for acute LRTI in that age group were lower in prepandemic seasons but though still higher than in 2024–25. For RSV infection, however, the 2024–25 season peak was similar to prepandemic levels; 38 EDVs (vs. 30–32 prepandemic) and 27 hospital admissions (vs. 32–36 prepandemic) were recorded (Appendix Table 4).

In the same ISO weeks in which EDVs for acute LRTI peaked across seasons among infants <12 months of age, a peak was also recorded among children 1–5 years of age (i.e., between ISO weeks 46 and 51); an average of 32 (range 24–37) EDVs for acute LRTI was recorded (Table 1). Unlike the pattern observed in children <12 months of age, the 2024–25 seasonal peak among children 1–5 years of age reached similar numbers of EDVs and hospital admissions for acute LRTI to the numbers seen in post-COVID seasons (Table 1; Figure 2).

When comparing the cumulative number of EDVs and hospital admissions for acute LRTI across different winter seasons among children <12 months

of age, the lowest counts were recorded in the 2024–25 season: 1,918 EDVs and 1,240 hospitalizations. The cumulative number of EDVs for acute LRTI was markedly higher in postpandemic seasons than in prepandemic seasons (Figure 3). Similar patterns were observed for RSV infection (Appendix Figure 1).

During the 2021–22 winter season, EDVs and hospitalizations for acute LRTIs increased among infants <12 months of age, resulting in 2,685 EDVs and 1,982 hospital admissions (Figure 3). Those numbers rose further in the 2022–23 and 2023–24 seasons, reaching 3,700 EDVs in 2022–23 and 3,572 EDVs in 2023–24.

In the 2024–25 season, only 1,918 EDVs for acute LRTI were recorded among children <12 months of age (Table 2; Appendix Figure 3, panel A), marking the lowest number of EDVs for the condition across all winter seasons studied, including both prepandemic and postpandemic periods. Compared with 3,700 EDVs in the 2022–23 season and 3,572 EDVs in the 2023–24 season, that difference represents a decline of >50%. Even more pronounced reductions were observed in hospital admissions for acute LRTI, which fell to 1,240 during the 2024–25 season, compared with 2,396 in the 2023–24 season (a 48% reduction) and 2,478 in the 2022–23 season (a 50% reduction) (Figure 3, panel B). Although the peak of EDVs and hospital admissions for RSV infection in the 2024–25 season was similar to that observed in prepandemic seasons (Appendix Table 4), cumulative counts in the postpandemic seasons (from 2021–2024) were substantially higher (Appendix Figure 1). Compared with the 2022–23 season, the 2024–25 season showed a 59% reduction in EDVs (from 644 to 265) and a 61% reduction in hospital admissions (from 704 to 273) among children <12 months of age.

Interrupted Time Series Analysis

Regression modeling suggested that EDVs and hospitalizations for acute LRTI and RSV infection plummeted among children <12 months of age during the 2024–25 season (Table 2; Figure 4; Appendix Figure 2). We observed comparable declines for LRTI and

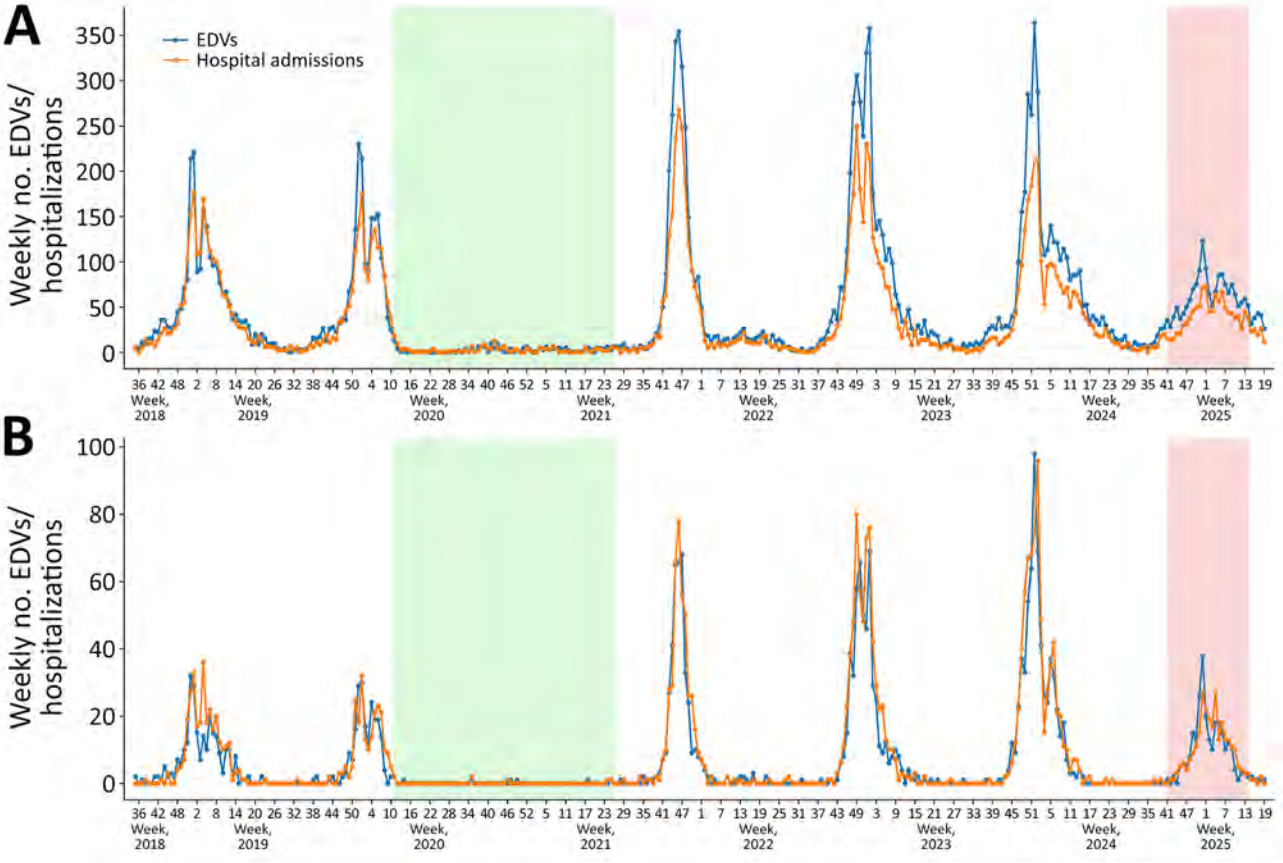

Figure 1. EDVs and hospitalizations among children <12 months of age in study of reduced EDVs and hospitalizations in infants after universal respiratory syncytial virus immunization, Italy, 2024–25. Numbers are shown for ISO week 35–2018 to ISO week 19–2025 for lower respiratory tract infection (A) and respiratory syncytial virus infections (B). Green shading indicates the period during which public health and social measures were implemented in response to the initial waves of the COVID-19 pandemic in the region. Red shading marks the prophylaxis period during which nirsevimab was administered. EDV, emergency department visit.

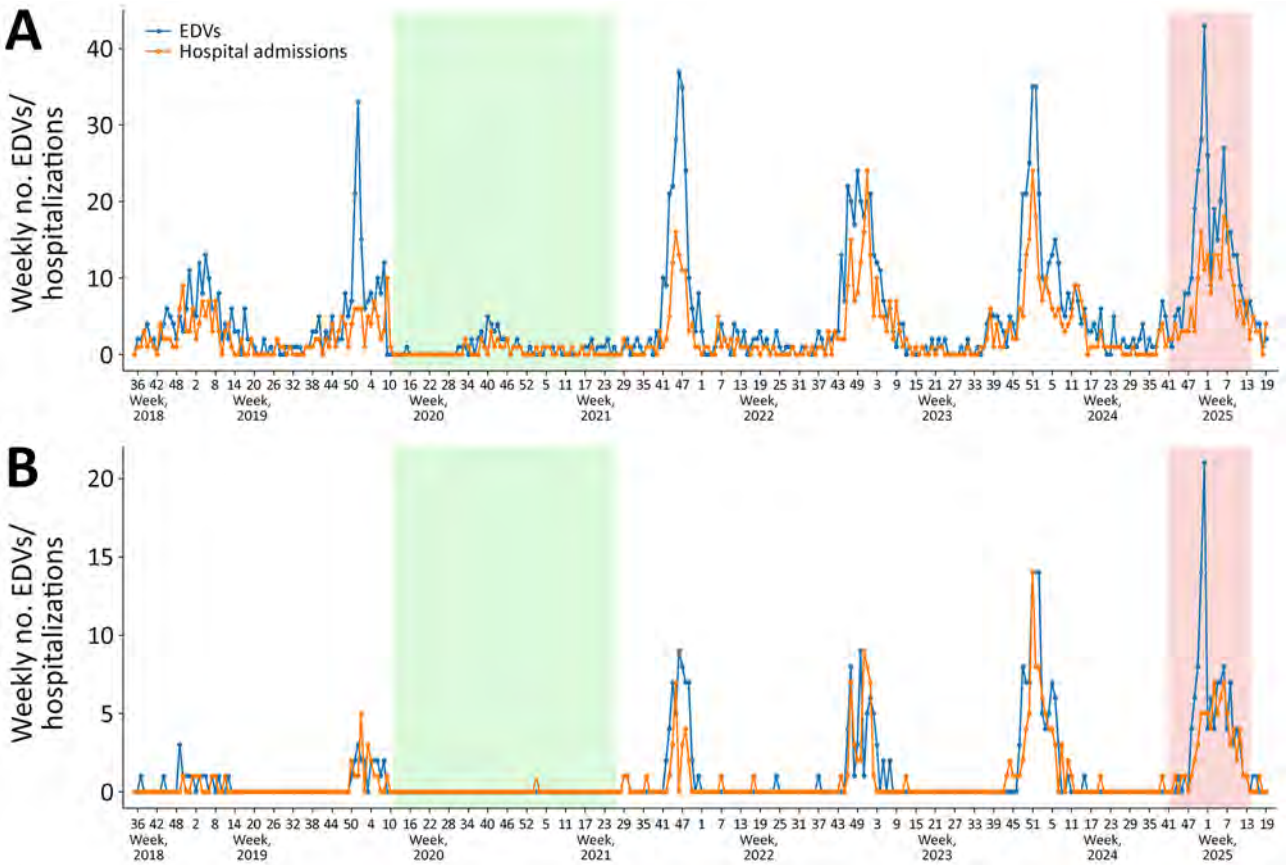

Figure 2. EDVs and hospitalizations in children 1–5 years of age in study of reduced EDVs and hospitalizations in infants after universal respiratory syncytial virus immunization, Italy, 2024–25. Numbers are shown for ISO week 35–2018 to ISO week 19–2025 for lower respiratory tract infection (A) and respiratory syncytial virus infections (B). Green shading indicates the period during which public health and social measures were implemented in response to the initial waves of the COVID-19 pandemic in the region. Red shading marks the prophylaxis period during which nirsevimab was administered. EDV, emergency department visit.

RSV infections among the same age group, both in EDVs (−42.7% for LRTIs and −49.3% for RSV infection) and hospital admissions (−46.5% for LRTIs and −55.0% for RSV infection). By contrast, children 1–5 years of age, who were not the target population of the immunization campaign, showed an opposite trend (Figure 5; Appendix Figure 3). Although those children had lower absolute numbers of both EDVs and hospitalization than infants <12 months of age, their indicator activity increased during the 2024–25 season. Specifically, predicted EDVs for RSV infection were 68 (95% UI 55–80), whereas observed visits were 116, a 70.6% (95% UI 26.5–114.7%) increase. Those values exceeded those observed in previous post-COVID seasons (2021–22 to 2023–24), confirming persistent RSV circulation among children 1–5 years of age. Similarly, predicted hospital admissions for RSV infection were 46 (95% UI 36–55), compared with 75 observed admissions, a 63.0% (95% UI 13.0– 113.0%) increase.

Table 1. EDVs and hospitalizations for lower respiratory tract infection at seasonal peak week among children in study of reduced EDVs and hospitalizations in infants after universal respiratory syncytial virus immunization, Italy, 2024–25*

	Children <12 mo		Children 1–5 y	
Winter season	EDVs	Hospital admission	EDVs	Hospital admission
2018–19	221 (week 1)	176 (week 1)	13 (week 5)	9 (week 50)
2019–20	230 (week 52)	175 (week 1)	33 (week 52)	10 (week 9)
2020–21	10 (week 41)	13 (week 42)	5 (week 40)	3 (week 41)
2021–22	354 (week 46)	268 (week 46)	37 (week 46)	16 (week 45)
2022–23	358 (week 1)	250 (week 49)	24 (week 49)	24 (week 52)
2023–24	364 (week 52)	212 (week 52)	35 (week 51)	24 (week 51)
2024–25	123 (week 52)	73 (week 1)	43 (week 52)	18 (week 6)

*Numbers shown are for winter seasons from 2018–19 to 2024–25. The ISO week in which the peak was reached is indicated in parentheses. EDV, emergency department visit.

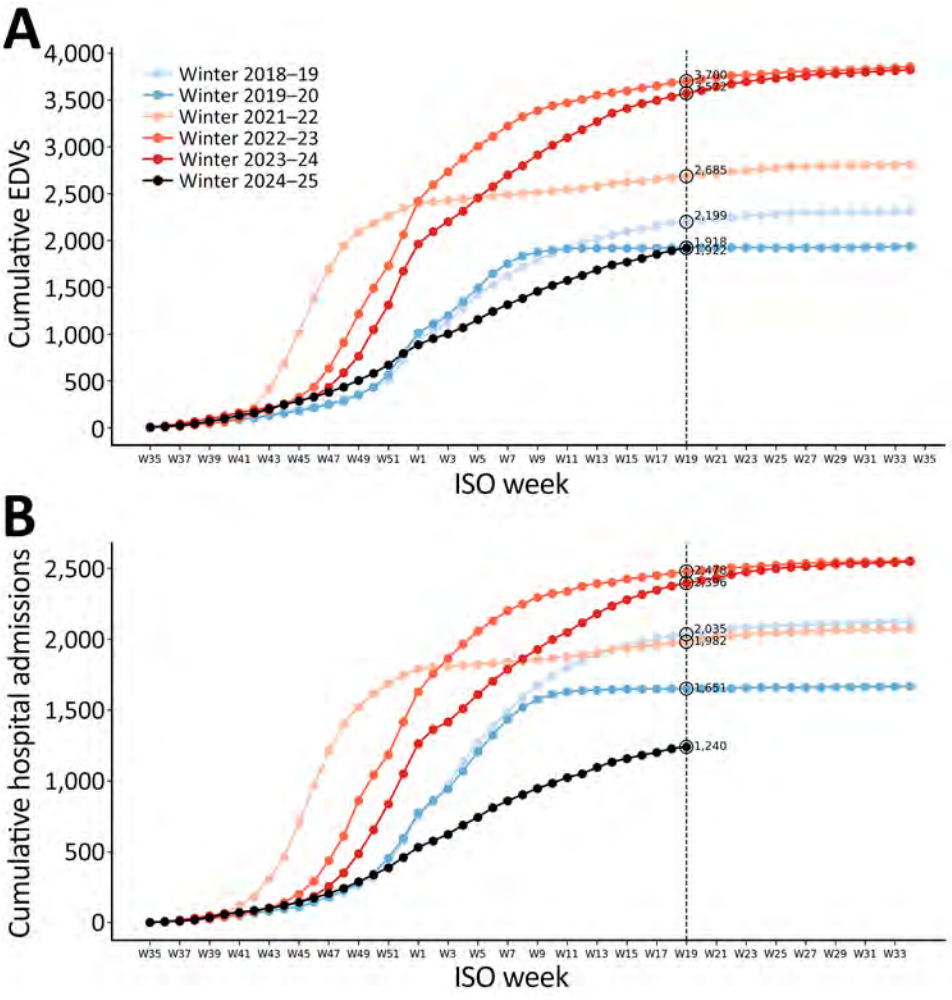

Figure 3. Comparison of cumulative EDVs (A) and hospitalizations (B) for lower respiratory tract infections among children <12 months of age from winter season 2018–19 to 2024–25 in study of reduced EDVs and hospitalizations in infants after universal respiratory syncytial virus immunization, Italy. To enable comparison between different epidemic years, a season was defined as the period going from the 35th week of 1 year to the end of the 34th week of the following year, covering the entire winter epidemic and accounting for shifts in its onset and conclusion. Pre-COVID and post-COVID seasons are colored in different shades of blue and red. EDV, emergency department visit.

Sensitivity Analysis

Diagnoses of ICD-9-CM code 07.96 (i.e., RSV infection) accounted for 0.2% of EDVs and hospitalizations for acute LRTIs among children <12 months of age and accounted for 2.0% of EDVs and 0.8% of hospital admissions among children 1–5 years of age (Appendix Table 5, Figures 4, 5). Excluding that diagnosis code from the acute LRTI definition produced only minor differences in the estimated impact of universal RSV immunization, underscoring the robustness of the analysis (Appendix Table 6).

Table 2. Impact of universal RSV immunization on EDVs and hospitalization in children <12 months of age and those 1–5 years of age, Italy, 2024–25*

	Indicator activity, winter 2024–25		Difference in indicator activity	
Age cohort	Predicted (95% UI)	Observed	Absolute change	% Change (95% UI)
Children <12 mo				
LRTI				
EDVs	3,347 (3,067–3,627)	1,918	−1,429	−42.7 (−48.1 to −37.3)
Hospitalizations	2,316 (2,120–2,513)	1,240	−1,076	−46.5 (−51.9 to −41.0)
RSV infection				
EDVs	523 (456–590)	265	−258	−49.3 (−58.2 to −40.4)
Hospitalizations	607 (523–691)	273	−334	−55.0 (−63.2 to −46.8)
Children 1–5 y				
LRTI				
EDVs	287 (262–312)	393	106	36.9 (18.9–55.0)
Hospitalizations	160 (145–176)	225	65	40.6 (17.6–63.6)
RSV infection				
EDVs	68 (55–80)	116	48	70.6 (26.5–114.7)
Hospitalizations	46 (36–55)	75	29	63.0 (13.0–113.0)

*EDV, emergency department visit; LRTI, lower respiratory tract infection; RSV, respiratory syncytial virus; UI, uncertainty interval.

Discussion

We present the results of an evaluation of the effectiveness of a large-scale nirsevimab immunization campaign for infants <12 months of age. The campaign aimed to reduce EDVs and hospital admissions for acute LRTI and RSV infection in the Lombardy region of northern Italy.

We observed a significant overall decline in EDVs and hospitalizations for acute LRTI and RSV infection among infants <12 months of age; we observed comparable percentage reductions in both EDVs and hospitalizations relative to both historical trends and model-predicted values. Starting November 2024, most infants were immunized at birth, ensuring timely protection. This campaign likely contributed to the observed impact, as opposed to outpatient-based strategies that rely on postdischarge follow-up. However, this decline is unlikely attributable to reduced or interrupted RSV circulation during the 2024–25 season, given that the trends observed in the 1–5–year age group remained consistent with or exceeded historical and predicted levels. The observed reduction in RSV-related outcomes in infants was not mirrored in children 1–5 years of age, suggesting that the intervention likely prevented disease among infants, not that levels of RSV circulation in the population were reduced.

A recent analysis modeled different immunization and vaccination scenarios in the Lombardy region using data collected before the RSV campaign was implemented to inform regional public health policies (*15*). That analysis estimated a considerable reduction in the number of hospitalizations caused by RSV: a 44% decrease with an estimated immunization coverage rate of 70% and a 60% decrease with an estimated immunization coverage rate of 95%. Those findings are consistent with the results of our analysis, which found that EDVs associated with RSV hospitalization decreased by 55% in the 2024–25 season. The previous study further predicted that the intervention

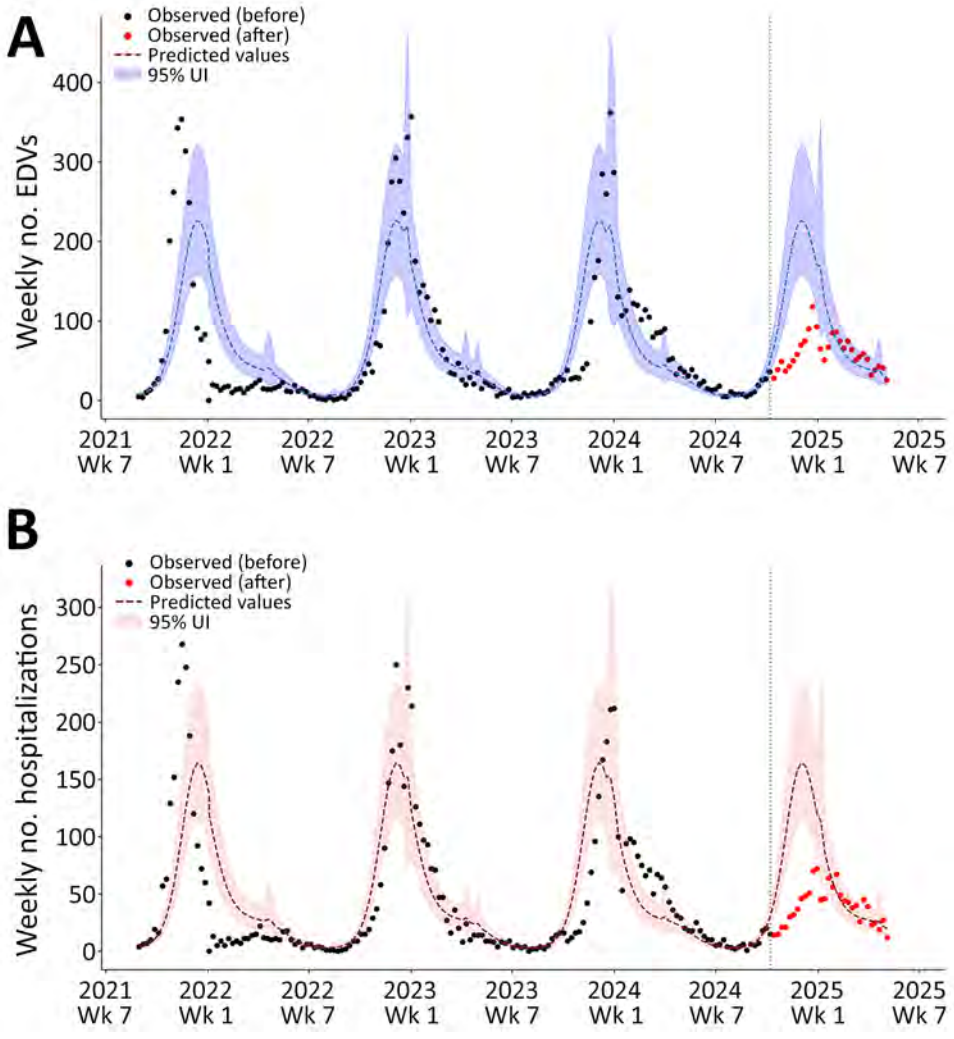

Figure 4. Interrupted time series analysis of EDVs (A) and hospitalizations (B) for lower respiratory tract infections among infants <12 months of age in study of reduced EDVs and hospitalizations in infants after universal respiratory syncytial virus immunization, Italy, 2024–25. Numbers are shown for ISO week 35–2021 to ISO week 19–2025. A negative binomial model incorporating a Fourier parameter was trained using historic data before the launch of the universal respiratory syncytial virus immunization program (before October 10, 2024; vertical dashed lines indicate launch date) and was then used to compute predicted values and 95% UIs. Those values are displayed against the observed weekly counts of EDVs and hospital admissions for lower respiratory tract infections. EDV, emergency department visit; UI, uncertainty interval.

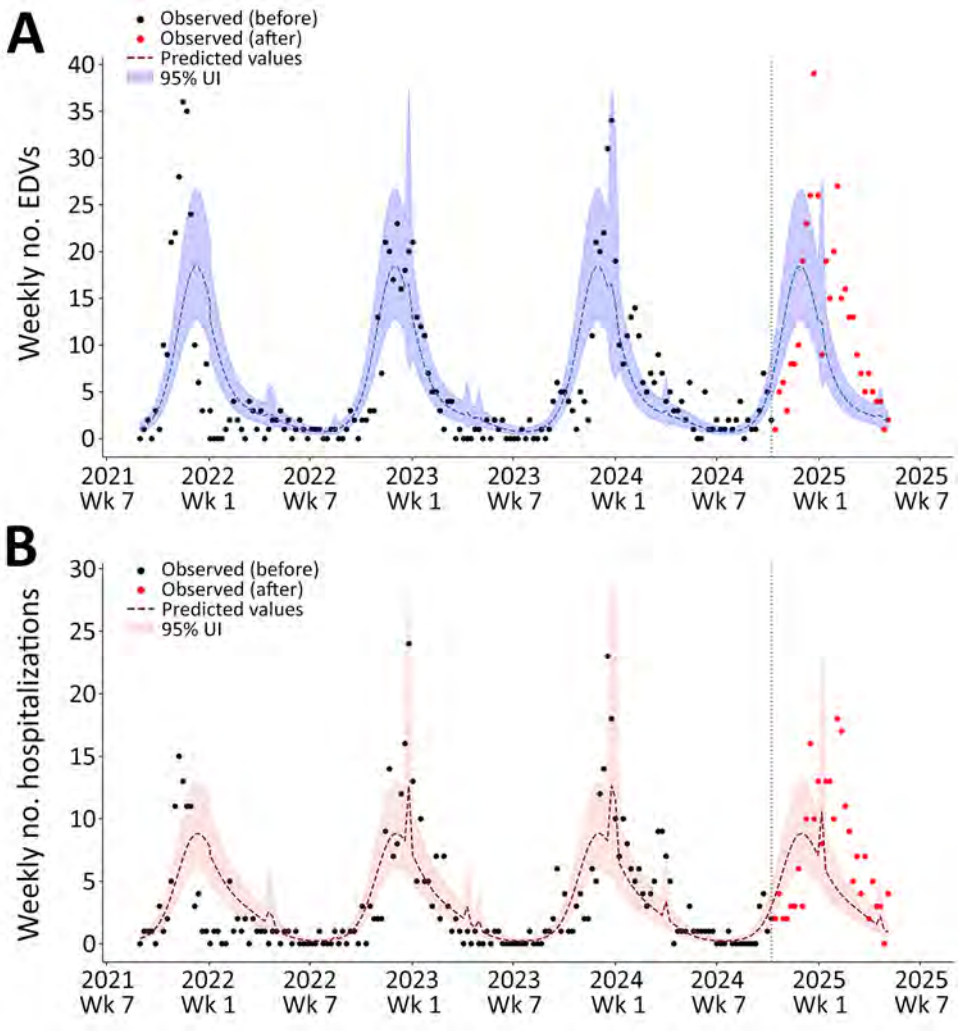

Figure 5. Interrupted time series analysis of EDVs (A) and hospitalizations (B) for lower respiratory tract infections among children 1–5 years of age in study of reduced EDVs and hospitalizations in infants after universal respiratory syncytial virus immunization, Italy, 2024–25. Numbers are shown for ISO week 35–2021 to ISO week 19–2025. A negative binomial model incorporating a Fourier parameter was trained using historic data before the launch of the universal respiratory syncytial virus immunization program (before October 10, 2024; vertical dashed lines indicate launch date) and was then used to compute predicted values and 95% UIs. Those values are displayed against the observed weekly counts of EDVs (and hospital admissions for lower respiratory tract infections. EDV, emergency department visit; UI, uncertainty interval.

would have had limited effects on reducing overall RSV circulation, because infants contribute relatively little to RSV community transmission (*15*). Our study corroborated that finding; an opposing trend was observed in children 1–5 years of age, supporting the use of this age group as a comparison population for deriving counterfactual estimates.

The effect of the RSV immunization campaign observed in our study is further supported by effectiveness estimates derived from a density case–control study (*16*), which were subsequently applied to the eligible infant population in Spain to estimate the national impact (*17*). That extrapolation suggests that, for every 1,000 infants immunized with the mAb, 14.7 cases of RSV-associated acute LRTIs are prevented. Likewise, we observed that, for every 1,000 mAb doses administered, 22.0 EDVs (1,429/64,903) and 16.6 hospital admissions (1,076/64,903) for acute LRTI were prevented.

Similar findings have been reported in Luxembourg (*10*), where an estimated coverage of 84% was achieved in maternity wards across the country's 4 hospitals (≈1,524 births), leading to a 69% reduction in hospitalizations among infants <6 months of age with laboratory-confirmed RSV infection. A notable increase in the mean age of RSV-associated hospitalizations was observed in that study for 2024–25 compared with 2022–23; the mean age shifted from 7.8 months in 2022–23 to 14.4 months in 2024–25. That shift in age distribution might partly explain the differences observed in our study, where EDVs and hospitalizations were considered in infants <12 months of age, in addition to potential variations in immunization coverage.

As expected, no surge in EDVs or hospitalizations for acute LRTI or RSV infection was observed during the rigorous implementation of public health and social measures in the initial phase of the pandemic in 2020 and 2021. Compared with previous epidemics, the postpandemic periods recorded the highest number of EDVs and hospital admissions.

That phenomenon might be attributed to waning immunity against RSV as a result of the stringent public health and social measures implemented to curb the surge of COVID-19 cases. Those measures ultimately reduced the circulation of several respiratory viruses, including RSV (*18*,*19*).

Our analysis has several limitations arising from the reliance on administrative anonymized datasets rather than laboratory RSV test results. First, testing intensity for RSV might have varied over the study period, particularly with increased diagnostic efforts in recent years (Appendix Table 5). Those differences might have led to greater detection of mild or non-LRTI RSV, affecting comparability across seasons. To mitigate that possibility, we adopted a broader case definition for acute LRTI that relied less on microbiological confirmation. Sensitivity analyses further suggested that non-LRTI RSV infections had only a marginal effect on the model estimates. Second, the datasets we used were not originally designed to identify individual cases. We made efforts to remove duplicates from EDVs and hospitalization data using a set of criteria, but that process was further complicated by the impossibility of ascertaining patients' exposure to the intervention under assessment. Therefore, an unimmunized infant might have visited different hospitals on different days, resulting in multiple counts without the possibility of deduplication. Third, because the case definition used for acute LRTI includes ICD-9-CM code 079.6, some episodes might include upper respiratory tract infections, leading to potential overestimation of RSV-related acute LRTI episodes. However, on the basis of the sensitivity analysis we conducted, that factor did not affect impact estimates when we removed diagnoses coded 079.6 from the case definition of acute LRTIs. Fourth, although most studies have focused on infants <6 months of age, we were unable to replicate that cutoff because of the nature of the ED data and the fact that the target population of the universal immunization campaign included all infants born during 2024–March 2025. Although the datasets used in our analysis encompass both date of birth and age group, only age group is a mandatory variable, because it is either directly recorded during the EDV or derived from date of birth. For children, the available age categories distinguish only between those <12 months of age and those 1–5 years of age. Consequently, our analysis was constrained to the infants <12 months of age, rather than infants <6 months of age. Fifth, the 2024–25 RSV season might not have been fully captured within the analysis period, potentially leading to underestimation of RSV-related outcomes for that season. That factor should be considered when comparing with earlier seasons that were fully observed. Last, because of the nature of the dataset used, persons residing outside the region who might have sought care at 1 of the ≈100 hospitals could not be excluded. That limitation is likely to have a minimal impact at the regional level, but it could be more relevant in areas near the borders of other regions in Italy or near Switzerland, where cross-border healthcare use could occur in both directions.

This study explored the effects of nirsevimab administration in a large territory with a population of ≈10 million persons and ≈64,500 births in 2024 (*20*) (63,053 of whom lived in the region), focusing on the number of EDVs and hospital admissions both for acute LRTIs and RSV infection among infants <12 months of age. We compared results with historical trends as well as to a comparison group to elucidate the effect of the immunization campaign. We found that use of nirsevimab for passive immunization of newborns and children <12 months of age, achieving an immunization coverage rate of ≈79% across the Lombardy region of Italy, resulted in a substantial reduction in EDVs and hospital admissions for acute LRTI and RSV infection. Further studies will be conducted upon the conclusion of the RSV epidemic to estimate the cost-effectiveness of the immunization campaign implemented. Our results, combined with those future analyses, will help inform policy decisions for future immunization programs.

Additional members of the Regional Immunization Council: Matteo Capobussi, Lorenzo Moja, Doriana Bertazzo, Andrea D'Adda, Monica De Angelis, Maria Grazia Manfredi, Chiara Marchisio, Alberto Moscariello, Sergio Abrignani, Paolo Bonfanti, Marino Faccini, Umberto Gelatti, Vania Giacomet, Andrea Gori, Carlo La Vecchia, Antonella Laiolo, Antonio Piro, Ian Schroeder, Giuliano Rizzardini, Pierachille Santus, and Carlo Signorelli.

AI tools were employed exclusively for copyediting purposes in this manuscript. No new content was generated by the AI system. All authors reviewed and approved the final manuscript. We affirm that the use of AI did not compromise the authenticity or integrity of the work.

Study conception and oversight were conducted by S.V., G.d.C., and D.C.; acquisition of data was performed by S.V., S.S., M. Maistrello, and G.B.; data analysis was performed by S.V., M. Maistrello, and G.B.; interpretation of data was performed by S.V., S.S., M. Maistrello, G.B., M. Maffeo, G.d.C., and D.C.; S.V. drafted the work; and M. Maffeo, G.d.C., D.C., S.S., C.B., E.P., and E.A. reviewed the work critically. All authors have read, reviewed, and approved the version of the manuscript to be published.

About the Author

Dr. Villa is a medical resident in public health at the University of Milan and an MSc candidate in epidemiology at the London School of Hygiene & Tropical Medicine. At the Regional Health Directorate of Lombardy Region, he works on various surveillance activities, including respiratory virus monitoring in the community and emergency departments, syndromic surveillance, antimicrobial resistance, and wastewater surveillance. Dr. Scarioni is a medical resident in public health at the University of Milan and a medical officer at the Regional Health Directorate of Lombardy Region. In her position, she works on vaccines and immunization, coordinating data-related activities in those areas.

References

1. Blau DM, Baillie VL, Els T, Mahtab S, Mutevedzi P, Keita AM, et al.; CHAMPS Consortium. Deaths attributed to respiratory syncytial virus in young children in high-mortality rate settings: report from Child Health and Mortality Prevention Surveillance (CHAMPS). Clin Infect Dis. 2021;73(Suppl_3):S218–28.
2. European Medicines Agency. Beyfortus (nirsevimab) [cited 2025 May 23]. https://www.ema.europa.eu/en/medicines/human/EPAR/beyfortus
3. Hammitt LL, Dagan R, Yuan Y, Baca Cots M, Bosheva M, Madhi SA, et al.; MELODY Study Group. Nirsevimab for prevention of RSV in healthy late-preterm and term infants. N Engl J Med. 2022;386:837–46.
4. Griffin MP, Yuan Y, Takas T, Domachowske JB, Madhi SA, Manzoni P, et al.; Nirsevimab Study Group. Single-dose nirsevimab for prevention of RSV in preterm infants. N Engl J Med. 2020;383:415–25.
5. Drysdale SB, Cathie K, Flamein F, Knuf M, Collins AM, Hill HC, et al.; HARMONIE Study Group. Nirsevimab for prevention of hospitalizations due to RSV in infants. N Engl J Med. 2023;389:2425–35.
6. Moline HL, Tannis A, Toepfer AP, Williams JV, Boom JA, Englund JA, et al.; New Vaccine Surveillance Network Product Effectiveness Collaborators. Early estimate of nirsevimab effectiveness for prevention of respiratory syncytial virus-associated hospitalization among infants entering their first respiratory syncytial virus season—New Vaccine Surveillance Network, October 2023–February 2024. MMWR Morb Mortal Wkly Rep. 2024;73:209–14.
7. Xu H, Aparicio C, Wats A, Araujo BL, Pitzer VE, Warren JL, et al. Estimated effectiveness of nirsevimab against respiratory syncytial virus. JAMA Netw Open. 2025;8:e250380.
8. Ares-Gómez S, Mallah N, Santiago-Pérez MI, Pardo-Seco J, Pérez-Martínez O, Otero-Barrós MT, et al.; NIRSE-GAL study group. Effectiveness and impact of universal prophylaxis with nirsevimab in infants against hospitalisation for respiratory syncytial virus in Galicia, Spain: initial results of a population-based longitudinal study. Lancet Infect Dis. 2024;24:817–28.
9. Sumsuzzman DM, Wang Z, Langley JM, Moghadas SM. Real-world effectiveness of nirsevimab against respiratory syncytial virus disease in infants: a systematic review and meta-analysis. Lancet Child Adolesc Health. 2025;9:393–403.
10. Ernst C, Bejko D, Gaasch L, Hannelas E, Kahn I, Pierron C, et al. Impact of nirsevimab prophylaxis on paediatric respiratory syncytial virus (RSV)-related hospitalisations during the initial 2023/24 season in Luxembourg. Euro Surveill. 2024;29:2400033.
11. López-Lacort M, Muñoz-Quiles C, Mira-Iglesias A, López-Labrador FX, Mengual-Chuliá B, Fernández-García C, et al. Early estimates of nirsevimab immunoprophylaxis effectiveness against hospital admission for respiratory syncytial virus lower respiratory tract infections in infants, Spain, October 2023 to January 2024. Euro Surveill. 2024;29:2400046.
12. Perramon-Malavez A, Buonsenso D, Morello R, Coma E, Foster S, Leonard P, et al. Real-world impact of nirsevimab immunisation against respiratory disease on emergency department attendances and admissions among infants: a multinational retrospective analysis. Lancet Reg Health Eur. 2025;55:101334.
13. Patton ME, Moline HL, Whitaker M, Tannis A, Pham H, Toepfer AP, et al. Interim evaluation of respiratory syncytial virus hospitalization rates among infants and young children after introduction of respiratory syncytial virus prevention products—United States, October 2024–February 2025. MMWR Morb Mortal Wkly Rep. 2025;74:273–81.
14. Villa S, Maffeo M, Maistrello M, Bagarella G, Porrello VN, Morani F, et al. Increased pneumonia-related emergency department visits, northern Italy. Emerg Infect Dis. 2025;31:1057–9.
15. Menegale F, Vezzosi L, Tirani M, Scarioni S, Odelli S, Morani F, et al. Impact of routine prophylaxis with monoclonal antibodies and maternal immunisation to prevent respiratory syncytial virus hospitalisations, Lombardy region, Italy, 2024/25 season. Euro Surveill. 2025;30:2400637.
16. Núñez O, Olmedo C, Moreno-Perez D, Lorusso N, Fernández Martínez S, Pastor Villalba PE, et al.; Nirsevimab Effectiveness Study Collaborators. Effectiveness of catch-up and at-birth nirsevimab immunisation against RSV hospital admission in the first year of life: a population-based case-control study, Spain, 2023/24 season. Euro Surveill. 2025;30:2400596.
17. Pastor-Barriuso R, Núñez O, Monge S; Nirsevimab Effectiveness Study Collaborators. Infants needed to immunise with nirsevimab to prevent one RSV hospitalisation, Spain, 2023/24 season. Euro Surveill. 2025;30:2500040.
18. Abu-Raya B, Viñeta Paramo M, Reicherz F, Lavoie PM. Why has the epidemiology of RSV changed during the COVID-19 pandemic? EClinicalMedicine. 2023;61:102089.
19. Ang HJ, Menegale F, Preziosi G, Pariani E, Migliari M, Pellegrinelli L, et al. Reconstructing the impact of COVID-19 on the immunity gap and transmission of respiratory syncytial virus in Lombardy, Italy. EBioMedicine. 2023;95:104745.
20. Istituto Nazionale di Statistica. Indicatori demografici–Anno 2024 [cited 2025 May 30]. https://www.istat.it/comunicato-stampa/indicatori-demografici-anno-2024

Address for correspondence: Simone Villa, U.O. Prevenzione, DG Welfare, Regione Lombardia, Piazza Città di Lombardia, 1, 20124, Milan, Italy; email: simone.villa@unimi.it

Genomic Insights into Marburg Virus Strains from 2023 and 2025 Outbreaks in Kagera, Tanzania

Lawrence A. Mapunda,[1] Medard Beyanga,[1] Nyambura Moremi, Jean N. Hakizimana, Doreen Kamori, Alfred Chacha, Edna Mgimba, Dennis Mrosso, Ambele E. Mwafulango, Jackson Mushumbusi, Ferdinand Ndunguru, Seif Abdul, Emmanuel Mkumbo, Maria E. Kelly, Céline Barnadas, Vida Mmbaga, Rogath Kishimba, Samwel Laizer, Ntuli Kapologwe, Michael Kiremeji, Erasto Sylvanus, Angela Samwel, Saumu Nungu, Emmanuel Achol, Julien Nguinkal, Hakimu Idris Lagu, Muna Affara, Florian Gehre, Calvin Sindato, Chacha Mangu, Elias Nyanda Ntinginya, Saida Murugwa, Pawan Angra, Shannon Whitmer, George Mgomella, Mahesh Swaminathan, Wangeci Gatei, Dorcas Wanjohi, Sofonias Tessema, Yenew Kebede, Said Aboud, Charles Sagoe-Moses, Alex Magesa, Gerald Misinzo, Tumaini Nagu, Grace Magembe

Marburg virus (MARV) is the primary cause of Marburg virus disease (MVD), a severe hemorrhagic fever with a high case-fatality rate. The first reported MVD outbreak in Tanzania occurred in 2023, followed by a second outbreak in 2025, both within the Kagera region. During those MVD outbreaks, 174 suspected cases were identified; of those, 10 were laboratory confirmed. After complete genome assembly and bioinformatic analyses, we found the MARV strains of the 2023 and 2025 outbreaks to be closely related and clustered with MARV strains that caused outbreaks in Rwanda (2024) and Uganda (2014). The sequences from both MVD outbreaks in Tanzania showed >99.71% nucleotide identity, suggesting a possible single spillover event followed by limited human-to-human virus transmission. Further ecologic studies are essential to identify potential spillover events, but our findings indicate that closely related MARV strains circulate in Kagera, Tanzania, posing a risk for future outbreak recurrence.

Viral hemorrhagic fevers (VHFs) are zoonotic or vectorborne diseases that pose a substantial threat to global health security and cause substantial economic burdens because of their rapid transmissibility and high fatality rates, as well as the limited availability of effective therapeutics and countermeasures. The incidence of VHFs is notably high in the tropical regions because environmental conditions favor the presence of vectors and reservoirs, as well as increased interactions between humans and animals (*1*). In addition, the threat of spread is magnified by delayed confirmatory diagnosis of VHFs in resource-limited settings, human displacement resulting from conflicts, and rapid increase in intercontinental travel and trade (*2*).

Marburg virus disease (MVD) is one of the VHFs caused by 2 orthomarburgviruses, Marburg virus (MARV) and Ravn virus (RAVV), classified into a

Author affiliation: National Public Health Laboratory, Dar es Salaam, Tanzania (L.A. Mapunda, N. Moremi, A. Chacha, E. Mgimba, D. Mrosso, A.E. Mwafulango, J. Mushumbusi, F. Ndunguru, S. Abdul); Ministry of Health, Dodoma, Tanzania (M. Beyanga, E. Mkumbo, V. Mmbaga, R. Kishimba, S. Laizer, N. Kapologwe, M. Kiremeji, E. Sylvanus, A. Samwel, S. Nungu, A. Magesa, T. Nagu, G. Magembe); Sokoine University of Agriculture, Morogoro, Tanzania (J.N. Hakizimana, G. Misinzo); Muhimbili University of Health and Allied Sciences, Dar es Salaam (D. Kamori); World Health Organization, Dar es Salaam (M.E. Kelly, C. Sagoe-Moses); World Health Organization, Geneva, Switzerland (C. Barnadas); East African Community, Arusha, Tanzania (E. Achol, J. Nguinkal, H.I. Lagu, M. Affara, F. Gehre); Bernhard Notch Institute for Tropical Medicine, Hamburg, Germany (M. Affara, F. Gehre); National Institute for Medical Research, Dodoma (C. Sindato, C. Mangu, E.N. Ntinginya, S. Aboud); US Centers for Disease Control and Prevention, Dar es Salaam (S. Murugwa, P. Angra, S. Whitmer, G. Mgomella, M. Swaminathan, W. Gatei); Africa Centres for Disease Control and Prevention, Addis Ababa, Ethiopia (D. Wanjohi, S. Tessema, Y. Kebede)

DOI: https://doi.org/10.3201/eid3201.251314

[1]These first authors contributed equally to this article.

single species, *Orthomarburgvirus marburgense*, genus *Orthomarburgvirus* of the *Filoviridae* family (*3*,*4*). MARV was the first filovirus discovered in 1967 during a concurrent outbreak of hemorrhagic fever among laboratory workers in Yugoslavia (Serbia) and Germany who had been in contact with tissues from African green monkeys imported from Uganda (*5*,*6*). The genome of MARV is composed of a nonsegmented negative-sense RNA with ≈19 kbp nucleotides. Genome sequencing is useful in MVD surveillance, contact tracing, and tracking the evolution of MARV and RAVV (*7*).

The Egyptian rousette bat (*Rousettus aegyptiacus*), a cave-dwelling bat, is the primary natural reservoir of MARV; transmission to humans occurs through spillover events from infected bats or contact with their bodily fluids or tissues (*8*). Outbreaks of MVD have frequently been associated with visits to bats' roosting sites, such as caves and mines, particularly within the geographic range of *R. aegyptiacus* bats (*9*,*10*). Two notable MVD outbreaks were reported in Africa: the 1998–2000 outbreaks in the Democratic Republic of the Congo (DRC), which resulted in 154 cases and 128 deaths (83% case-fatality rate [CFR]), and the 2004–2005 outbreak in Uige, Angola, which resulted in 252 cases and 227 deaths (90% CFR) (*10*–*13*). More recently, the third largest outbreak of MVD was reported in Rwanda in 2024, causing 66 confirmed cases and 15 deaths (23% CFR) (*14*). Other isolated MVD outbreaks have been identified in South Africa (1975), Kenya (1980, 1987), Russia (1990), Uganda (2007, 2008, 2012, 2014, 2017), Guinea (2021), Ghana (2022), and Equatorial Guinea (2023) (*15*).

The first MVD outbreak in Tanzania was declared in Kagera region in March 2023 and consisted of 9 cases (8 confirmed and 1 probable) and 6 deaths (66.6% CFR) (*16*). A second outbreak occurred in the same region in January 2025 and consisted of 10 cases (2 confirmed and 8 probable) and 10 deaths (100% CFR). In this article, we present genomic analyses and examine the genetic relationships among the MARV strains responsible for the 2023 and 2025 outbreaks in Tanzania and previously reported MARV strains reported in both humans and animal reservoirs. The Medical Research Coordinating Committee of the Tanzania National Institute for Medical Research granted ethics approval (certificate no. NIMR/HQ/R.8a/Vol.IX/4957) and permission to publish (ref. no. BD.242/437/01C/42).

Methods

Study Settings

The 2023 and 2025 outbreaks of MVD in Tanzania occurred in the Kagera region, northwestern Tanzania. The index case of the 2023 MVD outbreak was in a resident of Butahyaibega village in the Bukoba rural district who was engaged in fishing on Goziba Island, ≈80 km east of Lake Victoria shore (Figure 1). The outbreak primarily affected Butahyaibega village in Kanyangereko ward and Bulinda village in Maruku ward, both located ≈20 km south of the town of Bukoba. That area is notable for its numerous mining sites and caves that are inhabited by colonies of the Egyptian rousette bat (*R. aegyptiacus*).

The probable index case for the 2025 MVD outbreak was in a resident of Katerela village in Ruziba ward of Biharamulo district, situated in proximity to the Burigi and Biharamulo game reserves and ≈170 km south of the 2023 outbreak location (Figure 1). The 2025 outbreak was confined to the 2 neighboring villages of Katerela and Ruziba; contacts and cases were reported primarily within Biharamulo and Muleba districts in the Kagera region. Of note, a total of 8 probable case-patients died before sampling could be conducted. Those case-patients were epidemiologically linked to 2 laboratory-confirmed cases, both of whom died.

Sample Collection

During the MVD outbreaks, we collected blood samples in EDTA tubes for 84 suspected cases in 2023 and 81 suspected cases in 2025. We transported samples to a mobile laboratory stationed at Kabyaile Health Center in Missenyi district (Figure 1), which had been positioned in Kagera region as part of preparedness and response to the 2022–2023 Sudan Ebola virus outbreak in Uganda.

Confirmation of MARV by Real-Time Reverse Transcription PCR

We tested blood samples for filoviruses Ebolavirus (EBOV) and MARV using real-time reverse transcription PCR (RT-PCR). In brief, we extracted viral RNA from inactivated EDTA plasma collected using the QIAamp viral RNA mini kit (QIAGEN, https://www.qiagen.com), in accordance with the manufacturer's instructions. The extracted RNA served as a template for the diagnosis of filoviruses using the RealStar filovirus screen RT-PCR kit 1.0 (Altona Diagnostics, https://altona-diagnostics.com) using a CFX96 real-time PCR detection system (Bio-Rad Laboratories, https://www.bio-rad.com), in accordance with manufacturer's instructions. We conducted the initial real-time RT-PCR screening for both MARV and EBOV at the Kabyaile mobile laboratory before confirmation, cryopreservation, and next-generation sequencing at the national public health laboratory in Dar es Salaam.

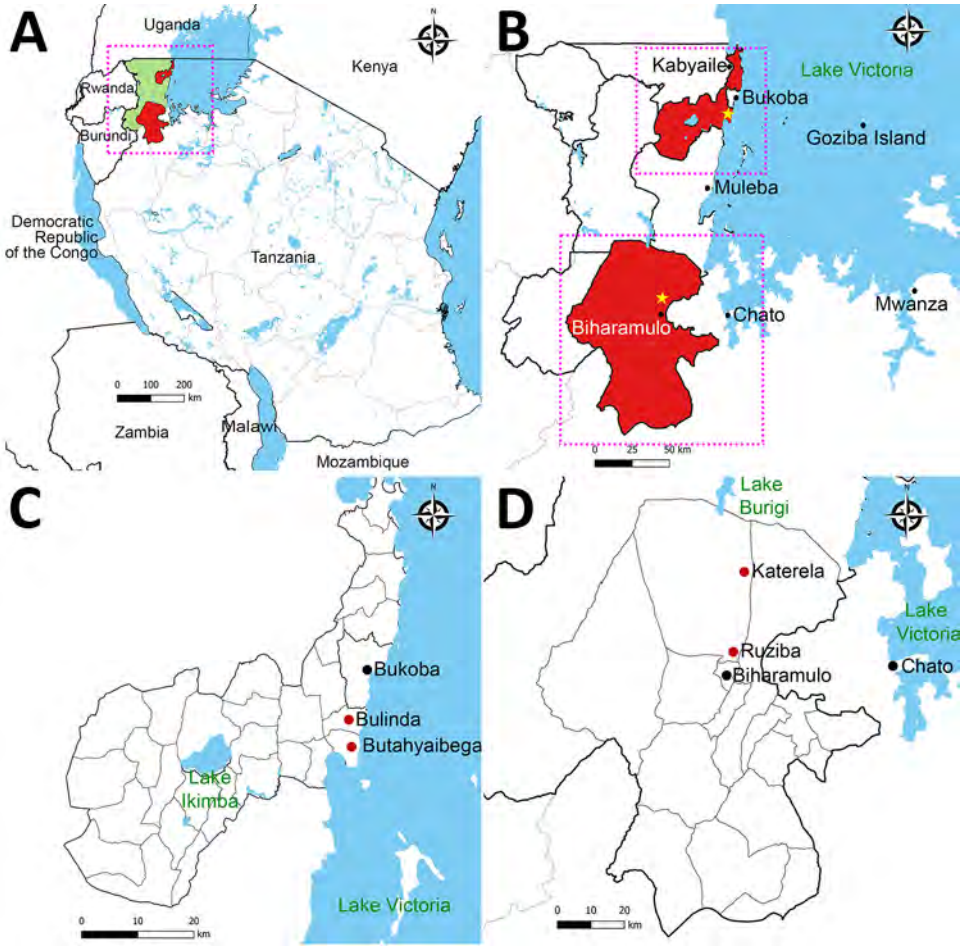

Figure 1. Locations of the 2023 and 2025 Marburg virus outbreaks in Kagera region, northwest Tanzania. A) The outbreaks occurred in northwest Tanzania, west of Lake Victoria, in Bukoba Rural and Biharamulo districts of the Kagera region. The region borders Uganda, Burundi and Rwanda. Green shading indicates Kagera region. Red shading indicates the affected districts. B) Expanded view of boxed area from panel A shows epicenters for both outbreaks (stars). Upper box marks the location of the 2023 outbreak in a village south of Bukoba town; lower box marks the location of the second outbreak in a village north of Biharamulo town. C) Locations of the 2023 outbreak in Bukoba Rural district. Red dots indicate affected villages. D) Locations of the 2025 outbreak in Biharamulo district. Red dots indicate affected villages.

Sequencing Library Preparation and Next-Generation Sequencing of MARV

We prepared sequencing libraries using the Illumina viral surveillance panel (Illumina, https://www.illumina.com), following the Illumina RNA prep with enrichment protocol. We pooled, normalized, and quantified the resulting libraries using the Qubit DNA high sensitivity kit (Thermo Fisher Scientific, https://www.thermofisher.com). We performed paired-end sequencing using MiSeq (Illumina) with a MiSeq 600 cycle V3 kit and generated sequencing reads with a configuration of 2 × 150 bp, yielding an average of 11 million reads per sample.

Bioinformatics Analysis

We subjected raw sequencing reads to quality control using FastQC version 0.11.9 (https://www.bioinformatics.babraham.ac.uk/projects/fastqc). We trimmed sequencing adapters and low-quality ends from reads using trim_galore version 0.6.4 (https://github.com/FelixKrueger/TrimGalore) powered by cutadapt version 4.5 (https://cutadapt.readthedocs.io/en/stable). We set the quality Phred score cutoff at 30 with a minimum read length of 75 bp. We aligned the quality-filtered sequencing reads to the isolate Marburg_virus/H.sapiens-tc/KEN/1980/Mt._Elgon-Musoke (GenBank accession no. NC_001608.3) as reference genome using Burrows-Wheeler Aligner version 0.7.17 with the maximum exact match (mem) algorithm (H. Li et al., unpub. data, https://doi.org/10.48550/arXiv.1303.3997). Subsequently, using the mapped sequencing reads, we performed de novo assembly using SPAdes version 3.13.1 (*17*) and Megahit version 1.2.9 (*18*), and evaluated the quality of the resulting assemblies using the Quality Assessment Tool (QUAST) program version 5.0.261 (*19*). We determined the MARV complete genome from each sample as the longest contig assembled.

For phylogenetic analysis, we aligned the MARV sequences generated in this study (deposited into GenBank under accession nos. PV700537–41) with those described previously available at GenBank by using MAFFT version 7.520 (https://mafft.cbrc.jp/alignment/software) to determine their evolutionary relationship (*20*). The alignment comprised 82 MARV complete genome sequences collected during 1967–

2025 in Angola (n = 13), DRC (n = 25), Guinea (n = 2), Kenya (n = 6), the Netherlands (n = 1), Rwanda (n = 5), Sierra Leone (n = 3), Tanzania (n = 5), and Uganda (n = 22) (Appendix 1 Table, https://wwwnc.cdc.gov/EID/article/32/1/25-1314-App1.xls). We used the model finder implemented in IQ-TREE version 1.6.12 (*21*) to determine the best-fitting model; we chose the general time reversible substitution model with estimated base frequencies, invariable sites, and gamma-distribution rate with 4 discrete categories in accordance with the Bayesian information criterion. We reconstructed a maximum-likelihood phylogenetic tree with IQ-TREE version 1.6.12 (*21*) and MEGA 12 using 1,000 bootstrap replications (*22*). We calculated the marginal likelihood estimation using Tracer version 1.7.2 (https://beast.community/tracer) to select the appropriate clock and demographic model. We used the uncorrelated relaxed clock with constant population model to generate the XML file in BEAUti version 1.10.4 (https://beast.community/beauti). We then analyzed the generated file using BEAST version 1.10.4 (https://github.com/beast-dev/beast-mcmc) for phylodynamic analysis, applying Monte Carlo Markov chain with a chain length of 20×10^6, sampling after every 1,000 cycles. We explored the results using Tracer version 1.7.2, targeting an effective sample size of ≥200 for each parameter (*23*,*24*). We annotated the time-scaled phylogenetic tree generated by BEAST using TreeAnnotator version 1.10.4 (https://beast.community/treeannotator) with a maximum clade credibility tree after a burn-in of 20% of the sample; we used FigTree version 1.4.4 (http://tree.bio.ed.ac.uk/software/figtree) for visualization. We used the Nextstrain build for Marburg and Ravn viruses (https://github.com/pvanheus/nextstrain-marv-and-ravv) for ancestral state reconstruction and then the Auspice tool (https://docs.nextstrain.org/projects/auspice/en/stable/index.html) for visualization as described previously (*25*,*26*). We used the snp-sites tool (https://github.com/andrewjpage/snp_sites) to identify variable positions in the alignment after excluding unsequenced regions, and used snp-dists (https://github.com/tseemann/snp-dists) to count the single-nucleotide polymorphisms between and within outbreaks, as described previously (*27*).

Results

Comparative Genomics Analysis of MARV

We attempted virus enrichment sequencing using specimens from 10 Marburg virus–positive persons and generated whole genomes from 5 persons; 3 of those persons were from the 2023 outbreak (sample nos. S6, S7, and S8) and 2 from the 2025 outbreak (S001 and S002) (Table 1). The genomes of MARV strains reported in our study were 18,943–19,070 nt long (Table 1). With the exception of unsequenced regions between the MARV strains, there were no nucleotide sequence variations between strains from the same outbreak, whereas there were 39 single-nucleotide polymorphisms between the 2023 and 2025 MARV strains.

When we compared the 2023 and 2025 MARV genomes to a Marburg virus reference genome (GenBank accession no. NC_001608.3), we found

Table 1. Patient metadata and sequence metrics from study of 2023 and 2025 MARV outbreaks in Kagera region, northwestern Tanzania*

Characteristic	Patient 1	Patient 2	Patient 3	Patient 4	Patient 5
Sequence ID	MARV/H.Sapiens/TZ/Kagera/S6/2023	MARV/H.Sapiens/TZ/Kagera/S7/2023	MARV/H.Sapiens/TZ/Kagera/S8/2023	MARV/H.Sapiens/TZ/Kagera/001/2025	MARV/H.Sapiens/TZ/Kagera/002/2025
Patient age, y/sex	26/M	27/M	36/M	28/M	30/M
Location	Bulinda	Butahyaibega	Butahyaibega	Katerela	Ruziba
Ct value	24.41	18.73	19.74	25.28	16.34
Total sequencing reads	10,899,272	5,213,734	7,809,532	23,905,276	9,523,562
Mean base Phred quality score	35.4	35.2	35.4	37.4	37.3
No. MARV-specific sequencing reads	17,339	256,285	1,132,206	7,049,308	4,245,624
Mapped reads, %	0.16	4.91	14.46	29.49	44
Assembled MARV genome size, bp	18,943	19,054	19,048	19,070	19,030
GC content, %	38.28	38.18	38.07	38.10	38.01
Mean genome coverage depth	128.166	1,875.16	8,344.77	46,400	29,600
Genome coverage, %	99.12	99.70	99.67	99.89	99.57
GenBank accession no.	PV700539	PV700540	PV700541	PV700537	PV700538

*Ct, cycle threshold; GC, percentage of guanine (G) and cytosine (C) nucleotides; ID, identification; MARV, Marburg virus.

99.12%–99.89% genome coverage. BLASTn (https://blast.ncbi.nlm.nih.gov) revealed that Tanzania MARV strains were closely related to a MARV isolate collected from a bat in the Python Cave, southwestern Uganda, in 2009 (GenBank accession no. JX458855) and from a human during the September 2014 MVD outbreak in Kampala, Uganda (GenBank accession no. KP985768). When we compared those genomes to the MARV reference genome (GenBank accession no. NC_001608.3), mean coverage depth was 128.166–46,400, with variability along the genome (Table 1; Appendix 2 Figure 1, https://wwwnc.cdc.gov/EID/article/32/1/25-1314-App2.pdf). We observed >99.68% nucleotide identity between MARV strains responsible for the 2023 and 2025 outbreaks in Tanzania and those of 2024 outbreak in Rwanda (GenBank accession nos. PQ552725–42) (Table 2).

Phylogenetic Analysis

A comparison of Tanzania MARV sequences with all available full-length MARV sequences from previous outbreaks across Africa demonstrated that the 2023 and 2025 sequences were closely related and clustered with MARV sequences from outbreaks in Rwanda in 2024 (bootstrap support 100%) and Uganda in 2014 (bootstrap support 100%) (Figure 2). The sequences from both MVD outbreaks in Tanzania showed >99.71% nucleotide identity, suggesting a possible local single spillover event in each of the Bukoba Rural and Biharamulo districts, followed by limited human-to-human virus transmission. The clock likeness analysis using TempEst version 1.5.3 (http://tree.bio.ed.ac.uk/software/tempest) revealed the existence of a positive temporal signal among representative full-length MARV sequences with a correlation coefficient of 0.7184 and a coefficient of determination (R^2) of 0.5161. The time to most recent common ancestor for the analyzed dataset was 1767 (95% highest posterior density interval range 1591–1966) and the evolution rate was 2.2233×10^{-4} (95% CI 1.8419×10^{-4} to 2.634×10^{-4}) substitutions/site/year. Bayesian evolutionary tree reconstruction analysis revealed that the Tanzania MARV strains clustered with the 2024 Rwanda MARV strains. In addition, the MARV strains from Tanzania were closely related to those collected in Uganda from bats in 2009 and humans in 2014.

Discussion

Marburg virus disease is a VHF with dramatic clinical manifestation and a high CFR that poses a substantial global health threat and negative economic consequences (*28*). The 3 MVD outbreaks reported in 2023, 2024 and 2025 in Tanzania and Rwanda occurred in a radius of ≈150 km, underscoring the common ecologic zone (Figure 1, panel A). We did not observe nucleotide substitutions in MARV from the same MVD outbreaks in Tanzania. Although the specific evolutionary origins of MARV in the Great Lakes ecosystem remains unresolved, we noted that the probable index cases in the Tanzania outbreaks in 2023 and 2025 were residents within the Kagera region with no foreign travel history. The Kagera region, where the Tanzania MVD outbreaks occurred, borders Uganda to the north, Rwanda to the west, and Burundi to the southwest; most of the area forms the Kagera River basin ecosystem, which is ecologically linked to the Albertine Rift montane forest ecoregion and the Greater Virunga Landscape. The Kagera River basin represents an interface of the highest biodiversity and diverse agro-ecosystems of Africa covering 5 countries; Burundi, DRC, Rwanda, Uganda, and Tanzania. High population mobility and diverse rich flora and fauna within the Kagera River basin ecosystem increase the risk for pathogen spillover and cross-border transmission of infectious diseases, including MVD. In East Africa, the distribution of Egyptian rousette bats encompasses Uganda, Rwanda, Burundi, and parts of the DRC, Kenya, and Tanzania. Although no study has reported MARV in bats in Tanzania, the virus has been isolated from bats in Uganda, DRC and Kenya (*9*,*29*,*30*). The area in Tanzania in which the 2023 and 2025 MVD outbreaks occurred is notable for its numerous mining sites and caves that are inhabited by colonies of Egyptian rousette bats, the reservoir host for MARV

Table 2. Comparison of amino acid mutations in Marburg virus strains in study of Marburg virus disease outbreaks in 2023 and 2025, Tanzania*

Gene	2023 outbreak, Tanzania	2024 outbreak, Rwanda	2025 outbreak, Tanzania
VP35	I94V (A3224G)	I94V (A3224G)	I94V (A3224G)
VP40	V57I (G4736)	V57I (G4736), Q159R (5043G)	V57I (G4736)
GP	P234S (C6640T), Y279D (6775G), H349N (C6985), S389G (A7105G)	P234S (C6640T), Y279D (6775G)	P234S (C6640T), Y279D (6775G), E241G (A6662G), H349N (C6985), S389G (A7105G)
L	I243L (A12207C), D699N (G13575A), V1673A (T16494C), M1734V (16680G), R1756S (A16748C),	R1756S (A16748C)	K174R (A12001G), V1673A (T16494C), R1756S (A16748C), S1820L (C16939T, T16940A), R1855K (G17044A)

*Study strains were compared with a reference isolate, GenBank accession number NC_001608.3. GP, glycoprotein; L, polymerase; VP, viral protein.

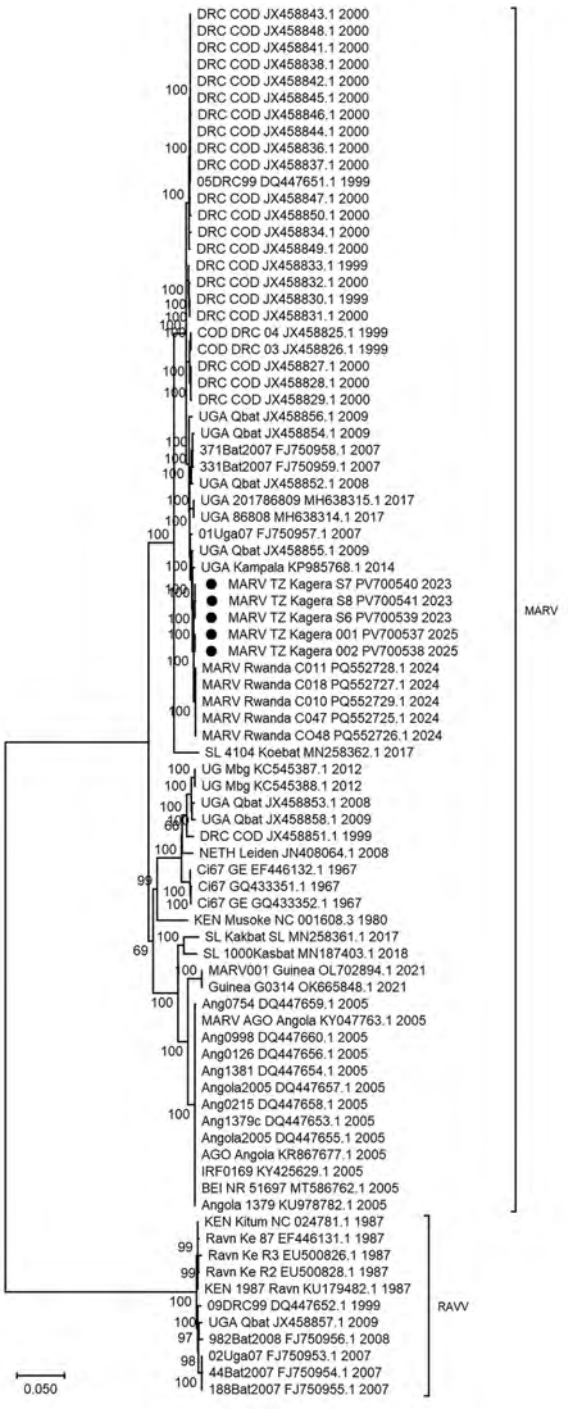

Figure 2. Maximum-likelihood phylogenetic tree from study of 2023 and 2025 MARV outbreaks in Kagera region, northwest Tanzania. Tree was reconstructed using 82 MARV complete genome sequences, including sequences responsible for the 2023 and 2025 outbreak in Tanzania described in this study (black dots) and previously reported sequences acquired from GenBank (accession numbers provided). Node values show the percentage of bootstrap support. Scale bar indicates nucleotide substitution per site. Ang, Angola; DRC, Democratic Republic of the Congo; KEN, Kenya; MARV, Marburg virus; NETH, the Netherlands; SL, Sierra Leone; UG or UGA, Uganda.

(*31*). The nucleotide sequences from both outbreaks were highly similar, suggesting a possible local single spillover event followed by limited human-to-human virus transmission.

The village where MVD was reported for the first time in Tanzania is the location of the Kanyangereko Cave, one of the largest Egyptian rousette bat roosting sites in the Kagera region, suggesting a likely source of the virus (*31*). High-risk human behavior and practices, including collection of bat-derived manure (guano) from caves for crop fertilization and direct contact with fruits partially eaten by Egyptian rousette bats, have been reported in the region, increasing the MARV spillover risk to humans (*9*,*31*). The possibility of virus dispersion from Kagera to other location in Tanzania or neighboring countries through movement of possibly infected bats cannot be excluded; average flight distances of 60.18 km for Egyptian rousette bats and interactions with other animal species and humans have been documented (*9*).

Reported MVD outbreaks in Africa, including within eastern Africa, highlight the growing MVD public threat (*32*). It is difficult to determine whether the number of MARV outbreaks has increased in recent years or if more cases have been identified through improved diagnostics capacity and public health surveillance systems. Investigation of MARV in Egyptian rousette bats in Tanzania is crucial to understand the extent of the risk posed to the human population in the Kagera region and beyond. The fact that the exact origin of the MVD outbreaks in Tanzania is not identified poses a continued threat to the population in the Kagera River basin. We recommend anthropologic and ecologic studies to identify the virus reservoirs and factors that enhance MVD transmission dynamics in this ecosystem.

Our findings indicated that genetically closely related MARV strains were responsible for the 2023 and 2025 MVD outbreak in Kagera region of Tanzania, which supports the hypothesis of a local zoonotic spillover event followed by limited human-to-human virus transmission. More MARV complete genomes from humans and bats and other reservoirs from eastern Africa countries are needed to accurately understand the evolution and spread pattern of MARV, which can help public health authorities to design effective prevention and control strategies. Furthermore, obtaining complete genome sequences during outbreaks are crucial for effective monitoring, management of new waves of infection, and improved understanding of the transmission dynamics.

Acknowledgments

We thank all development and implementing partners who supported the response to MVD outbreaks in Tanzania and in particular those who provided the technical assistance to the laboratory pillar, including the World Health Organization, the Africa Centres for Disease Control and Prevention, the East African Community, and the US Centers for Disease Control and Prevention.

About the Author

Dr. Mapunda is head of the virology department at the Tanzania National Public Health Laboratory. His primary research interests are pathogen genomics and public health surveillance.

References

1. Gonzalez JP, Souris M, Valdivia-Granda W. Global spread of hemorrhagic fever viruses: predicting pandemics. Methods Mol Biol. 2018;1604:3–31. https://doi.org/10.1007/978-1-4939-6981-4_1
2. Bloom DE, Cadarette D. Infectious disease threats in the twenty-first century: strengthening the global response. Front Immunol. 2019;10:549. https://doi.org/10.3389/fimmu.2019.00549
3. Geisbert TW. Marburg and Ebola hemorrhagic fevers (filoviruses). Mandell, Douglas, and Bennett's principles and practice of infectious diseases. 2015;1995–99:e1. https://doi.org/10.1016/B978-1-4557-4801-3.00166-1
4. Mahanty S, Bray M. Pathogenesis of filoviral haemorrhagic fevers. Lancet Infect Dis. 2004;4:487–98. https://doi.org/10.1016/S1473-3099(04)01103-X
5. Luby JP, Sanders CV. Green monkey disease ("Marburg virus" disease): a new zoonosis. Ann Intern Med. 1969;71:657–60. https://doi.org/10.7326/0003-4819-71-3-657
6. Siegert R, Shu HL, Slenczka HL, Peters D, Müller G. The aetiology of an unknown human infection transmitted by monkeys (preliminary communication). Ger Med Mon. 1968;13:1–2.
7. Wolf YI, Kazlauskas D, Iranzo J, Lucía-Sanz A, Kuhn JH, Krupovic M, et al. Origins and evolution of the global RNA virome. mBio. 2018;9:e02329-18. https://doi.org/10.1128/mbio.02329-18
8. Amman BR, Bird BH, Bakarr IA, Bangura J, Schuh AJ, Johnny J, et al. Isolation of Angola-like Marburg virus from Egyptian rousette bats from West Africa. Nat Commun. 2020;11:510. https://doi.org/10.1038/s41467-020-14327-8
9. Amman BR, Schuh AJ, Akurut G, Kamugisha K, Namanya D, Sealy TK, et al. Micro–global positioning systems for identifying nightly opportunities for Marburg virus spillover to humans by Egyptian rousette bats. Emerg Infect Dis. 2023;29:2238–45. https://doi.org/10.3201/eid2911.230362
10. Bausch DG, Borchert M, Grein T, Roth C, Swanepoel R, Libande ML, et al. Risk factors for Marburg hemorrhagic fever, Democratic Republic of the Congo. Emerg Infect Dis. 2003;9:1531–7. https://doi.org/10.3201/eid0912.030355
11. Eneh SC, Okonji OC, Chiburoma AG, Francisca Ogochukwu O, Tuwleh L, Gideon I, et al. Marburg virus disease amid COVID-19 in West Africa: an emerging and re-emerging zoonotic epidemic threat, future implications and way forward. Ther Adv Infect Dis. 2023;10:20499361231168520. https://doi.org/10.1177/20499361231168520
12. Ligon BL. Outbreak of Marburg hemorrhagic fever in Angola: a review of the history of the disease and its biological aspects. Semin Pediatr Infect Dis. 2005;16:219–24. https://doi.org/10.1053/j.spid.2005.05.001
13. Towner JS, Khristova ML, Sealy TK, Vincent MJ, Erickson BR, Bawiec DA, et al. Marburgvirus genomics and association with a large hemorrhagic fever outbreak in Angola. J Virol. 2006;80:6497–516. https://doi.org/10.1128/JVI.00069-06
14. Butera Y, Mutesa L, Parker E, Muvunyi R, Umumararungu E, Ayitewala A, et al. Genomic and transmission dynamics of the 2024 Marburg virus outbreak in Rwanda. Nat Med. 2025;31:422–6. https://doi.org/10.1038/s41591-024-03459-9
15. Kinimi E. Marburg virus disease in sub-Saharan Africa: a review of currently available comprehensive genomic data up to 2024. Zoonotic Dis. 2025;5:6. https://doi.org/10.3390/zoonoticdis5010006
16. World Health Organization. Marburg virus disease—Equatorial Guinea and the United Republic of Tanzania. 2023 [cited 2023 Nov 1]. https://www.who.int/emergencies/disease-outbreak-news/item/2023-DON467
17. Bankevich A, Nurk S, Antipov D, Gurevich AA, Dvorkin M, Kulikov AS, et al. SPAdes: a new genome assembly algorithm and its applications to single-cell sequencing. J Comput Biol. 2012;19:455–77. https://doi.org/10.1089/cmb.2012.0021
18. Li D, Liu CM, Luo R, Sadakane K, Lam TW. MEGAHIT: an ultra-fast single-node solution for large and complex metagenomics assembly via succinct de Bruijn graph. Bioinformatics. 2015;31:1674–6. https://doi.org/10.1093/bioinformatics/btv033
19. Gurevich A, Saveliev V, Vyahhi N, Tesler G. QUAST: quality assessment tool for genome assemblies. Bioinformatics. 2013;29:1072–5. https://doi.org/10.1093/bioinformatics/btt086
20. Katoh K, Standley DM. MAFFT multiple sequence alignment software version 7: improvements in performance and usability. Mol Biol Evol. 2013;30:772–80. https://doi.org/10.1093/molbev/mst010
21. Nguyen LT, Schmidt HA, von Haeseler A, Minh BQ. IQ-TREE: a fast and effective stochastic algorithm for estimating maximum-likelihood phylogenies. Mol Biol Evol. 2015;32:268–74. https://doi.org/10.1093/molbev/msu300
22. Kumar S, Stecher G, Suleski M, Sanderford M, Sharma S, Tamura K. MEGA12: Molecular Evolutionary Genetic Analysis version 12 for adaptive and green computing. Mol Biol Evol. 2024;41:msae263. https://doi.org/10.1093/molbev/msae263
23. Bouckaert R, Vaughan TG, Barido-Sottani J, Duchêne S, Fourment M, Gavryushkina A, et al. BEAST 2.5: an advanced software platform for Bayesian evolutionary analysis. PLoS Comput Biol. 2019;15:e1006650. https://doi.org/10.1371/journal.pcbi.1006650
24. Rambaut A, Drummond AJ, Xie D, Baele G, Suchard MA. Posterior summarization in Bayesian phylogenetics using Tracer 1.7. Syst Biol. 2018;67:901–4. https://doi.org/10.1093/sysbio/syy032
25. Hadfield J, Megill C, Bell SM, Huddleston J, Potter B, Callender C, et al. Nextstrain: real-time tracking of pathogen evolution. Bioinformatics. 2018;34:4121–3. https://doi.org/10.1093/bioinformatics/bty407
26. Sagulenko P, Puller V, Neher RA. TreeTime: maximum-likelihood phylodynamic analysis. Virus Evol. 2018;4:vex042. https://doi.org/10.1093/ve/vex042
27. Page AJ, Taylor B, Delaney AJ, Soares J, Seemann T, Keane JA, et al. *SNP-sites*: rapid efficient extraction of

SNPs from multi-FASTA alignments. Microb Genom. 2016;2:e000056. https://doi.org/10.1099/mgen.0.000056
28. Srivastava S, Sharma D, Kumar S, Sharma A, Rijal R, Asija A, et al. Emergence of Marburg virus: a global perspective on fatal outbreaks and clinical challenges. Front Microbiol. 2023;14:1239079. https://doi.org/10.3389/fmicb.2023.1239079
29. Amman BR, Carroll SA, Reed ZD, Sealy TK, Balinandi S, Swanepoel R, et al. Seasonal pulses of Marburg virus circulation in juvenile *Rousettus aegyptiacus* bats coincide with periods of increased risk of human infection. PLoS Pathog. 2012;8:e1002877. https://doi.org/10.1371/journal.ppat.1002877
30. Towner JS, Amman BR, Sealy TK, Carroll SAR, Comer JA, Kemp A, et al. Isolation of genetically diverse Marburg viruses from Egyptian fruit bats. PLoS Pathog. 2009; 5:e1000536. https://doi.org/10.1371/journal.ppat.1000536
31. Kinimi E, Joo-Yeon L, Jeong-Su L, Hee-Young L, Yim MS, Misinzo G, et al. Conservation and zoonotic risk implications of Egyptian fruit bats amid Marburg virus disease outbreaks in Tanzania and the broader sub-Saharan African region. Zoonotic Dis. 2025;5:30. https://doi.org/10.3390/zoonoticdis5040030
32. Simiyu B. Wafula, Ndabashinze R, Sah S, Bushi G, Mehta R, Verma A. First Marburg virus outbreak in Rwanda: a new public health challenge. Clin Infect Pract. 2024;24:100392. https://doi.org/10.1016/j.clinpr.2024.100392

Address for correspondence: Nyambura Moremi, United Republic of Tanzania Ministry of Health—National Public Health Laboratory, S.L.P. 9083, Dar es Salaam, United Republic of Tanzania; email: nyamburasogone@gmail.com

Emergence of New Delhi Metallo-β-Lactamase 14–Producing *Klebsiella pneumoniae* Sequence Type 147 Clone in Spain and Outbreak in the Canary Islands

Pablo Aja-Macaya,[1] Tania Blanco-Martín,[1] Cristian Mateo-León,[1] Cristóbal del Rosario-Quintana, Carmen Piña, Enrique de la Cruz-Tabares, Salud Rodríguez-Pallares, Lucía González-Pinto, Alejandro Beceiro, Marina Oviaño, Germán Bou, Diego García-Martínez de Artola,[2] Jorge Arca-Suárez[2]

The emergence of a high-risk New Delhi metallo-β-lactamase 14–producing *Klebsiella pneumoniae* sequence type 147 clone is of public health concern because of its rapid international spread. We report cross-border emergence and rapid dissemination of that clone in the Canary Islands, Spain, during 2023–2025. We analyzed 30 isolates recovered during 2023 in detail by reviewing clinical and epidemiologic data, conducting whole-genome sequencing to assess clonal relatedness and analyze resistomes, and performing antimicrobial susceptibility testing of novel therapeutic options through reference broth microdilution. The isolates formed a well-defined cluster, with minimal genomic distance and identical resistomes, confirming the local outbreak. Those clones were also closely related to other international New Delhi metallo-β-lactamase 14–producing *K. pneumoniae* sequence type 147 isolates, supporting the ongoing cross-border expansion of that clone. Aztreonam/avibactam was the most active therapeutic option (MICs ≤0.125 mg/L). Our findings highlight the need for close monitoring to prevent further dissemination of this clone.

The global rise of New Delhi metallo-β-lactamase (NDM)–producing *K. pneumoniae*, highlighted by surveillance programs such as ATLAS, is becoming an alarming concern (*1*). First detected in Europe in patients who had received healthcare in India in 2009 (*2*), NDM-producing strains have since spread widely, particularly among countries in Europe (*3*), and are closely associated with successful *K. pneumoniae* clones, including sequence types (ST) 147, 11, and 15 (*4*). In Spain, the first NDM-1–producing isolate was detected in 2009 in a *K. pneumoniae* isolate from a man from Spain who had received medical attention in India (*5*). Recent nationwide carbapenemase surveillance studies in Spain have reported prevalence rates of <5% for NDM-producing Enterobacterales in most regions but also a gradual spread across different geographic areas (*6*). However, according to recent data from the country's Network of Laboratories for the Surveillance of Resistant Microorganisms (RedLabRA; https://cnm.isciii.es/redlabra), among 6,756 carbapenemase-producing Enterobacterales (CPE) isolates detected in 2023, a total of 396 (7.9%) were NDM-producing *K. pneumoniae*, making this type the third most prevalent carbapenemase/microorganism association in Spain (*7*).

Among the lineages of *K. pneumoniae* involved in the spread of NDM enzymes, ST147 is likely one of

Author affiliations: Servicio de Microbiología Clínica and Instituto de Investigación Biomédica A Coruña (INIBIC), Complexo Hospitalario Universitario, A Coruña, Spain (P. Aja-Macaya, T. Blanco-Martín, S. Rodríguez-Pallares, L. González-Pinto, A. Beceiro, M. Oviaño, G. Bou, J. Arca-Suárez); CIBER de Enfermedades Infecciosas (CIBERINFEC), Instituto de Salud Carlos III, Madrid, Spain (T. Blanco-Martín, A. Beceiro, M. Oviaño, G. Bou, J. Arca-Suárez); Hospital Universitario Nuestra Señora de la Candelaria, Santa Cruz de Tenerife, Spain (C. Mateo-León, D. García-Martínez de Artola); Complejo Hospitalario Universitario Insular-Materno Infantil de Gran Canaria, Las Palmas de Gran Canaria, Spain (C. del Rosario-Quintana, C. Piña); Complejo Hospitalario Universitario Insular-Materno Infantil de Gran Canaria, Las Palmas de Gran Canaria (Enrique de la Cruz-Tabares)

DOI: https://doi.org/10.3201/eid3201.251504

[1]These first authors contributed equally to this article.

[2]These senior authors contributed equally to this article.

the most prevalent sequence types globally (*8*). That clone first appeared in the early 1990s and became globally disseminated over the next decade, probably catalyzed by successful selection of alterations in the quinolone resistance-determining regions, as well as by acquisition of the plasmid-encoded $bla_{CTX\text{-}M\text{-}15}$ (*9*). NDM-producing *K. pneumoniae* ST147 isolates have been circulating in Spain for at least a decade (*10*). Treatment of infection with those isolates represents a substantial challenge because the strains often carry multiple antimicrobial resistance determinants, including extended-spectrum β-lactamases, aminoglycoside-modifying enzymes, or other carbapenemases, such as *K. pneumoniae* carbapenemase or oxacillinase (OXA) 48–like oxacillinases (*11,12*). Moreover, NDM enzymes also display strong catalytic activity against most β-lactams and are increasingly associated with resistance to recently approved or investigational options, such as cefiderocol and cefepime/taniborbactam (*13,14*).

A total of 84 NDM carbapenemase variants had been described as of August 28, 2025 (*15*). Whereas most differ from the prototype NDM-1 by only 1 or a few amino acid substitutions, some of those variants have notable effects on β-lactam hydrolysis (e.g., NDM-5) or resistance to newly developed boronate inhibitors (e.g., NDM-9) (16,17). In 2023, an alarming report described rapid emergence and dissemination of an NDM-14–producing ST147 clone in France, a single NDM-1 amino acid variant (D130G) known to enhance carbapenem-hydrolyzing activity (*18*). The authors identified Morocco as a potential origin and noted high levels of antimicrobial resistance.

Within the framework of the Network of Diagnostic Laboratories for Healthcare-Associated Infection Surveillance in the Canary Islands (*19*), a total of 99 cases of infection with the ST147 clone were identified during January 2023–March 2025 across 3 islands. That outbreak of the NDM-14–producing clone in Spain is among the largest reported in Europe. In line with European Centre for Disease Prevention and Control guidelines for genomic surveillance and multicountry outbreak investigations, we performed a genomic surveillance study, assessed the outbreak's dimension, and evaluated newly developed therapeutic options to generate timely information for infection control and therapeutic alternatives.

Methods

Bacterial Isolates

During January 2023–March 2025, a total of 99 NDM-14–producing *K. pneumoniae* isolates were recovered from clinical or surveillance samples from patients admitted to 4 hospitals on 3 Canary Islands: the Complejo Hospitalario Universitario Insular-Materno Infantil (CHUIMI; Gran Canaria), the Hospital Universitario de Gran Canaria Doctor Negrín (Gran Canaria), the Hospital Universitario Doctor José Molina Orosa (Lanzarote), and the Hospital General de Fuerteventura Virgen de la Peña (Fuerteventura). The isolates were submitted to the reference laboratory of the Laboratory Network for Infection Surveillance System of the Canary Islands (RELAP; Hospital Universitario Nuestra Señora de la Candelaria, Tenerife, Spain). Of the 99 isolates, 30 corresponded to the first nonduplicate NDM-14–producing *K. pneumoniae* isolates identified in the archipelago, all recovered from patients admitted to CHUIMI in 2023. We further selected those 30 isolates for subsequent whole-genome sequence-guided phylogenomic analysis and evaluation of recently approved and investigational β-lactams and β-lactam/β-lactamase inhibitor combinations (Appendix 1 Table 1, https://wwwnc.cdc.gov/EID/article/32/1/25-1504-App1.xlsx).

Clinical and Epidemiologic Data Collection

We screened for carbapenemase production among patients admitted to CHUIMI (Appendix 2, https://wwwnc.cdc.gov/EID/article/32/1/25-1504-App2.pdf) and collected clinical and epidemiologic information related to patients with positive samples for NDM-14–producing *K. pneumoniae*. Researchers anonymized demographic and clinical data with an alphanumeric code and compiled complete details of each sample and the information collected in the initial 2023 outbreak (Appendix 1 Table 1).

Whole-Genome Sequencing

We sequenced the 30 isolates with an Illumina NovaSeq 6000 (https://www.illumina.com) and obtained total genomic DNA using a Genomic DNA Buffer Set with a Genomic-tip 20/G (QIAGEN, https://www.qiagen.com). We generated Illumina indexed paired-end libraries from a Nextera DNA XT Library Prep Kit (Illumina). In addition, we sequenced the isolate from the index case (I238) identified at CHUIMI, as well as isolate I542 (an NDM-14–producing *K. pneumoniae* isolate that belonged to a phylogenomically distant ST, 997), in parallel with a PacBio platform (Pacific Biosciences, https://www.pacb.com) to obtain high-quality hybrid assemblies and plasmid reconstruction. To understand the evolutionary trajectory, we also sequenced 3 isolates from 2024 (n = 1) and 2025 (n = 2) by using the Illumina NovaSeq 6000.

Bioinformatic Analysis

We quality controlled reads for bioinformatic assembly with Unicycler version 0.5.0 (https://github.com/rrwick/Unicycler), using a hybrid approach when possible. We then assessed reads for contamination and completeness by using CheckM version 1.1.3 (https://github.com/Ecogenomics/CheckM). We deposited raw reads and assemblies in the National Center for Biotechnology Information under Bioproject PRJNA1216752 and provide complete accession numbers for all databases (Appendix 1 Table 2).

Using *K. pneumoniae* ST147 isolate TGH13 (GenBank accession no. CP012745.1) as a reference, we performed core-genome phylogenomic analysis in snippy version 4.6.0 (https://github.com/tseemann/snippy) with the phylogenetically closest 863 ST147 international isolates from multiple databases (Appendix 1 Table 3). We created a phylogenomic tree by using fasttree version 2.1.11 (https://morgannprice.github.io/fasttree; parameters "-nt -gtr"). We described the complete methodology in detail, including phylogenomic analysis and genomic characterization of isolates (Appendix 2).

Antimicrobial Drug Susceptibility Testing

We tested for antimicrobial drug susceptibility by using Sensititer EUMDRXXF microdilution plates (Thermo Fisher Scientific, https://www.thermofisher.com), using reference broth microdilution assays with cation-adjusted Müeller-Hinton broth for newly developed β-lactam/β-lactamase inhibitor combinations, and, for cefiderocol, iron-depleted cation-adjusted Müeller-Hinton broth prepared according to Clinical and Laboratory Standards Institute guidelines (*20*). We interpreted MIC values according to EUCAST guidelines (*21*) (Appendix 1 Table 4).

Molecular Cloning

We cloned the genes $bla_{\text{NDM-1}}$ and $bla_{\text{NDM-14}}$ into pUCP-24, then transformed the recombinant plasmids by electroporation into *Escherichia coli* TG1 (wild-type permeability) and *E. coli* HB4 (OmpC and OmpF deficient) and selected on LB agar plates containing 10 mg/L of gentamicin. MICs were determined as described for drug susceptibility (Appendix 1 Table 5).

Results

Index Case

The first case of NDM-14–producing *Klebsiella pneumoniae* ST147 (strain I238) in this outbreak was identified on January 13, 2023, in a 34-year-old female patient admitted to CHUIMI. The patient, originally from Laayoune, administered by Morocco, was transferred for urgent intervention after she had a major bile duct injury develop as a complication of a laparoscopic cholecystectomy performed in Morocco in 2022. Bile duct reconstruction surgery was performed on December 28, 2022, and the NDM-14–producing ST147 *K. pneumoniae* isolate was detected 26 days later from the catheter tip and biliary drainage. Targeted intravenous colistin therapy was initiated (4.5 million IU/12 h for 12 days), and the patient was discharged after favorable clinical evolution with continued antimicrobial therapy and outpatient follow-up.

Epidemiologic Investigation, Outbreak Detection, and Current Extension

The hospital admission of the index case-patient subsequently caused a 3-case transmission event in the digestive surgery unit (ward 10S) at CHUIMI. Control measures were performed, including epidemiologic investigations; systematic screenings of carbapenemase-producing organisms, including culture and molecular-based approaches; enhanced hygiene; transfer to a dedicated high-risk ward (8N); cohorting of patients; and environmental sampling, if needed. Despite control efforts and apparent early containment of cases in ward 10S, RELAP later identified 98 additional NDM-14–producing ST147 *K. pneumoniae* isolates through March 2025, for a total of 99 isolates.

We compiled a comprehensive representation of the contribution of NDM-14–producing ST147 *K. pneumoniae* to the overall proportion of carbapenemase-producing *K. pneumoniae* isolates submitted by CHUIMI to RELAP during the study period (Figure 1). Isolates that fulfilled ≥1 of the following criteria were submitted: isolates from clinical samples associated with invasive infection (excluding colonization); isolates from clinical or environmental sources during outbreak or epidemic events; or detection of emerging pathogens requiring enhanced surveillance, including the NDM-14–producing *K. pneumoniae* isolates we describe. The peak of the reported cases occurred during June 2023–September 2024. During that period, the mean (±SD) percentage of submitted *K. pneumoniae* isolates producing NDM-14 among all submitted carbapenemase-producing *K. pneumoniae* isolates was 41.56% (SD ±14.40%). The maximum peak of incidence occurred in January 2024, when production of NDM-14 accounted for 67% of the 35 cases.

During the study period, most cases were identified at CHUIMI (n = 93), where the index case was detected. However, during 2024, additional cases

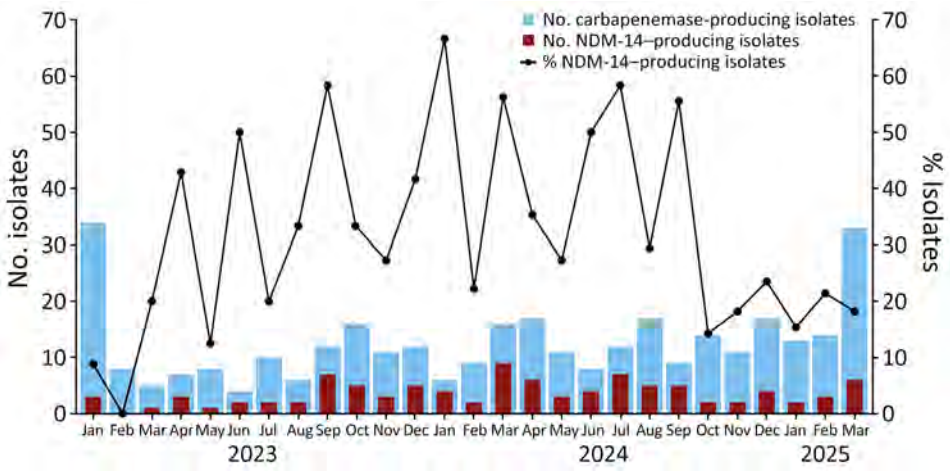

Figure 1. Carbapenemase-producing *Klebsiella pneumoniae* isolates submitted to the Laboratory Network for Infection Surveillance System of the Canary Islands by Complejo Hospitalario Universitario Insular-Materno Infantil (Gran Canaria) during January 2023–March 2025 from study of emergence of NDM-14–producing *K. pneumoniae* sequence type 147 clone in Spain and outbreak in the Canary Islands. Numbers and percentages of NDM-14–producing *K. pneumoniae* isolates compared with all isolates are shown. Isolates were submitted if they fulfilled ≥1 of the following criteria: recovery from clinical samples associated with invasive infection (excluding colonization); recovery from clinical or environmental sources during outbreak or epidemic events; or detection of emerging pathogens requiring enhanced surveillance, including the NDM-14–producing *K. pneumoniae* isolates described. NDM, New Delhi metallo-β-lactamase.

were also reported at Hospital Universitario de Gran Canaria Doctor Negrín (n = 4), a hospital in Gran Canaria, the same island as the index case, as well as at Hospital Universitario Doctor José Molina Orosa on the neighboring island of Lanzarote (n = 1) and Hospital General de Fuerteventura Virgen de la Peña on the neighboring island of Fuerteventura (n = 1). Those detections confirmed not only interhospital transmission but also cross-island emergence of NDM-14–producing ST147 *K. pneumoniae*.

To clarify the origin and early epidemiologic dynamics of that clone, we focused on the first 30 cases detected in 2023 at CHUIMI (Appendix 1 Table 1). The isolates were collected from patients across different medical and surgical wards: internal medicine (n = 12); general digestive surgery (n = 4); digestive, hematology, neurology, and neurosurgery (n = 2 each); and pneumology, endocrinology, emergency, vascular surgery, oncology, and infectious diseases (n = 1 each) (Appendix 1 Table 1). The spread of the clone among those wards and departments occurred despite implementation of control measures and could not be clearly linked or assigned to a specific reservoir or transmission chain on which to act, limiting the effectiveness of measures adopted for containment. The spread beyond the hospital was later reflected by cases detected through emergency services or with onset in the community, although most cases of community acquisition showed previous contact with healthcare institutions (data not shown).

Patients from whom isolates were recovered had a median age of 70.5 years (range 34–96 years); sex distribution was similar (17 [56.7%] male and 13 [44.3%] female). Median time from admission to positive $bla_{\text{NDM-14}}$ culture was 14 days (range 0–309 days) (Appendix 2 Figure 1). Most (n = 28) cases were in Canary Islands residents, despite the presence of 2 nonresidents (1 from Morocco, 1 from Germany) in the initial 3-case cluster in ward 10S. Most cases were colonization (19/30 [63.3%]), and 30-day mortality among patients with positive cultures was low (2/30 [6.7%]). With the exception of the index case-patient, who was treated with colistin, most patients with documented infection were treated with ceftazidime/avibactam combined with aztreonam (Appendix 1 Table 1).

Genomic Investigation and Cross-Border Emergence Linked to Morocco and France

We performed core-genome phylogenomic reconstruction of the 30 NDM-14–producing *K. pneumoniae* isolates identified at CHUIMI in comparison with the closest 863 genomes of the ST147 available in multiple databases and using the genome of *K. pneumoniae* isolate TGH13 (GenBank accession number CP012745.1) as reference. The NDM-14–producing ST147 *K. pneumoniae* isolates from the Canary Islands grouped into a cluster belonging to core-genome multilocus sequence type (MLST) 8081/8250 (Figure 2), which included other genetically related $bla_{\text{NDM-14}}$–positive ST147 *K. pneumoniae* isolates from other countries, such as France, the Netherlands, the United States, and the United Kingdom. Isolates from the Canary Islands formed a well-defined subcluster, highlighting their close phylogenomic relationship.

We detected 3 core-genome clusters of 5 single-nucleotide polymorphisms (SNPs) among the isolates (Appendix 2 Figure 2). The Canary Islands sublineage

had an average core-genome distance among any 2 isolates of 2.7 SNPs and a maximum distance of 9 SNPs. Finally, the mean (±SD) whole-genome distance of any Canary Islands isolate against the index case, I238, was 4 (± 3) mutations (including insertions and deletions). To visualize the strain evolution, we sequenced 3 additional isolates from 2024 (n = 1) and 2025 (n = 2) (Appendix 1 Table 2); those isolates showed an average whole-genome distance of 28 (± 13) mutations against I238.

Virulome, Resistome, and Plasmidome of NDM-14–Producing *K. pneumoniae* ST147 Isolates from the Canary Islands

Whole-genome sequencing analysis of the 30 isolates identified in 2023 (I238-I440) confirmed clonal dissemination of this ST147 clone (core-genome MLST ≈8081/8250; wzi64, O1/O2v1). Putative virulence was influenced by the presence of aerobactin (*iuc*) and yersiniabactin (*ybt*) and the absence of colibactin (*clb*). The multidrug-resistant profile was associated with the presence of multiple β-lactamase-encoding genes, including bla_{NDM-14}, $bla_{CTX-M-15}$, bla_{OXA-1}, bla_{OXA-9}, bla_{SHV-11}, and bla_{TEM-1}, as well as detection of a truncated *ompK35* (R60fs), impairing outer membrane permeability. Additional resistance determinants were identified for aminoglycosides (*aac(6')-Ib'*, *aac(6')-Ib-cr*, *aadA*, *aph(3')-VI*, *aph3-Ia*, *armA*), fluoroquinolones (*qnrS1*), and other antimicrobial families (*sul1*, *sul2*, *dfrA5*, *catB3*, *arr-3*, *mphA*, *mphE*, *mrx*, *msrE*). Furthermore, all isolates carried 6 plasmids: incompatiability group (Inc) FIB+IncHI1B (≈330 kbp), IncFIB (≈1,12 kbp),

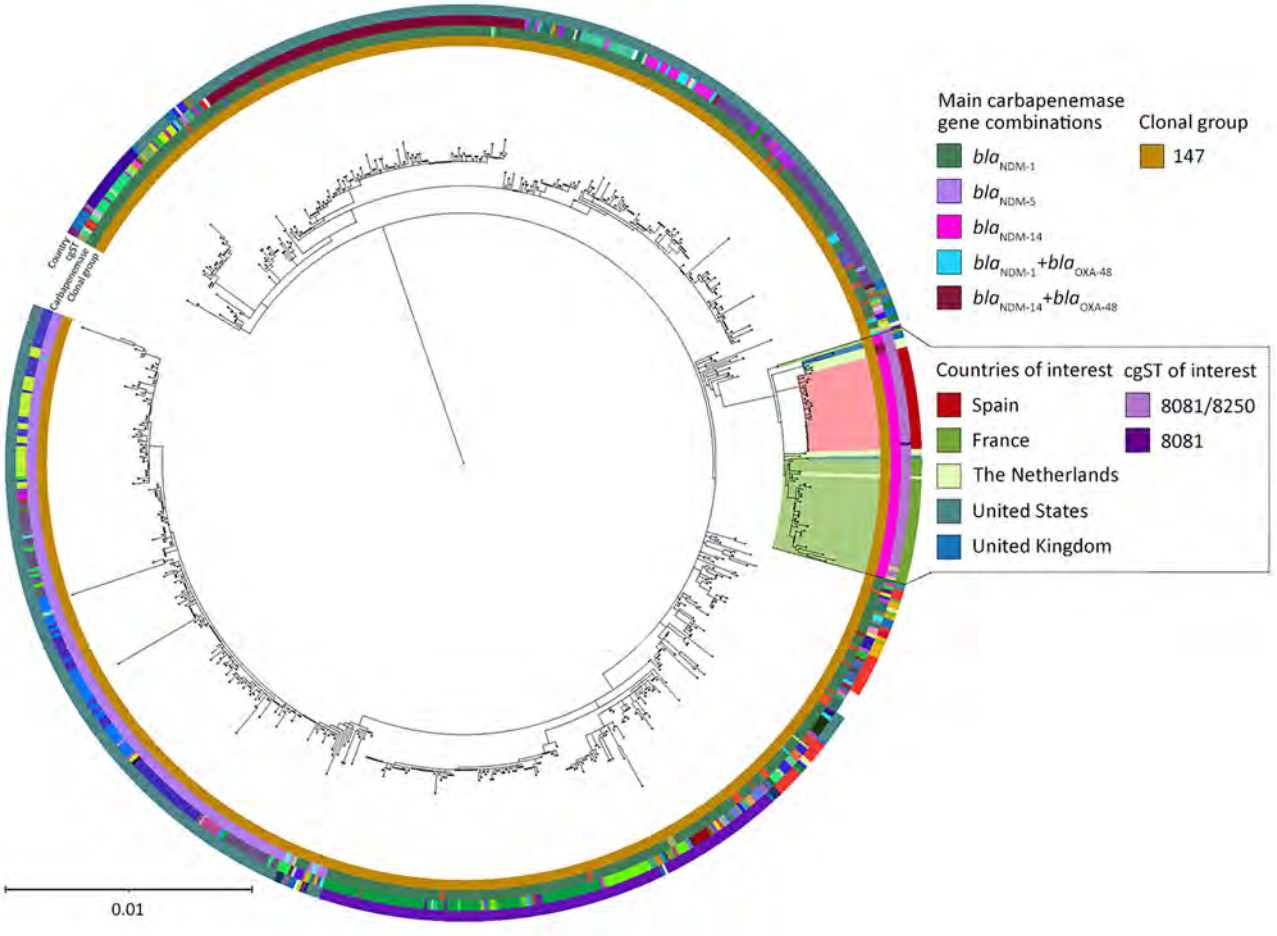

Figure 2. Core-genome phylogenomic tree of New Delhi metallo-β-lactamase (NDM) 14–producing *Klebsiella pneumoniae* ST147 isolates from a Canary Islands outbreak and related isolates from study of emergence of NDM-14–producing *K. pneumoniae* ST147 clone in Spain and outbreak in the Canary Islands. The tree includes the closest 863 genomes of *K. pneumoniae* isolates belonging to the ST147 clone, found in PasteurMLST (https://bigsdb.pasteur.fr/klebsiella), the National Center for Biotechnology Information Genome Database (https://www.ncbi.nlm.nih.gov/genome), and Pathogenwatch (https://pathogen.watch). Red shading indicates the Canary Island outbreak isolates; other countries and STs of interest are also highlighted. The most prevalent carbapenemases appearing in the dataset of the most similar isolates are noted. *K. pneumoniae* isolate TGH13 (GenBank accession no. CP012745.1) was used as the reference strain. Scale bar indicates nucleotide substitutions per site. cgST, core-genome ST; ST, sequence type.

IncFIB (54 kbp), IncR (≈40 kbp), Col(pHAD28) (4 kbp), and ColRNAI (≈9 kbp). Of note, the *bla*$_{NDM-14}$ gene was located on the nonconjugative IncFIB plasmid of ≈54 kbp. We compiled comparative data regarding the differential genomic features of the isolates from the Canary Islands cluster with other nearby isolates (Figure 2; Appendix 2 Figure 2).

Genetic Context of β-Lactamases

The *bla*$_{NDM-14}$ gene was embedded in an IncFIB (54 kbp) plasmid also carrying *bla*$_{CTX-M-15}$ and *bla*$_{OXA-1}$. Another large IncFIB+IncHI1B (≈330 kbp) plasmid harbored multiple resistance genes but also multiple conjugative transfer proteins not present in the IncFIB (54 kbp) plasmid. Of particular interest, an additional isolate, designated I542, which corresponded to a *bla*$_{NDM-14}$–positive *K. pneumoniae* sample detected during the outbreak but belonging to a phylogenomically distant sequence type (ST997), also carried the same plasmids, which confirmed the ability of the *bla*$_{NDM-14}$ gene to spread horizontally among different *K. pneumoniae* sequence types. We further analyzed the IncFIB+IncHI1B (≈330 kbp) and IncFIB (54 kbp) plasmids and compared them with international isolates and MLSTs (Figure 3), finding that they matched almost perfectly with each other. Further analysis of the pNDM-14 plasmid (Figure 4) showed complete synteny at the nucleotide level. The *bla*$_{NDM-14}$ gene was surrounded by an S630 family ISSpu2 transposase upstream and an IS6 family IS15DIV transposase downstream.

Antimicrobial Susceptibility to β-Lactams and β-Lactam/β-Lactamase Inhibitor Combinations and Mechanisms of Cefepime/Taniborbactam Resistance

Among the 30 *K. pneumoniae* clinical isolates associated with the outbreak, the most active antimicrobial combinations were aztreonam/avibactam and aztreonam/nacubactam, both demonstrating activity against the whole collection (100% susceptibility rate; 30/30 isolates). Aztreonam/avibactam showed the greatest potency; 50% MIC and 90% MIC values were both 0.125 mg/L. Combinations of cefepime with the novel diazabicyclooctane β-lactamase inhibitors zidebactam and nacubactam also exhibited high levels of activity; susceptibility rates were 96.7% (29/30 isolates), and MIC ranges were 1–16 mg/L for zidebactam and 2 to >32 mg/L for nacubactam. Cefiderocol and colistin both demonstrated similarly high susceptibility rates (96.7% susceptibility rate; 29/30 isolates);

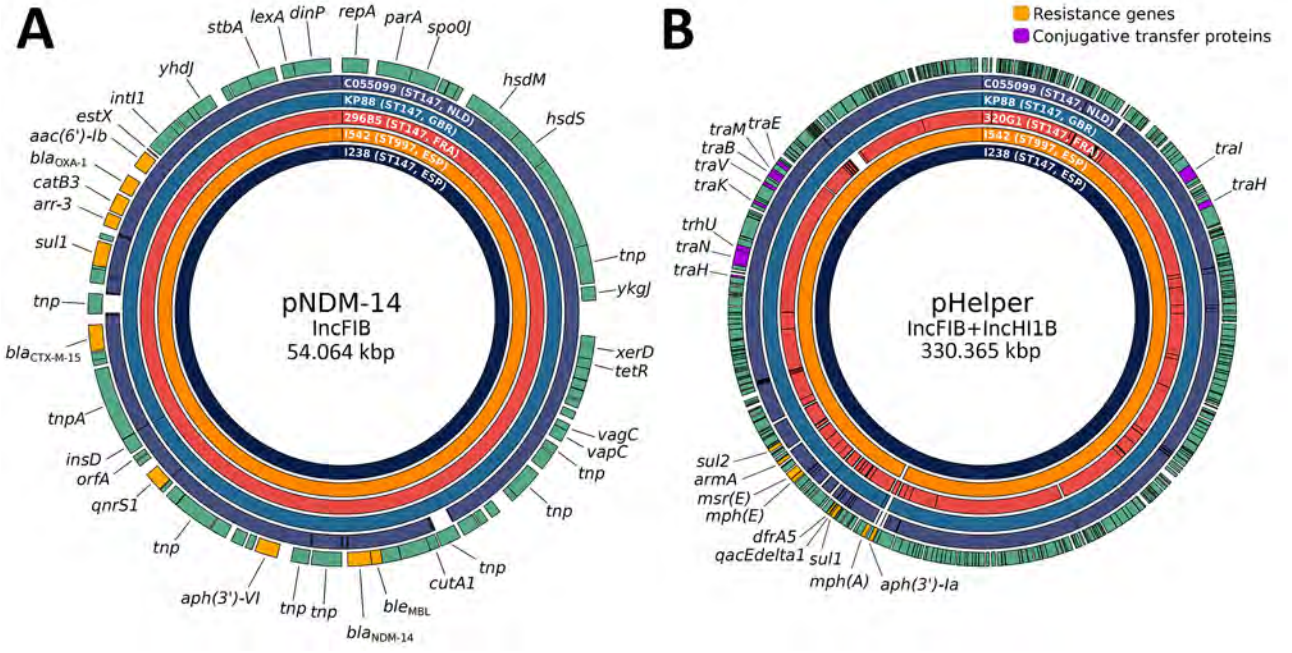

Figure 3. Comparison of 2 of the most relevant plasmids in isolates from study of emergence of New Delhi metallo-β-lactamase (NDM) 14–producing *Klebsiella pneumoniae* ST147 clone in Spain and outbreak in the Canary Islands. The *bla*$_{NDM-14}$–containing plasmid pNDM-14 (A) and its probable helper for conjugation and intraspecies transmission pHelper (B) are shown, comparing multiple *K. pneumoniae* ST147 strains from different countries (Spain, I238; France, 296B5 and 320G1; United Kingdom, KP88; the Netherlands, C055099) and a phylogenomically distant *K. pneumoniae* ST997 carrying the same plasmids (I542, Spain). The outer ring shows loci, including resistance genes and conjugative transfer proteins. Because of the large size of pHelper, only those 2 types of features are shown. The other rings represent the presence or absence of parts of the plasmid relative to the I238 reference plasmid. ESP, Spain; FRA, France; GBR, United Kingdom; Inc, incompatibility group; NLD, the Netherlands; ST, sequence type.

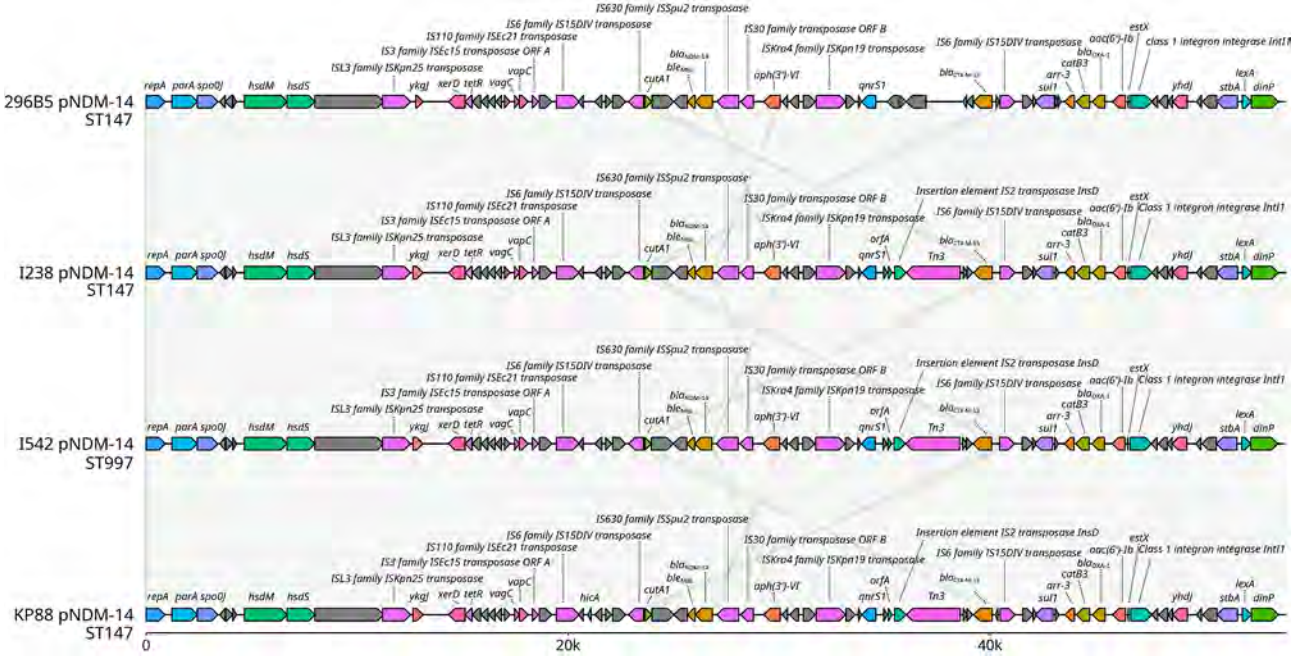

Figure 4. Detailed comparison of circularized *bla*$_{NDM-14}$ plasmids from study of emergence of New Delhi metallo-β-lactamase (NDM) 14–producing *Klebsiella pneumoniae* ST147 clone in Spain and outbreak in the Canary Islands. Plasmids are from multiple countries (Spain, I238 and I542; France, 296B5; United Kingdom, KP88) and 2 different STs. Gray lines indicate synteny at the nucleotide level. Gray shading indicates loci without gene names or named hypothetical proteins; other colors are randomized on the basis of gene order. *ble*$_{MBL}$, bleomycin resistance gene; CTX, cholera toxin; IS, insertion sequence; ORF, open reading frame; OXA, oxacillin; pNDM-14, NDM-14–producing plasmid; ST, sequence type.

cefiderocol displayed a MIC range of 1–4 mg/L and a 50%/90% MIC of 2/2 mg/L, at the clinical breakpoint for susceptibility.

By contrast, all isolates were resistant to piperacillin/tazobactam, ceftazidime, ceftazidime/avibactam, cefepime, aztreonam, imipenem, imipenem/relebactam, meropenem, meropenem/vaborbactam, tobramycin, and amikacin (Appendix 1 Table 4). Of note, the combination of cefepime and the boronate-type β-lactamase inhibitor taniborbactam showed limited activity, inhibiting only 10% of isolates (3/30), with MIC values ranging from 4 to 32 mg/L.

We also evaluated production of NDM-1 or NDM-14 β-lactamases in either the wild-type *E. coli* TG1 host or the porin-deficient *E. coli* HB4 host (Appendix 1 Table 5). The susceptibility profile remained largely unchanged between hosts, with the notable exception of cefepime/taniborbactam, for which the MIC increased substantially, from 4 mg/L in *E. coli* TG1 to 64 mg/L in *E. coli* HB4.

Discussion

RELAP (*19*) was launched in 2022, aligning with the European Centre for Disease Prevention and Control roadmap for integrating genomic typing in surveillance and outbreak investigations (*22*). The network provides timely, high-resolution WGS-based data on pathogen emergence within the archipelago, with particular focus on high-priority carbapenem-resistant Enterobacterales designated by the World Health Organization.

Using that network, RELAP, located in Tenerife (Spain), was able to carry out WGS-guided monitoring of the emergence of a large outbreak caused by a highly resistant NDM-14–producing *K. pneumoniae* ST147 clone in the Canary Islands. The outbreak affected 99 patients and spread rapidly across 4 hospitals on 3 islands in 27 months. Whereas the ST147 *K. pneumoniae* clone is a known disseminator of NDM-type carbapenemases (*23*,*24*), its association with the NDM-14 enzyme had not previously been reported in Spain. Our findings are consistent with and expand upon a previous report of this clone's involvement in multiple outbreaks across France (*18*). Direct epidemiologic links with Morocco were detected in both the Canary Islands and France outbreaks.

The Canary Islands' insular geography makes them highly vulnerable to pathogen importation through intense cross-border mobility (e.g., tourism, medical transfers), whereas their compartmentalized structure contributes to concentrated early transmission within a single island. This effect is further

amplified by a tightly interconnected healthcare circuit relying on few reference hospitals, but interisland mobility eventually enables dissemination to other islands. Consequently, whereas the focal nosocomial cluster in this outbreak was controlled, the lineage appears to have disseminated across the community and various islands through patient movement and interisland healthcare referral, no longer limited to a single transmission chain or hospital ward. Therefore, the situation seems to have evolved from a focal outbreak to a scenario of cryptic dissemination. Those aspects highlight the necessity for robust surveillance measures to limit CPE spread in island settings, reinforcing the importance of surveillance networks using high-resolution, WGS-guided methods for rapid outbreak typing and control.

Comparative genomic analysis of the first 30 cases of the outbreak confirmed the NDM-14 enzyme was not acquired by existing *K. pneumoniae* ST147 lineages circulating in Spain, where this clone has been present for more than a decade (*25*,*26*). None of the outbreak isolates were clustered with previously reported ST147 genomes from Spain, suggesting a recent introduction of this specific sublineage of the clone into the country. All isolates from the Canary Island outbreak (average core-genome SNP distance of 2.7) fell within the clonality range (*27*). We also found them to be closely related to NDM-14–producing ST147 *K. pneumoniae* isolates from France, further supporting the hypothesis of a common origin in North Africa, where this high-risk clone was reported in 2025 (*28*). Its presence in the Netherlands, the United States, and the United Kingdom further underscores its global spread. Recent public health communications have argued for improved surveillance of NDM-producing isolates in patients transferred from Ukraine (*29*,*30*). In this context, the ongoing outbreaks in France and the Canary Islands, both linked to patients transferred from Morocco, also illustrate the need to maintain and reinforce surveillance on patient transfers from neighboring North Africa regions with a high burden of CPEs, such as Morocco (*28*), Tunisia (*31*), and Egypt (*32*).

The Canary Islands isolates' resistome showed remarkable similarity to other NDM-14–producing *K. pneumoniae* isolates publicly available, including carriage of $bla_{\text{NDM-14}}$, $bla_{\text{CTX-M-15}}$, $bla_{\text{OXA-1}}$, $bla_{\text{OXA-9}}$, $bla_{\text{SHV-11}}$, and $bla_{\text{TEM-1}}$. All those genes are also present in genomes found in France, the Netherlands, the United States, and the United Kingdom, highlighting the still limited evolution of the β-lactam resistance mechanisms in this expanding strain. Alarmingly, some recent isolates from the Canary Islands appear to have also acquired $bla_{\text{OXA-48}}$, as observed in the Netherlands. Another worrying finding is the first identification of the NDM-14–bearing plasmid outside of the ST147 clone in a phylogenomically distant *K. pneumoniae* ST997 isolate from the Canary Islands. Of note, that isolate not only contained the $bla_{\text{NDM-14}}$ IncFIB (54 kbp) plasmid, which lacks putative genes involved in mobilization, but also the pHelper plasmid previously found to be necessary for transmission. Those observations confirm previous laboratory conjugation experiments (*18*) and demonstrate that conjugation can also occur between clinical strains, highlighting that this gene might disseminate further. Currently, its interspecies distribution seems limited to *Acinetobacter lwoffii* and *K. pneumoniae*. A very similar $bla_{\text{NDM-1}}$–carrying ≈54 kbp IncFIB plasmid has been seen in Enterobacterales, primarily in *K. pneumonia*e in multiple STs globally. Nonetheless, the NDM-14 variant has only been detected in isolates epidemiologically associated with the North Africa region. That fact, combined with the distinct clustering of the *K. pneumoniae* lineage in which it appears, strongly suggests that the $bla_{\text{NDM-14}}$–carrying plasmid evolved independently within the North Africa region from a common $bla_{\text{NDM-1}}$ ancestor.

NDM-producing Enterobacterales are commonly resistant to all classic β-lactams, including aztreonam because of simultaneous production of AmpCs or extended-spectrum β-lactamases. As expected, all our isolates fit this assumption. Cefiderocol was active against the first 30 outbreak isolates analyzed here, although in all cases, MICs were borderline at 2 mg/L. The use of cefiderocol against NDM-producing Enterobacterales is to some extent concerning, because of measurable hydrolysis of this cephalosporin at the biochemical level (*33*) but also because of previously reported cases of drug resistance. By contrast, aztreonam/avibactam was highly active (MICs ≤0.125–0.25 mg/L), as previously reported (*18*), confirming that combination as the therapeutic option of choice for combating infections caused by the strain. We also analyzed the performance of some developmental combinations in clinical trial evaluation (cefepime/taniborbactam [*34*,*35*], cefepime/zidebactam [*36*], cefepime/nacubactam [*37*], and aztreonam/nacubactam [*37*]) with potential activity against MBL-producing Enterobacterales. However, none of those options was more active than aztreonam/avibactam, because none of them yielded MICs <1 mg/L, thus reinforcing the prominent role that aztreonam/avibactam is expected to have against NDM-producing Enterobacterales in the future (*38*). However, of concern is that some of the

newly developed agents, particularly cefepime/taniborbactam, for which phase 3 clinical trial evaluations have recently been completed (*39*), were not active against many of the isolates included here (considering a clinical breakpoint of 4 mg/L). Resistance to that combination might not be caused by direct NDM-mediated resistance to taniborbactam inhibition but instead by a combination of NDM production with loss-of-function mutations affecting the *ompK35* porin channel, as previously observed (*40*). Parallel production of both NDM-1 and NDM-14 in wild-type (*E. coli* TG1) and porin-deficient (*E. coli* HB4) hosts confirmed that NDM production under low-permeability conditions markedly increases cefepime MICs (from 64–128 to >256 mg/L) and cefepime/taniborbactam MICs (from 4 to 64 mg/L), providing further evidence on the interplay between NDM production and reduced outer membrane permeability in cefepime/taniborbactam resistance.

In conclusion, we report a large outbreak and the rapid, widespread emergence of NDM-14–producing *K. pneumoniae* ST147 in the Canary Islands of Spain during 2023–2025. The outbreak began after the direct transfer of a patient from Morocco. This clone is genetically closely related to isolates currently expanding in France and other countries, thus highlighting its clonal cross-border dissemination. The study findings also demonstrate that the blaNDM-14–carrying plasmid can be efficiently transferred to distantly related K. pneumoniae lineages and investigational β-lactam/β-lactamase inhibitor combinations show limited activity against these strains, for which aztreonam/avibactam is likely to become a key therapeutic option in severe infections.

No ethics approval was needed for this outbreak investigation. Demographic and clinical data were anonymized with an alphanumeric code. Raw reads and produced assemblies are available in the National Center for Biotechnology Information (BioProject no. PRJNA1216752). Complete accession numbers (BioSample, Sequence Read Archive, GenBank) are provided in Appendix 1 Table 2.

This work was supported by the Instituto de Salud Carlos III (ISCIII project nos. PI24/00920, PI23/00851, and PI22/01212) and co-funded by the European Union. The research was also funded by Centro de Investigación Biomédica en Red de Enfermedades Infecciosas (CIBERINFEC; CB21/13/00055), integrated in the National Plan for Scientific Research, Development and Technological Innovation 2013-2016, and funded by the ISCIII-General Subdirection of Assessment and Promotion of the Research-European Regional Development Fund (FEDER) "A way of making Europe." The study was also funded by Axencia Galega de Innovacion (GAIN), Conselleria de Innovacion, Conselleria de Emprego e Industria through "Proxectos de excelencia" (IN607D 2021/12 to A.B. and IN607D 2024/008 to J.A.-S.) and "Axudas para a consolidación de grupos de investigación que pola súa produción científica e a súa actividade de I + D constitúan unha referencia no Sistema galego de I + D + I" (IN607A 2024/09 to G.B.). T.B.-M. was financially supported by the Río Hortega Program (ISCIII, CM23/00095). S.R.-P. was financially supported by the Río Hortega Program (ISCIII, CM23/00104). L.G.-P. was financially supported by the PFIS Program (ISCIII, FI23/00074). J.A.-S. was financially supported by the Juan Rodés Program (ISCIII, JR21/00026).

P.A.-M, T.B.-M, C.M.-L, C.R.-Q, C.P, E.C.-T, S.R.-P, L.G.-P, A.B., and M.O performed the main investigation and analyzed the data. D.G.-M.A., G.B., and J.A.-S. conceived, designed, and supervised the study. All authors analyzed and interpreted the data, revised the manuscript, and approved the final version of the article.

About the Author

Mr. Aja-Macaya is a bioinformatician in the Microbiology Service of the University Hospital of A Coruña, A Coruña, Spain. His research interests involve working with multidrug-resistant pathogens through genomics.

References

1. Wise MG, Karlowsky JA, Mohamed N, Hermsen ED, Kamat S, Townsend A, et al. Global trends in carbapenem- and difficult-to-treat-resistance among World Health Organization priority bacterial pathogens: ATLAS surveillance program 2018-2022. J Glob Antimicrob Resist. 2024;37:168–75. https://doi.org/10.1016/j.jgar.2024.03.020
2. Kumarasamy KK, Toleman MA, Walsh TR, Bagaria J, Butt F, Balakrishnan R, et al. Emergence of a new antibiotic resistance mechanism in India, Pakistan, and the UK: a molecular, biological, and epidemiological study. Lancet Infect Dis. 2010;10:597–602. https://doi.org/10.1016/S1473-3099(10)70143-2
3. Johnson AP, Woodford N. Global spread of antibiotic resistance: the example of New Delhi metallo-β-lactamase (NDM)-mediated carbapenem resistance. J Med Microbiol. 2013;62:499–513. https://doi.org/10.1099/jmm.0.052555-0
4. Pérez-Vázquez M, Sola Campoy PJ, Ortega A, Bautista V, Monzón S, Ruiz-Carrascoso G, et al.; Spanish NDM Study Group. Emergence of NDM-producing *Klebsiella pneumoniae* and *Escherichia coli* in Spain: phylogeny, resistome, virulence and plasmids encoding $bla_{\text{NDM-like}}$ genes as determined by WGS. J Antimicrob Chemother. 2019;74:3489–96. https://doi.org/10.1093/jac/dkz366
5. Oteo J, Domingo-García D, Fernández-Romero S, Saez D, Guiu A, Cuevas O, et al. Abdominal abscess due to NDM-1-producing *Klebsiella pneumoniae* in Spain. J Med Microbiol. 2012;61:864–7. https://doi.org/10.1099/jmm.0.043190-0

6. Cañada-García JE, Moure Z, Sola-Campoy PJ, Delgado-Valverde M, Cano ME, Gijón D, et al.; GEMARA/GEIRAS-SEIMC/REIPI CARB-ES-19 Study Group. CARB-ES-19 multicenter study of carbapenemase-producing *Klebsiella pneumoniae* and *Escherichia coli* from all Spanish provinces reveals interregional spread of high-risk clones such as ST307/OXA-48 and ST512/KPC-3. Front Microbiol. 2022;13:1331657. https://doi.org/10.3389/fmicb.2022.918362
7. Cañada-García JE, Pérez-Vázquez M, Oteo-Iglesias J. RedLabRA: Molecular surveillance of carbapenemase-producing *Klebsiella pneumoniae, Enterobacter cloacae* complex, and *Escherichia coli* in Spain. RedLabRA Annual Report 2023 [in Spanish]. Majadahonda (Madrid): Instituto de Salud Carlos III, Centro Nacional de Microbiología; 2025 [cited 2025 Dec 3]. https://cnm.isciii.es/redlabra
8. Peirano G, Chen L, Kreiswirth BN, Pitout JDD. Emerging antimicrobial-resistant high-risk *Klebsiella pneumoniae* clones ST307 and ST147. Antimicrob Agents Chemother. 2020;64:e01148–20. https://doi.org/10.1128/AAC.01148-20
9. Rodrigues C, Desai S, Passet V, Gajjar D, Brisse S. Genomic evolution of the globally disseminated multidrug-resistant *Klebsiella pneumoniae* clonal group 147. Microb Genom. 2022;8:000737. https://doi.org/10.1099/mgen.0.000737
10. Arca-Suárez J, Rodiño-Janeiro BK, Pérez A, Guijarro-Sánchez P, Vázquez-Ucha JC, Cruz F, et al.; GEMARA-SEIMC/REIPI Enterobacterales Study Group. Emergence of 16S rRNA methyltransferases among carbapenemase-producing Enterobacterales in Spain studied by whole-genome sequencing. Int J Antimicrob Agents. 2022;59:106456. https://doi.org/10.1016/j.ijantimicag.2021.106456
11. Sandfort M, Hans JB, Fischer MA, Reichert F, Cremanns M, Eisfeld J, et al. Increase in NDM-1 and NDM-1/OXA-48-producing *Klebsiella pneumoniae* in Germany associated with the war in Ukraine, 2022. Euro Surveill. 2022;27:2200926. https://doi.org/10.2807/1560-7917.ES.2022.27.50.2200926
12. Rigatou A, Afolayan AO, Tatsi EB, Deliolanis I, Michos A, Reuter S, et al. Double carbapenemases in *Klebsiella pneumoniae* blood isolates: dissemination in a single medical center via multiple plasmids and a variety of highly efficient clones. Antimicrob Agents Chemother. 2025;69:e0146224. https://doi.org/10.1128/aac.01462-24
13. Blanco-Martín T, Alonso-García I, González-Pinto L, Outeda-García M, Guijarro-Sánchez P, López-Hernández I, et al.; GEMARA/SEIMC-CIBERINFEC Study Group on the activity and resistance mechanisms to new β-lactams and β-lactamase inhibitors (PROTECT). Activity of cefiderocol and innovative β-lactam/β-lactamase inhibitor combinations against isogenic strains of *Escherichia coli* expressing single and double β-lactamases under high and low permeability conditions. Int J Antimicrob Agents. 2024;63:107150. https://doi.org/10.1016/j.ijantimicag.2024.107150
14. Warecki BA, Tomatis PE, Mojica MF, Bethel CR, Rodríguez Saravia M, Drusin SI, et al. Cefiderocol "under siege"? Understanding the rise of NDM-mediated resistance to novel agents. Chem Sci (Camb). 2025;16:12519–33. https://doi.org/10.1039/D5SC02122G
15. Naas T, Oueslati S, Bonnin RA, Dabos ML, Zavala A, Dortet L, et al. Beta-lactamase database (BLDB) - structure and function. J Enzyme Inhib Med Chem. 2017;32:917–9. https://doi.org/10.1080/14756366.2017.1344235
16. Hornsey M, Phee L, Wareham DW. A novel variant, NDM-5, of the New Delhi metallo-β-lactamase in a multidrug-resistant *Escherichia coli* ST648 isolate recovered from a patient in the United Kingdom. Antimicrob Agents Chemother. 2011;55:5952–4. https://doi.org/10.1128/AAC.05108-11
17. Le Terrier C, Gruenig V, Fournier C, Nordmann P, Poirel L. NDM-9 resistance to taniborbactam. Lancet Infect Dis. 2023;23:401–2. https://doi.org/10.1016/S1473-3099(23)00069-5
18. Emeraud C, Mahamat A, Jousset AB, Bernabeu S, Goncalves T, Pommier C, et al. Emergence and rapid dissemination of highly resistant NDM-14-producing *Klebsiella pneumoniae* ST147, France, 2022. Euro Surveill. 2023;28:2300095. https://doi.org/10.2807/1560-7917.ES.2023.28.42.2300095
19. Servicio Canario de la Salud. Instruction no. 3/2022, from the director of the Canary Islands health service establishing the Canary Islands network of microbiology laboratories to support the healthcare-associated infection surveillance system for the control and monitoring of resistant microorganisms [in Spanish]. Gobierno de Canarias. 2022 [cited 2025 Dec 3]. https://www3.gobiernodecanarias.org/sanidad/scs/content/b9e742a3-0466-11ee-8455-eff8b3f8079e/Intruccion_3_22.pdf
20. Clinical and Laboratory Standards Institute. Performance standards for antimicrobial susceptibility testing, 34th edition (M100-S34). Wayne (PA): The Institute; 2024.
21. European Committee on Antimicrobial Susceptibility Testing. Clinical breakpoints (v. 15.0). Växjö (Sweden); The Committee; 2025.
22. European Centre for Disease Prevention and Control. ECDC strategic framework for the integration of molecular and genomic typing into European surveillance and multi-country outbreak investigations. Stockholm: The Centre; 2019.
23. Marí-Almirall M, Cosgaya C, Pitart C, Viñes J, Muñoz L, Campo I, et al.; MERCyCAT Study Group. Dissemination of NDM-producing *Klebsiella pneumoniae* and *Escherichia coli* high-risk clones in Catalan healthcare institutions. J Antimicrob Chemother. 2021;76:345–54. https://doi.org/10.1093/jac/dkaa459
24. Linkevicius M, Alm E, Roer L, Svartström O, Dada-Olorunwa M, Räisänen K, et al. Cross-border spread of a mosaic resistance (OXA-48) and virulence (aerobactin) plasmid in *Klebsiella pneumoniae*: a European Antimicrobial Resistance Genes Surveillance Network investigation, Europe, February 2019 to October 2024. Euro Surveill. 2025;30:2500439. https://doi.org/10.2807/1560-7917.ES.2025.30.27.2500439
25. Papagiannitsis CC, Izdebski R, Baraniak A, Fiett J, Herda M, Hrabák J, et al.; MOSAR WP2, WP3 and WP5 study groups; MOSAR WP2 WP3 and WP5 study groups. Survey of metallo-β-lactamase-producing *Enterobacteriaceae* colonizing patients in European ICUs and rehabilitation units, 2008-11. J Antimicrob Chemother. 2015;70:1981–8. https://doi.org/10.1093/jac/dkv055
26. Oteo J, Ortega A, Bartolomé R, Bou G, Conejo C, Fernández-Martínez M, et al.; GEIH-GEMARA (SEIMC) and REIPI. Prospective multicenter study of carbapenemase-producing *Enterobacteriaceae* from 83 hospitals in Spain reveals high in vitro susceptibility to colistin and meropenem. Antimicrob Agents Chemother. 2015;59:3406–12. https://doi.org/10.1128/AAC.00086-15
27. Schürch AC, Arredondo-Alonso S, Willems RJL, Goering RV. Whole genome sequencing options for bacterial strain typing and epidemiologic analysis based on single nucleotide polymorphism versus gene-by-gene-based approaches. Clin Microbiol Infect. 2018;24:350–4. https://doi.org/10.1016/j.cmi.2017.12.016
28. Khazaz A, El Otmani F, Benzaarate I, El Hamouchi A, Bourjilat F, Brisse S, et al. First detection of the high-risk

Klebsiella pneumoniae ST147 clone producing NDM-14 in a community setting in Morocco: A new public health concern. J Glob Antimicrob Resist. 2025;40:96–7. https://doi.org/10.1016/j.jgar.2024.11.010
29. Pallett SJC, Morkowska A, Woolley SD, Potochilova VV, Rudnieva KL, Iungin OS, et al. Evolving antimicrobial resistance of extensively drug-resistant Gram-negative severe infections associated with conflict wounds in Ukraine: an observational study. Lancet Reg Health Eur. 2025;52:101274. https://doi.org/10.1016/j.lanepe.2025.101274
30. Witteveen S, Hans JB, Izdebski R, Hasman H, Samuelsen Ø, Dortet L, et al. Dissemination of extensively drug-resistant NDM-producing *Providencia stuartii* in Europe linked to patients transferred from Ukraine, March 2022 to March 2023. Euro Surveill. 2024;29:2300616. https://doi.org/10.2807/1560-7917.ES.2024.29.23.2300616
31. Jaidane N, Tilouche L, Oueslati S, Girlich D, Azaiez S, Jacquemin A, et al. Clonal dissemination of NDM-producing *Proteus mirabilis* in a teaching hospital in Sousse, Tunisia. Pathogens. 2025;14:298. https://doi.org/10.3390/pathogens14030298
32. Gamal D, Fernández-Martínez M, Salem D, El-Defrawy I, Montes LÁ, Ocampo-Sosa AA, et al. Carbapenem-resistant *Klebsiella pneumoniae* isolates from Egypt containing bla_{NDM-1} on IncR plasmids and its association with *rmtF*. Int J Infect Dis. 2016;43:17–20. https://doi.org/10.1016/j.ijid.2015.12.003
33. Poirel L, Sadek M, Nordmann P. Contribution of PER-type and NDM-type β-lactamases to cefiderocol resistance in *Acinetobacter baumannii.* Antimicrob Agents Chemother. 2021;65:e0087721. https://doi.org/10.1128/AAC.00877-21
34. ClinicalTrials.gov. Safety and efficacy study of cefepime/VNRX-5133 in patients with complicated urinary tract infections (CERTAIN-1). 2019 [cited 2025 Dec 3]. https://clinicaltrials.gov/study/NCT03840148
35. ClinicalTrials.gov. Cefepime-taniborbactam vs meropenem in adults with VABP or ventilated HABP (CERTAIN-2). 2024 [cited 2025 Dec 3]. https://www.clinicaltrials.gov/study/NCT06168734
36. ClinicalTrials.gov. Study of cefepime-zidebactam (FEP-ZID) in complicated urinary tract infection (cUTI) or acute pyelonephritis (AP). 2021 [cited 2025 Dec 3]. https://clinicaltrials.gov/study/NCT04979806
37. ClinicalTrials.gov. P3 study to assess efficacy and safety of cefepime/nacubactam and aztreonam/nacubactam versus best available therapy for adults with infection due to carbapenem resistant Enterobacterales (Integral-2). 2023 [cited 2025 Dec 3]. https://clinicaltrials.gov/study/NCT05905055
38. Vázquez-Ucha JC, Alonso-Garcia I, Guijarro-Sánchez P, Lasarte-Monterrubio C, Álvarez-Fraga L, Cendón-Esteve A, et al.; GEMARA-SEIMC/REIPI Enterobacterales Study Group. Activity of aztreonam in combination with novel β-lactamase inhibitors against metallo-β-lactamase-producing Enterobacterales from Spain. Int J Antimicrob Agents. 2023;61:106738. https://doi.org/10.1016/j.ijantimicag.2023.106738
39. Wagenlehner FM, Gasink LB, McGovern PC, Moeck G, McLeroth P, Dorr M, et al.; CERTAIN-1 Study Team. Cefepime-taniborbactam in complicated urinary tract infection. N Engl J Med. 2024;390:611–22. https://doi.org/10.1056/NEJMoa2304748
40. Blanco-Martín T, López-Hernández I, Aracil B, González-Pinto L, Aja-Macaya P, Alonso-García I, et al.; GEMARA-SEIMC/CIBERINFEC Study Group on the activity and resistance mechanisms to new β-lactams and β-lactamase inhibitors (PROTECT). Assessment of the activity and mechanisms of resistance to cefiderocol and combinations of β-lactams and the novel β-lactamase inhibitors avibactam, taniborbactam, zidebactam, nacubactam, xeruborbactam, and ANT3310 in emerging double-carbapenemase-producing Enterobacterales. Antimicrob Agents Chemother. 2024;68:e0092424. https://doi.org/10.1128/aac.00924-24

Address for correspondence: Jorge Arca-Suárez, Complexo Hospitalario Universitario de A Coruña, As Xubias s/n, 15006, A Coruña, Spain; email: jorge.arca.suarez@sergas.es

Effect of Chloramine Disinfection of Community Water System on Legionnaires' Disease Outbreak, Minnesota, USA, 2024

Molly E. Bledsoe,[1] Apoorva Goel, Maya Adelgren, Timothy M. LaPara,[2] Raymond M. Hozalski[2]

The Minnesota Department of Health identified an outbreak of Legionnaires' disease in a city in northern Minnesota, USA, in April 2023 that continued until chloramine disinfection of the community water system was implemented. Before chloramine disinfection was implemented, *Legionella pneumophila* was detected in 1 of 16 samples from the drinking water distribution system and in 5 of 10 premise plumbing samples using both cultivation-dependent (Legiolert) and cultivation-independent (digital PCR) assays in this independent investigation. Approximately 11 weeks after disinfection was implemented, all distribution system samples tested negative; however, 1 of 6 Legiolert-tested and 3 of 6 digital PCR–tested premise plumbing samples were positive. After 24 weeks of disinfection, all samples collected from the distribution system and premise plumbing tested negative. Our results show that a community water system supplied by groundwater supported substantial growth of *L. pneumophila* in premise plumbing and that chloramine disinfection halted the outbreak.

Legionnaires' disease, a severe pneumonia caused by *Legionella pneumophila* bacteria, is an increasingly common disease caused by waterborne pathogens in the United States and other developed countries (*1*–*5*). *L. pneumophila* occurs naturally in surface waters and soils and is commonly found in various engineered water system components, including cooling towers, water distribution systems, showerheads, spas, hot tubs, and humidifiers (*6*,*7*). The primary mode of *L. pneumophila* exposure is through inhalation of contaminated aerosols (*8*).

Author affiliations: University of Minnesota–Twin Cities, Minneapolis, Minnesota, USA (M.E. Bledsoe, A. Goel, M. Adelgren, T.M. LaPara, R.M. Hozalski); Biotechnology Institute, University of Minnesota–Twin Cities, St. Paul, Minnesota, USA (T.M. LaPara, R.M. Hozalski)

DOI: https://doi.org/10.3201/eid3201.251232

Although Legionnaires' disease outbreaks are typically associated with local sources of contamination, a few researchers have attributed Legionnaires' disease outbreaks to entire community water systems. For example, an outbreak of Legionnaires' disease occurred concomitantly with the catastrophic lead corrosion event in Flint, Michigan, USA, in 2014 (*9*); however, such associations of outbreaks with entire water systems are rare (*10*). To limit exposure to *L. pneumophila* via building water systems, multiple approaches have been suggested, including the maintenance of a residual disinfectant (*11*–*14*), flushing of infrequently used plumbing systems to minimize stagnation (*15*,*16*), and the maintenance of germicidal temperatures in residential and institutional water heaters (*17*,*18*). Reducing the availability of assimilable organic carbon (AOC) is another strategy to minimize overall growth of bacteria and opportunistic pathogens (*19*).

Beginning in April 2023, a city in northern Minnesota, USA, had 1–2 confirmed cases of Legionnaires' disease reported each month for 7 consecutive months. After an investigation, the Minnesota Department of Health (MDH) subsequently announced in February 2024 that the community water system was the only common source of exposure among the reported cases, which had continued to mount into 2024. Because the groundwater-supplied system routinely tested negative for total coliforms, that community water system was not required to disinfect its water in accordance with the Ground Water Rule (*20*). In response to the outbreak, the affected utility implemented chloramine disinfection to reduce or eliminate Legionnaires' disease in the community. We report on the results of an independent investigation in which we collected water samples from the drinking

[1]Current affiliation: Black & Veatch, Bloomington, Minnesota, USA.
[2]These authors contributed equally to this manuscript.

water distribution system and premise plumbing before and after the implementation of chloramine disinfection and analyzed the samples for *L. pneumophila* and other microorganisms of concern (i.e., *Legionella* spp., *Acanthamoeba* spp., *Vermamoeba vermiformis*).

Materials and Methods

Study Site

The community water system is located in northern Minnesota and serves a population of >10,000 persons. Water is withdrawn from 2 aquifers via 5 groundwater wells, supplying as much as 2.25 million gallons/day. The water treatment process includes aeration and filtration for iron and manganese removal, fluoride addition, and softening. The drinking water distribution system comprises ≈81 miles of distribution mains servicing 10.6 square miles; estimated maximum residence time in the system (i.e., water age) is 2–3 days.

Sample Collection

We collected water samples on 2 occasions before the implementation of chloramine disinfection (February 2024 and May 2024) and 2 occasions after the implementation of chloramine disinfection (September 2024 and December 2024). We collected the samples at the water treatment facility (i.e., raw water and finished water) and from multiple locations throughout the distribution system (Figure; Appendix Table, https://wwwnc.cdc.gov/EID/article/32/1/25-1232-App1.pdf) to provide thorough geographic coverage of the system and a gradient of distances from the water utility. We selected sampling locations, consisting primarily of accessible public buildings, on the basis of recommendations from MDH and utility personnel. No samples were collected from residential buildings. We collected distribution system samples (n = 27) from either a hydrant (n = 4) or from inside buildings at the tap closest to where the service line entered the building (n = 23). We collected additional premise plumbing water samples (cold, n = 11; hot, n = 11) in 3 large institutional buildings from kitchen faucets, utility faucets, or showers. One of those institutional buildings (location B) had a substantial decline in occupancy and water use around the time that chloramine disinfection was implemented. Another one of the institutional buildings (location C) implemented a remediation strategy before the initiation of this study. Location E was included after the first sample collection event. We performed sample collection and analyses for this study independent of other sample collection and analyses done by MDH and utility personnel.

For water sample collection, we flushed water for 5–10 minutes until it reached a constant temperature. Then, we collected water samples (≈1 L) for digital PCR in autoclaved polypropylene bottles containing sodium thiosulfate to quench any residual disinfectant. Similarly, we collected 100-mL samples in manufacturer-provided sterile bottles containing sodium thiosulfate for culture-based analyses of *L. pneumophila* and total coliforms. We collected samples for total organic carbon and AOC, a measure of the organic carbon readily available for assimilation by bacteria, in carbon-free glass bottles. We immediately placed all water samples on ice for same-day transport back to the laboratory and processed all samples within 48 hours of collection.

Water Quality Analyses

We measured temperature, pH, and chlorine concentrations onsite immediately before water sample collection. We measured temperature and pH using a handheld meter (PH60 pH tester; Apera Instruments, https://aperainst.com). We determined total chlorine using the N,N-diethyl-p-phenylenediamine method and a portable colorimeter (DR3000 or SL1000; Hach, https://www.hach.com) according to the manufacturer's protocol. We determined total organic carbon concentrations using a TOC analyzer (TOC-L series; Shimadzu, https://www.shimadzu.com) calibrated using potassium hydrogen phthalate standards. We measured AOC by inoculating pasteur-

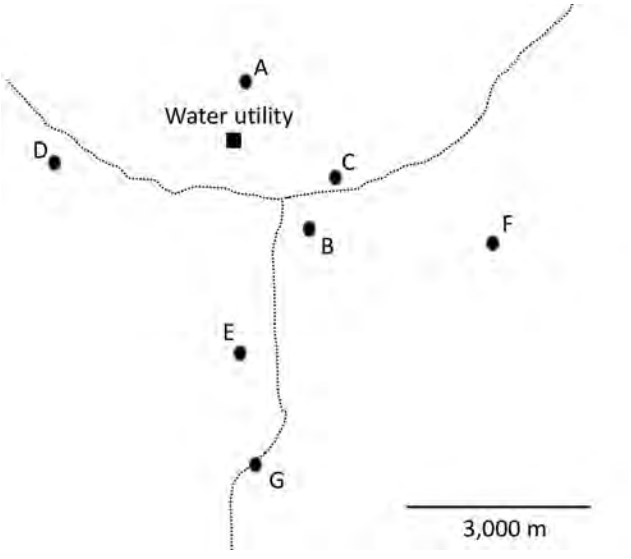

Figure. Approximate locations of the sites from which water samples were collected in study of the effect of chloramine disinfection of community water system on Legionnaires' disease outbreak, Minnesota, USA. Circles indicate community sampling sites A–G. Square indicates water utility. Dotted lines represent 2 major roads that pass through the community.

ized water samples with 2 strains of bacteria obtained from the American Type Culture Collection, *Pseudomonas fluorescens* strain P17 (ATCC 49642) and *Spirillum* sp. strain NOX (ATCC 49643), incubating them at room temperature, and enumerating the organisms over time via plating as described previously (*21*).

Culture-Based Enumeration of Microorganisms

We enumerated *L. pneumophila* via cultivation using the Legiolert method and total coliforms by the Colilert method (IDEXX Laboratories, https://www.idexx.com), in accordance with the manufacturer's instructions. We performed quality assurance and quality control of the Legiolert assay using samples of *L. pneumophila* (ATCC 33156; positive control) and *Enterococcus faecalis* (ATCC 29212; negative control). We extracted DNA from ≥1 positive well from every sample positive by the Legiolert method and subjected it to digital PCR, targeting the *mip* and *wzm* genes to validate the results.

Sample Processing and DNA Extraction

We concentrated microorganisms from each water sample (≈1 L) onto a mixed cellulose ester filter 47 mm in diameter with nominal pore size of 0.2 μm (MilliporeSigma, https://www.sigmaaldrich.com) via vacuum filtration. We prepared blank (control) filters (n = 15) by filtering 2 mL of autoclaved tap water through a clean filter. We immediately placed each filter into a PowerWater Bead Pro Tube (QIAGEN, https://www.qiagen.com) containing PW1 lysis buffer and stored them at −20°C. We then extracted DNA from the filter membranes and from biomass removed from positive Legiolert wells via syringe, using the DNeasy PowerWater Kit and a QIAcube Connect system (QIAGEN) according to the manufacturer's protocol. All blank (control) filters were negative for all PCR targets except for 16S rRNA genes.

Quantitative PCR

We performed real-time quantitative PCR to quantify total bacteria (i.e., 16S rRNA genes) (*22*) and *Vermamoeba vermiformis* (i.e., 18S rRNA genes) (*23*) using a CFX Connect Real-Time System (Bio-Rad Laboratories, https://www.bio-rad.com). We determined the quantities of unknown samples against calibration curves prepared with known quantities of synthetic gBlock gene fragments (Integrated DNA Technologies, https://www.idtdna.com). The limit of detection (LOD) for all bacteria was $10^{5.0}$ gene copies/L; the LOD for *V. vermiformis* was $10^{3.0}$ gene copies/L. We used digital PCR to quantify *Legionella* spp. (*ssrA*), *L. pneumophila* (*mip*), *L. pneumophila* serogroup 1 (*wzm*), and *Acanthamoeba* (18S rRNA for *Acanthamoeba*) (*24*,*25*). Each digital PCR involved multiplexing 4 target genes using the QIAcuity One on the QIAcuity Nanoplate 8.5K 96-well (QIAGEN) following manufacturer's standard operational procedures. The LOD for the digital PCRs was $10^{2.34}$ gene copies/L based on a minimum requirement of 3 positive partitions for an assay to be designated as a valid detection (Appendix Tables 7, 8).

We compared pairwise concentrations of microorganisms by Wilcoxon rank sum test. Differences of $p<0.05$ were statistically significant.

Results

Water Quality Characteristics

We tested all water samples collected from the distribution system (Appendix Tables 2–6); all tested negative for total coliforms (Appendix Tables 2–5). Typical temperatures of the distribution system samples were 4.4°C–15.5°C, except for the September samples that had higher temperatures (11.3°C–20.9°C) (Appendix Tables 2–5). Among the premise plumbing samples, hot water temperatures ranged from 21.4°C (water heater was not in use at the time of sample collection) to 47.2°C (Appendix Tables 2–5). Similarly, cold water temperatures typically ranged from 9.4°C to 15.5°C, except for the September samples, for which temperature range was 19.7°C–21.7°C. Water sample pH range was 7.2–8.4; median pH was 8.1.

We assumed negligible total chlorine concentrations and did not measure levels in February 2024 and May 2024 before disinfection was initiated. Total chlorine concentration in the distribution system in September 2024 was 0.3–1.8 mg/L as Cl_2 and in December 2024 was 1.2–2.4 mg/L as Cl_2. Total chlorine concentrations in the cold-water premise plumbing samples were similar to the distribution system samples. In contrast, the total chlorine concentrations in the hot-water samples were lower (0.1–0.8 mg/L as Cl_2).

Total organic carbon concentrations were consistent from the source water through the distribution system (mean ±SD = 2.2 ±0.4 mg/L) (Appendix Table 6). In contrast, AOC concentrations varied substantially depending on sample location and date. AOC concentrations in the source water collected from 5 different wells (before treatment) and in the finished water (after treatment) were similar; the range was 2.2–37.5 μg/L. In December 2024, AOC concentrations in the distribution system were similar to the well water and finished water (8.8–20.3 μg/L). In contrast, in

September 2024, AOC concentrations increased from 37.1 μg/L in the finished water to 117–157 μg/L in the distribution system.

Quantification of Total Bacteria in Distribution System and in Premise Plumbing Water

We observed significantly lower concentrations of bacteria (Wilcoxon $p<10^{-5}$) in the distribution system and premise plumbing samples after introduction of chloramines (Appendix Tables 9–12). Before disinfection, we quantified substantial concentrations of bacteria in both distribution system samples ($10^{5.9}$–$10^{7.7}$ gene copies/L; median $10^{7.5}$ gene copies/L) and in premise plumbing samples ($10^{7.1}$–$10^{9.5}$ gene copies/L; median $10^{7.5}$ gene copies/L). After disinfection, we observed substantial decreases in the concentrations of bacteria in the distribution system samples ($10^{5.2}$–$10^{7.3}$ gene copies/L; median $10^{5.7}$ gene copies/L) and in the premise plumbing samples ($10^{5.0}$–$10^{8.8}$ gene copies/L; median $10^{6.1}$ gene copies/L).

Quantification of *V. vermiformis* and *Acanthamoeba* spp.

All distribution system and premise plumbing samples were negative for *Acanthamoeba* organisms (n = 53). In contrast, we detected *V. vermiformis* frequently in both the distribution system and premise plumbing samples. Before disinfection, the frequency of detection (FOD) in the distribution system samples was 100% (n = 16), corresponding to concentrations of $10^{3.0}$–$10^{4.7}$ gene copies/L (median $10^{4.2}$ gene copies/L). After chloramine disinfection was implemented, the FOD decreased to 62.5% (10/16 samples), with corresponding significantly lower concentrations of LOD to $10^{5.0}$ gene copies/L (median $10^{3.0}$ gene copies/L) (Wilcoxon p = 0.003). Similarly, the FOD in the premise plumbing samples was 100% (n = 10) before disinfection but decreased to 58.3% (7/12 samples) after chloramine disinfection was implemented.

Quantification of *L. pneumophila* via Legiolert

Before the use of chloramine disinfection, *L. pneumophila* was rarely detected in the distribution system but was frequently detected in premise plumbing samples via Legiolert (Table 1). We detected *L. pneumophila* in 1 distribution system sample before disinfection (1/16 samples) at the LOD ($10^{1.0}$ most probable number [MPN]/L). In contrast, half (5/10 samples) of the premise plumbing samples before disinfection were positive by the Legiolert assay; most of the Legiolert-negative results came from location C, which had performed a remediation procedure to prevent additional cases of Legionnaires' disease before we began our study. The 3 positive hot water samples had *L. pneumophila* concentrations of $10^{2.4}$–$10^{4.0}$ MPN/L; the corresponding cold water samples had concentrations ranging from below the LOD to $10^{3.7}$ MPN/L.

After disinfection was implemented, we noted a substantial decrease in the FOD and in the concentrations of *L. pneumophila* determined via Legiolert. We did not detect *L. pneumophila* in any of the distribution system samples (n = 16) and in only 1/12 premise plumbing samples. That positive sample, which was collected from the hot water at location B in September 2024, had an *L. pneumophila* concentration of $10^{1.6}$ MPN/L.

Quantification of *Legionella* by Digital PCR

We detected *Legionella* spp. (target gene *ssrA*) by digital PCR in numerous distribution system and premise plumbing samples (Appendix Tables 9–12). Before disinfection, the concentrations of *Legionella*

Table 1. Concentrations of *Legionella pneumophila* as determined by Legiolert assay in water samples collected in study of *Legionella* and chloramine disinfection within a community water system, Minnesota, USA*

Location	Description	Concentration, $\log_{10}$ MPN/L			
		2024 Feb	2024 May	2024 Sep	2024 Dec
Water utility	Finished water	<LOD	<LOD	<LOD	<LOD
A	Distribution system	1	<LOD	<LOD	<LOD
B	Distribution system	<LOD	<LOD	<LOD	<LOD
	Premise, cold	3.7	2.0	<LOD	<LOD
	Premise, hot	3.7	2.4	1.6	<LOD
C	Distribution system	<LOD	<LOD	<LOD	<LOD
	Premise, cold	<LOD	<LOD	<LOD	<LOD
	Premise, hot	<LOD	<LOD	<LOD	<LOD
D	Distribution system	<LOD	<LOD	<LOD	<LOD
E	Distribution system	ND	<LOD	<LOD	<LOD
	Premise, cold	ND	<LOD	<LOD	<LOD
	Premise, hot	ND	4.0	<LOD	<LOD
F	Distribution system	<LOD	<LOD	<LOD	<LOD
G	Distribution system	<LOD	<LOD	<LOD	<LOD

*Samples were collected on different dates and from different locations. Samples were classified as being from the distribution system or from the premise plumbing (cold or hot). Chloramine disinfection was initiated in June 2024. LOD, limit of detection; MPN, most probable number; ND, not determined because no sample was collected.

Table 2. Concentrations of *Legionella pneumophila* as determined by digital PCR targeting *mip* genes in water samples collected in study of *Legionella* and chloramine disinfection within a community water system, Minnesota, USA*

Location	Description	Concentration, log_{10} gene copies/L			
		2024 Feb	2024 May	2024 Sept	2024 Dec
Water utility	Finished water	<LOD	<LOD	<LOD	<LOD
A	Distribution system	<LOD	<LOD	<LOD	<LOD
B	Distribution system	<LOD	<LOD	<LOD	<LOD
	Premise, cold	3.2	<LOD	3.9	<LOD
	Premise, hot	4.3	3.1	8.2	<LOD
C	Distribution system	<LOD	<LOD	<LOD	<LOD
	Premise, cold	<LOD	<LOD	<LOD	<LOD
	Premise, hot	2.5	<LOD	<LOD	<LOD
D	Distribution system	<LOD	<LOD	<LOD	<LOD
E	Distribution system	ND	<LOD	<LOD	<LOD
	Premise, cold	ND	<LOD	<LOD	<LOD
	Premise, hot	ND	3.9	2.6	NM
F	Distribution system	<LOD	<LOD	<LOD	<LOD
G	Distribution system	<LOD	<LOD	<LOD	<LOD

*Samples were collected on different dates and from different locations. Samples were classified as being from the distribution system or from the premise plumbing (cold or hot). Chloramine disinfection was initiated in June 2024. LOD, limit of detection; ND, not determined because no sample was collected; NM, not measured because the sample was lost during processing.

spp. in the distribution system samples (range from below the LOD to $10^{4.2}$ gene copies/L) were slightly lower than those in premise plumbing (range $10^{2.6}$–$10^{4.7}$ gene copies/L). A significant (Wilcoxon $p<0.001$) decrease in the concentration of *Legionella* spp. in the distribution system samples (range from below the LOD to $10^{3.4}$ gene copies/L) and in the premise plumbing samples (range from below the LOD to $10^{4.8}$ gene copies/L, with 1 outlier at $10^{8.2}$ gene copies/L) occurred after implementation of chloramine disinfection.

We quantified the concentrations of both *L. pneumophila* (target gene *mip*) and *L. pneumophila* serogroup 1 (target gene *wzm*) in distribution system and premise plumbing samples (Appendix Tables 9–12). Because the results for those 2 assays were very similar, we describe here only the results for *L. pneumophila* (target gene *mip*). We did not detect *L. pneumophila* by digital PCR in any distribution system samples either before or after the implementation of disinfection (Table 2). Before disinfection, however, we detected *L. pneumophila* in several premise plumbing samples (Table 2). The FOD of *L. pneumophila* was greater for hot water samples (80%; 4/5 samples) than for cold water samples (20%; 1/5 samples) with concentrations in hot water samples ranging from below the LOD to $10^{4.3}$ gene copies/L and in cold water samples from below the LOD to $10^{3.2}$ gene copies/L. We collected most of the PCR-negative samples from location C, which had undergone a building remediation in response to the Legionnaires' disease outbreak before our sample collection campaign.

After disinfection, the FODs and concentrations of *L. pneumophila* in premise plumbing samples decreased substantially. *L. pneumophila* was detected in 2/6 premise plumbing samples collected in September 2024 but not in any sample (n = 6) collected in December 2024. One of the samples collected in September 2024 had the highest observed concentration of *L. pneumophila* ($10^{8.2}$ gene copies/L); that sample was collected at the same time and location as the lone Legiolert-positive sample after chloramine disinfection had been implemented.

Discussion

Most Legionnaires' disease outbreaks are attributed to a specific, localized issue such as water stagnation in a large building or an improperly maintained cooling tower (*6*,*7*). In February 2024, however, MDH publicly announced that the community water supply was the likely source of *L. pneumophila* connected to an outbreak of Legionnaires' disease that eventually comprised 34 confirmed cases (Appendix Figure), including 2 deaths and 30 hospitalizations. After the announcement, personnel from MDH, which is also responsible for regulating drinking water quality in the state of Minnesota, asked us to perform an independent, complementary analysis of the community water system. Our initial analysis identified *L. pneumophila* in multiple institutional buildings throughout the community water system at concentrations sufficiently high (>1,000 MPN or gene copies/L) to require corrective action (*12*). Our subsequent analysis, performed after the implementation of chloramine disinfection in June 2024, revealed less frequent detections and lower concentrations of *L. pneumophila*. In addition, there were no additional cases of Legionnaires' disease after the implementation of chloramine disinfection. Our results, therefore, demonstrate that the community water system was susceptible to growing substantial concentrations of *L. pneumophila* within premise plumbing, contributing to an outbreak of

Legionnaires' disease, and that chloramine disinfection effectively halted the outbreak.

To our knowledge, researchers have previously identified community water systems in the United States as the principal factor in outbreaks of Legionnaires' disease on 3 previous occasions. One of those was associated with the water crisis in Flint, Michigan (*9*), and the other 2 were attributed to a failure to maintain a strong residual disinfectant in community water systems supplied by surface water (*26*,*27*). The Minnesota outbreak of Legionnaires' disease, therefore, was unique because it was triggered by a community water system supplied by groundwater. The source of the water supply is particularly pertinent because in the United States, community water systems supplied by groundwater that routinely test negative for total coliforms are not required to disinfect the water before distribution or maintain a residual disinfectant throughout the distribution system (*20*).

We suspect that an unexpectedly high AOC content in the groundwater supply was a factor contributing to this outbreak of Legionnaires' disease. It is believed that *L. pneumophila* growth in water distribution systems primarily occurs inside amoeba (e.g., *V. vermiformis*) that graze on biofilms that form on the interior surfaces of water distribution and premise plumbing rather than in the drinking water directly (*28*). Thus, the AOC in water supplies could indirectly contribute to *L. pneumophila* proliferation by enabling the growth of biofilms on distribution system mains and premise plumbing piping (*19*). Although ground water typically has low concentrations of bioavailable organic carbon (*21*,*29*–*31*), AOC levels in the drinking water in our study routinely exceeded the suggested threshold for microbiologically stable water in the absence of a residual disinfectant of 10–20 μg/L (*21*) and at times exceeded the threshold for water containing a residual disinfectant of 50–100 μg/L (*32*). Of note, AOC concentrations in the distribution system often were greater than those in the raw groundwater and finished water; identifying the cause of this increase within the distribution system warrants further investigation.

From a practical perspective, our study demonstrates that maintaining a residual disinfectant throughout the distribution system is a robust approach to suppress the growth of *Legionella* spp. bacteria (as *ssrA* genes), *L. pneumophila* bacteria (via Legiolert and digital PCR targeting *mip* and *wzm* genes), other bacteria (as 16S rRNA genes), and amoebas (especially *V. vermiformis*) (*28*,*33*). Another theory is that the lack of residual disinfectant was a pertinent factor contributing to this outbreak of Legionnaires' disease. Although most public water systems in the United States practice primary disinfection (i.e., as part of the treatment process before distribution) and maintain a residual disinfectant, the Ground Water Rule (*20*) enables community water systems that test negative for total coliforms to forego disinfection. As of December 2025, there are >250 community water systems in Minnesota that do not practice disinfection, including 10 such systems that serve populations of ≥1,000 persons.

In conclusion, our study provides evidence that a community water system was the source of a Legionnaires' disease outbreak that was subsequently resolved by implementing chloramine as a residual disinfectant throughout the drinking water distribution system. The principal water quality factor leading to the outbreak was a lack of residual disinfectant in the drinking water distribution system. Perhaps more important, however, we conjecture that unexpectedly high concentrations of AOC contributed to the overall growth of bacteria and the occurrence of *L. pneumophila*. Although groundwater is generally low in AOC (≤50 μg/L [*34*]), that water quality parameter is rarely monitored in the United States. We advocate, therefore, for AOC testing to identify community water systems at greater risk for bacterial and possibly *L. pneumophila* growth, especially those supplied by ground water that do not use disinfection and any disinfected system that struggles to maintain a residual throughout their distribution system. Furthermore, nondisinfected ground water systems and disinfected systems that struggle to maintain a residual also should consider periodic monitoring for *L. pneumophila* and disinfection or disinfection boosting when positive samples or cases of Legionnaires' disease are encountered.

Acknowledgments

We thank Sandeep Burman for inviting our team to participate in the investigation. We also thank water utility personnel for their assistance in collecting water samples and in collecting some of the water quality data. Finally, we thank Josie Gatto, Kailey Kaltenbrun, Ethan Schnettler, and Alexis Swanson for assistance in processing water samples.

The US Environmental Protection Agency supported this research (EPA grant no. R840605 awarded to R.H.)

About the Author

Ms. Bledsoe recently received her master's degree from the University of Minnesota. She is an environmental engineer currently employed by Black & Veatch Corporation.

References

1. Barskey AE, Derado G, Edens C. Rising incidence of Legionnaires' disease and associated epidemiologic patterns, United States, 1992–2018. Emerg Infect Dis. 2022;28:527–38. https://doi.org/10.3201/eid2803.211435
2. Beauté J; The European Legionnaires' Disease Surveillance Network. Legionnaires' disease in Europe, 2011 to 2015. Euro Surveill. 2017;22:30566. https://doi.org/10.2807/1560-7917.ES.2017.22.27.30566
3. Kunz JM, Lawinger H, Miko S, Gerdes M, Thuneibat M, Hannapel E, et al. Surveillance of waterborne disease outbreaks associated with drinking water—United States, 2015–2020. MMWR Surveill Summ. 2024;73:1–23. https://doi.org/10.15585/mmwr.ss7301a1
4. US Centers for Disease Control and Prevention. Legionnaires' disease surveillance summary report, United States 2018–2019. https://www.cdc.gov/legionella/health-depts/surv-reporting/2018-19-surv-report-508.pdf
5. Farnham A, Alleyne L, Cimini D, Balter S. Legionnaires' disease incidence and risk factors, New York, New York, USA, 2002–2011. Emerg Infect Dis. 2014;20:1795–802. https://doi.org/10.3201/eid2011.131872
6. Armstrong TW, Haas CN. Legionnaires' disease: evaluation of a quantitative microbial risk assessment model. J Water Health. 2008;6:149–66. https://doi.org/10.2166/wh.2008.026
7. van Heijnsbergen E, Schalk JAC, Euser SM, Brandsema PS, den Boer JW, de Roda Husman AM. Confirmed and potential sources of *Legionella* reviewed. Environ Sci Technol. 2015;49:4797–815. https://doi.org/10.1021/acs.est.5b00142
8. Schoen ME, Ashbolt NJ. An in-premise model for *Legionella* exposure during showering events. Water Res. 2011;45:5826–36. https://doi.org/10.1016/j.watres.2011.08.031
9. Rhoads WJ, Garner E, Ji P, Zhu N, Parks J, Schwake DO, et al. Distribution system operational deficiencies coincide with reported Legionnaires' disease clusters in Flint, Michigan. Environ Sci Technol. 2017;51:11986–95. https://doi.org/10.1021/acs.est.7b01589
10. Gleason JA, Cohn PD. A review of legionnaires' disease and public water systems—scientific considerations, uncertainties, and recommendations. Int J Hyg Environ Health. 2022;240:113906. https://doi.org/10.1016/j.ijheh.2021.113906
11. Kim T, Zhao X, Hozalski RM, LaPara TM. Residual disinfectant effectively suppresses *Legionella* species in drinking water distribution systems supplied by surface water in Minnesota, USA. Sci Total Environ. 2024;940:173317. https://doi.org/10.1016/j.scitotenv.2024.173317
12. LeChevallier MW. Managing *Legionella pneumophila* in water systems. J Am Water Works Assoc. 2020;112:10–23. https://doi.org/10.1002/awwa.1444
13. Lee-Masi M, Coulter C, Chow SJ, Zaitchik B, Jacangelo JG, Exum NG, et al. Two-year evaluation of *Legionella* in an aging residential building: assessment of multiple potable water remediation approaches. Sci Total Environ. 2024;941:173710. https://doi.org/10.1016/j.scitotenv.2024.173710
14. Prest EI, Hammes F, van Loosdrecht MCM, Vrouwenvelder JS. Biological stability of drinking water: controlling factors, methods, and challenges. Front Microbiol. 2016;7:45. https://doi.org/10.3389/fmicb.2016.00045
15. Hozalski RM, LaPara TM, Zhao X, Kim T, Waak MB, Burch T, et al. Flushing of stagnant premise water systems after the COVID-19 shutdown can reduce infection risk by *Legionella* and *Mycobacterium* spp. Environ Sci Technol. 2020;54:15914–24. https://doi.org/10.1021/acs.est.0c06357
16. Kim T, Zhao X, LaPara TM, Hozalski RM. Flushing temporarily improves microbiological water quality for buildings supplied with chloraminated surface water but has little effect for groundwater supplies. Environ Sci Technol. 2023;57:5453–63. https://doi.org/10.1021/acs.est.2c08123
17. Ji P, Rhoads WJ, Edwards MA, Pruden A. Impact of water heater temperature setting and water use frequency on the building plumbing microbiome. ISME J. 2017;11:1318–30. https://doi.org/10.1038/ismej.2017.14
18. Proctor CR, Dai D, Edwards MA, Pruden A. Interactive effects of temperature, organic carbon, and pipe material on microbiota composition and *Legionella pneumophila* in hot water plumbing systems. Microbiome. 2017;5:130. https://doi.org/10.1186/s40168-017-0348-5
19. van der Kooij D, Veenendaal HR, Italiaander R, van der Mark EJ, Dignum M. Primary colonizing *Bertaproteobacteriales* play a key role in the growth of *Legionella pneumophila* in biofilms on surfaces exposed to drinking water treated by slow sand filtration. Appl Environ Microbiol. 2018;84:e01732–18. https://doi.org/10.1128/AEM.01732-18
20. United States Environmental Protection Agency. Ground water rule [cited 2025 July 22]. https://www.epa.gov/dwreginfo/ground-water-rule
21. van der Kooij D. Assimilable organic carbon as an indicator of bacterial regrowth. J Am Water Works Assoc. 1992;84:57–65. https://doi.org/10.1002/j.1551-8833.1992.tb07305.x
22. LaPara TM, Burch TR, McNamara PJ, Tan DT, Yan M, Eichmiller JJ. Tertiary-treated municipal wastewater is a significant point source of antibiotic resistance genes into Duluth-Superior Harbor. Environ Sci Technol. 2011;45:9543–9. https://doi.org/10.1021/es20277tr
23. Kuiper MW, Valster RM, Wullings BA, Boonstra H, Smidt H, van der Kooij D. Quantitative detection of the free-living amoeba *Hartmannella vermiformis* in surface water by using real-time PCR. Appl Environ Microbiol. 2006;72:5750–6. https://doi.org/10.1128/AEM.00085-06
24. Benitez AJ, Winchell JM. Clinical application of a multiplex real-time PCR assay for simultaneous detection of *Legionella* species, *Legionella pneumophila*, and *Legionella pneumophila* serogroup 1. J Clin Microbiol. 2013;51:348–51. https://doi.org/10.1128/JCM.02510-12
25. Qvarnstrom Y, Visvesvara GS, Sriram R, da Silva AJ. Multiplex real-time PCR assay for simultaneous detection of *Acanthamoeba* spp., *Balamuthia mandrillaris*, and *Naegleria fowleri*. J Clin Microbiol. 2006;44:3589–95. https://doi.org/10.1128/jcm.00875-06
26. Cohn PD, Gleason JA, Rudowski E, Tsai SM, Genese CA, Fagliano JA. Community outbreak of legionellosis and an environmental investigation into a community water system. Epidemiol Infect. 2015;143:1322–31. https://doi.org/10.1017/S0950268814001964
27. Rhoads WJ, Keane T, Spencer MS, Pruden A, Edwards MA. Did municipal water distribution system deficiencies contribute to a Legionnaires' disease outbreak in Quincy, IL? Environ Sci Technol Lett. 2020;7:896–902. https://doi.org/10.1021/acs.estlett.0c00637
28. National Academies of Sciences, Engineering, and Medicine. Management of *Legionella* in water systems. Washington: The National Academies Press; 2020.
29. Lesnik R, Brettar I, Höfle MG. *Legionella* species diversity and dynamics from surface reservoir to tap water: from cold adaptation to thermophily. ISME J. 2016;10:1064–80. https://doi.org/10.1038/ismej.2015.199
30. Miettinen IT, Vartiainen T, Martikainen PJ. Determination of assimilable organic carbon in humus-rich drinking waters. Water Res. 1999;33:2277–82. https://doi.org/10.1016/S0043-1354(98)00461-8

31. Pick FC, Fish KE, Biggs CA, Moses JP, Moore G, Boxall JB. Application of enhanced assimilable organic carbon method across operational drinking water systems. PLoS One. 2019;14:e0225477. https://doi.org/10.1371/journal.pone.0225477
32. LeChevallier MW, Welch NJ, Smith DB. Full-scale studies of factors related to coliform regrowth in drinking water. Appl Environ Microbiol. 1996;62:2201–11. https://doi.org/10.1128/aem.62.7.2201-2211.1996
33. Flannery B, Gelling LB, Vugia DJ, Weintraub JM, Salerno JJ, Conroy MJ, et al. Reducing *Legionella* colonization in water systems with monochloramine. Emerg Infect Dis. 2006;12:588–96. https://doi.org/10.3201/eid1204.051101
34. Bradford SM, Palmer CJ, Olson BH. Assimilable organic carbon concentrations in Southern California surface and groundwater. Water Res. 1994;28:427–35. https://doi.org/10.1016/0043-1354(94)90280-1

Address for correspondence: Raymond M. Hozalski, University of Minnesota, Department of Civil, Environmental, and Geo-Engineering, 500 Pillsbury Dr SE, Minneapolis, MN 55455-0116, USA; email: hozal001@umn.edu

Detection of Novel Thermotolerant *Tepidimonas* sp. Bacteria in Human Respiratory Specimens, Hong Kong, China, 2024

Kelvin Hei-Yeung Chiu, Shuk-Ching Wong, Edwin Kwan-Yeung Chiu, Raymond Hon-Man Ng, Jonathan Hon-Kwan Chen, Jordan Yik-Hei Fong, Lithia Lai-Ha Yuen, Simon Yung-Chun So, David Christopher Lung, Vincent Chi-Chung Cheng, Kwok-Yung Yuen, Jade Lee-Lee Teng

In patients with acute respiratory infections (ARIs), routine diagnostic tests often fail to identify the microbial cause; thus, many ARIs have undetermined etiology. We investigated potential involvement of thermotolerant bacteria in ARIs among patients in Hong Kong, China, by incubating blood agar inoculated with respiratory specimens at 50°C for 5 days. Among 7,257 specimens analyzed, 58 specimens from 57 patients grew thermotolerant bacteria not identified by other methods. We identified *Tepidimonas* spp. in 42 isolates, 3 of which appear to be a novel *Tepidimonas* species (tentatively *Tepidimonas hongkongensis* sp. nov). Genomic analysis revealed various virulence, resistance, and stress-related genomes in the 3 isolates. *Tepidimonas* spp. bacteria were predominantly isolated from patients with chronic lung disease and malignancies. We also detected *T. hongkongensis* in hospital water samples but at a lower percentage than in respiratory specimens, suggesting colonization potential. Clinical implications of *T. hongkongensis* remain unknown; continued surveillance could determine its role in ARIs.

Although routine bacterial culture and multiplex reverse transcription PCR for respiratory viruses and fastidious organisms are commonly performed in respiratory specimens from patients with acute respiratory syndrome, the distinct microbial cause remains unidentified in most patients. A study from China showed that among school-age children with acute respiratory infections (ARIs), 46.9% of viral and 30.9% of bacterial etiologies could be identified, but the other patients had ARIs of unknown etiology (*1*).

The routine practice of bacterial culture of expectorated sputum relies on blood and chocolate agar plates incubated at 35°C–37°C for 48 hours. Those methods could miss bacteria that grow poorly or very slowly at body temperature and might be overgrown by common oropharyngeal commensals. Although most respiratory pathogens are not thermotolerant, pathogens such as *Aspergillus* spp. fungi and the bacterium *Mycobacterium xenopi* are thermotolerant and have been described as causing respiratory infections, especially in patients with chronic lung disease (*2*).

We hypothesized that increasing the incubation temperature during culture can suppress normal flora and enable fastidious, thermotolerant bacteria to grow, possibly revealing novel pathogens contributing to ARIs. We investigated respiratory specimens by prolonged incubation of agar plates at high temperature, then subjected cultured bacterial isolates to matrix-assisted laser desorption/ionization time-of-flight (MALDI-TOF) mass spectrometry and partial 16S rRNA gene sequencing to determine whether thermotolerant bacteria were the cause of ARIs.

Materials and Methods

Study Design and Specimen Collection

We conducted a multicenter, retrospective study in a hospital network in Hong Kong, China, including a 1,700-bed university-affiliated teaching hospital (Queen Mary Hospital) and 3 extended care hospitals ranging in size from 270 to 530 beds. We included all respiratory specimens, including sputum and

Author affiliations: Queen Mary Hospital, Hong Kong, China (K.H.-Y. Chiu, S.-C. Wong, E.K.-Y. Chiu, R.H.-M. Ng, J.H.-K. Chen, L.L.-H. Yuen, S.Y.-C. So, V.C.-C. Cheng); University of Hong Kong, Hong Kong (S.-C. Wong, J.H.-K. Chen, J.Y.-H. Fong, K.-Y. Yuen, J.L.-L. Teng); Queen Elizabeth Hospital, Hong Kong (D.C. Lung); Hong Kong Children's Hospital, Hong Kong (D.C. Lung)

DOI: https://doi.org/10.3201/eid3201.250818

bronchoalveolar lavage fluid (BALF) samples, collected during January 19–May 19, 2024, and sent to the microbiology laboratory at Queen Mary Hospital for routine bacterial culture. This study was approved by the Institutional Review Board of the University of Hong Kong Special Administrative Region, People's Republic of China/Hospital Authority Hong Kong Special Administrative Region, People's Republic of China West Cluster (UW 25-135).

Routine Investigations Methodology

As part of routine screening, we performed Gram stains on all lower respiratory specimens to semiquantify the number of leukocytes and assess specimen quality. We observed Gram stains under light microscopy at ×100 magnification and graded stains on the basis of the number of leukocytes as trace (<25 cells), 2+ (25–75 cells), or 3+ (>75 cells) and epithelial cells as 1+ (<10 cells), 2+ (10–25 cells), or 3+ (>25 cells) in an average of 10 fields. We inoculated all samples on blood and chocolate agar plates for routine bacterial culture and also inoculated BALF samples on MacConkey agar plates. Plates routinely are incubated at 35°C at 5% CO_2 and examined every 24 hours for 2 days. For this study, we also inoculated all respiratory tract samples on separate blood agar plates, incubated at 50°C, and examined plates every 24 hours for 5 days. We defined any colonies that grew from the blood agar plates at 50°C as thermotolerant bacteria, and subjected those to MALDI-TOF spectrometry and 16S rRNA PCR (*3*), when necessary, for bacterial identification. If the MALDI-TOF In Vitro Diagnostic database (Bruker, https://www.bruker.com) failed to identify bacteria, we performed subsequent Sanger sequencing.

16S rRNA, MALDI-TOF Spectrometry, and Whole-Genome Sequencing Methods

When MALDI-TOF spectrometry failed to identify bacterial isolates, we performed 16S rRNA sequencing. We used universal bacterial primers 16S-1F and 16S-2R and the QIAmp DNA Minikit (QIAGEN, https://www.qiagen.com) to extract DNA and sequenced on the 3500 Genetic Analyzer system (Thermo Fisher Scientific, https://www.thermofisher.com) (Appendix).

We considered bacteria that had suboptimal similarity percentages with existing bacteria in the BLAST (https://blast.ncbi.nlm.nih.gov) as possible novel species (*4*). We subjected those bacteria to whole-genome sequencing by using a dual platform of short- and long-read sequencing. For short-read sequencing, we performed DNA preparation by using the Nextera DNA Prep Kit, then sequenced on the iSeq100 (Illumina, https://www.illumina.com). For long-read sequencing, we used the Ligation Sequencing Kit for DNA preparation and MinION for sequencing (both Oxford Nanopore Technologies, https://nanoporetech.com) (Appendix, https://wwwnc.cdc.gov/EID/article/32/1/25-0818-App1.pdf).

Covariates of Interest

We retrieved data on patients who had thermotolerant bacterial species identified from electronic health records. Patient information included demographic data, underlying medical conditions, signs and symptoms, time from hospital admission to sample collection, hematologic parameters, inflammatory markers, and radiologic findings.

Statistical Analysis

We reported descriptive statistics as median and range and categorical variables as frequency and percentage. We used Fisher exact or χ^2 tests for 2-group comparisons. We performed statistical analyses in SPSS Statistics 24.0 (IBM, https://www.ibm.com) and considered $p<0.05$ statistically significant.

Results

During January 19–May 19, 2024, the microbiology laboratory collected 7,257 respiratory specimens, of which 6,766 were lower respiratory tract specimens: 5,922 expectorated sputum, 388 tracheal aspirates, and 456 bronchial specimens, including BALF and endobronchial biopsy specimens. The other 491 respiratory specimens were upper respiratory tract specimens: 113 nasal or nasopharyngeal swab samples, 283 oral or throat swab samples, and 95 gastric aspirates.

Among collected specimens, 66 (64 sputum and 2 throat swab) specimens from 65 patients grew thermotolerant bacteria that could not be identified by MALDI-TOF spectrometry (Table 1). Among the 66 thermotolerant bacterial specimens, we identified *Tepidimonas* spp. in 42 (63.6%, 0.6% of all respiratory specimens, 41 sputum and 1 throat swab) specimens from 41 patients by 16S rRNA sequencing; 37 were *T. aquatica*, 3 were undetermined *Tepidimonas* spp., 1 was *T. taiwanensis*, and 1 was *T. fonticaldi.*

Patients with *Tepidimonas* spp. bacterial isolates were from all age groups; 56.1% of patients were female and 43.9% were male (Table 2). The most common underlying conditions in the cohort were solid organ malignancy (41.5%), hypertension (36.6%), chronic lung disease (24.4%), and hyperlipidemia (24.4%). Among *Tepidimonas* spp. isolates, 58.5% were from sputum saved in the outpatient setting or collected ≤48 hours of hospital admission, suggesting a

Table 1. Bacteria from respiratory specimens collected in a study on detection of novel thermotolerant *Tepidimonas* spp. bacteria in human respiratory specimens, Hong Kong, China, 2024*

Thermotolerant bacteria	No. (%) specimens
Tepidimonas spp.	42 (63.6)
T. aquatica	37
T. taiwanensis	1
T. fonticaldi	1
Unidentified *Tepidimonas* spp.†	3
Schlegelella aquatica	14 (12.1)
Vulcaniibacterium thermophilum	4 (6.1)
Thermomonas spp.	2 (3.0)
Lactobacillus delbrueckii	1 (1.5)
Bacillus species	3 (4.5)
B. gelatini	1
B. licheniformis	1
B. safensis	1

*Identified by matrix-assisted laser desorption/ionization time-of-flight mass spectrometry.
†Unable to identify species-level by 16S rRNA sequencing.

possible community source. Common clinical signs and symptoms included cough, fever, and shortness of breath. Some of the patients had abnormal chest radiograph findings, including consolidation or pulmonary infiltrates (26.8%), pleural effusion (19.5%), and chronic lung changes (24.4%). However, 34.1% of patients with *Tepidimonas* spp. isolated had unremarkable findings on chest radiographs, representing possible bacterial colonization of the respiratory tract.

Table 2. Demographic characteristics of 41 patients from whom *Tepidimonas* spp. bacteria were detected in respiratory specimens, Hong Kong, China, 2024*

Characteristics	Value
Median age, y (range)	70 (15–97)
Sex	
F	23 (56.1)
M	18 (43.9)
Underlying conditions	
Hypertension	15 (36.6)
Diabetes mellitus	7 (17.1)
Hyperlipidemia	10 (24.4)
Cardiovascular disease	9 (22.0)
Renal impairment	7 (17.1)
Cerebral vascular accident	1 (2.4)
Chronic lung disease	10 (24.4)
Chronic liver disease	7 (17.1)
Solid organ malignancy	17 (41.5)
Hematologic malignancy	1 (2.4)
Autoimmune disease	1 (2.4)
Timing of positive growth	
Outpatient or ≤48 h of admission	24 (58.5)
>48 h after admission	17 (41.5)
Clinical signs and symptoms	
Fever	13 (31.7)
Cough	14 (34.1)
Sputum	11 (26.8)
Shortness of breath	13 (31.7)
Chest radiography	
Not done	2 (4.9)
Unremarkable	14 (34.1)
Consolidation or pulmonary infiltrates	11 (26.8)
Pleural effusion	8 (19.5)
Chronic lung changes	10 (24.4)
Blood parameters, median (range)	
Leukocytes, $\times 10^9$ cells/L	8.34 (1.77–23.10)
Neutrophils, $\times 10^9$ cells/L	5.94 (1.29–20.95)
C-reactive protein, mg/dL	5.21 (0.17–18.53)

*Values are no. (%) except as indicated.

Among laboratory characteristics of the 41 sputum specimens, 51.2% had trace leukocytes, and 46.3% had <10 epithelial cells per field (Table 3). In addition, 36.6% had growth of other pathogenic organisms, the most common of which were *Haemophilus influenzae* and *Flavobacterium* species.

Novel Species Identification

Our study identified 3 clinical isolates of a novel *Tepidimonas* sp. bacterium. Here, we report phenotypic characteristics and genomic features of those bacteria, including detection of virulence, antimicrobial resistance (AMR), and stress-related genes. To investigate potential sources of this bacterium, we also performed environmental sampling in the hospital.

Phenotypic Analysis and Biochemical Characteristics

The 3 undetermined sequences detected by 16S rRNA sequencing displayed 96.68%–97.59% sequence identity to known *Tepidimonas* spp. available in the BLAST database, suggesting that the taxonomic position of those isolates remained uncertain. The sequences were from 3 isolates (HKU77, HKU78, and HKU79) from 3 patients: 1 with pulmonary metastasis, 1 with community-acquired pneumonia, and 1 with underlying Graves' disease and schizophrenia who had fever during hospitalization.

Gram stain of isolates HKU77, HKU78, and HKU79 revealed gram-negative, non–spore-forming, motile rods with occasional spherical enlargement (Appendix Figure, panel A). We observed small translucent and nonpigmented colonies with no hemolysis on blood agar after 24 hours of incubation. The size of colonies gradually increased with prolonged incubation. We noted no pigment production at 35°C or 42°C, but colonies displayed a slight brown pigmentation after prolonged incubation at 50°C. Optimal growth of those bacteria occurred at 50°C, and we noted no visible growth at 25°C (Appendix Figure, panels B–D). The 3 isolates did not grow in anaerobic conditions. Growth on chocolate agar and *Haemophilus* test medium at 50°C was similar to that for blood agar; we observed slower growth on *Brucella* agar. However, we noted no growth on buffered charcoal yeast extract agar or brain heart infusion agar supplemented with X and V factor. We observed no fluorescence under ultraviolet light (Table 4).

Biochemically, all 3 isolates were oxidase-positive and weakly catalase-positive (with 15% hydrogen

peroxide) and tested negative for lipase, lecithinase, DNAase, and gelatinase at 50°C. The isolates were positive for nitrate reductase, glutamyl arylamidase, and tyrosine arylamidase and weakly positive for urease. Sugar fermentation (glucose, lactose, sucrose, citrate), indole, H_2S production, and ortho-nitrophenyl-β-galactoside were all negative after incubation at 50°C. We evaluated enzymatic activity by using the VITEK AutoMicrobic GNI+ card (bioMérieux, https://www.biomerieux.com), which was positive for glutamyl arylamidase and tyrosine arylamidase, and 1 strain (HKU78) showed additional enzymatic activity of L-proline arylamidase and a positive Ellman's test result.

The 3 isolates were susceptible to piperacillin, piperacillin/tazobactam, ceftazidime, amikacin, ciprofloxacin, tobramycin, and cefepime, according to the Clinical Laboratory Standards Institute *Pseudomonas* breakpoints (*5*). The MICs of penicillin for the 3 isolates were ≤0.016 μg/mL, and MICs of vancomycin were 48–64 μg/mL. Comparison with phenotypic characteristics of *T. aquatica* and *T. taiwanensis* showed that the *Tepidimonas* species from our 3 strains did not grow on buffered charcoal yeast extract agar, but both *T. aquatica* and *T. taiwanensis* did. Furthermore,

Table 3. Characteristics of isolate cultures from 41 sputum specimens in study of novel thermotolerant *Tepidimonas* spp. bacteria in human respiratory specimens, Hong Kong, China, 2024

Characteristics	No. (%)
Leukocyte quantified by Gram stain	
Negative	7 (17.1)
Trace	21 (51.2)
2+	7 (17.1)
3+	6 (14.6)
Epithelial cells quantified by Gram stain	
Negative	4 (9.8)
1+	19 (46.3)
2+	10 (24.4)
3+	8 (19.5)
Other organisms grown	15 (36.6)
Acinetobacter species	2 (4.9)
Candida species	2 (4.9)
Escherichia coli	1 (2.4)
Flavobacterium species	3 (7.3)
Haemophilus influenzae	4 (9.8)
Pseudomonas aeruginosa	2 (4.9)
Methicillin-resistant *Staphylococcus aureus*	1 (2.4)
Stenotrophomonas maltophilia	2 (4.9)

Table 4. Laboratory characteristics of 3 strains of novel thermotolerant *Tepidimonas* spp. bacteria isolated in human respiratory specimens, Hong Kong, China, 2024*

Test	HKU77^T	HKU78	HKU79
Gram stain	Gram-negative rod	Gram-negative rod	Gram-negative rod
Anaerobic growth	No growth	No growth	No growth
Motility	Motile	Motile	Motile
Oxidase	Positive	Positive	Positive
Catalase, 15% H_2O_2	Weakly positive	Weakly positive	Weakly positive
Yellow pigment	Slightly brown	Slightly brown	Slightly brown
Hemolysis	Negative	Negative	Negative
UV fluorescence	Negative	Negative	Negative
Growth, 72 h			
25°C	No growth	No growth	No growth
37°C	Very slow growth	Very slow growth	Very slow growth
42°C	Slow growth	Slow growth	Slow growth
50°C	Growth	Growth	Growth
Growth rate, 50°C, 72 h			
Chocolate agar	Same as blood agar	Same as blood agar	Same as blood agar
Haemophilus test medium	Nearly same as blood agar	Nearly same as blood agar	Nearly same as blood agar
Brucella agar	Slower than blood agar	Slower than blood agar	Slower than blood agar
BCYE agar	No growth	No growth	No growth
Oxoid brain–heart infusion agar	No growth	No growth	No growth
Egg yolk agar, 50°C	Negative	Negative	Negative
DNAase agar, 50°C	Negative	Negative	Negative
Gelatinase agar, 50°C	Negative	Negative	Negative
Glucose oxidation and fermentation test, 50°C	Inert	Inert	Inert
Nitrate, 50°C	Positive	Positive	Positive
Urease, 50°C	Weakly positive	Weakly positive	Weakly positive
ONPG, 50°C	Negative	Negative	Negative
Positive by VITEK AutoMicrobic GNI+ system†, McFarland 2	Glutamyl arylamidsae, tyrosine arylamidase	Glutamyl arylamidsae, tyrosine arylamidase, L-proline arylamidase, Ellman's test	Glutamyl arylamidsae, tyrosine arylamidase
MIC, μg/mL at 50°C			
Vancomycin	64	48	64
Penicillin	≤0.016	≤0.016	≤0.016

*Strains of novel *T. hongkongensis*. BCYE, buffered charcoal yeast extract; ONPG, ortho-Nitrophenyl-β-galactoside; UV, ultraviolet.
†bioMérieux, https://www.biomerieux.com.

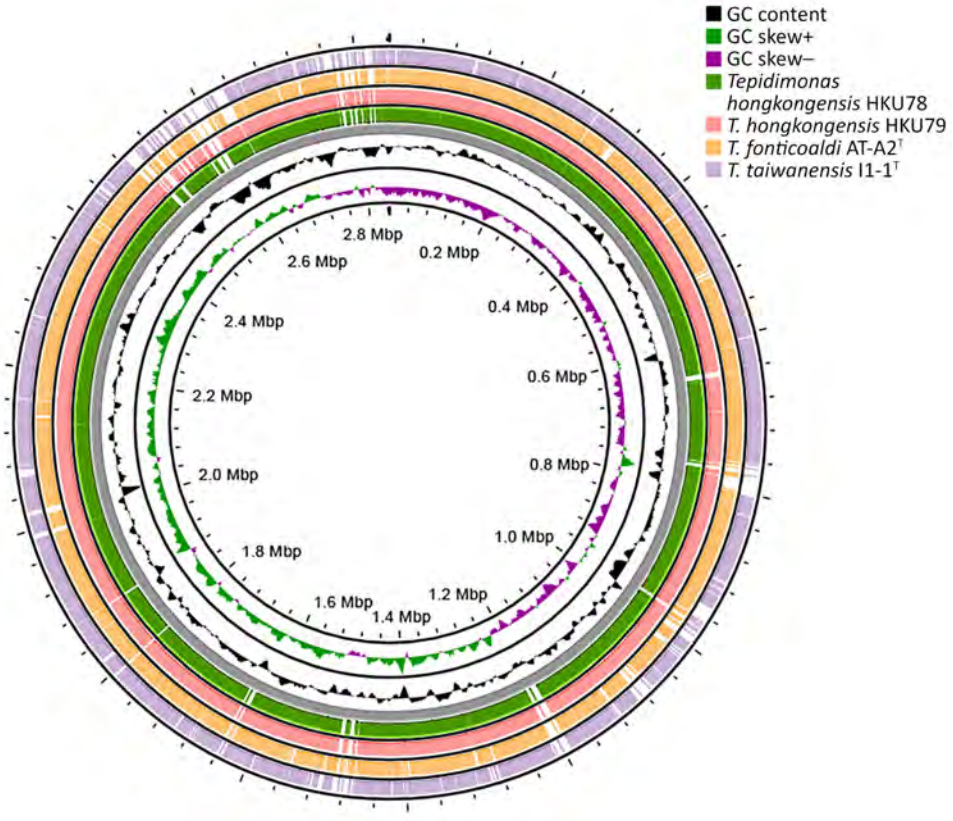

Figure 1. Circular genome map of novel thermotolerant *Tepidimonas* spp. bacteria detected in human respiratory specimens, Hong Kong, China, 2024. Using patient strain HKU77^T as the reference genome forming the backbone, the ring compares genome matches from patient strains HKU78 and HKU79 and the 2 closest *Tepidimonas* species, *T. fonticoaldi* AT-A2^T and *T. taiwanensis* I1–1^T genomes. The genome features include GC content and plus (+) or minus (–) GC skew.

T. taiwanensis is gelatinase- and nitrate-positive, but *T. aquatica* and the novel *Tepidimonas* species from our study are not (Table 4).

Comparative Genomic Characterizations

The de novo assembly, using Illumina and Oxford Nanopore Technology reads, yielded complete genomes for the strains HKU77, HKU78, and HKU79 (Figure 1). The genome sizes of the 3 strains ranged from 2,842,968 to 2,891,522 bp, and GC content spanned 67.1%–67.2% (Table 5). We submitted the assembled genome sequences to PROKKA (https://github.com/tseemann/prokka) for annotation, which resulted in 2,695–2,786 protein-coding sequences, 3 rRNA operons, and 50–52 tRNA-coding genes (Table 5). Annotation via the RAST pipeline (Rapid Annotations using Subsystems Technology; Argonne National Laboratory, https://www.anl.gov/mcs/rast-rapid-annotation-using-subsystem-technology) indicated that the 3 strains possess a similar number of genes and subsystems, except for strain HKU78, which harbored a phage genome containing an additional integron integrase *IntI1* gene related to the phages, prophages, transposable elements, and plasmids subsystem in RAST (Figure 2).

Table 5. Genome characteristics and functional annotation in study of novel thermotolerant *Tepidimonas* spp. bacteria in human respiratory specimens, Hong Kong, China, 2024*

Features	HKU77^T	HKU78	HKU79
Size, bp	2,842,968	2,875,687	2,891,522
No. contigs	1	1	1
% GC	67.2	67.1	67.2
No. coding sequences	2,695	2,744	2,786
No. rRNA sequences	3	3	3
No. tRNA sequences	51	52	50

*Genome statistics obtained from PROKKA (https://github.com/tseemann/prokka) annotation and seqkit (https://github.com/shenwei356/seqkit/releases) results.

To determine the phylogenetic positions of the 3 strains within the genus *Tepidimonas*, we used Type (Strain) Gene Server (Leibniz Institute, https://tygs.dsmz.de) results to construct a phylogenetic tree incorporating genome data from the 3 strains and complete genomes of other *Tepidimonas* spp. type strains. That analysis revealed that HKU77, HKU78, and HKU79 cluster together, forming a distinct and well-supported phylogenetic clade, separate from other *Tepidimonas* species, and are most closely related to *T. fonticaldi* (Figure 3, panel A). Similarly, the phylogenetic tree constructed from core-genome sequences displayed a consistent topology (Figure 3, panel B). In silico genome-to-genome comparison demonstrated that the 3 strains from our study shared pairwise digital DNA-DNA hybridization (dDDH) values ranging from

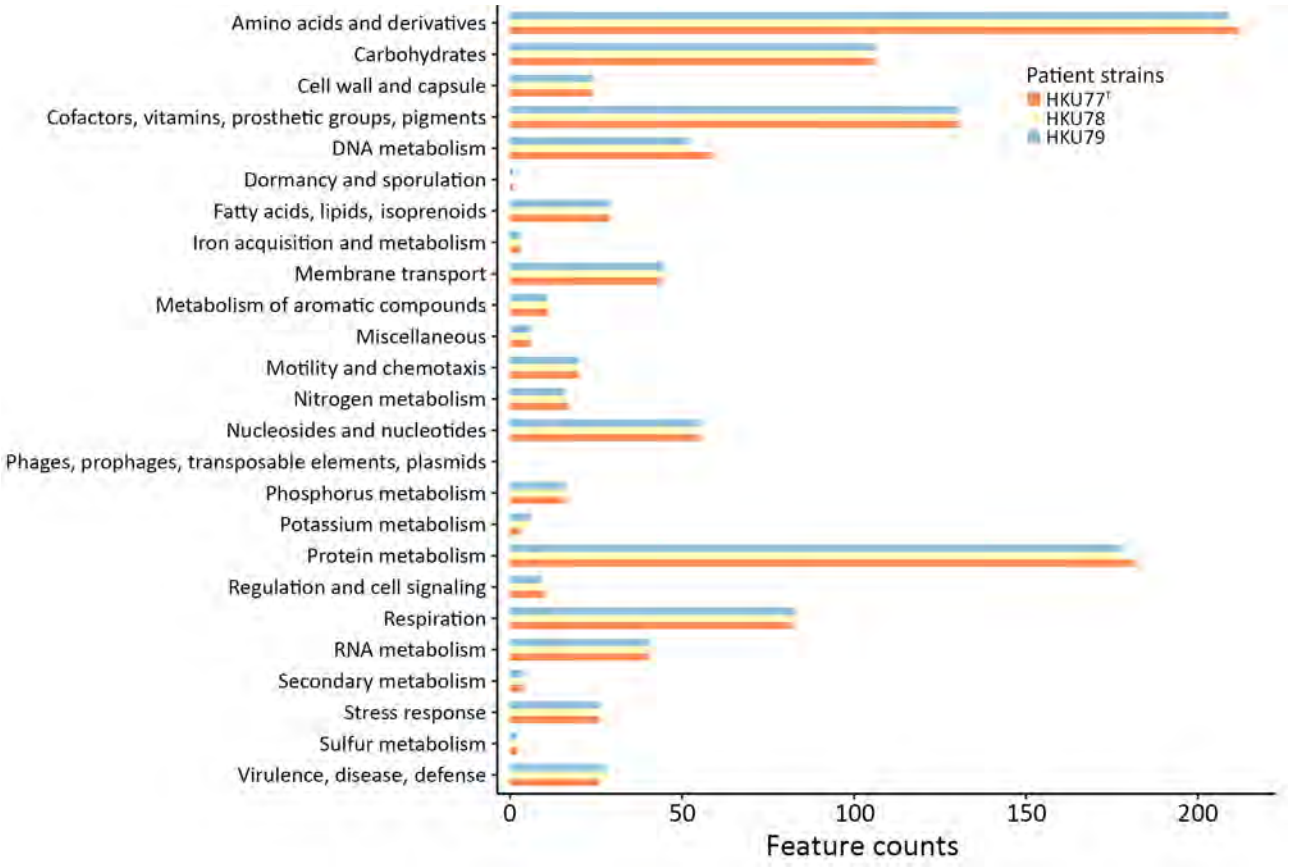

Figure 2. Comparison of feature counts of functional annotations from detection of novel thermotolerant *Tepidimonas* spp. bacteria in human respiratory specimens, Hong Kong, China, 2024. Annotations were determined by using Rapid Annotations using Subsystems Technology (Argonne National Laboratory, https://www.anl.gov/mcs/rast-rapid-annotation-using-subsystem-technology). Each functional category is represented by bars corresponding to the 3 patient strains of *T. hongkongensis* identified in this study.

95.3% to 97.8% among each other. Those 3 strains were most closely related to *T. fonticaldi* AT-A2 (dDDH value 26.1%–26.2%), followed by *T. taiwanensis* I1–1 (dDDH value 24.7%–24.8%), and *T. charontis* SPSP-6T (dDDH value 24.0%–24.3%), but the dDDH values were below the 70.0% threshold, indicating the 3 strains from our study are a different species (Table 6). On the basis of those results, we propose that strains HKU77, HKU78, and HKU79 represent a newly identified *Tepidimonas* species. We suggest the name *Tepidimonas hongkongensis* sp. nov. for the location of isolation and that strain HKU77^{T} (GenBank accession no. CP187300) be designated as the type strain.

Virulence, AMR, and Stress-Related Genes

We characterized virulence factors of *T. hongkongensis* by using the Virulence Factors of Pathogenic Bacteria database (https://www.mgc.ac.cn/VFs/main.htm), on the basis of available sequences (Appendix Table 1). We identified several genes that contribute to the function of motility and adherence, some of which are similar to genes of type IV pili of *Pseudomonas* spp., including *pilB*, *pilC*, and *pilT*, contributing to the adhesion of *T. hongkongensis* to other cells. We also detected different genes related to immune evasion and several genes that contribute to counteracting phagocytosis in humans. Those genes included *uge*, which is observed to generate the capsule in *Klebsiella* spp. bacteria, and *algC*, *algU*, and *algW*, which are responsible for alginate regulation and biosynthesis in *Pseudomonas* spp. bacteria. In addition, we observed genes in *T. hongkongensis* that are associated with secretion systems in other bacteria, including *clpV* (type VI secretory system), *epsE*, and *lspG* (type II secretory system). *T. hongkongensis* strains also contained *hemE* and *hemL* genes, which are observed in heme biosynthesis in *Haemophilus* spp. bacteria.

Another species, *T. taiwanensis*, has previously been reported to produce alkaline protease and polyhydroxyalkanoates (PHA), renewable and biodegradable polymers that can replace conventional plastic (*6*). Comparison of *T. hongkongensis* and type strain *T. taiwanensis* LMG22826T (GenBank

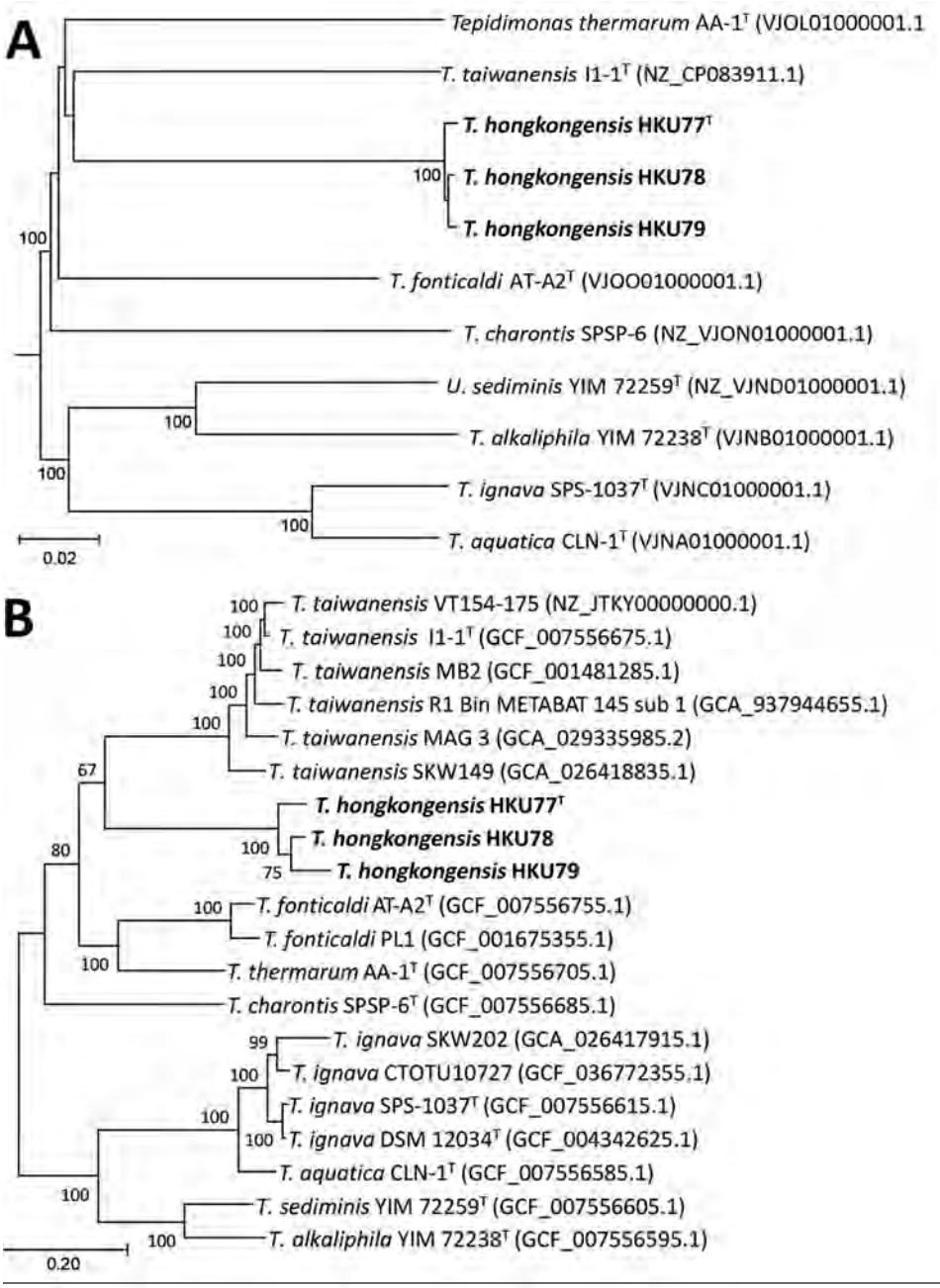

Figure 3. Phylogeny of novel thermotolerant *Tepidimonas* spp. bacteria isolated from human respiratory specimens, Hong Kong, China, 2024. Phylogenetic trees show the relationship between 3 patient strains identified in this study (bold font) and global representative *Tepidimonas* spp. strains. A) Tree was inferred using whole-genome data with Type (Strain) Gene Server (Leibniz Institute, https://tygs.dsmz.de). B) Tree inferred from the species-specific core genes and compared with existing *Tepidimonas* spp. in GenBank. Scale bar indicates nucleotide substitutions per site.

accession no. CP083911) showed that *T. hongkongensis* contained alkaline proteases, except lysyl endopeptidase. Furthermore, *T. taiwanensis* possesses *phaC* and *phaR* genes that are necessary for PHA production, as well as *phaZ* coding PHA depolymerase. Similarly, all 3 *T. hongkongensis* strains possessed the *phaC*, *phaR*, and *phaZ*, suggesting that *T. hongkongensis* is associated with PHA production. Oxidation of thiosulfate to sulfate has been reported in all *Tepidimonas* species through the *sox* pathway (*7*), and all 3 *T. hongkongensis* strains contained the genes encoding the sulfur-oxidizing protein.

Using the National Center for Biotechnology Information AMRfinder (https://www.ncbi.nlm.nih.gov/pathogens/antimicrobial-resistance/AMRFinder), we found that all 3 *T. hongkongensis* harbored aminoglycoside resistance genes (*aadA2*) and a β-lactamase gene (bla_{OXA-2}). We also identified stress-related genes, including multiple heat-shock proteins and efflux pumps, including *qacL* (Appendix Table 2).

Characteristics for Patients with *T. hongkongensis* Strains

The isolate of strain HKU77^T was from a patient with pulmonary metastases. The DNA GC content was

Table 6. Pairwise genomic alignments in study of novel thermotolerant *Tepidimonas* spp. bacteria in human respiratory specimens, Hong Kong, China, 2024*

Tepidimonas species	ID	Genome size, bp	GC, %	No. proteins	No. rRNA	No. tRNA	% d4
T. hongkongensis reference	HKU77^T	2,842,968	67.2	2,695	3	51	NA
T. hongkongensis	HKU78	2,924,694	67.1	2,807	6	52	95.3
T. hongkongensis	HKU79	2,891,522	67.2	2,786	3	50	95.5
T. fonticaldi	AT-A2	3,009,526	69.0	2,761	6	54	26.1
T. taiwanensis	I1–1	2,915,587	68.8	2,671	9	56	24.7
T. charontis	SPSP-6T	2,808,982	66.6	2,634	8	55	24.0
T. thermarum	AA1	2,703,753	68.7	2,552	6	51	23.8
T. aquatica	CLN-1	2,672,904	68.6	2,506	4	58	23.4
T. ignava	DSM 12034	2,715,700	68.8	2,562	6	54	22.7
T. sediminis	YIM 72259	2,533,936	71.8	2,337	5	58	22.5
T. alkaliphila	YIM 72238	2,465,445	69.0	2,279	3	54	21.8

*Comparison through digital DNA-DNA hybridization by using Type (Strain) Gene Server (Leibniz Institute, https://tygs.dsmz.de). ID, identification.

67.2% mol; we considered this the type strain. The isolate of the second strain, HKU78, was from a patient with community-acquired pneumonia and had DNA GC content of 67.1% mol. The isolate of the third strain, HKU79, was from a patient with underlying Graves' disease and paranoid schizophrenia and had DNA GC content of 67.2% mol.

Environmental Sample Collection and Clinical Correlations

We collected 101 water samples from the faucets in various areas of the hospital, including wards, utility rooms, bathrooms, and the pantry, after the study period in April 2025. Among collected samples, 47 (46.5%) grew thermotolerant bacteria (Table 7). From those 47 samples, we subsequently identified 43 (91.5%; 42.6% of all water samples collected) thermotolerant bacteria as *Schlegelella aquatica*. We identified *T. hongkongensis* in 2 (2.0%) water samples and *Prophyrobacter cryptus* bacteria in 1 (1.0%) water sample. The percentages of water samples growing *S. aquatica* (42.6%) and *T. hongkongensis* (2.0%) were higher than the rates in respiratory specimens: 0.6% *S. aquatica* and 0.2% *T. hongkongensis* ($p<0.05$). Although we identified >20 times more *S. aquatica* isolates than *Tepidimonas* spp. isolates in the water samples, we isolated 3 times as many *Tepidimonas* spp. bacteria than *S. aquatica* in respiratory specimens. Furthermore, among the 17 patients with *Tepidimonas* spp. bacteria isolated from sputum 48 hours after hospitalization (Table 2), none were hospitalized in the 2 wards from which we isolated *T. hongkongensis* in the water samples.

Discussion

Thermotolerant bacteria can thrive under elevated temperatures, typically 45°C–60°C. Examples of thermotolerant bacteria causing human infection include *Campylobacter fetus* (*8*) and *Mycobacterium xenopi* (*2*). Various thermotolerant bacteria, such as *Tepidimonas* spp., have been isolated or detected in environmental hot water samples, including hot springs (*9*–*11*). However, the clinical consequences of most thermotolerant bacteria are uncertain.

In addition to *Tepidimonas* spp., our study identified different thermotolerant bacteria in clinical specimens, including *S. aquatica*, which belongs to the Comamonadaceae family and was first isolated from a hot spring in Taiwan (*9*) but was not known to cause human infection. In addition, we identified *Vulcaniibacterium thermophilum* in 4 patient samples; it was first isolated from a geothermal soil sample in Tengchong, Yunnan Province, in southwest China in 2012 (*10*) and was the reported cause of prosthetic joint infection in 1 case (*13*). In addition, *Thermomonas* spp. bacteria, which we detected in 2 specimens, frequently have been isolated from hot water (*11*,*14*), marine sediment (*15*), and soil (*16*–*18*). One study reported its detection in the naso-oropharyngeal microbiome from breast cancer patients with severe COVID-19 (*19*). *Lactobacillus delbrueckii* bacteria, which we detected in 1 specimen, commonly are used for probiotics and food fermentation (*20*); however, that bacterium has been reported to cause urinary tract infection and bacteremia (*21*–*24*). Finally, we detected 3 *Bacillus* spp. bacteria, which are known to form heat-resistant spores; although non–*B. anthracis Bacillus* are usually considered environmental bacteria, they can cause infection in patients with prostheses and central catheters (*25*,*26*).

The genus *Tepidimonas* was established in 2000 (*27*), and its members are gram-negative bacilli with positive catalase and oxidase activity that are motile

Table 7. Bacteria from 101 water samples collected in hospital for study of novel thermotolerant *Tepidimonas* spp. bacteria in human respiratory specimens, Hong Kong, China, 2024*

Thermotolerant bacteria	No. (%) samples
Schlegelella aquatica	43 (42.6)
Tepidimonas hongkongensis sp. nov.	2 (2.0)
Prophyrobacter cryptus	1 (1.0)
Alphaproteobacterium	1 (1.0)

*Water samples were collected from faucets in various areas of the hospital, including wards, utility rooms, bathrooms, and the pantry.

due to a single polar flagellum. *Tepidimonas* spp. bacteria typically exhibit optimal growth at temperatures >45°C; therefore, most have been isolated from relatively high-temperature environments, such as hot springs and spas worldwide (*9*–*11*). As of January 25, 2026, only 8 *Tepidimonas* species have been validly published in the List of Prokaryotic names with Standing in Nomenclature: *T. ignava*, *T. aquatica*, *T. taiwanensis*, *T. thermarum*, *T. fonticaldi*, *T. sediminis*, *T. alkaliphila*, and *T. charontis* (https://lpsn.dsmz.de/genus/tepidimonas). Within the genus, *T. taiwanensis* is the only strain that uses glucose and fructose for growth, due to the presence of putative ABC glucose/mannose (*gtsABCD*) and fructose (*frcABC*) transporters (*7*), whereas other species are frequently referred to as asaccharolytic. Similar to a previous report (*7*), the novel *T. hongkongensis* bacterium does not use glucose and fructose for growth. Of note, *T. taiwanensis* produces alkaline protease and PHA, renewable and biodegradable polymers that can replace conventional plastic (*6*). Genome analysis revealed that *T. hongkongensis* contains most of the alkaline protease genes found in *T. taiwanensis*, as well as genes associated with PHA production (*12*). Analysis of stress-related genes in *T. hongkongensis* revealed the presence of heat-resistant protein and ATPase genes, which explain its thermotolerant characteristic.

In our study, 0.6% of respiratory specimens grew *Tepidimonas* spp. bacteria after prolonged incubation at 50°C, and most patients from whom specimens were collected had solid organ malignancy and chronic lung disease, although ages were wide ranging. Other *Tepidimonas* spp. bacteria have been detected in clinical samples. For instance, a proposed new *Tepidimonas* species, *T. arfidensis*, was cultured from a bone marrow aspirate sample from a patient with leukemia with neutropenic fever (*28*). Other *Tepidimonas* spp. bacteria have been implicated in different human microbiome studies, including the urine microbiome for urinary incontinence (*29*,*30*), the endometrial microbiome for endometriosis (*31*), the gut microbiome in primary sclerosing cholangitis (*32*), and the sinus microbiome in chronic rhinosinusitis (*33*). In our study, only 36.6% of the patients had growth of other pathogenic bacteria in the sputum (Table 3), suggesting that *Tepidimonas* spp. are pathogenic and can cause lower respiratory tract infection.

The tap water samples collected from the hospital revealed the presence of *T. hongkongensis* sp. nov. and a high percentage of *S. aquatica*. Those results align with previous findings that *Tepidimonas* spp. and *S. aquatica* bacteria are commonly found in the environment (*9*,*34*). Of note, we detected *Tepidimonas* spp. bacteria more frequently than *S. aquatica* in the water samples, but we detected more *Tepidimonas* spp. than *S. aquatica* in respiratory specimens (Tables 1, 7), suggesting that *Tepidimonas* spp. bacteria could have a greater potential for colonizing the human respiratory tract than other environmental bacteria.

Comparative genomic analysis revealed that all 3 *T. hongkongensis* strains contained various virulence genes spanning critical functional classes, including adherence, iron uptake, lipid metabolism, nutritional virulence, serum resistance, and stress adaptation, but those genes are absent in *S. aquatica* LMG 23380 (Appendix Table 1). Those genes support colonization of host tissue, nutrient scavenging, immune evasion, and persistence under stress, further underscoring the potential pathogenicity of *T. hongkongensis.* Although resistome profiling did not demonstrate substantial antimicrobial resistance in *T. hongkongensis* (Appendix Table 2), we did detect it in environmental samples, and its ability to acquire other resistance, such as colistin resistance, through horizontal gene transfer from other gram-negative bacteria, is not known (*35*,*36*). Therefore, further surveillance is warranted.

Whether detection of *T. hongkongensis* in the hospital water systems warrants interventions requires further risk assessments and studies. First, the infectious threshold of *T. hongkongensis* should be established to assess the risk that patients could acquire it from the water system. Furthermore, whether usual water disinfection protocols, such as chlorine or ultraviolet light, are effective against this bacterium is unknown. Ongoing vigilance and documentation will help define the baseline incidence and clinical significance for this bacterium and guide future recommendations.

The first limitation of our study is that it was conducted in a hospital network in Hong Kong; whether similar observations occur in other hospitals and countries requires further investigation. Second, we only used 50°C for agar incubation to isolate thermotolerant bacteria, which might have failed to recover other clinically relevant pathogens that do not grow at such high temperatures. Third, although isolation of *Tepidimonas* spp. bacteria from the clinical specimens in our study might be related to a hot water source, other studies have isolated various *Tepidimonas* spp. bacteria in sterile clinical specimens, suggesting this genus might not solely be an environmental contaminant. Finally, isolation of *Tepidimonas* spp. and other thermotolerant bacteria in respiratory specimens could represent colonization instead of respiratory pathogens. However, many patients in our study had underlying solid organ malignancy, suggesting pathogenicity is still possible in severely

immunocompromised patients, such as bone marrow transplant recipients. Further studies are required to investigate the pathogenic potential of *T. hongkongensis* and the range of illnesses the bacteria can cause.

In conclusion, we successfully isolated 42 thermotolerant *Tepidimonas* spp. bacterial strains from clinical specimens, including 3 novel strains confirmed by whole-genome sequencing. We propose the name *T. hongkongensis* sp. nov. to describe the 3 novel strains and designation of HKU77^{T} as the type strain of this novel species. The combination of high incubation temperature for selection, prolonged incubation for growth, and MALDI-TOF mass spectrometery and 16S rRNA sequencing enabled discovery of this novel species. Analysis of water samples from the hospital further confirmed the presence of *T. hongkongensis* in the environment. Although clinical implications of *T. hongkongensis*, especially in immunocompromised patients, are not yet known, its potential spread in water systems is concerning. Ongoing vigilance and documentation will help define the baseline incidence and clinical significance of *T. hongkongensis* and guide future recommendations.

Acknowledgments

We thank the laboratory staff for additional work in processing the respiratory specimens and water samples collected during the study period.

Whole-genome sequences for strains HKU77^{T} (GenBank accession no. CP187300), HKU78 (GenBank accession no. CP187547), and HKU79 (GenBank accession no. CP187301) are available in National Center for Biotechnology Information BioProject database (https://www.ncbi.nlm.nih.gov/bioproject) under BioProject no. PRJNA1245643.

This study was partly supported by funding from the start-up fund for new staff at the Faculty of Dentistry, The University of Hong Kong; and donations from May Tam Mak Mei Yin, Richard Yu and Carol Yu, the Shaw Foundation Hong Kong, Michael Seak-Kan Tong, Mow Lum Yip, Lee Wan Keung Charity Foundation Limited, Providence Foundation Limited (in memory of the late Lui Hac-Minh), Hui Ming, Hui Hoy and Chow Sin Lan Charity Fund Limited, The Chen Wai Wai Vivien Foundation Limited, Chan Yin Chuen Memorial Charitable Foundation, and Marina Man-Wai Lee. The funding sources had no role in the study design, data collection, analysis, interpretation, or writing of the report.

About the Author

Dr. Chiu is an associate consultant in the Department of Microbiology, Queen Mary Hospital, Hong Kong, China. His research interests are emerging infectious diseases and antimicrobial stewardship.

References

1. Li ZJ, Zhang HY, Ren LL, Lu QB, Ren X, Zhang CH, et al.; Chinese Centers for Disease Control and Prevention (CDC) Etiology of Respiratory Infection Surveillance Study Team. Etiological and epidemiological features of acute respiratory infections in China. Nat Commun. 2021;12:5026. https://doi.org/10.1038/s41467-021-25120-6
2. Marušić A, Katalinić-Janković V, Popović-Grle S, Janković M, Mazuranić I, Puljić I, et al. *Mycobacterium xenopi* pulmonary disease—epidemiology and clinical features in non-immunocompromised patients. J Infect. 2009;58:108–12. https://doi.org/10.1016/j.jinf.2009.01.001
3. Munson E, Carella A, Carroll KC. Valid and accepted novel bacterial taxa derived from human clinical specimens and taxonomic revisions published in 2022. J Clin Microbiol. 2023;61:e0083823. https://doi.org/10.1128/jcm.00838-23
4. Woo PC, Lau SK, Teng JL, Tse H, Yuen KY. Then and now: use of 16S rDNA gene sequencing for bacterial identification and discovery of novel bacteria in clinical microbiology laboratories. Clin Microbiol Infect. 2008;14:908–34. https://doi.org/10.1111/j.1469-0691.2008.02070.x
5. Clinical and Laboratory Standards Institute. Performance standards for antimicrobial susceptibility testing: thirty-fourth informational supplement (M100–ED34), Wayne (PA): The Institute; 2024.
6. Hermankova K, Kourilova X, Pernicova I, Bezdicek M, Lengerova M, Obruca S, et al. Complete genome sequence of the type strain *Tepidimonas taiwanensis* LMG 22826T, a thermophilic alkaline protease and polyhydroxyalkanoate producer. Genome Biol Evol. 2021;13:evab280. https://doi.org/10.1093/gbe/evab280
7. Albuquerque L, Castelhano N, Raposo P, Froufe HJC, Tiago I, Severino R, et al. Comparative genome sequence analysis of several species in the genus *Tepidimonas* and the description of a novel species *Tepidimonas charontis* sp. nov. Int J Syst Evol Microbiol. 2020;70:1596–604. https://doi.org/10.1099/ijsem.0.003942
8. Woo PC, Leung KW, Tsoi HW, Wong SS, Teng JL, Yuen KY. Thermo-tolerant *Campylobacter fetus* bacteraemia identified by 16S ribosomal RNA gene sequencing: an emerging pathogen in immunocompromised patients. J Med Microbiol. 2002;51:740–6. https://doi.org/10.1099/0022-1317-51-9-740
9. Chou YJ, Sheu SY, Sheu DS, Wang JT, Chen WM. *Schlegelella aquatica* sp. nov., a novel thermophilic bacterium isolated from a hot spring. Int J Syst Evol Microbiol. 2006;56:2793–7. https://doi.org/10.1099/ijs.0.64446-0
10. Wei DQ, Yu TT, Yao JC, Zhou EM, Song ZQ, Yin YR, et al. *Lysobacter thermophilus* sp. nov., isolated from a geothermal soil sample in Tengchong, south-west China. Antonie van Leeuwenhoek. 2012;102:643–51. https://doi.org/10.1007/s10482-012-9761-8
11. Alves MP, Rainey FA, Nobre MF, da Costa MS. *Thermomonas hydrothermalis* sp. nov., a new slightly thermophilic gamma-proteobacterium isolated from a hot spring in central Portugal. Syst Appl Microbiol. 2003;26:70–5. https://doi.org/10.1078/072320203322337335
12. Chen TL, Chou YJ, Chen WM, Arun B, Young CC. *Tepidimonas taiwanensis* sp. nov., a novel alkaline-protease-producing bacterium isolated from a hot spring. Extremophiles. 2006;10:35–40. https://doi.org/10.1007/s00792-005-0469-9
13. Dhawan B, Sebastian S, Malhotra R, Kapil A, Gautam D. Prosthetic joint infection due to *Lysobacter thermophilus* diagnosed by 16S rRNA gene sequencing. Indian J Med Microbiol. 2016;34:100–2. https://doi.org/10.4103/0255-0857.174124

14. Ju JH, Kim JS, Lee DH, Jeon JH, Heo SY, Seo JW, et al. *Thermomonas aquatica* sp. nov., isolated from an industrial wastewater treatment plant. Int J Syst Evol Microbiol. 2019;69:3399–404. https://doi.org/10.1099/ijsem.0.003630
15. Wu XT, He YQ, Li GX, Xiao H, Dai XR, Yang MR, et al. Genome sequence of sulfide-dependent denitrification bacterium *Thermomonas* sp. strain XSG, isolated from marine sediment. Microbiol Resour Announc. 2021;10:e00057-21. https://doi.org/10.1128/MRA.00057-21
16. Xu S, Chen J, Chen S, Lai Q, Liu Z, Xu Y. *Thermomonas mangrovi* sp. nov., isolated from soil of a mangrove nature reserve. Int J Syst Evol Microbiol. 2023;73:5. https://doi.org/10.1099/ijsem.0.005915
17. Wang L, Zheng S, Wang D, Wang L, Wang G. *Thermomonas carbonis* sp. nov., isolated from the soil of a coal mine. Int J Syst Evol Microbiol. 2014;64:3631–5. https://doi.org/10.1099/ijs.0.063800-0
18. Kim MK, Im WT, In JG, Kim SH, Yang DC. *Thermomonas koreensis* sp. nov., a mesophilic bacterium isolated from a ginseng field. Int J Syst Evol Microbiol. 2006;56:1615–9. https://doi.org/10.1099/ijs.0.64049-0
19. Viana MC, Curty G, Furtado C, Singh B, Bendall ML, Viola JPB, et al. Naso-oropharyngeal microbiome from breast cancer patients diagnosed with COVID-19. Front Microbiol. 2023;13:1074382. https://doi.org/10.3389/fmicb.2022.1074382
20. Hemmi J, Makino S, Yokoo T, Kano H, Asami Y, Takeda K, et al. Consumption of yogurt fermented with *Lactobacillus delbrueckii* ssp. *bulgaricus* OLL1073R-1 augments serum antibody titers against seasonal influenza vaccine in healthy adults. Biosci Microbiota Food Health. 2023;42:73–80. https://doi.org/10.12938/bmfh.2022-037
21. Neonakis IK, Skamagkas I, Stafylaki D, Maraki S. *Lactobacillus delbrueckii* urinary tract infection in a male patient: a case report. Germs. 2022;12:304–7. https://doi.org/10.18683/germs.2022.1333
22. Maillet F, Passeron A, Podglajen I, Ranque B, Pouchot J. *Lactobacillus delbrueckii* urinary tract infection in a male patient. Med Mal Infect. 2019;49:226–8. https://doi.org/10.1016/j.medmal.2018.11.006
23. Darbro BW, Petroelje BK, Doern GV. *Lactobacillus delbrueckii* as the cause of urinary tract infection. J Clin Microbiol. 2009;47:275–7. https://doi.org/10.1128/JCM.01630-08
24. DuPrey KM, McCrea L, Rabinowitch BL, Azad KN. Pyelonephritis and bacteremia from *Lactobacillus delbrueckii*. Case Rep Infect Dis. 2012;2012:745743. https://doi.org/10.1155/2012/745743
25. Shimada T, Ishikawa K, Kawai F, Yoneoka D, Mori N. Risk factors associated with infection-related mortality of *Bacillus cereus* bacteremia in hematologic disorders. Int J Hematol. 2023;118:726–30. https://doi.org/10.1007/s12185-023-03671-2
26. Castedo E, Castro A, Martin P, Roda J, Montero CG. *Bacillus cereus* prosthetic valve endocarditis. Ann Throac Surg. 1999;68:2351–2. https://doi.org/10.1016/s0003-4975(99)01163-7
27. Moreira C, Rainey FA, Nobre MF, da Silva MT, da Costa MS. *Tepidimonas ignava* gen. nov., sp. nov., a new chemolitho-heterotrophic and slightly thermophilic member of the beta-Proteobacteria. Int J Syst Evol Microbiol. 2000;50:735–42. https://doi.org/10.1099/00207713-50-2-735
28. Ko KS, Lee NY, Oh WS, Lee JH, Ki HK, Peck KR, et al. *Tepidimonas arfidensis* sp. nov., a novel gram-negative and thermophilic bacterium isolated from the bone marrow of a patient with leukemia in Korea. Microbiol Immunol. 2005;49:785–8. https://doi.org/10.1111/j.1348-0421.2005.tb03669.x
29. Carnes MU, Siddiqui NY, Karstens L, Gantz MG, Dinwiddie DL, Sung VW, et al.; Eunice Kennedy Shriver National Institute of Child Health and Human Development Pelvic Floor Disorders Network. Urinary microbiome community types associated with urinary incontinence severity in women. Am J Obstet Gynecol. 2024;230:344.e1–20. https://doi.org/10.1016/j.ajog.2023.10.036
30. Richter HE, Carnes MU, Komesu YM, Lukacz ES, Arya L, Bradley M, et al.; Eunice Kennedy Shriver National Institute of Child Health and Human Development Pelvic Floor Disorders Network. Association between the urogenital microbiome and surgical treatment response in women undergoing midurethral sling operation for mixed urinary incontinence. Am J Obstet Gynecol. 2022;226:93.e1–15. https://doi.org/10.1016/j.ajog.2021.07.008
31. Wessels JM, Domínguez MA, Leyland NA, Agarwal SK, Foster WG. Endometrial microbiota is more diverse in people with endometriosis than symptomatic controls. Sci Rep. 2021;11:18877. https://doi.org/10.1038/s41598-021-98380-3
32. Denoth L, Juillerat P, Kremer AE, Rogler G, Scharl M, Yilmaz B, et al.; on behalf ff the Swiss Ibd Cohort Study. Modulation of the mucosa-associated microbiome linked to the PTPN2 risk gene in patients with primary sclerosing cholangitis and ulcerative colitis. Microorganisms. 2021;9:1752. https://doi.org/10.3390/microorganisms9081752
33. Kim JH, Kim SH, Lim JY, Kim D, Jeong IS, Lee DK, et al. Association between the sinus microbiota with eosinophilic inflammation and prognosis in chronic rhinosinusitis with nasal polyps. Exp Mol Med. 2020;52:978–87. https://doi.org/10.1038/s12276-020-0458-1
34. Freitas M, Rainey FA, Nobre MF, Silvestre AJ, da Costa MS. *Tepidimonas aquatica* sp. nov., a new slightly thermophilic beta-proteobacterium isolated from a hot water tank. Syst Appl Microbiol. 2003;26:376–81. https://doi.org/10.1078/072320203322497400
35. Gao R, Hu Y, Li Z, Sun J, Wang Q, Lin J, et al. Dissemination and mechanism for the MCR-1 colistin resistance. PLoS Pathog. 2016;12:e1005957. https://doi.org/10.1371/journal.ppat.1005957
36. Sun J, Li XP, Fang LX, Sun RY, He YZ, Lin J, et al. Co-occurrence of mcr-1 in the chromosome and on an IncHI2 plasmid: persistence of colistin resistance in *Escherichia coli*. Int J Antimicrob Agents. 2018;51:842–7. https://doi.org/10.1016/j.ijantimicag.2018.01.007

Address for correspondence: Kwok-Yung Yuen, Department of Microbiology, School of Clinical Medicine, Li Ka Shing Faculty of Medicine, University of Hong Kong, Daniel & Mayce Yu Administration Wing, 21 Sassoon Rd, Pokfulam, Hong Kong, China; email: kyyuen@hku.hk; or Jade Lee-Lee Teng, Faculty of Dentistry, Prince Philip Dental Hospital, 34 Hospital Rd, Sai Ying Pun, Hong Kong, China; email: llteng@hku.hk

Clinical Manifestations of Emerging *Trichosporon* spp. Infections, France

Marie Desnos-Ollivier, Alexandre Alanio, Maud Gits-Muselli, Karine Boukris-Sitbon, Agathe Bertho, Aude Sturny-Leclère, Emilie Guemas, Philippe Poirier, Christine Bonnal, Marie-Elisabeth Bougnoux, Sophie Brun, Taieb Chouaki, Nicole Desbois-Nogard, Elisabeth Chachaty, Florence Persat, Marc Pihet, André Paugam, Françoise Botterel, Magalie Demar, Loïc Favennec, Florent Morio, Frédéric Gabriel, Arnaud Fekkar, Jean-Pierre Gangneux, Caroline Mahinc, Valérie Letscher-Bru, Laurence Millon, Frédéric Dalle, Julie Bonhomme, Muriel Nicolas, Boualem Sendid, Milène Sasso, Laure Courtellemont, Anne-Laure Roux, Estelle Perraud-Cateau, Juliette Guitard, Edith Mazars, Olivier Lortholary, Fanny Lanternier

Fungi in the family Trichosporonaceae are rarely involved in invasive disease but are frequently associated with colonization or respiratory allergic infection. Trichosporonaceae exhibit intrinsic resistance to echinocandin antimicrobial drugs, posing challenges for treatment and contributing to high mortality rates. We compiled a nationwide analysis of 112 cases of invasive disease caused by *Trichosporon* spp. and related fungi, diagnosed in France over 20 years, that combined clinical data, susceptibility profiles, and molecular identification. We identified 12 species; *T. asahii* was the most common species recovered, and the new species *T. austroamericanum* was next. Comparison of clinical data highlighted species and genotypic differences, such as a much higher proportion of children infected by *T. asahii* and major differences in antimicrobial drug susceptibility. Correct identification is not only of epidemiologic interest but also necessary for patient management because of the varying clinical and microbiological characteristics found in different species.

Among the wide range of fungi responsible for invasive infections in humans, species within the Trichosporonaceae family are generally considered rare or uncommon pathogens (*1*–*4*). However, recent reports indicate an increasing incidence in both high-income and resource-limited countries over the past decade (*2*,*4*–*6*).

Author affiliations: Institut Pasteur, Paris, France (M. Desnos-Ollivier, A. Alanio, K. Boukris-Sitbon, A. Bertho, A. Sturny-Leclère, O. Lortholary, F. Lanternier); Hôpital Saint-Louis, Paris (A. Alanio, M. Gits-Muselli); Hôpital Robert Debré, APHP, Université Paris Cité, Paris (M. Gits-Muselli); Université Paris Cité, INSERM, IAME, Paris (M. Gits-Muselli); Centre National de la Recherche Scientifique, Toulouse, France (E. Guemas); Centre Hospitalier Universitaire Clermont-Ferrand, Clermont-Ferrand, France (P. Poirier); Université Blaise Pascal, Clermont-Ferrand (P. Poirier); Hôpital Bichat–Claude-Bernard, Paris (C. Bonnal); Hôpital Necker-Enfants Malades, Paris (M.-E. Bougnoux, O. Lortholary, F. Lanternier); Hôpital Avicenne, Bobigny, France (S. Brun); Centre Hospitalier Universitaire Amiens-Picardie, Amiens, France (T. Chouaki); University Hospital of Martinique, Fort-de-France, Martinique (N. Desbois-Nogard); Gustave Roussy, Villejuif, France (E. Chachaty); Centre Hospitalier Universitaire de Lyon, Lyon, France (F. Persat); CHU d'Angers, University Angers, University Brest, GEIHP, SFR ICAT, Angers, France (M. Pihet); Cochin Port Royal University Hospial AP-AP (A. Paugam); Université Paris-Est Créteil, Créteil, France (F. Botterel); Centre Hospitalier Andree Rosemon, Cayenne, Guyana (M. Demar); University Hospital Charles Nicolle, Rouen, France (L. Favennec); Nantes University Hospital, Nantes, France (F. Morio); Centre Hospitalier Universitaire de Bordeaux, Bordeaux, France (F. Gabriel); Centre d'Immunologie et des Maladies Infectieuses, Paris (A. Fekkar); Hôpital Pontchaillou, Rennes, France (J.-P. Gangneux); Centre Hospitalier Universitaire de Saint-Étienne, Saint-Étienne, France (C. Mahinc); Hôpitaux Universitaires de Strasbourg, Strasbourg, France (V. Letscher-Bru); University Hospital J Minjoz, Besancon, France (L. Millon); Dijon University Hospital, Dijon, France (F. Dalle); Centre Hospitalier Universitaire Côte de Nacre, Caen, France (J. Bonhomme); Centre Hospitalier Universitaire de Guadeloupe, Pointe-à-Pitre, Guadeloupe, France (M. Nicolas); Lille University Hospital Center, Lille, France (B. Sendid); Centre Hospitalier Universitaire Nîmes et Université de Montpellier, Nîmes, France (M. Sasso); Centre Hospitalier Universitaire d'Orléans, Orléans, France (L. Courtellemont); Assistance Publique-Hôpitaux de Paris, Boulogne-Billancourt, France (A.-L. Roux); Centre Hospitalier Universitaire Poitiers, Poitiers, France (E. Perraud-Cateau); Hôpital Saint-Antoine, Paris (J. Guitard); Centre Hospitalier de Valenciennes, Valenciennes, France (E. Mazars)

DOI: https://doi.org/10.3201/eid3201.250504

Trichosporonaceae is a family of basidiomycetous, yeast-like fungi that produce arthroconidia and are commonly found in air, soil, and water worldwide (*7*). Trichosporonaceae can also be recovered from contaminated materials or medical devices. Some species are part of the normal or transient human microbiota, particularly on the skin and in the gastrointestinal tract (*8*–*11*). After taxonomic revisions, clinically relevant Trichosporonaceae are now distributed into 3 genera, *Trichosporon*, *Apiotrichum*, and *Cutaneotrichosporon*. Each genus contains multiple species known to cause invasive infections in humans (*12*–*14*). *T. asahii* remains the most frequently reported species responsible for invasive fungal disease (IFD) caused by Trichosporonaceae (*5*,*6*,*9*,*15*–*17*), but it is also known to cause summer-type hypersensitivity pneumonitis, particularly in Japan (*18*,*19*). This species is also considered the most virulent among Trichosporonaceae and demonstrates higher MICs for amphotericin B and azoles than other fungi (*15*,*17*,*20*–*22*). The distribution of other species varies, but typically *Cutaneotrichosporon dermatis*, *T. asteroides*, *C. mucoides*, *T. inkin*, and *T. faecale* are relatively commonly involved in IFD (*2*,*4*,*5*,*17*,*21*,*23*,*24*), and *T. inkin* is recognized as a leading cause of white piedra (*25*).

IFD caused by Trichosporonaceae has a high mortality rate, ranging from 30% to 90% (*4*,*24*,*26*,*27*). Such infections are commonly associated with hematologic malignancies (*1*,*2*,*28*) and are frequently reported in pediatric populations (*26*). Immunosuppressed patients are particularly at risk, especially those with central venous catheters, urinary or peritoneal catheters, broad-spectrum antimicrobial drug use, corticosteroid therapy, intensive care unit (ICU) stays, or prior exposure to echinocandins such as caspofungin, to which Trichosporonaceae fungi are intrinsically resistant (*1*,*3*,*4*,*23*,*29*,*30*). Clusters of infection have been described previously (*16*). Current treatment guidelines recommend voriconazole monotherapy for IFD caused by Trichosporonaceae (*28*,*31*), although other azoles and amphotericin B are also commonly used. Some studies advocate combination therapy with amphotericin B and voriconazole (*17*,*20*).

Despite the clinical relevance of Trichosporonaceae infections, epidemiologic data from multicentric studies remain scarce (*4*), and most information stems from case reports or small patient cohorts (*6*,*27*). Because of the variability in antimicrobial drug susceptibility across species, accurate identification is essential for both epidemiologic understanding and clinical management (*1*,*21*). In this article, we report 112 episodes of IFD caused by Trichosporonaceae, diagnosed during 2002–2022 in France. The cases were documented across 41 centers and are supported by clinical data, precise molecular identification, and antimicrobial susceptibility testing.

Materials and Methods

Clinical Data

We included in the study all first episodes of IFD caused by Trichosporonaceae notified at the National Reference Center for Invasive Mycoses and Antifungals (NRCMA) during 2002–2022. Demographic and clinical data concerning the patients were collected during prospective national surveillance programs. The surveillance of the NRCMA was approved by the Institut Pasteur Institutional Review Board 1 (approval no. 2009–34/IRB) and the Commission National de l'Informatique et des Libertés, according to French regulations. The YEASTS program collected information and strains corresponding to fungemia episodes in hospitals near Paris during 2002–2022 (*1*). The Réseau de Surveillance des Infections Fongiques (RESSIF) program centralized data on IFD episodes, without selection bias, from 36 hospitals throughout France, diagnosed during 2012 and 2022 (*32*).

We collected demographic and clinical data by using electronic case report form designed on the VOOZANOO platform (http://www2.voozanoo.net). We conducted statistical analyses by using Stata software version 17 (StataCorp, LLC, https://www.stata.com). We expressed categorical variables as percentages and continuous variables as medians ±SD. We evaluated differences between the groups by using χ^2 or Fisher exact tests and considered p values <0.05 statistically significant. We conducted Shapiro-Wilk tests to determine the distribution of MIC values for genotypes 1, 3, and 4 of *T. asahii* and then performed a Kruskal Wallis or analysis of variance test.

Isolates

As part of this prospective surveillance program, clinical isolates were sent to the NRCMA for complementary investigations, including species identification and in vitro antifungal susceptibility testing by the EUCAST method. Depending on the period, methods for identification were different (ID32C carbon assimilation profiles or matrix-assisted laser desorption/ionization time-of-flight mass spectrometry profiles associated with internal transcribed spacer [ITS] or intergenic spacer [IGS] region sequencing), but when it was possible ITS+IGS regions were sequenced prospectively or retrospectively. For the isolates (n = 3) not sent to the active surveillances programs YEASTS or RESSIF (*32*,*33*) and from before 2008, retrospective identification was not possible.

We amplified ITS regions by PCR by using panfungal primers V9D (5′-TTAAGTCCCTGCCCTTTGTA-3′) (*34*) and LS266 (5′-GCATTCCCAAACAACTCGACTC-3′) (*35*) and the IGS region by using 26SF and 5SR, as previously reported (*14*). We edited sequences by using Geneious Prime software (https://www.geneious.com). We trimmed ITS region sequences with sequences of primers ITS1 (5′-TCCGTAGGTGAACCTGCGG-3′) and ITS4 (5′-GCATATCAATAAGCGGAGGA-3′) and IGS1 region sequences by using sequences SCTTTGSACT and ACYGCATCC, adapted from previous reports (*14*).

For species identification, we compared concatenated sequences of ITS and IGS regions of the clinical isolates with concatenated sequences of type strains. When sequences of isolates had a percentage of similarity with sequence of type strain >98%, we considered isolates as belonging to the same species. When the percentage was 90%–98%, we suggested that isolates could belong to a putative undescribed species, and we named them with a *cf.* in front of the species name. For those isolates, we deposited sequences into GenBank (accession nos. PV575975–8).

We conducted multiple alignments of 106 ITS+IGS concatenated sequences of 1,556 bp (95 clinical isolates and 11 type strains) by using multiple sequence comparison by log-expectation alignment and constructed a neighbor-joining tree by using a Hasegawa-Kishino-Yano model with a bootstrap analysis of 1,000 replicates. We used a newick tree to design a cladogram with Itol software version 1.9 (https://itol.embl.de). We used IGS1 sequences for *T. asahii* isolates to determine genotype.

Antimicrobial Susceptibility Profile

We determined MICs for fluconazole, voriconazole, posaconazole, and flucytosine for all isolates according to the EUCAST broth microdilution standardized method (https://www.eucast.org/fileadmin/src/media/PDFs/EUCAST_files/AFST/Files/EUCAST_E.Def_7.4_Yeast_definitive_revised_2023.pdf). We also determined caspofungin, micafungin, and amphotericin B MICs with a modified version of the protocol, which uses AM3 medium instead of RPMI medium as described previously (*36*).

We calculated values of MIC inhibiting at least 50% (MIC_{50}) or 90% (MIC_{90}) of the isolates among 1 species. Of note, neither EUCAST nor Clinical and Laboratory Standards Institute currently publish breakpoints for any Trichosporonacea species. Recently, EUCAST proposed interpretation of amphotericin B and anidulafungin MICs for *Trichosporon* spp.; but because we did not use standard conditions to determine MICs for amphotericin B, we cannot take those values into account. However, epidemiologic cutoffs have been proposed for fluconazole for *T. asahii* and for fluconazole and voriconazole for *C. dermatis* (https://www.eucast.org/fileadmin/src/media/PDFs/EUCAST_files/AFST/Files/EUCAST_guidance_for_Rare_yeast_with_no_breakpoints_final_clean_19-06-2024.pdf).

Phenotypic Observation

We examined the macroscopic appearance of 10 isolates belonging to species of the ovoides clade, containing the main *Trichosporon* species involved in IFD. Those isolates were CBS 4828 type of *T. faecale*, CNRMA15.795 *T. cf. faecale*, CBS 5585 neotype of *T. inkin*, CNRMA20.443 *T. austroamericanum*, CBS 2482 type of *T. coremiiforme*, CNRMA19.523 *T. cf. coremiiforme*, CBS 7556 neotype of *T. ovoides*, CBS 9051 type of *T. lactis*, CBS 9052 type of *T. caseorum*, and CBS 2479 type of *T. asahii.*

We prepared a suspension concentrated at 2.10^5 cells/mL on the basis of a fresh culture of isolates in sterile water. We determined concentration by using luna cell counting slides (Logos Biosystems Inc., https://logosbio.com). Then, we deposited 2 μL of the solution on Sabouraud agar plates and incubated at 20°C. We measured the size of the colony after 4, 5, 6, 7, and 10 days and noted color and appearance.

Results

Episode Characteristics

During 2002–2022, a total of 112 cases of IFD caused by Trichosporonaceae, mainly bloodstream infection (77.7%), concerning 112 patients, were reported to the NRCMA from 41 hospitals in France (37 metropolitan and 4 overseas) (Table 1). Most patients were male (66.1% vs. 33.9% female); median age was 43.77 years, and a high percentage were extreme ages (18.8% children <15 years of age and 17.9% adults >65 years of age). The main underlying conditions were hematologic malignancies (39.3%), recent surgery (≤30 days from diagnosis; 28.6%), and solid organ transplantation (11.6%). Twelve patients also had diabetes mellitus, 7 had traumas (generally serious accidents involving contact with plants, such as being crushed by a tree, or mower or rototiller accidents resulting in multiple fractures or amputations), and 23 were neutropenic. Risk factors associated were stay in ICU (45.9%), presence of catheter (56.3%), immunosuppressive drugs (37.5%), or administration of steroids (22.3%). At least 33.9% of patients received antimicrobial drugs before IFD diagnosis, mainly echinocandins (24.1%). Most patients received antimicrobial drugs after diagnosis (90.2%),

Table 1. Demographic and clinical characteristics of patients in study of clinical manifestations of emerging *Trichosporon* species infections, France, 2002–2022*

Characteristics	Value
Sex	
M	74 (66.1)
F	38 (33.9
Age, years, mean ±SD (range)	43.77 ±24.39 (1–90)
<15 y	21 (18.8)
>65 y	20 (17.7)
Clinical information	
Bloodstream infection	87 (77.7)
Bone infection	12 (10.7)
Stay in intensive care unit, n = 98	45 (45.9)
Underlying conditions	
Hematologic malignancy	44 (39.3)
Acute leukemia	25
Lymphoma	13
Recent surgery	32 (28.6)
Solid organ transplantation	14 (11.6)
Kidney	5
Heart	4
Liver	4
Lung	1
Diabetes	12 (10.7)
Risk factors	
Neutropenia	23 (20.5)
Presence of catheter	63 (56.3)
Immunosuppressive treatment	42 (37.5)
Steroids	25 (22.3)
Antifungal exposure	38 (33.9)
Echinocandins	27 (24.1)
Antifungal treatment	101 (90.2)
Containing voriconazole	64 (57.1)
Containing amphotericin B	24 (21.4)
Outcome, n = 99	
Death within 30 days of diagnosis	38 (38.4)

*Values are no. (%) except as indicated.

mainly with voriconazole (57.1%). Mortality by day 30 after diagnosis was 38.4%.

Of note, among the 112 episodes, 14 corresponded to mixed infections. Those patients were simultaneously infected with 1 or 2 additional fungal species, mainly ascomycetous yeast (n = 9) at the same infection site (Appendix Table, http://wwwnc.cdc.gov/EID/article/32/1/25-0504-App1.pdf). Those episodes were caused by 6 different species of Trichosporonaceae, although *T. asahii* was involved in most cases (9/14).

Species Diversity

Among the 112 episodes studied, 101 isolates from 101 episodes were sent to the NRCMA. On the basis of the ITS+IGS sequencing, 94 isolates belonged to 9 already described species, distributed across 3 genera (*Trichosporon* [n = 5], *Apiotrichum* [n = 2], *Cutaneotrichosporon* [n = 2]). Seven isolates corresponded to 3 putative unknown species: 4 closely related to *T. faecale* (GenBank accession nos. PV575976 and PV575977), 2 to *T. coremiiforme* (GenBank accession no. PV575975) and 1 to *A. loubierii* (GenBank accession no, PV575978) (Figure 1).

Most isolates belonged to the *Trichosporon* genus (90.1%). Two species represented most cases of IFD caused by *Trichosporonaceae* in France: *T. asahii* (51.5%) and the species recently described as *T. austroamericanum* (22.8%), which is closely related to *T. inkin* (Figure 2). Among the 58 cases of *T. asahii*, 51 isolates were received at the NRCMA. On the basis of IGS sequencing, 6 genotypes were identified, mainly genotype 1 (n = 25) and genotypes 3 (n = 11) and 4 (n = 11), followed by genotype 7 (n = 2), genotype 5 (n = 1), and 1 isolate with an undefined allele.

Episodes of IFD caused by Trichosporonaceae were reported under several national surveillance programs. If we compare the distribution of species and the number of episodes by year over the same period for the RESSIF program and the YEASTS program, the proportion of *T. asahii* is higher among the YEASTS program than among the RESSIF survey but the opposite for *T. austroamericanum.* A trend for an increased number of episodes over time in the RESSIF survey was seen (Figure 3).

In Vitro Antimicrobial Drug Susceptibility

Voriconazole appears to be the most active antifungal agent in vitro (Table 2), with the lowest MIC_{50} or MIC_{90} values and ranges of MICs for all species, except for *A. mycotoxinivorans*, for which both isolates have lower values for posaconazole than voriconazole. Conversely, all isolates of all species have high MICs to flucytosine (>4 mg/L and all MIC_{50} determined ≥32 mg/L) and to echinocandins (data not shown). *Trichosporon asahii*, *A. loubieri*, *A. mycotoxinivorans*, and isolates closely related to *T. faecale* have reduced susceptibility to amphotericin B compared with other Trichosporonaceae species. More precisely, *T. asahii* isolates belonging to genotype 4 tend toward lower MIC_{50} or MIC_{90} values for azoles and amphotericin B than isolates of genotypes 1 and 3 (genotype 1 displayed the highest MIC_{50} or MIC_{90} for all antimicrobial drugs), but the differences were statistically significant only for amphotericin B (p = 0.0073). EUCAST recently defined epidemiologic cutoff values for fluconazole (wild-type ≤16 mg/L) for *T. asahii* and for fluconazole (wild-type ≤16 mg/L) and voriconazole (wild-type ≤0.125 mg/L) for *C. dermatis*. Taking those values into account, we can see only 4 isolates of genotype 1 can be considered resistant to fluconazole. We found no resistant isolates among the other genotypes or for *C. dermatis* strains. Furthermore, *T. asahii* have higher MICs for azoles and amphotericin B than *T. austroamericanum* and *T. inkin* with a difference in voriconazole MIC distribution (Figure 4).

Growth Rate and Morphologic Aspect

On the basis of the growth rate measured for 10 isolates belonging to different species of *Trichosporon* (Appendix Figure), we observed that *T. coremiiforme* and isolates corresponding to the potential *T. cf. coremiiforme* (isolate name CNRMA19.523) species had the highest growth rate, whereas *T. inkin* and *T. austroamericanum* had reduced but similar growth rate. All isolates grew as white colonies on Sabouraud agar plate and were generally creamy, although some species appeared smooth or flat to domed and wrinkled (Figure 5).

T. asahii versus *T. austroamericanum*

Episodes involving only 1 species (excluding mixed infections) and those with isolates sent to NRCMA were included in this comparison, which corresponds to 44 episodes of *T. asahii* infection and 22 of *T. austroamericanum*. A higher proportion of women and children among the patients infected with *T. asahii* were observed, whereas the proportion of men was much higher among patients infected with *T. austroamericanum*. Furthermore, infections because of *T. austroamericanum* were more frequently associated with recent surgery (p = 0.03) or solid organ transplantation (p = 0.008) (Table 3).

Discussion

In this report, we describe demographic, clinical, and molecular characteristics of a large collection of 112 cases of IFD caused by Trichosporonaceae fungi diagnosed in France throughout 2 decades during multicentric national prospective surveillance programs. As mentioned in other studies, we observed a high proportion of children among the patients (18.8%) but with a significant difference in proportion depending on the species (*26*). As outlined in this study, most cases of IFD caused by Trichosporonaceae are bloodstream infections (77.7%) and occur in patients with underlying conditions such as hematologic malignancy (39.3%), recent surgery (28.6%), or solid organ transplant (11.6%) (*1*,*2*,*28*). A recent study concluded that, in cases of fungemia caused by *Trichosporon* spp., advanced age, use of mechanical ventilation, and persistent neutropenia were associated with poor prognosis (*4*). Another study demonstrated that exposure to caspofungin is a risk factor associated with fungemia caused by *Trichosporon* spp. (*1*).

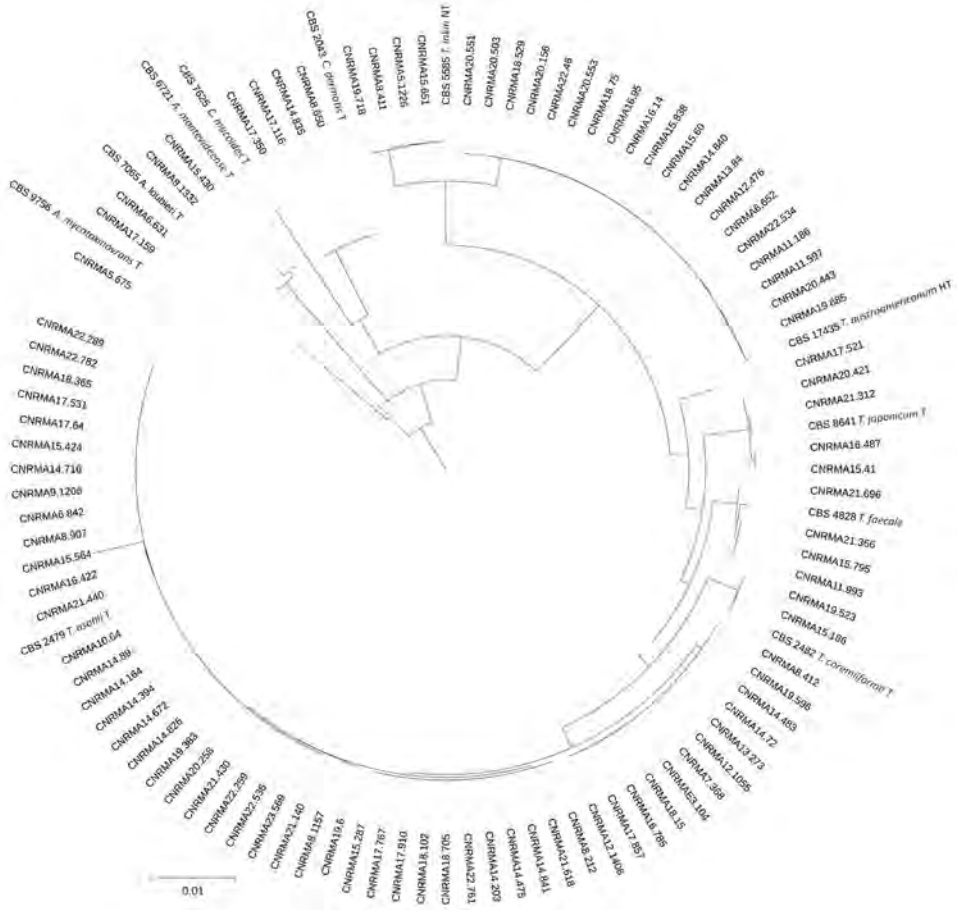

Figure 1. Cladogram of 94 clinical isolates and 11 reference strains from study of clinical manifestations of emerging *Trichosporon* species infections, France, 2002–2022. Tree was designed using Itol software version 1.9 (https://itol.embl.de) on the basis of the newick tree obtained from the Hasegawa-Kishino-Yano model analysis after multiple alignment of concatenation of trimmed sequences of internal transcribed spacer and intergenic spacer regions (Geneious Prime, https://www.geneious.com). GenBank accession numbers or type strain identification numbers are provided for each isolate. Scale bar indicates substitutions per site.

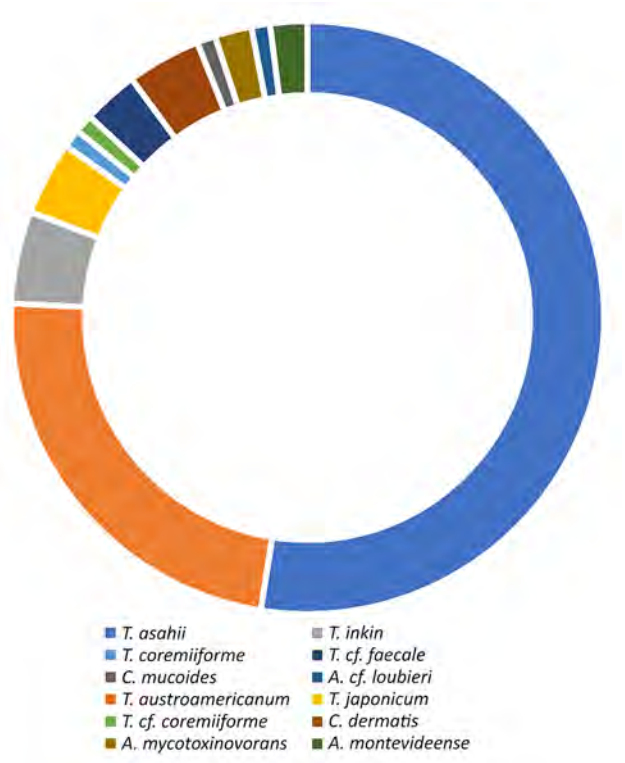

Figure 2. Proportions of species involved in invasive trichosporonosis cases from study of clinical manifestations of emerging *Trichosporon* species infections, France, 2002–2022. The *cf.* designation indicates putative undescribed species.

Similarly, the risk factors that we found frequently were hospitalization in ICU (45.9%), presence of catheter (56.3%), and exposure to antimicrobial drugs (33.9%), primarily echinocandins (27/38).

On the basis of the data from RESSIF, we seem to be observing a trend in France toward an increase in the number of cases of IFD caused by Trichosporonaceae. However, the incidence of those infections is difficult to determine precisely, because some participating centers did not participate exhaustively over the entire study period.

Sequencing of ITS+IGS regions of rDNA enabled us to identify ≥12 different species of Trichosporonaceae responsible for 112 IFD cases in 41 different hospitals in France during 2002–2022. Of note, all cases reported from overseas territories were because of *T. asahii* only. We suggest that 7 cases were because of putative undescribed species, for which additional molecular characterizations such as whole-genome sequencing analysis are now warranted. As expected, most cases were caused by *T. asahii*, but unexpectedly, the recently described species *T. austroamericanum* ranked second (*12*). The percentage of children was significantly lower among patients infected with this new species (4.5%) than among those infected with *T. asahii* (29.5%; p = 0.024). On the other hand, the percentage of men was much higher (86% vs. 52%; p = 0.007). In addition, *T. asahii* was more frequently involved in bloodstream infections or exposure to an antimicrobial drug, whereas *T. austroamericanum* was more frequently associated with recent surgery (p = 0.03) and solid organ transplant (p = 0.008) (Table 3).

Sequencing of the IGS region for *T. asahii* isolates is described as a useful tool for genotyping this species. At least 13 different genotypes have already been identified, some of which appear to have geographic preferences. Genotypes 1, 3, and 4 seem to be more frequent worldwide (*5*,*15*,*16*,*23*,*37*). Among the 101 isolates received at the NRCMA during the study period we report, the 51 isolates of *T. asahii* belonged to 6 different genotypes, and we confirmed the major genotype was 1 (49%), followed by genotypes 3 (21%) and 4 (21%). Of note, genotype 3 is frequently reported in the United

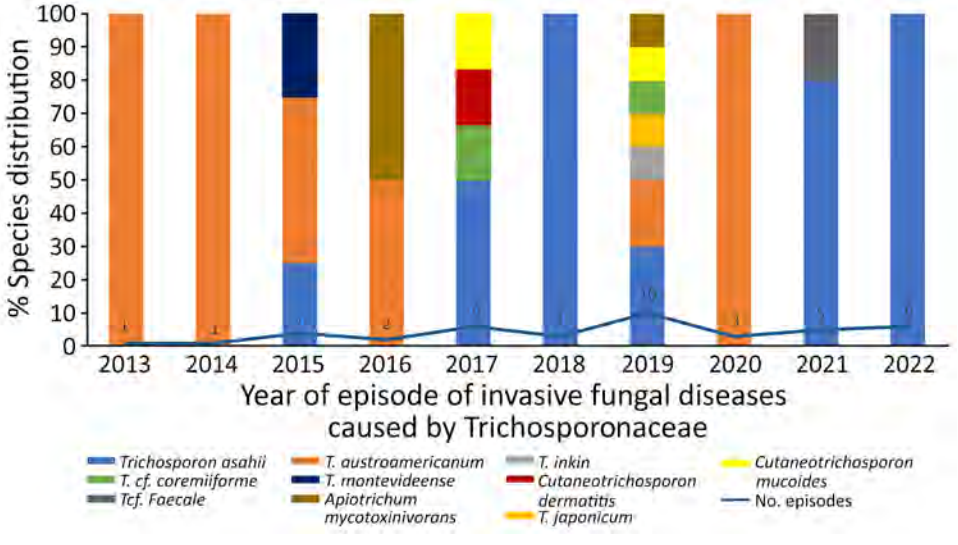

Figure 3. Species distribution over time for RESSIF survey used in a study of the clinical manifestations of emerging *Trichosporon* species infections, France, 2002–2022. Number of episodes diagnosed in the centers participating in the survey are reported for each year. The *cf.* designation indicates putative undescribed species.

Table 2. Antimicrobial susceptibility profiles of 101 clinical isolates determined by using the EUCAST method, according to species and genotypes recovered, in study of clinical manifestations of emerging *Trichosporon* species infections, France, 2002–2022*

Species and genotype (no. isolates)	MIC_{50}/MIC_{90}, mg/L (range of MICs)				
	AMB	5FC	FLUCO	VORI	POSA
Trichosporon asahii (52)	2/>4 (0.25–>4)	64/>64 (4–>64)	4/16 (0.25–64)	0.06/0.25 (<0.015–1)	0.25/0.5 (<0.015–1)
Genotype 1 (25)	2/>4 (0.25–>4)	64/>64 (4–>64)	4/32 (0.25–64)	0.125/0.25 (<0.015–1)	0.25/0.5 (<0.015–1)
Genotype 3 (12)	1/2 (0.5–4)	32/>64 (8–>64)	1 /4 (0.5–8)	0.06/0.25 (0.03–0.5)	0.25/0.5 (0.06–0.5)
Genotype 4 (11)	1/1 (0.25–2)	32/>64 (8–>64)	2/4 (0.25–16)	0.06/0.125 (<0.015–0.25)	0.06/0.25 (<0.015–0.5)
Genotype 7 (2)	−/− (2)	−/− (>64)	−/− (2–16)	−/− (0.06–0.5)	−/− (0.03–0.5)
Genotype 5 (1)	−/− (4)	−/− (32)	−/− (2)	−/− (0.03)	−/− (0.25)
Genotype 13† (1)	−/− (>4)	−/− (>64)	−/− (8)	−/− (0.125)	−/− (1)
T. austroamericanum (21)	0.25/1 (0.06–2)	>64/>64 (64–>64)	0.5/4 (0.25–4)	0.03/0.06 (<0.015–0.125)	0.06/0.25 (<0.015–0.25)
T. inkin (7)	0.5/− (0.125–>4)	>64/− (16–>64)	2/− (1–16)	0.03/− (<0.015–0.25)	0.125/− (<0.015–0.5)
T. cf. coremiiforme (2)	−/− (0.5–2)	−/− (8–32)	−/− (0.5–1)	−/− (0.03–0.125)	−/− (0.06–0.125)
T. coremiiforme (1)	−/− (0.5)	−/− (16)	−/− (2)	−/− (0.03)	−/− (0.125)
T. cf. faecale (4)	−/− (1–>4)	−/− (16–>64)	−/− (1–16)	−/− (0.03–0.25)	−/− (0.03–0.5)
T. japonicum (4)	−/− (0.25–4)	−/− (8–>64)	−/− (0.5–4)	−/− (<0.015–0.125)	−/− (0.03–0.125)
Cutaneotrichosporon dermatis (4)	−/− (0.06–0.25)	−/− (>64)	−/− (2–16)	−/− (0.03–0.125)	−/− (<0.015–0.125)
C. mucoides (1)	−/− (0.06)	−/− (8)	−/− (2)	−/− (0.125)	−/− (0.5)
Apiotrichum loubieri (1)	−/− (1)	−/− (8)	−/− (2)	−/− (0.03)	−/− (0.06)
A. montevideense (2)	−/− (0.06–0.25)	−/− (>64)	−/− (1)	−/− (0.03–0.06)	−/− (0.03–0.125)
A. mycotoxinivorans (2)	−/− (2)	−/− (16–32)	−/− (2–8)	−/− (0.125–1)	−/− (<0.015–0.25)

*AMB, amphotericin B; *cf*., putative undescribed species; FLUCO, fluconazole; POSA, posaconazole; VORI, voriconazole; 5FC, flucytosine.
†Genotype 13 corresponds to the genotype described previously (GenBank accession no. MN936175)

States, in Thailand, and in the houses of summer-type hypersensitivity pneumonitis patients in Japan (*14*,*17*). Of interest, among the 11 patients infected with genotype 3 in this study, at least 6 were recovered from patients born or diagnosed in the Americas. Surprisingly, according to the genotype and excluding cases of mixed infections, 13 of 21 patients infected by genotype 1 died within 30 days of diagnosis: 5 of 11 for genotype 3 and only 1 of 8 for genotype 4. Those results could suggest some epidemiologic characteristic related to genotype or some difference in terms of virulence.

We confirmed that no matter the species or genotypes, voriconazole is the most effective antimicrobial drug in vitro against isolates belonging to the Trichosporonaceae family (*17*,*20*). Because of the small number of isolates for 10 species, we can only give the MIC values obtained for informational purposes. However, there are some differences worth noting: *T. asahii*, *A. loubieri*, *A. mycotoxinivorans*, and the isolates closely related to *T. faecale* have a lower susceptibility to amphotericin B compared with other species. Furthermore, *T. asahii* has higher MICs for azoles and amphotericin B than do *T. austroamericanum* and *T. inkin*. Some differences are noticed between genotypes; genotype 1 has the highest MIC for all antimicrobial drugs tested, whereas genotype 4 has lower MICs to azoles and amphotericin B than isolates of genotypes 1 and 3. Some studies reported a lower susceptibility for certain genotypes (*17*,*37*,*38*) and one study found that genotype 7 isolates have the highest MIC90 values for azoles, suggesting those isolates contributed to the increasing rates of voriconazole non-wild–type isolates observed in the past 10 years (*37*). In this study, the proportion of genotype 7 was

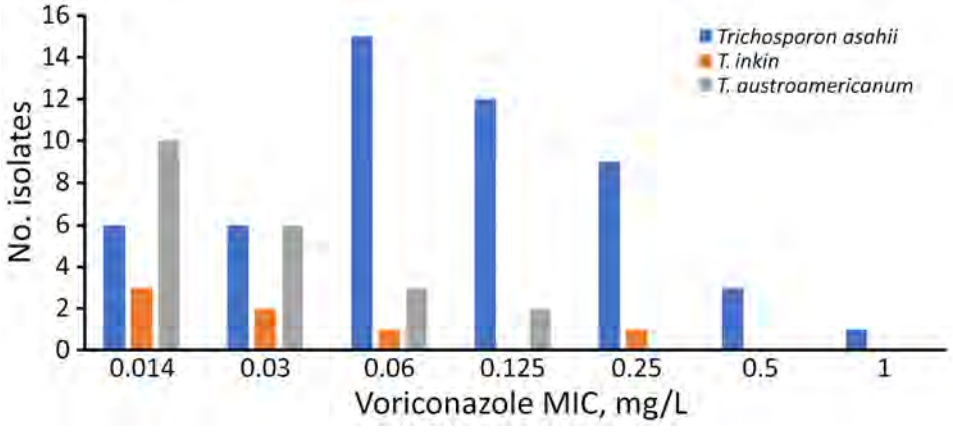

Figure 4. Voriconazole MIC distribution for 3 species of *Trichosporon* from study of clinical manifestations of emerging *Trichosporon* species infections, France, 2002–2022. MICs determined by using the EUCAST method.

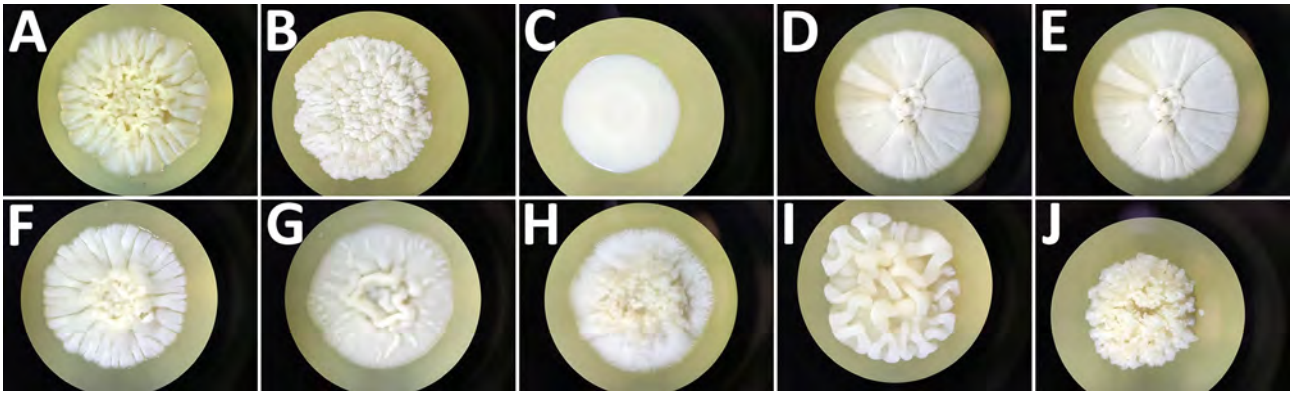

Figure 5. Macroscopic aspect of colonies grown on Sabouraud agar plates incubated 10 days at 20°C for 10 isolates recovered from study of clinical manifestations of emerging *Trichosporon* species infections, France, 2002–2022. A) *T. asahii* type strain isolate CBS 2479. B) *T. austroamericanum* isolate CNRMA20.443. C) *T. inkin* neotype strain isolate CBS 5585. D) *T. coremiiforme* type strain isolate CBS 2482. E) *T. cf. coremiiforme* isolate CNRMA19.523. F) *T. faecale* type strain isolate CBS 4828. G) *T. cf. coremiiforme* isolate CNRMA15.795. H) *T. ovoides* neotype strain isolate CBS 7556. I) *T. caseorum* type strain isolate CBS 9052. J) *T. lactis* isolate CBS 9051. *T. coremiiforme* and isolates corresponding to the potential *T. cf. coremiiforme* species (E, G) had the highest growth rate, whereas *T. inkin* and *T. austroamericanum* had reduced but similar growth rate. The *cf.* designation indicates putative undescribed species.

too small to calculate MIC_{90}s. Nevertheless, determining natural diversity would be useful to explain differences in susceptibility or even virulence, possibly linked to environmental pressures such as repeated exposure to azoles, because that mechanism is known in other pathogenic fungi (*39*–*41*).

We confirmed that *T. asahii*, especially genotype 1, is the major species of the Trichosporonaceae family involved in human IFD. We also confirmed that the pediatric population is at a higher risk and that the most frequent underlying conditions associated with infection are hematologic malignancies, recent surgery, and solid

Table 3. Comparison of demographic and clinical characteristics of the patients with single trichosporonosis episodes caused by *Trichosporon asahii* versus *T. austroamericanum* from study of clinical manifestations of emerging *Trichosporon* species infections, France, 2002–2022*

Characteristics	*T. asahii*, n = 44	*T. austroamericanum*, n = 22	p value
Sex			
M	23 (52.2)	19 (86.4)	0.007
F	21 (47.8)	3 (13.6)	
Mean age, y, ±SD (range)	43 ±24.5 (1–83)	50 ±19.7 (8–83)	0.159
<15 y	13 (29.5)	1 (4.5)	0.024
>65 y	6 (13.6)	5 (22.7)	0.35
Site of infection			
Bloodstream infection	37 (84.1)	15 (68.2)	0.038
Bone	3 (6.8)	4 (18.2)	
Skin	3 (6.8)	1 (4.5)	
Intensive care unit admission	15 (34.1)	8 (36.4)	0.903
Hematologic malignancy	22 (50)	6 (27.3)	0.082
Acute leukemia	12 (27.3)	3 (13.6)	
Lymphoma	8 (18.2)	1 (45)	
Recent surgery	6 (13.6)	8 (36.4)	0.03
Orthopedic	2 (4.5)	2 (9.1)	
Cardiac	0	2 (9.1)	
Kidney-urinary tract	0	2 (9.1)	
Solid organ transplantation	3 (6.8)	8 (36.4)	0.008
Liver	2 (4.5)	1 (4.5)	
Kidney	1 (2.3)	3 (13.6)	
Heart	0	3 (13.6)	
Lung	0	1 (4.5)	
Presence of catheter	29 (65.9)	10 (45.5)	0.315
Exposure to antimicrobial drugs	13 (29.5)	10 (45.5)	0.175
Neutropenia	11 (25)	3 (13.6)	0.535
Immunosuppresive drugs	19 (43.2)	11 (50)	0.571
Corticotherapy	12 (27.3)	4 (18.2)	0.665
Death within 30 days of diagnosis	14 (31.8)	5 (22.7)	0.389

*Values are no. (%) except as indicated.

organ transplantation. We identified 3 main genotypes recovered among the patients diagnosed in French hospitals (genotypes 1, 3, and 4). Of note, we observed that genotype 4 seems to be more frequently associated with trauma and having lower MICs values for amphotericin B and azoles, compared with other genotypes. Species and genotype identification of environmental isolates will be necessary to increase the knowledge about natural reservoirs, diversity, and virulence.

We observed that the recently described *T. austroamericanum*, closely related to *T. inkin* and frequently misidentified by using carbon profile assimilation pattern, 26S, ITS sequencing, or matrix-assisted laser desorption/ionization time-of-flight mass spectrometry, was the second most common Trichosporonaceae family involved in human IFD. When compared with the clinical data of patients infected with *T. asahii,* we found very different species characteristics. In contrast, *T. inkin*, *T. faecale*, and *C. dermatis*, which are frequently identified as responsible for non–*T. asahii* IFD, were rarely involved in our survey (*4*,*17*,*21*).

In conclusion, this study confirms that the correct identification of Trichosporonaceae species and genotypes is not only of epidemiologic interest but also critical for patient management. Certain clinical and microbiological characteristics, such as in vitro susceptibility to antimicrobial agents, can vary according to species. Clinicians must have the correct organism identification to treat patients correctly.

Acknowledgments

Funding was provided by Santé Publique France.

About the Author

Dr. Desnos-Ollivier is a deputy director of the French National Reference Center for invasive Mycoses and Antifungals at the Institut Pasteur, Paris, France. She is involved in managing the national surveillance program of invasive fungal infections in yeast identification, the study of antifungal resistance, cluster cases, and the emergence of new yeast species.

References

1. Bretagne S, Renaudat C, Desnos-Ollivier M, Sitbon K, Lortholary O, Dromer F; French Mycosis Study Group. Predisposing factors and outcome of uncommon yeast species-related fungaemia based on an exhaustive surveillance programme (2002–14). J Antimicrob Chemother. 2017;72:1784–93. https://doi.org/10.1093/jac/dkx045
2. Colombo AL, Padovan AC, Chaves GM. Current knowledge of *Trichosporon* spp. and Trichosporonosis. Clin Microbiol Rev. 2011;24:682–700. https://doi.org/10.1128/CMR.00003-11
3. Lima YP, Dias VC. *Trichosporon* spp.: what's new? Future Microbiol. 2024;19:373–5. https://doi.org/10.2217/fmb-2023-0281
4. Nobrega de Almeida J, Francisco EC, Holguín Ruiz A, Cuéllar LE, Rodrigues Aquino V, Verena Mendes A, et al. Epidemiology, clinical aspects, outcomes and prognostic factors associated with Trichosporon fungaemia: results of an international multicentre study carried out at 23 medical centres. J Antimicrob Chemother. 2021;76:1907–15. https://doi.org/10.1093/jac/dkab085
5. Kuo SH, Lu PL, Chen YC, Ho MW, Lee CH, Chou CH, et al. The epidemiology, genotypes, antifungal susceptibility of *Trichosporon* species, and the impact of voriconazole on *Trichosporon* fungemia patients. J Formos Med Assoc. 2021;120:1686–94. https://doi.org/10.1016/j.jfma.2020.12.007
6. Liao Y, Lu X, Yang S, Luo Y, Chen Q, Yang R. Epidemiology and outcome of *Trichosporon* fungemia: a review of 185 reported cases from 1975 to 2014. Open Forum Infect Dis. 2015;2:ofv141. https://doi.org/10.1093/ofid/ofv141
7. Sugita T, Nishikawa A, Ichikawa T, Ikeda R, Shinoda T. Isolation of *Trichosporon asahii* from environmental materials. Med Mycol. 2000;38:27–30. https://doi.org/10.1080/mmy.38.1.27.30
8. Cho O, Matsukura M, Sugita T. Molecular evidence that the opportunistic fungal pathogen *Trichosporon asahii* is part of the normal fungal microbiota of the human gut based on rRNA genotyping. Int J Infect Dis. 2015;39:87–8. https://doi.org/10.1016/j.ijid.2015.09.009
9. Li H, Guo M, Wang C, Li Y, Fernandez AM, Ferraro TN, et al. Epidemiological study of *Trichosporon asahii* infections over the past 23 years. Epidemiol Infect. 2020;148:e169. https://doi.org/10.1017/S0950268820001624
10. Mehta V, Nayyar C, Gulati N, Singla N, Rai S, Chandar J. A comprehensive review of *Trichosporon* spp.: an invasive and emerging fungus. Cureus. 2021;13:e17345. https://doi.org/10.7759/cureus.17345
11. Zhang E, Sugita T, Tsuboi R, Yamazaki T, Makimura K. The opportunistic yeast pathogen *Trichosporon asahii* colonizes the skin of healthy individuals: analysis of 380 healthy individuals by age and gender using a nested polymerase chain reaction assay. Microbiol Immunol. 2011;55:483–8. https://doi.org/10.1111/j.1348-0421.2011.00341.x
12. Francisco EC, Desnos-Ollivier M, Dieleman C, Boekhout T, Santos DWCL, Medina-Pestana JO, et al. Unveiling *Trichosporon austroamericanum* sp. nov.: a novel emerging opportunistic basidiomycetous yeast species. Mycopathologia. 2024;189:43. https://doi.org/10.1007/s11046-024-00851-4
13. Liu XZ, Wang QM, Göker M, Groenewald M, Kachalkin AV, Lumbsch HT, et al. Towards an integrated phylogenetic classification of the *Tremellomycetes*. Stud Mycol. 2015;81:85–147. https://doi.org/10.1016/j.simyco.2015.12.001
14. Sugita T, Nakajima M, Ikeda R, Matsushima T, Shinoda T. Sequence analysis of the ribosomal DNA intergenic spacer 1 regions of *Trichosporon* species. J Clin Microbiol. 2002;40:1826–30. https://doi.org/10.1128/JCM.40.5.1826-1830.2002
15. Arabatzis M, Abel P, Kanellopoulou M, Adamou D, Alexandrou-Athanasoulis H, Stathi A, et al. Sequence-based identification, genotyping and EUCAST antifungal susceptibilities of *Trichosporon* clinical isolates from Greece. Clin Microbiol Infect. 2014;20:777–83. https://doi.org/10.1111/1469-0691.12501
16. Desnos-Ollivier M, Maufrais C, Pihet M, Aznar C, Dromer F; French Mycoses Study Group. Epidemiological investigation for grouped cases of *Trichosporon asahii* using whole genome and IGS1 sequencing. Mycoses. 2020;63:942–51. https://doi.org/10.1111/myc.13126
17. Guo LN, Yu SY, Hsueh PR, Al-Hatmi AMS, Meis JF, Hagen F, et al. Invasive infections due to *Trichosporon*: species distribution, genotyping, and antifungal susceptibilities from

a multicenter study in China. J Clin Microbiol. 2019;57:e01505–18. https://doi.org/10.1128/JCM.01505-18
18. Nakajima A, Saraya T, Mori T, Ikeda R, Sugita T, Watanabe T, et al. Familial summer-type hypersensitivity pneumonitis in Japan: two case reports and review of the literature. BMC Res Notes. 2013;6:371. https://doi.org/10.1186/1756-0500-6-371
19. Sugita T, Ikeda R, Nishikawa A. Analysis of *Trichosporon* isolates obtained from the houses of patients with summer-type hypersensitivity pneumonitis. J Clin Microbiol. 2004;42:5467–71. https://doi.org/10.1128/JCM.42.12.5467-5471.2004
20. Desnos-Ollivier M, Lortholary O, Bretagne S, Dromer F. Azole susceptibility profiles of more than 9,000 clinical yeast isolates belonging to 40 common and rare species. Antimicrob Agents Chemother. 2021;65:e02615–20. https://doi.org/10.1128/AAC.02615-20
21. Francisco EC, de Almeida Junior JN, de Queiroz Telles F, Aquino VR, Mendes AVA, de Andrade Barberino MGM, et al. Species distribution and antifungal susceptibility of 358 *Trichosporon* clinical isolates collected in 24 medical centres. Clin Microbiol Infect. 2019;25:909.e1–5. https://doi.org/10.1016/j.cmi.2019.03.026
22. Kurakado S, Miyashita T, Chiba R, Sato C, Matsumoto Y, Sugita T. Role of arthroconidia in biofilm formation by *Trichosporon asahii*. Mycoses. 2021;64:42–7. https://doi.org/10.1111/myc.13181
23. Parashar A, Rastogi V, Prakash H, Pandey A, Rudramurthy SM. Intergenic spacer (IGS-1) region sequence-based identification, genotypic analysis, and antifungal susceptibility of clinical *Trichosporon* species. Indian J Med Microbiol. 2023;45:100390. https://doi.org/10.1016/j.ijmmb.2023.100390
24. Chagas-Neto TC, Chaves GM, Melo AS, Colombo AL. Bloodstream infections due to *Trichosporon* spp.: species distribution, *Trichosporon asahii* genotypes determined on the basis of ribosomal DNA intergenic spacer 1 sequencing, and antifungal susceptibility testing. J Clin Microbiol. 2009;47:1074–81. https://doi.org/10.1128/JCM.01614-08
25. Guerrero-Ponce AE, Araiza J, Tirado-Sánchez A, Bonifaz A. Review article white piedra: review of 131 cases. Mycoses. 2024;67:e13668. https://doi.org/10.1111/myc.13668
26. Akaslan Kara A, Çay Ü, Yalçınkaya R, Erdeniz EH, Tural Kara T, Özdemir H, et al. Bloodstream infections due to *Trichosporon* species in paediatric patients: results from the first national study from Turkey. J Mycol Med. 2022;32:101229. https://doi.org/10.1016/j.mycmed.2021.101229
27. de Almeida Júnior JN, Hennequin C. Invasive *Trichosporon* infection: a systematic review on a re-emerging fungal pathogen. Front Microbiol. 2016;7:1629. https://doi.org/10.3389/fmicb.2016.01629
28. Chen SC, Perfect J, Colombo AL, Cornely OA, Groll AH, Seidel D, et al. Global guideline for the diagnosis and management of rare yeast infections: an initiative of the ECMM in cooperation with ISHAM and ASM. Lancet Infect Dis. 2021;21:e375–86. https://doi.org/10.1016/S1473-3099(21)00203-6
29. Bayramoglu G, Sonmez M, Tosun I, Aydin K, Aydin F. Breakthrough *Trichosporon asahii* fungemia in neutropenic patient with acute leukemia while receiving caspofungin. Infection. 2008;36:68–70. https://doi.org/10.1007/s15010-007-6278-6
30. Cordeiro RA, Aguiar ALR, da Silva BN, Pereira LMG, Portela FVM, de Camargo ZP, et al. *Trichosporon asahii* and *Trichosporon inkin* biofilms produce antifungal-tolerant persister cells. Front Cell Infect Microbiol. 2021;11:645812. https://doi.org/10.3389/fcimb.2021.645812
31. Arendrup MC, Boekhout T, Akova M, Meis JF, Cornely OA, Lortholary O; European Society of Clinical Microbiology and Infectious Diseases Fungal Infection Study Group; European Confederation of Medical Mycology. ESCMID and ECMM joint clinical guidelines for the diagnosis and management of rare invasive yeast infections. Clin Microbiol Infect. 2014;20(Suppl 3):76–98. https://doi.org/10.1111/1469-0691.12360
32. Bretagne S, Sitbon K, Desnos-Ollivier M, Garcia-Hermoso D, Letscher-Bru V, Cassaing S, et al.; French Mycoses Study Group. Active surveillance program to increase awareness on invasive fungal diseases: the French RESSIF network (2012 to 2018). MBio. 2022;13:e0092022. https://doi.org/10.1128/mbio.00920-22
33. Dannaoui E, Paugam A, Develoux M, Chochillon C, Matheron J, Datry A, et al. Comparison of antifungal MICs for yeasts obtained using the EUCAST method in a reference laboratory and the Etest in nine different hospital laboratories. Clin Microbiol Infect. 2010;16:863–9. https://doi.org/10.1111/j.1469-0691.2009.02997.x
34. de Hoog GS, Gerrits van den Ende AH. Molecular diagnostics of clinical strains of filamentous *Basidiomycetes*. Mycoses. 1998;41:183–9. https://doi.org/10.1111/j.1439-0507.1998.tb00321.x
35. Masclaux F, Guého E, de Hoog GS, Christen R. Phylogenetic relationships of human-pathogenic *Cladosporium* (*Xylohypha*) species inferred from partial LS rRNA sequences. J Med Vet Mycol. 1995;33:327–38. https://doi.org/10.1080/02681219580000651
36. Desnos-Ollivier M, Bretagne S, Lortholary O, Dromer F; French Mycoses Study Group. Echinocandins susceptibility patterns of 2,787 yeast isolates: importance of the thresholds for the detection of FKS mutations. Antimicrob Agents Chemother. 2022;66:e0172521. https://doi.org/10.1128/aac.01725-21
37. Francisco EC, de Almeida Junior JN, Queiroz-Telles F, Aquino VR, Mendes AVA, de Oliveira Silva M, et al. Correlation of *Trichosporon asahii* genotypes with anatomical sites and antifungal susceptibility profiles: data analyses from 284 isolates collected in the last 22 years across 24 medical centers. Antimicrob Agents Chemother. 2021;65:e01104–20. https://doi.org/10.1128/AAC.01104-20
38. Sun W, Su J, Xu S, Yan D. *Trichosporon asahii* causing nosocomial urinary tract infections in intensive care unit patients: genotypes, virulence factors and antifungal susceptibility testing. J Med Microbiol. 2012;61:1750–7. https://doi.org/10.1099/jmm.0.049817-0
39. Casadevall A, Kontoyiannis DP, Robert V. On the emergence of *Candida auris*: climate change, azoles, swamps, and birds. MBio. 2019;10:e01397–19. https://doi.org/10.1128/mBio.01397-19
40. Lestrade PPA, Meis JF, Melchers WJG, Verweij PE. Triazole resistance in *Aspergillus fumigatus*: recent insights and challenges for patient management. Clin Microbiol Infect. 2019;25:799–806. https://doi.org/10.1016/j.cmi.2018.11.027
41. Padovan ACB, Rocha WPDS, Toti ACM, Freitas de Jesus DF, Chaves GM, Colombo AL. Exploring the resistance mechanisms in *Trichosporon asahii*: triazoles as the last defense for invasive trichosporonosis. Fungal Genet Biol. 2019;133:103267. https://doi.org/10.1016/j.fgb.2019.103267

Address for correspondence: Marie Desnos-Ollivier, Institut Pasteur, 28 rue du Docteur Roux, 75015 Paris, France; email: mdesnos@pasteur.fr

Enhanced Isolation and Detection of COVID-19 in Hospitalized Patients Undergoing Antiviral Therapy

Ranawaka A.P.M. Perera, Andrew Marques, Jevon Graham-Wooten, Li Hui Tan, Noam Cohen, Kyle Rodino, Ronald G. Collman, Frederic D. Bushman, Susan R. Weiss

We evaluated the efficiency of SARS-CoV-2 detection from patient respiratory specimens by comparing 3 cell lines: Vero E6, Vero E6 expressing transmembrane protease serine 2 (Vero E6 T2), and Vero E6 expressing angiotensin-converting enzyme 2 and transmembrane protease serine 2 (Vero E6 A2T2). We compared a range of sample types, clinical conditions, and real-time reverse transcription PCR cycle threshold values. Vero E6 A2T2 exhibited enhanced sensitivity by supporting efficient virus entry and replication with faster cytopathic effect. Vero E6 culture isolated infectious virus only up to 3 days after PCR confirmation but with Vero E6 A2T2 cells, culture occurred up to 7 days after confirmation. Whole-genome sequencing showed no evidence of adaptive mutations when Vero E6 A2T2 was used for viral culture, supporting use for downstream analyses. Optimized infectious virus detection systems are needed for research and clinical settings, particularly for high-risk, immunocompromised populations that produce virus longer and contribute to variant emergence.

After infection, SARS-CoV-2 is produced from the respiratory tract, which is the primary mode of secondary transmission between contacts (*1*–*3*). Therefore, it is essential to identify and isolate patients producing infectious virus to minimize transmission. Developing sensitive methods for identifying infectious virus and defining the kinetics of infectious viral production are critical for informing measures aimed at reducing the community and hospital transmission risk. This goal is particularly crucial for hospitalized or immunocompromised persons who might experience prolonged viral replication with consequences of both prolonged infectivity and new variant emergence, as well as receiving antiviral treatments whose effect on infectious virus produced is not well understood (*4*,*5*)

Infected persons might remain real-time reverse transcription (qRT-PCR) positive for extended periods well after the resolution of clinical symptoms and detectable infectious virus (*6*–*8*). Previous studies have associated antigen positivity with detectable infectious virus (*9*). Alternatively, some practitioners use specific qRT-PCR cycle thresholds (Cts) or defined time after initial PCR positivity (*10*–*12*). However, sensitive detection of infectious virus is essential to know which patients might contribute to forward transmission and to calibrate other methodologies.

Typically, the Vero E6 cell line has been used for the detection of infectious virus production and the resultant data was the basis for designating isolation measures during the initial pandemic phase (*13*–*15*). This cell line is particularly advantageous because of its genetic deficiency in type I interferon production, which enables efficient viral propagation by evading host antiviral defenses (*16*,*17*) However, highly sensitive methods are necessary to understand the nature of infectious virus production, particularly in hospitalized patients undergoing antiviral treatment. Subsequent studies have used modified Vero E6 lines expressing transmembrane protease serine 2 (TMPRSS2) and angiotensin-converting enzyme 2 (ACE2) for improved viral culture (*18*–*21*) but without systematic parallel comparisons across these lines. The purpose of this study was to compare viral culture

Author affiliations: Department of Veterans Affairs, Philadelphia, Pennsylvania, USA (R.A.P.M. Perera); University of Pennsylvania, Philadelphia (R.A.P.M. Perera, A. Marques, J. Graham-Wooten, L.H. Tan, N. Cohen, K. Rodino, R.G. Collman, F.D. Bushman, S.R. Weiss)

DOI: https://doi.org/10.3201/eid3201.251011

methods for the detection of infectious SARS-CoV-2 to identify improved and optimized methods.

Materials and Methods

Patient Population

We obtained respiratory samples from 246 SARS-CoV-2 positive patients at the Hospital of the University of Pennsylvania (Philadelphia, PA, USA), determined by Cepheid (https://www.cepheid.com), Thermo Fisher TaqPath EUA (Thermo Fisher Scientific, https://www.thermofisher.com), or Roche Cobas (https://www.roche.com) clinical assay, depending on period. We determined Ct values for all samples before virus isolation by the qRT-PCR protocol as described previously (*22*). Nasopharyngeal swab and endotracheal aspirate specimens were collected during April 2020–February 2024 from critically ill hospitalized patients who provided consent (University of Pennsylvania internal review board protocol no. 823392), and we extracted clinical data from the electronic medical record system. We obtained additional nasopharyngeal swab specimens as deidentified specimens that remained after clinical patient testing from several timepoints during April 2020–February 2024 (University of Pennsylvania internal review board protocol no. 814859). Nasopharyngeal swab specimens were collected in viral transport medium (VTM; BD, https://www.bd.com) or in some cases phosphate-buffered saline (PBS) because of VTM shortage, and endotracheal aspirates were collected without media. Specimens were stored at −80C until analysis.

Cell Lines and Viruses

We cultured Vero E6 (ATCC-CRL-1586), Vero E6 TMPRSS2 (kindly provided by Dr. Sara Cherry), and Vero E6 ACE2 TMPRSS2 (kindly provided by Dr. Luis Martinez-Sobrido) in Dulbecco minimum essential medium (DMEM) with 10% L-glutamine, 4.5 g/L D-glucose (ThermoFisher Scientific), 10% heat-inactivated fetal bovine serum (FBS; Cytiva, https://www.cytivalifesciences.com), and 1× penicillin/streptomycin (Thermo Fisher Scientific). rSARS-CoV-2-mCherry virus was kindly provided by Dr. Luis Martinez-Sobrido.

Human Primary Epithelial Cell Air-Liquid Interface Cultures

We derived nasal epithelial stem cells from cytologic brushings obtained from patients without respiratory infection undergoing sinonasal surgery at the University of Pennsylvania and the Philadelphia Veterans Affairs Medical Center, after receiving informed consent and under protocols approved by the University of Pennsylvania internal review board (protocol no. 800614) and the Philadelphia Veterans Affairs internal review board (protocol no. 00781). We pooled nasal cells from 4–6 patients and differentiated as previously described to prepare air-liquid interface cell cultures (*23*).

Virus Culture

We seeded Vero E6, Vero E6 TMPRSS2, and Vero E6 ACE2 TMPRSS2 cells at 100,000 cells/well into 48-well plates (TPP Techno Plastic Products, https://www.tpp.ch) to achieve subconfluent monolayers after 24 hours in a CO_2 incubator. We removed the medium and inoculated 50 μL of PCR-positive clinical specimen diluted 1:1 in DMEM with 2% fetal calf serum (both Thermo Fisher Scientific) in triplicate. After 1 hour incubation at 37°C, we added 1 mL of 2% FBS DMEM. We incubated the plates at 37°C in a CO_2 incubator. We observed the cells daily and harvested when 40%–50% demonstrated cytopathic effect.

Whole-Genome Sequence Analysis

We sequenced genomes by using the ARTIC POLAR protocol as described previously (*24*,*25*). We analyzed the genomes after aligning to the SARS-CoV-2 wild-type reference sequence (GenBank accession no. NC_045512.2). We used the BWA aligner tool version 0.7.17 (https://github.com/lh3/bwa/releases/tag/v0.7.17) with a filter requiring a minimum mapping score of 30. We removed reads that did not align to the reference by using Samtools version 1.10 (https://github.com/samtools/samtools/releases/tag/1.10). We called variants by using Bcftools version 1.10.2-34 (https://github.com/samtools/bcftools/releases/tag/1.10.2). We used a previously published bioinformatics pipeline to assign point mutations (*26*–*29*).

Infection of Nasal Air-Liquid Interface Cultures

We diluted virus isolates in 2% FBS DMEM to 50 μL at multiplicity of infection (MOI) of 0.01 and added apically to nasal air-liquid interface (ALI) cultures for 1 hour adsorption. Then, we apically washed the cells 3 times. We added 100 μL of 2% FBS DMEM apically to collect the produced virus.

Tissue Culture Infectious Dose Assays

We used Vero E6, Vero E6 TMPRSS2, or Vero E6 ACE2 TMPRSS2 cells for 50% tissue culture infectious dose ($TCID_{50}$) assays. We added serial dilutions onto cell plates that were incubated at 37°C for 1 hour. We added a liquid overlay (DMEM with L-Glut, 2% heat-inactivated FBS, 1% sodium pyruvate, 0.01%

agarose) and incubated for 16 hours. We removed the overlay and added 4% paraformaldehyde for ≥30 minutes to fix monolayers. We removed the paraformaldehyde and washed 3 times in 0.05% Tween/PBS (Thermo Fisher Scientific) and blocked with 2% bovine serum albumin in PBS with Tween 20 (Thermo Fisher Scientific). Then, we added 50 µL SARS-CoV-2 nucleocapsid antibody and incubated overnight. We washed the plates 3 times, added 50 µL horseradish peroxidase-conjugated secondary antibody, incubated for 1 hour, washed the plates again, added 50 µL KPL TrueBlue substrate (SeraCare, https://www.seracare.com), and incubated for 15 minutes at room temperature. After that incubation, we washed the plates 3 times with distilled water. We estimated the endpoint titer (50% of wells positive) by using the Reed-Muench method.

Western Blots

We rinsed cells with PBS stored on ice. We prepared lysates by using lysis buffer (1% nucleocapsid-40, 2 mM EDTA, 10% glycerol, 150 mM NaCl, 50 mM Tris-HCl, pH 8.0) with protease and phosphatase inhibitors (Roche). We conducted Western blots as previously described (*23*).

Statistics

We graphed and analyzed data by using GraphPad Prism (https://www.graphpad.com), showing individual values or mean ±SD. Unless stated, we determined significance by Fisher exact test for pairwise comparisons.

Biosafety

We conducted all procedures in a certified Biohazard Safety Level 3 laboratory. Procedures were approved by the University of Pennsylvania Office of Environmental Health and Safety.

Results

Nasal swab or endotracheal aspirate specimens were collected and analyzed from a total of 246 patients infected with SARS-CoV-2. The cohort included cross-sectional samples (n = 178) and longitudinal samples (n = 68) collected from patients. Among the patients from whom longitudinal samples were collected, 10 had asymptomatic infection, 54 had symptomatic respiratory illness and survived, and 4 died (Tables 1, 2). Of those 68 patients, 23 were male and 45 were female. The median patient age was 61 (range 24–101) years. Major comorbidities and immunosuppression were noted in 25 cases. Hematologic malignancies such as leukemia and lymphoma were present in 11 patients, 5 patients had undergone solid organ transplantation, and 10 had solid malignancies on active therapy.

Table 1. SARS-CoV-2 strains recovered from PCR positive patients in study on the enhanced isolation and detection of COVID-19 in hospitalized patients undergoing antiviral therapy

	PCR positive patients	
SARS-CoV-2 strain	Cross-sectional	Longitudinal
Wild-type	5	30
Delta	6	0
BA.1	12	0
BA.2	34	0
BQ	25	0
BA.5	70	0
XBB.1	26	0
Unknown	0	38
Subtotal	178	68
Total	246	

From the longitudinal cohort, 38 patients who sought care during the later stages of the pandemic were vaccinated and had received booster doses, whereas the remaining 30 patients, who sought care during the early stages of the pandemic, were unvaccinated. Of patients who received therapy, 27 received remdesivir, 3 Paxlovid (Pfizer, https://www.pfizer.com), and 6 monoclonal antibody therapy before specimen collection. Most patients also received corticosteroids as part of the treatment regime.

We carried out virus culture isolations by using the routinely used parental Vero E6 cell line; Vero E6 expressing the serine protease TMPRSS2 (Vero E6 T2), which enables SARS-CoV-2 spike protein processing and enhances viral entry; and Vero E6 expressing both TMPRSS2 and ACE2, which serves as the receptor for SARS-CoV-2 entry (Vero E6 A2T2). We evaluated those 3 cell lines in parallel

Table 2. Longitudinal patient cohort demographics from study on the enhanced isolation and detection of COVID-19 in hospitalized patients undergoing antiviral therapy*

Characteristics	Value
Patients	68
Age range, y	24–101
Sex	
M	23
F	45
Clinical manifestation	
Asymptomatic	10
Symptomatic, survived	54
Symptomatic, died	4
Vaccinated	38
Nonvaccinated	30
Antiviral treatment	
Remdesivir	27
Paxlovid	3
Monoclonal antibody	6
No antivirals	7
Immunosuppressed	25

*Values are no. patients except as indicated. Paxlovid, http://www.pfizer.com.

for their efficiency in supporting virus culture isolation (Figure 1, panel A).

To assess the effect of collection medium on virus isolation efficiency, we inoculated nasal swab specimens collected with PBS and VTM and confirmed to contain the BA.5 SARS-CoV-2 variant onto 3 cell lines (n = 30 per group with comparable Ct values). The virus isolation rates from PBS samples were 3.3% (n = 1) in Vero E6, 6.6% (n = 2) in Vero E6 T2, and 16.6% (n = 5) in Vero E6 A2T2. In contrast, VTM samples demonstrated markedly higher isolation efficiencies: 20% (n = 6) in Vero E6, 40% (n = 12) in Vero E6 T2, and 83.3% (n = 25) in Vero E6 A2T2 ($p<0.001$) (Figure 1, panel B).

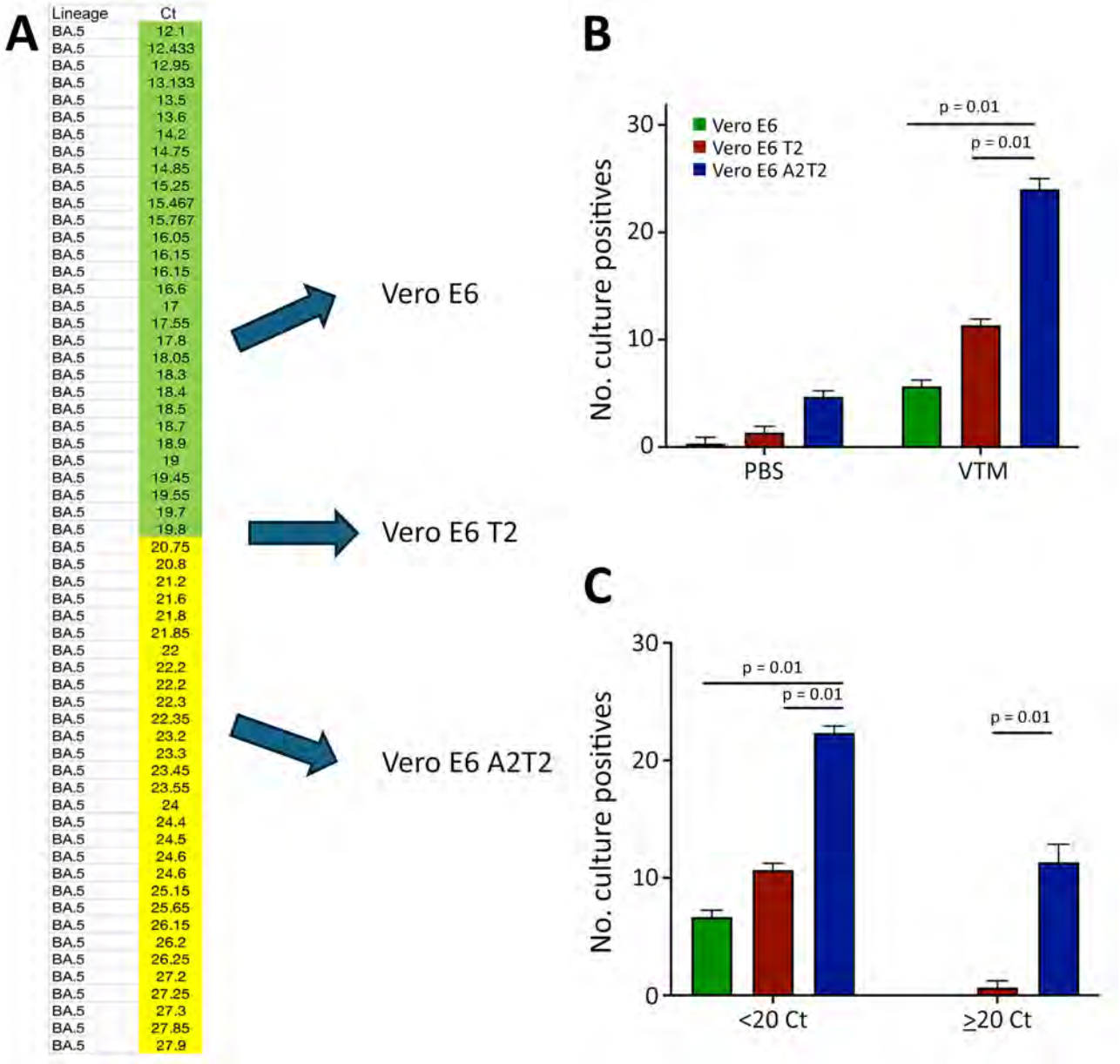

Figure 1. Comparative analysis of SARS-CoV-2 infectious virus isolation using Vero E6–derived cell lines from study on the enhanced isolation and detection of COVID-19 in hospitalized patients undergoing antiviral therapy. A) Thirty nasal swab specimens confirmed by real time PCR to contain the SARS-CoV-2 BA.5 variant, representing a range of Ct values from 12.1–27.9, were inoculated in triplicate onto Vero E6, Vero E6 T2, and Vero E6 A2T2 cell lines. B) Number of BA.5-positive nasal swab specimens collected in either PBS or VTM and inoculated in triplicate onto the 3 cell lines. C) BA.5-positive nasal swab specimens collected in VTM and stratified by Ct values; samples with values ≤20 or >20 were inoculated in triplicate into the 3 cell lines, and the number of successful virus isolations was plotted with corresponding means ±SD. Error bars indicate SDs. Ct, cycle threshold; PBS, phosphate-buffered saline; Vero E6 T2, Vero E6 cells expressing transmembrane protease serine 2; Vero E6 A2T2, Vero E6 cells expressing both transmembrane protease serine 2 and angiotensin-converting enzyme 2; VTM, viral transport medium.

To evaluate the sensitivity across a range of viral copy numbers in nasal swab specimens, we stratified samples collected only in VTM confirmed to contain BA.5 by qRT-PCR Ct values, ≤20 (n = 30) or >20 (n = 30), and inoculated both onto the 3 cell lines separately. When Ct values were <20, all 3 cell lines supported virus isolation, with efficiencies of 23.3% (n = 7) for Vero E6, 36.6% (n = 11) for Vero E6 T2, and 76.6% (n = 23) for Vero E6 A2T2 (p<0.001). However, for samples with Ct values >20, only Vero E6 T2 (3.3%, n = 1) and Vero E6 A2T2 (43.3%, n = 13) successfully supported viral isolation (p<0.001); Vero E6 failed to yield virus (Figure 1, panel C).

We confirmed nasal VTM samples (n = 148) by qRT-PCR and sequencing to contain several SARS-CoV-2 variants, including wild-type, Delta, BA.1, BA.2, BQ, BA.5, and XBB.1. We inoculated samples in triplicate onto the 3 cell lines to evaluate their capacity for isolating viruses from swab specimens that were positive for variants other than BA.5. The mean ±SD isolation success rates were 28.3 ±1.24 per 148 samples for Vero E6, 48 ±2.44 for Vero E6 T2, and 114.6 ±3.29 for Vero E6 A2T2, suggesting greater efficiency of Vero E6 A2T2 cells (p<0.001) (Figure 2).

To assess suitability for high titer virus stock production, we inoculated nasal swab specimens from 3 patients onto all 3 cell lines and ALI primary human nasal epithelial cultures. We subsequently passaged virus isolates in the same cells to obtain second-generation virus stocks. The final log mean ±SD viral titers (measured by $TCID_{50}$ assays that used Vero E6 A2T2) after the second passage in ALI cultures were 7.3 ±0.1, 7.5 ±0.1, and 7.0 ±0.3 for the 3 patients. In comparison, second-passage titers were 6.3 ±0.2, 6.2 ±0.3, and 6.6 ±0.3 for Vero E6; 6.1 ±0.3, 5.2 ± 0.3, and 5.5 ±0.2 for Vero E6 T2; and 5.1 ±0.2, 5.5 ±0.3, and 5.5 ±0.2 for Vero E6 A2T2. Thus, although sensitive for viral isolation, Vero E6 A2T2s produced viral stocks with much lower viral titers (Table 3).

We selected 3 clinical specimens (patients 1, 17, and 20) confirmed by qRT-PCR to be positive for the SARS-CoV-2 BA.5 Omicron variant and each sample was inoculated onto Vero E6, Vero E6 T2, and Vero E6 A2T2 cell lines. We conducted whole-genome sequencing on the parent swab and viral isolates obtained after the first passage in each of the cell lines to assess if there were any cell line-specific mutations introduced during culture. We also whole-genome sequenced the original swab material from patients 17 and 20, but insufficient nucleic acid was available from patient 1 for sequencing. Comparative genomic analysis revealed no noteworthy differences between the viral genomes from the parental swab material and those derived from each cell line (Figure 3). Furthermore, there were no consensus mutations, and the changes in minor variants were fairly limited, with <0.15 change in proportion (Figure 4).

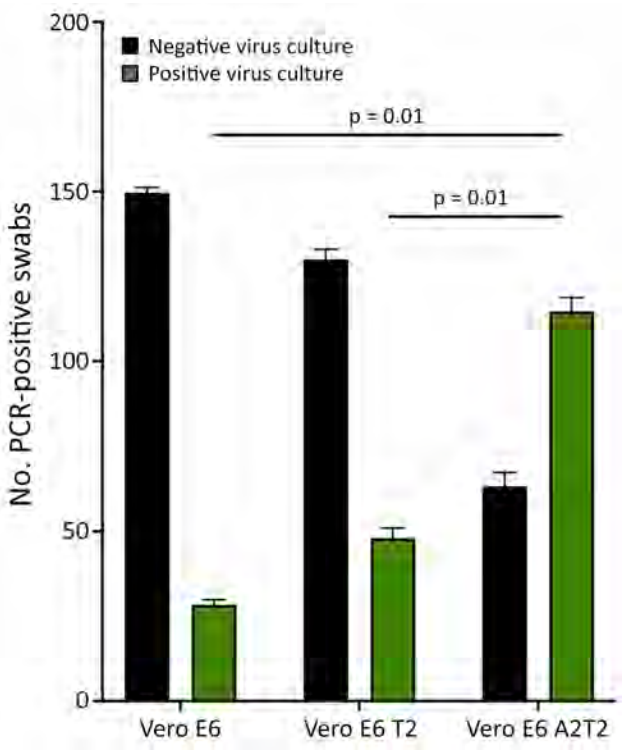

Figure 2. Viral culture isolation rates from nasal swabs of nonimmunocompromised patients infected with SARS-CoV-2 variants of concern from study on the enhanced isolation and detection of COVID-19 in hospitalized patients undergoing antiviral therapy. Nasal swabs (n = 148) PCR-confirmed positive for wild-type, Delta, BA.1, BA.2, BQ, BA.5, and XBB.1 SARS-CoV-2 variants of concern were cultured in triplicate on 3 different cell lines. Error bars indicate SDs. Vero E6 T2, Vero E6 cells expressing transmembrane protease serine 2; Vero E6 A2T2, Vero E6 cells expressing both transmembrane protease serine 2 and angiotensin-converting enzyme 2.

Table 3. Three clinical specimens confirmed positive by real time reverse transcriptase PCR for the SARS-CoV-2 BA.5 Omicron variant from study on the enhanced isolation and detection of COVID-19 in hospitalized patients undergoing antiviral therapy

Nasal swab ID	ALI	Vero E6	Vero E6 T2	Vero E6 A2T2	p value
1	7.3 ±0.1	6.3 ±0.2	6.1 ±0.3	5.1 ±0.2	<0.001
17	7.5 ±0.1	6.2 ±0.3	5.2 ±0.3	5.5 ±0.3	<0.01
20	7.0 ±0.3	6.6 ±0.3	5.5 ±0.2	5.5 ±0.2	<0.01

*Values are mean ±SD. ID, identification.

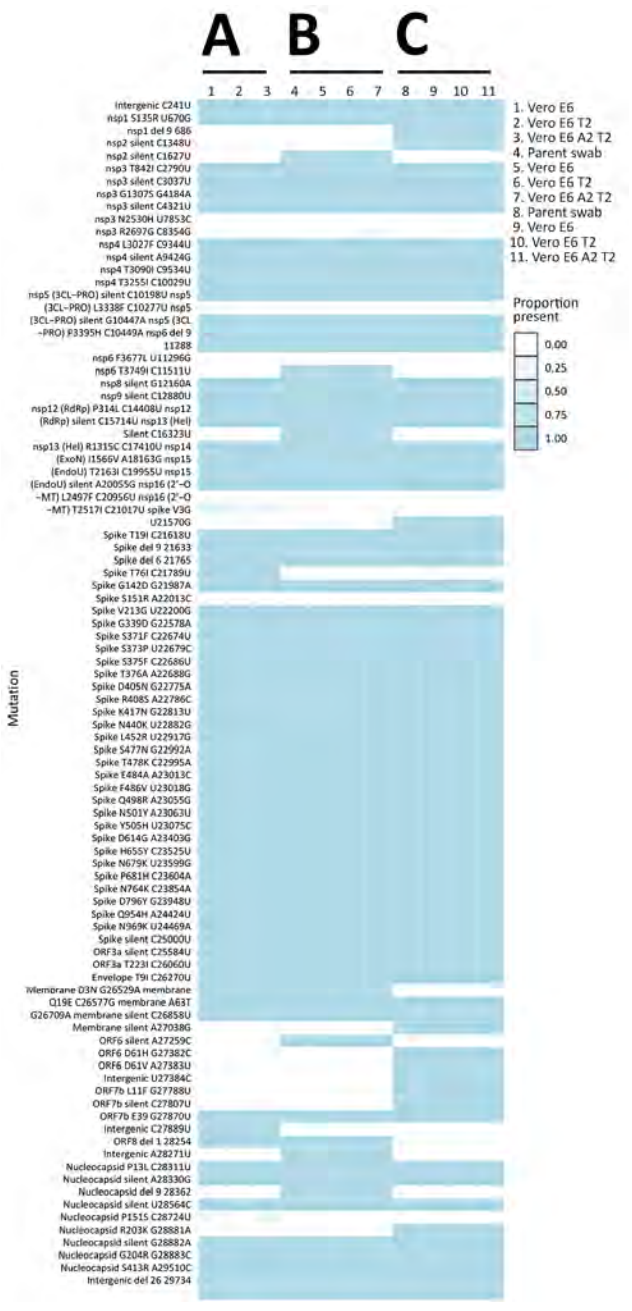

Figure 3. Heatmap of viral whole genome sequences of patient swab specimens after first passage in the 3 cell lines Vero E6, Vero E6 T2, and Vero E6 A2T2 from study on the enhanced isolation and detection of COVID-19 in hospitalized patients undergoing antiviral therapy. Columns represent sequenced samples; rows correspond to mutations relative to the wild-type reference SARS-CoV-2 strain. Darker blue shades indicate an increased prevalence of specific mutations relative to the wild-type strain. Del, deletion; nsp, nonstructural protein; ORF, open reading frame; RdRp, RNA-dependent RNA polymerase; Vero E6 T2, Vero E6 cells expressing transmembrane protease serine 2; Vero E6 A2T2, Vero E6 cells expressing both transmembrane protease serine 2 and angiotensin-converting enzyme 2.

Successful virus culture isolation depends on the efficient entry of viral particles from clinical specimens into susceptible cells through cell surface or endosomal pathways and then by replication. To compare the efficiency and route of viral entry in the 3 Vero-derived cell lines, we inoculated nasal swab samples qRT-PCR-positive for SARS-CoV-2 variants WA.1, Delta, and XBB.1 (viral titers measured by Vero E6 A2T2) at a MOI of 0.01. Western blot confirmed higher expression levels of TMPRSS2 in Vero E6 T2 cells and ACE2 in Vero E6 A2T2 cells (Figure 5, panel A).

We harvested cells 12 hours postinfection to probe for SARS-CoV-2 spike and nucleocapsid proteins. We detected nucleocapsid and spike protein in all the cell lines that were inoculated with nasal swab material positive for wild-type and Delta strain, with the highest expression observed in Vero E6 A2T2. In contrast, we only observed nucleocapsid and spike expression with Vero E6 A2T2 cells inoculated with nasal swab material positive for XBB.1 variant (Figure 5, panel B). Infection with mCherry-expressing wild-type virus at 0.01 MOI revealed much greater membrane fusion events in Vero E6 A2T2 cells, as indicated by broader areas of red fluorescence aligned with cytopathic effect seen from the brightfield image compared with the other 2 cell lines that demonstrated a more localized cellular infection at 12 hours postinfection (Figure 6, panel A). Cytopathic effect observations at 12 hours postinfection for wild-type, Delta, and XBB.1 variants at 0.01 MOI revealed numerous pronounced syncytia and fewer single cell infections in Vero E6 A2T2, whereas Vero E6 and Vero E6 T2 cells primarily exhibited isolated infected cells (Figure 6, panel B).

To compare the sensitivity of the 3 Vero E6-derived cell lines in quantifying infectious viral load present in respiratory swab specimens relative to Ct values, we performed a modified $TCID_{50}$ assay on the basis of detecting foci of infection by using clinical samples from a subset of hospitalized patients with SARS-CoV-2 infection. Modified $TCID_{50}$ assays conducted by using parental Vero E6 cells yielded viral titers of log 1.8–4.3 $TCID_{50}$/mL. In contrast, assays that used Vero E6 T2 cells demonstrated higher viral titers of 1.8–6.8 $TCID_{50}$/mL, and assays that used Vero E6 A2T2 cells exhibited the broadest and most sensitive detection range, spanning 1.8–9.8 $TCID_{50}$/mL. Across all 3 cell lines, viral titers demonstrated a strong inverse correlation with the qRT-PCR Ct values of the respective respiratory samples, with inverse Pearson correlation coefficients of 0.85 for both Vero E6 and Vero E6 T2, and 0.86 for Vero E6 A2T2. Of note, Vero E6 A2T2 cells demonstrated superior

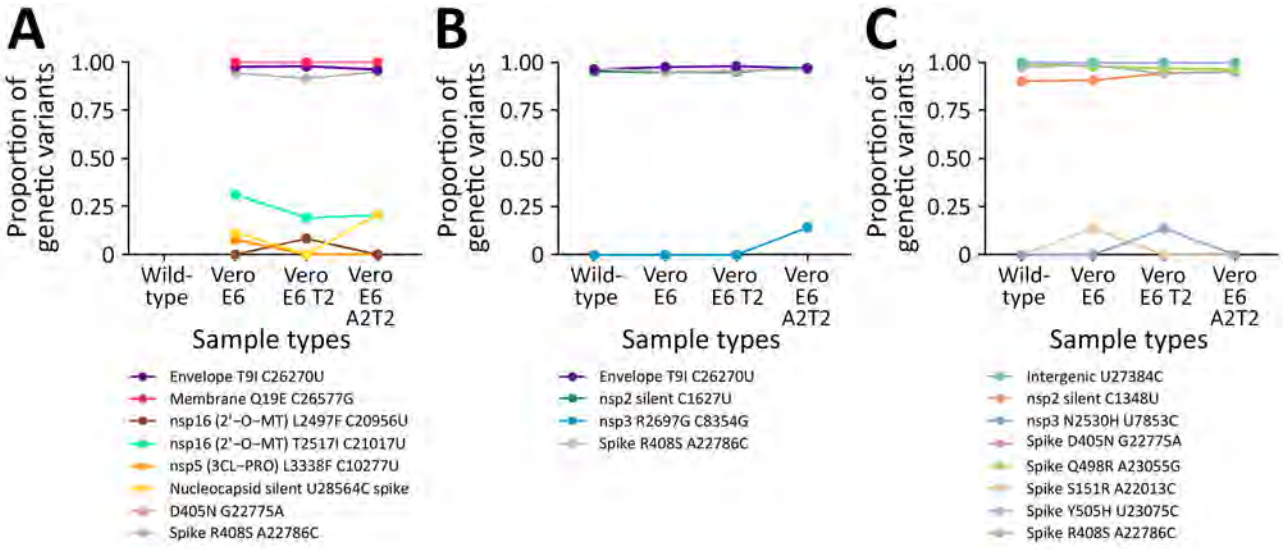

Figure 4. Minor variants identified after passage 1 from SARS-CoV-2 BA.5 Omicron variant positive nasal swab specimens in 3 cell lines Vero E6, Vero E6 T2, and Vero E6 A2T2 from study on the enhanced isolation and detection of COVID-19 in hospitalized patients undergoing antiviral therapy. This figure shows the minor variants observed in the 3 virus culture isolates obtained after passage 1 from nasal swab samples from patients 1, 17, and 20 that were SARS-CoV-2 positive and were a BA.5 Omicron variant. Vero E6 T2, Vero E6 cells expressing transmembrane protease serine 2; Vero E6 A2T2, Vero E6 cells expressing both transmembrane protease serine 2 and angiotensin-converting enzyme 2.

sensitivity, consistently yielding higher infectious titers and detecting infectious virus even in specimens with the highest Ct values. The highest Ct threshold level for detecting infectious virus was 27.3 (Figure 7).

After assessing the correlation of $TCID_{50}$ infectious titers with Ct values in each cell type in hospitalized patients, we measured the duration of the infectious viral production by the patients after qRT-PCR confirmed SARS-CoV-2 infection (n = 68) by $TCID_{50}$ assays that used Vero E6, Vero E6 T2, and Vero E6 A2T2 cell lines. First, we measured the upper respiratory tract viral titers from a subset of patients (n = 38) (Figure 8, panel A). Those patients received remdesivir, Paxlovid, or monoclonal antibody therapy. The titers obtained in Vero E6 revealed only 3 patients (3/38) to have infectious virus in their upper respiratory tract up to 3 days (log 2 $TCID_{50}$/mL). When Vero E6 T2 cells were used, we detected infectious virus (log 2–3 $TCID_{50}$/mL) in 7 patients (7/38) up to 4 days. However, Vero E6 A2T2 cells detected infectious virus in more patients (16/38), with viral titers of log 0.5–6 $TCID_{50}$/mL, and 2 patients showed detectable virus at 7 days.

We also assessed lower respiratory tract viral titers in a subset of patients (n = 30) by using endotracheal aspirates. The lower respiratory tract titers of those patients were log 3.17–8.17 $TCID_{50}$/mL from assays that used Vero E6 cells, log 4.17–9.17 $TCID_{50}$/

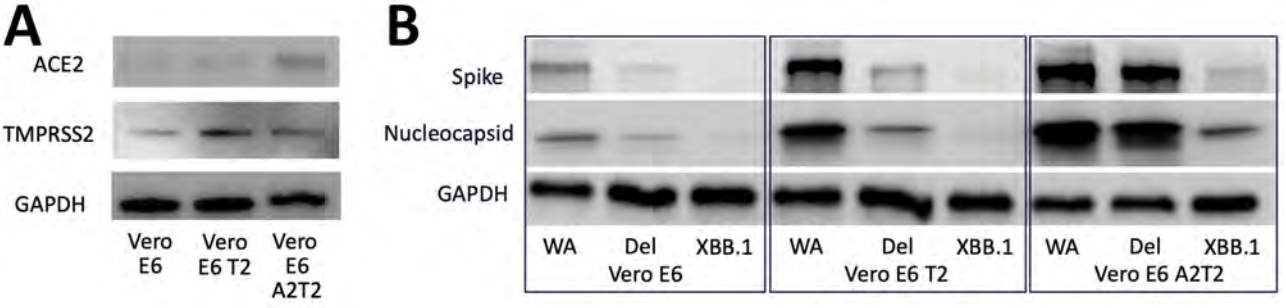

Figure 5. Efficiency and possible routes of infectious viral particle internalization of SARS-CoV-2 in Vero E6, Vero E6 T2, and Vero E6 A2T2 cell lines from study on the enhanced isolation and detection of COVID-19 in hospitalized patients undergoing antiviral therapy. Samples were separated by using sodium dodecyl sulfate–polyacrylamide gel electrophoresis and transferred to a polyvinylidene difluoride membrane for detection of ACE2, TMPRSS2, GAPDH (A) or SARS-CoV-2 spike and nucleocapsid antibodies (B). GAPDH, glyceraldehyde-3-phosphate dehydrogenase; ACE2, angiotensin-converting enzyme 2; del, deletion; TMPRSS2, transmembrane protease serine 2; Vero E6 T2, Vero E6 cells expressing TMPRSS2; Vero E6 A2T2, Vero E6 cells expressing both TMPRSS2 and ACE2.

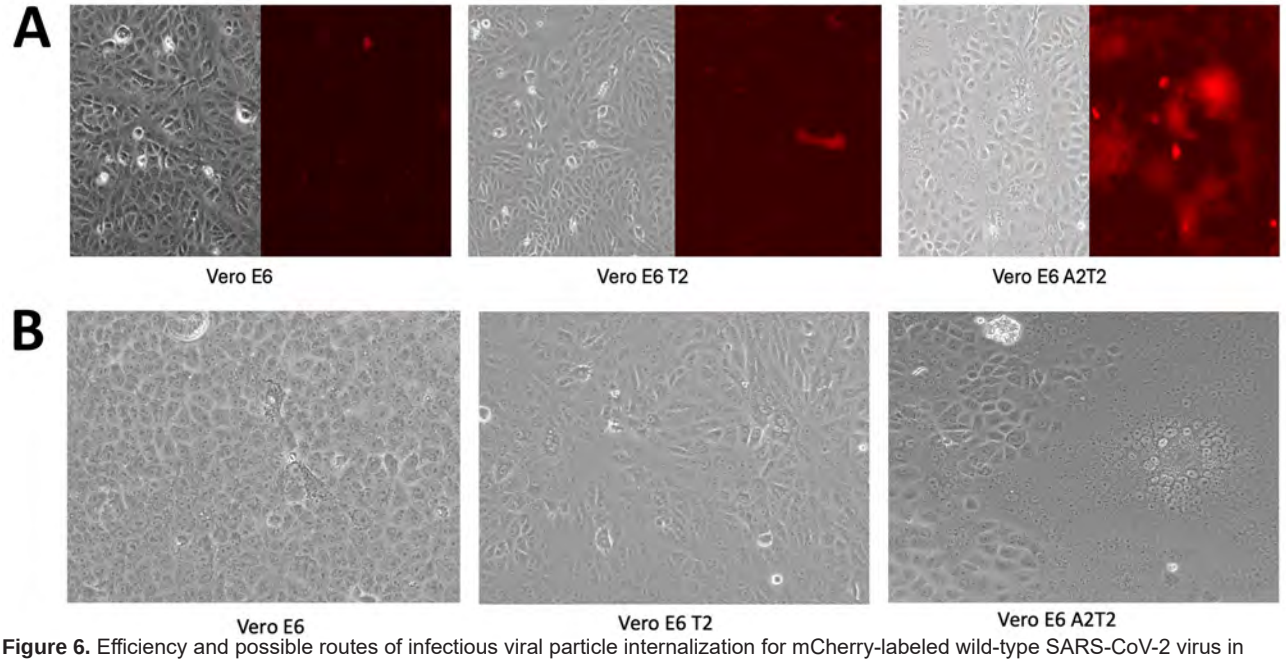

Figure 6. Efficiency and possible routes of infectious viral particle internalization for mCherry-labeled wild-type SARS-CoV-2 virus in Vero E6, Vero E6 T2, and Vero E6 A2T2 cell lines from study on the enhanced isolation and detection of COVID-19 in hospitalized patients undergoing antiviral therapy. A) Inoculated cells, singular cells or fused (in red). B) Cytopathic effects induced by SARS-CoV-2 XBB.1 viral inoculation, focal areas of rounded cells or regions of fused cells forming syncytia or giant cell structures across the different cell lines. Vero E6 T2, Vero E6 cells expressing transmembrane protease serine 2; Vero E6 A2T2, Vero E6 cells expressing both transmembrane protease serine 2 and angiotensin-converting enzyme 2.

mL from assays that used Vero E6 T2 cells, and log 2.67–14.17 $TCID_{50}$/mL from assays that used Vero E6 A2T2 cells (Figure 8, panel B). Assays that used Vero E6 and Vero E6 T2 cells showed viral production in the lower respiratory tract up to 9 days after PCR confirmation and assays that used Vero E6 A2T2 cells showed infectious virus in the lower respiratory tract up to 11 days after PCR confirmation. Vero E6

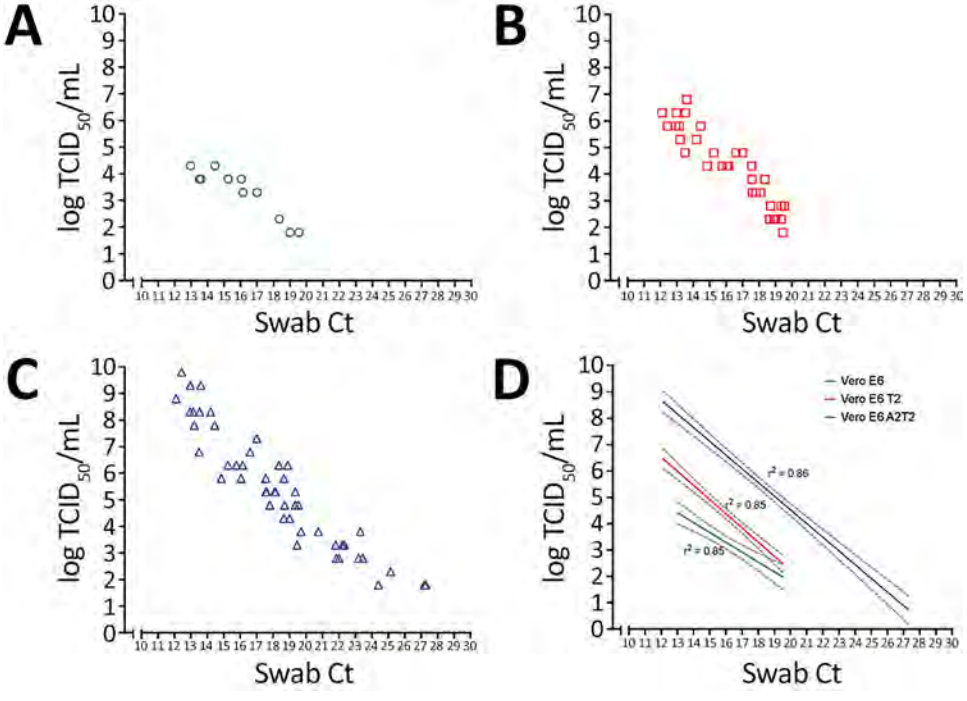

Figure 7. Threshold sensitivity SARS-CoV-2 viral titers by $TCID_{50}$ assays that used different cell types in upper respiratory tract specimens across a range of Ct values from a study on the enhanced isolation and detection of COVID-19 in hospitalized patients undergoing antiviral therapy. A–C) Viral titers were measured in samples with varying Ct values using $TCID_{50}$ assays for 3 cell lines: A) Vero E6, B) Vero E6 T2, and C) Vero E6 A2T2. D) Pearson correlation coefficient of the respiratory viral titers determined by each cell line versus the Ct value. Dotted lines indicate 95% CIs. Ct, cycle threshold; $TCID_{50}$, 50% tissue culture infectious dose; Vero E6 T2, Vero E6 cells expressing transmembrane protease serine 2; Vero E6 A2T2, Vero E6 cells expressing both transmembrane protease serine 2 and angiotensin-converting enzyme 2.

A2T2 cells appear to detect infectious virus production from patients for substantially longer than the Vero E6 that is traditionally used for virus isolation.

Discussion

Through a comparative evaluation of 3 Vero E6–derived cell lines, our data provide insights for improving the detection and quantification of infectious SARS-CoV-2 from clinical samples, including hospitalized, critically ill, or immunocompromised patients. This investigation highlights the substantial value of the optimization of the level of TMPRSS2 and ACE2 expression in the cell lines used for the isolation and quantification of infectious virus from clinical samples. Compared with PCR-based methods or the traditional Vero cells, cell lines expressing both the ACE2 receptor and TMPRSS2 protease were much more effective and had a multifold increase in sensitivity for detecting infectious virus. Although we did not find a similar comprehensive mechanistic comparison in the literature, similar findings have been reported by using different Vero E6 cell lines (*19*–*21*). We observed that Vero E6 A2T2 consistently outperformed the parental Vero E6 and intermediate Vero E6 T2 in virus isolation efficiency, infectious titer quantification, and sensitivity of detection from specimens with low viral RNA loads. This performance was evident in both standard isolation and $TCID_{50}$ assay viral quantification. In contrast, when titers of viral stock grown in the different cells were compared, Vero E6 A2T2 performed poorly, likely because of the rupture of syncytia before optimal titers were reached. This poor performance suggests that although ideal for virus isolation, Vero E6 A2T2 might not be ideal for virus stock preparation. Of note, Vero E6 A2T2 cells did not induce adaptation mutations in the viral genome after initial passages, indicating they preserve virus integrity while enhancing sensitivity and are well-suited for downstream genomic and phenotypic analyses. Mechanistic studies confirmed initiation of early replication after 12 hours of incubation, higher levels of spike protein expression, and robust syncytia formation of fluorescent reporter viruses, reinforcing the utility of Vero E6 A2T2 for detection, isolation, and quantification. This confirmation underscores the value of implementing optimized virus detection methods in the clinical settings, particularly when monitoring viral kinetics in patients with prolonged infections. Of note, although Vero E6 cells expressing only ACE2 might slightly improve over parental cells because of higher receptor density, lacking TMPRSS2 directly affects entry, resulting in inferior efficiency versus TMPRSS2 expressing cell lines (*30*). We found that a Ct value of 27.3 would be the threshold of infectious virus isolation by using the high sensitivity Vero E6 A2T2 line, although this threshold might depend on different variants.

One limitation of this study is that we did not have enough sample size to get estimates for each variant. Accurate measurement of infectious virus is also critical in basic science and animal studies to achieve correct conclusions. Vero E6 A2T2 cells detected higher titers and durations of viral production in patients relative to other cell lines. A second limitation

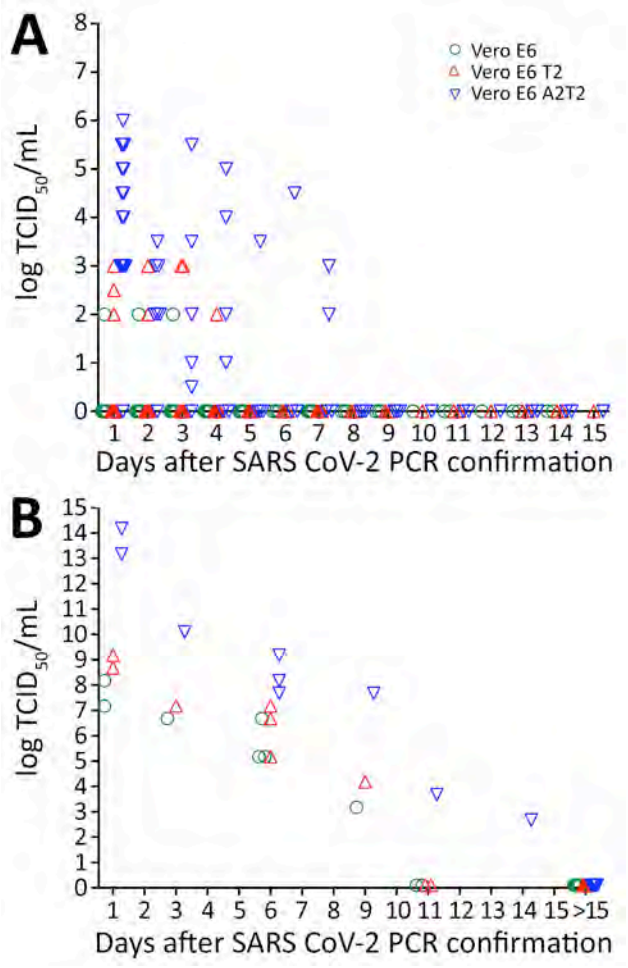

Figure 8. Infectious SARS-CoV-2 virus detection over time in the upper and lower respiratory tract of hospitalized patients when assayed using Vero E6, Vero E6 T2, and Vero E6 A2T2 cell lines from study on enhanced isolation and detection of COVID-19 in hospitalized patients undergoing antiviral therapy. Viral titers shed after PCR-confirmed SARS-CoV-2 infection were measured by $TCID_{50}$ assays that used the 3 cell lines. A) Upper respiratory tract viral titers obtained from nasal swab specimens; B) lower respiratory tract titers obtained from endotracheal aspirates. $TCID_{50}$, 50% tissue culture infectious dose; Vero E6 T2, Vero E6 cells expressing transmembrane protease serine 2; Vero E6 A2T2, Vero E6 cells expressing both transmembrane protease serine 2 and angiotensin-converting enzyme 2.

of the study was that the period between patients' symptom onset and hospital admission after PCR confirmation likely varied among different patients. Therefore, although the relative sensitivity of the different cell lines is clear, the kinetics of infectious virus decline is not generalizable. In our patients, infectious virus was detected up to 11 days post-PCR, and titers reached log 14.17 $TCID_{50}$/mL in endotracheal aspirates. This study highlights the need to apply optimal infectious virus detection methodologies to studies of therapy and infection control to prevent prolonged viral transmission.

In conclusion, the Vero E6 A2T2 cell line represents a sensitive, robust, and reliable platform for SARS-CoV-2 isolation and quantification particularly in complex cases involving immunocompromised patients. Our findings offer an optimized methodological framework for enhanced virologic surveillance and therapeutic monitoring, supporting better clinical and public health management during outbreaks.

Acknowledgment

We thank Ayannah Fitzgerald and Layla Khatib for their assistance in this study.

The study was supported by the National Institutes of Health (award nos. 5R01AI169537-04, R21DE03190, and R33HL13706).

About the Author

Dr. Perera is a research assistant professor in the Department of Microbiology at the Perlman School of Medicine, The University of Pennsylvania, Philadelphia. His main research interest is emerging and reemerging zoonotic viral diseases.

References

1. Carraturo F, Del Giudice C, Morelli M, Cerullo V, Libralato G, Galdiero E, et al. Persistence of SARS-CoV-2 in the environment and COVID-19 transmission risk from environmental matrices and surfaces. Environ Pollut. 2020;265(Pt B):115010.
2. Perera RAPM, Tso E, Tsang OTY, Tsang DNC, Fung K, Leung YWY, et al. SARS-CoV-2 virus culture and subgenomic RNA for respiratory specimens from patients with mild coronavirus disease. Emerg Infect Dis. 2020;26:2701–4. https://doi.org/10.3201/eid2611.203219
3. Puhach O, Meyer B, Eckerle I. SARS-CoV-2 viral load and shedding kinetics. Nat Rev Microbiol. 2023;21:147–61.
4. Embi PJ, Levy ME, Naleway AL, Patel P, Gaglani M, Natarajan K, et al. Effectiveness of 2-dose vaccination with mRNA COVID-19 vaccines against COVID-19-associated hospitalizations among immunocompromised adults—nine states, January–September 2021. MMWR Morb Mortal Wkly Rep. 2021;70:1553–9. https://doi.org/10.15585/mmwr.mm7044e3
5. Pham MN, Murugesan K, Banaei N, Pinsky BA, Tang M, Hoyte E, et al. Immunogenicity and tolerability of COVID-19 messenger RNA vaccines in primary immunodeficiency patients with functional B-cell defects. J Allergy Clin Immunol. 2022;149:907–911.e3. https://doi.org/10.1016/j.jaci.2021.11.022
6. Braunstein GD, Schwartz L, Hymel P, Fielding J. False positive results with SARS-CoV-2 RT-PCR tests and how to evaluate a RT-PCR-positive test for the possibility of a false positive result. J Occup Environ Med. 2021;63:e159–62. https://doi.org/10.1097/JOM.0000000000002138
7. Layfield LJ, Camp S, Bowers K, Miller DC. SARS-CoV-2 detection by reverse transcriptase polymerase chain reaction testing: analysis of false positive results and recommendations for quality control measures. Pathol Res Pract. 2021;225:153579. https://doi.org/10.1016/j.prp.2021.153579
8. Yang C, Jiang M, Wang X, Tang X, Fang S, Li H, et al. Viral RNA level, serum antibody responses, and transmission risk in recovered COVID-19 patients with recurrent positive SARS-CoV-2 RNA test results: a population-based observational cohort study. Emerg Microbes Infect. 2020;9:2368–78. https://doi.org/10.1080/22221751.2020.1837018
9. Ke R, Martinez PP, Smith RL, Gibson LL, Mirza A, Conte M, et al. Daily longitudinal sampling of SARS-CoV-2 infection reveals substantial heterogeneity in infectiousness. Nat Microbiol. 2022;7:640–52. https://doi.org/10.1038/s41564-022-01105-z
10. Centers for Disease Control and Prevention. Ending isolation and precautions for people with COVID-19: interim guidance 2025 [cited 2025 Apr 21]. https://archive.cdc.gov/www_cdc_gov/coronavirus/2019-ncov/hcp/duration-isolation.html
11. Mowrer CT, Creager H, Cawcutt K, Birge J, Lyden E, Van Schooneveld TC, et al. Evaluation of cycle threshold values at deisolation. Infect Control Hosp Epidemiol. 2022;43:794–6. https://doi.org/10.1017/ice.2021.132
12. Rhee C, Kanjilal S, Baker M, Klompas M. Duration of severe acute respiratory syndrome coronavirus 2 (SARS-CoV-2) infectivity: when is it safe to discontinue isolation? Clin Infect Dis. 2021;72:1467–74. https://doi.org/10.1093/cid/ciaa1249
13. Avanzato VA, Matson MJ, Seifert SN, Pryce R, Williamson BN, Anzick SL, et al. Case study: prolonged infectious SARS-CoV-2 shedding from an asymptomatic immunocompromised individual with cancer. Cell. 2020;183:1901–1912.e9. https://doi.org/10.1016/j.cell.2020.10.049
14. Aydillo T, Gonzalez-Reiche AS, Aslam S, van de Guchte A, Khan Z, Obla A, et al. Shedding of viable SARS-CoV-2 after immunosuppressive therapy for cancer. N Engl J Med. 2020;383:2586–8. https://doi.org/10.1056/NEJMc2031670
15. Choi B, Choudhary MC, Regan J, Sparks JA, Padera RF, Qiu X, et al. Persistence and evolution of SARS-CoV-2 in an immunocompromised host. N Engl J Med. 2020;383:2291–3. https://doi.org/10.1056/NEJMc2031364
16. Miorin L, Kehrer T, Sanchez-Aparicio MT, Zhang K, Cohen P, Patel RS, et al. SARS-CoV-2 Orf6 hijacks Nup98 to block STAT nuclear import and antagonize interferon signaling. Proc Natl Acad Sci U S A. 2020;117:28344–54. https://doi.org/10.1073/pnas.2016650117
17. Ogando NS, Dalebout TJ, Zevenhoven-Dobbe JC, Limpens RWAL, van der Meer Y, Caly L, et al. SARS-coronavirus-2 replication in Vero E6 cells: replication kinetics, rapid adaptation and cytopathology. J Gen Virol. 2020;101:925–40. https://doi.org/10.1099/jgv.0.001453
18. Chang CW, Parsi KM, Somasundaran M, Vanderleeden E, Liu P, Cruz J, et al. A newly engineered A549 cell line expressing ACE2 and TMPRSS2 is highly permissive to

SARS-CoV-2, including the delta and omicron variants. Viruses. 2022;14:1369. https://doi.org/10.3390/v14071369
19. Kinoshita H, Yamamoto T, Kuroda Y, Inoue Y, Miyazaki K, Ohmagari N, et al. Improved efficacy of SARS-CoV-2 isolation from COVID-19 clinical specimens using VeroE6 cells overexpressing TMPRSS2 and human ACE2. Sci Rep. 2024;14:24858. https://doi.org/10.1038/s41598-024-75038-4
20. Matsuyama S, Nao N, Shirato K, Kawase M, Saito S, Takayama I, et al. Enhanced isolation of SARS-CoV-2 by TMPRSS2-expressing cells. Proc Natl Acad Sci U S A. 2020;117:7001–3. https://doi.org/10.1073/pnas.2002589117
21. Yazawa S, Yamazaki E, Saga Y, Itamochi M, Inasaki N, Shimada T, et al. Evaluation of SARS-CoV-2 isolation in cell culture from nasal/nasopharyngeal swabs or saliva specimens of patients with COVID-19. Sci Rep. 2023;13:8893. https://doi.org/10.1038/s41598-023-35915-w
22. Marques AD, Sherrill-Mix S, Everett JK, Adhikari H, Reddy S, Ellis JC, et al. Multiple introductions of SARS-CoV-2 alpha and delta variants into white-tailed deer in Pennsylvania. MBio. 2022;13:e0210122. https://doi.org/10.1128/mbio.02101-22
23. Li Y, Renner DM, Comar CE, Whelan JN, Reyes HM, Cardenas-Diaz FL, et al. SARS-CoV-2 induces double-stranded RNA-mediated innate immune responses in respiratory epithelial-derived cells and cardiomyocytes. Proc Natl Acad Sci U S A. 2021;118:e2022643118. https://doi.org/10.1073/pnas.2022643118
24. Marques AD, Graham-Wooten J, Fitzgerald AS, Sobel Leonard A, Cook EJ, Everett JK, et al. SARS-CoV-2 evolution during prolonged infection in immunocompromised patients. MBio. 2024;15:e0011024. https://doi.org/10.1128/mbio.00110-24
25. Marques AD, Hogenauer M, Bauer N, Gibison M, DeMarco B, Sherrill-Mix S, et al. Evolution of SARS-CoV-2 in white-tailed deer in Pennsylvania 2021–2024. PLoS Pathog. 2025;21:e1012883. https://doi.org/10.1371/journal.ppat.1012883
26. Everett J, Hokama P, Roche AM, Reddy S, Hwang Y, Kessler L, et al. SARS-CoV-2 Genomic variation in space and time in hospitalized patients in Philadelphia. MBio. 2021;12:e03456–20. https://doi.org/10.1128/mBio.03456-20
27. Li H. A statistical framework for SNP calling, mutation discovery, association mapping and population genetical parameter estimation from sequencing data. Bioinformatics. 2011;27:2987–93. https://doi.org/10.1093/bioinformatics/btr509
28. Li H, Durbin R. Fast and accurate short read alignment with Burrows-Wheeler transform. Bioinformatics. 2009;25:1754–60. https://doi.org/10.1093/bioinformatics/btp324
29. Li H, Handsaker B, Wysoker A, Fennell T, Ruan J, Homer N, et al.; 1000 Genome Project Data Processing Subgroup. The sequence alignment/map format and SAMtools. Bioinformatics. 2009;25:2078–9. https://doi.org/10.1093/bioinformatics/btp352
30. Hoffmann M, Kleine-Weber H, Schroeder S, Krüger N, Herrler T, Erichsen S, et al. SARS-CoV-2 cell entry depends on ACE2 and TMPRSS2 and is blocked by a clinically proven protease inhibitor. Cell. 2020;181:271–280.e8. https://doi.org/10.1016/j.cell.2020.02.052

Address for correspondence: Ranawaka Perera, Department of Microbiology, Perelman School of Medicine, University of Pennsylvania, 3400 Civic Center Blvd, Bldg 421, Philadelphia, PA 19104, USA; email: ranawaka.perera@pennmedicine.upenn.edu

Detection of Oropouche and Punta Toro Virus Infections by Enhanced Surveillance, Panama, 2023–2024

Maria Chen-Germán, Claudia González, Dimelza Araúz, Celestino Aguilar, Melanie Vega, Oris Chavarria, Ambar Moreno, Erika Santiago, Danilo Franco, Elimelec Valdespino, Jessica Gondola, Mayla Pinedo, Domicio Espino, Tamara Salcedo, Leticia Franco, Nicanor Obaldía III, Blas Armien, Alexander A. Martínez,[1] Brechla Moreno[1]

Enhanced arboviral surveillance in Panama revealed an Oropouche virus case, 5 months before the 2025 national outbreak, in samples that tested negative for routinely screened arboviruses. Subsequent contact tracing identified an additional case of Punta Toro virus. Our findings highlight the importance of expanding diagnostic efforts to identify circulating arboviruses.

In recent years, arbovirus incidence and geographic range have expanded markedly, leading to multiple outbreaks worldwide. Nevertheless, a substantial proportion of patients remain undiagnosed, largely because of the predominant focus on dengue clinical suspicion. We report findings from an enhanced surveillance initiative in Panama that reanalyzed dengue-negative samples, leading to the identification of other viral agents, including Oropouche virus (OROV) and Punta Toro virus (PTV). Our results highlight the need to broaden diagnostic approaches in arbovirus endemic regions.

OROV is a single-stranded, negative-sense, segmented RNA virus classified within the family *Peribunyaviridae*, genus *Orthobunyavirus*, primarily transmitted by the anthropophilic biting midge, *Culicoides paraensis*. OROV, first identified in Trinidad and Tobago in 1955, has circulated across Central and South America (*1*). In Panama, it was first isolated in 1989, although there is serologic evidence of earlier circulation in 1968 and 1978 (*2*).

In 2024, the Pan American Health Organization/World Health Organization reported rising OROV cases across the Americas, including areas with no previous evidence of circulation (*3*). Health officials linked this geographic expansion to severe clinical outcomes, including fatalities, vertical transmission, fetal loss, and microcephaly (*4*). Studies from Brazil identified a novel recombination event in OROV genomes (*5*).

PTV belongs to the *Phenuiviridae* family, *Phlebovirus* genus. This highly diverse genus encompasses numerous species globally distributed and transmitted by vectors like sandflies and ticks (*6*). Key members include Toscana virus and Rift Valley fever virus, which cause epidemics and neurologic disease across the Mediterranean Basin, Europe, and the Middle East (*7*). Reports from the Americas have identified *Phlebovirus* species in Brazil, Peru (*8*), Colombia (*9*) and Panama (*10*), although PTV appears to be reported only in Panama. Human infections, mainly detected in metropolitan areas of Panama, cause nonspecific febrile illness characterized by fever, headache, weakness, and retro-orbital pain (*10*).

The Study

In 2023–2024, the Gorgas Memorial Institute (Panama City, Panama) analyzed 3,589 serum samples. After a Pan American Health Organization/World Health Organization alert on rising regional OROV incidence

Author affiliations: Instituto Conmemorativo Gorgas de Estudios de la Salud, Panama City, Panama (M. Chen-Germán, C. González, D.J. Araúz, M. Vega, O. Chavarria, A. Moreno, E. Santiago, D. Franco, E. Valdespino, J. Gondola, N. Obaldia III, B. Armien, A.A. Martínez, B. Moreno); University of Panama, Panama City (C. Gonzalez, C. Aguilar, A.A. Martínez); Dr. Hugo Spadafora Polyclinic, Colon City, Panama (M. Pinedo); Ministry of Health, Penonome City, Panama (D. Espino); Ministry of Health, Panama City (T. Salcedo, B. Armien); Organización Panamericana de la Salud/Organización Mundial de la Salud, Panama City (L. Franco); Sistema Nacional de Investigación-SENACYT, Panama City (B. Armien, A.A. Martínez); Interamerican University of Panama, Panama City (B. Moreno)

DOI: http://doi.org/10.3201/eid3201.251224

[1]These authors were co–principal investigators.

and because of the lack of confirmed cases in Panama, we retrospectively tested a subset (24%) of dengue virus (DENV)–negative samples from that set for OROV by reverse transcription PCR (*11*). We later integrated this assay into a broader diagnostic algorithm for samples testing negative for DENV, Zika virus, and Chikungonya virus, which included testing for *Alphavirus*, *Orthoflavivirus*, and *Phlebovirus* (Appendix 1, https://wwwnc.cdc.gov/EID/article/32/1/25-1224-App1.pdf).

Through this surveillance, we identified an OROV-positive case from August 2024. The patient, a 31-year-old male environmental officer stationed in a forested area of the Soberanía National Park, Panama, sought treatment for an acute febrile syndrome characterized by severe frontal-occipital headache, chills, arthralgia, and marked asthenia. The man underwent an initial clinical evaluation at a primary healthcare facility, where the result of a dengue NS1 antigen test was negative. Treating clinicians reported no neurologic manifestations or relapses. Health officials conducted contact tracing, covering the patient's residence and workplace, collecting serum and urine samples from 36 contacts. Twelve symptomatic persons underwent testing for OROV, DENV, Zika virus, chikungunya virus, *Orthoflavivirus*, *Phlebovirus*, and *Alphavirus* (Table 1). Of those, 1 contact tested positive for the *Phlebovirus* genus, with symptoms including fever, chills, myalgia, arthralgia, headache, retro-orbital pain, and conjunctivitis.

We sequenced aliquots from both positive samples (OROV and *Phlebovirus* genus) using an in-house metagenomic approach (A. Martinez et al., unpub. data, https://dx.doi.org/10.17504/protocols.io.36wgq6545lk5/v1) (Appendix 1), yielding a complete OROV genome (GenBank accession nos. PV942050–2) (Table 2). We performed phylogenetic analysis using the Nextstrain OROV database (https://github.com/nextstrain/oropouche), which placed the sample at the basal node of the BR-2015–2024 clade (*5*), notably separated from the sequences circulating in the Brazil outbreak (Figure).

We performed a comparative analysis of OROV using the Panama sequence (hOROV/Panama/A003066/2024), recent Brazil sequences (OROV/Saul/17225/2020, LACENAM_ILMD_3228ZCF, and ILMD_TF29; GenBank accession nos. PP154170–2), and the ancestral BeAn19991 strain as reference. The Panama sequence showed multiple amino acid substitutions across structural and nonstructural proteins sharing 96.8% amino acid identity for the large (L) segment, 97%–99% for the medium (M) segment, and 98%–100% for the small (S) segment with BeAn19991. The Panama sequence also shared 99% amino acid identity for the L segment, 98%–99% for the M segment, and 100% for the S segment with the Brazil sequences (Appendix 1 Figure 1). We theorized that the differences may influence viral replication or transcription efficiency (K.B. Gunter et al., unpub. data, http://dx.doi.org/10.1101/2025.08.02.668287).

Further testing identified the *Phlebovirus* genus–positive sample as PTV (GenBank accession nos. PV942053–5) (Appendix 1 Figure 2; Appendix 2, https://wwwnc.cdc.gov/EID/article/32/1/25-1224-App1.xlsx). Compared against the prototype strain (GenBank accession nos. KP272028–30), amino acid identity was 87% for the L segment, 94% for the M segment, and 95%–97% for the S segment. Comparison with a 2004 sequence (GenBank accession nos. KP272031–3) showed amino acid identity as 99% with the L segment, 99% with the M segment, and 98%–99% with the S segment (Appendix 1 Figures 3, 4).

Before the OROV outbreak that began in January 2025 in Panama, the last documented case occurred in 1989 in Bejuco, a coastal community ≈35 miles west of Panama City, a region surrounded predominantly by mature broadleaf forest at the time (*2*). The OROV case we identified was likely acquired in a similar ecologic setting, at the interface between the metropolitan region and the Soberanía National Park. The geographic proximity between Bejuco and Soberanía National Park (22–25 miles) suggests shared ecologic characteristics and supports the hypothesis of ongoing cryptic OROV circulation before the 2025 cases reported in Darién province.

Although the absence of genomic data over the intervening decades limits reconstruction of OROV's full evolutionary history in Panama, our case provides valuable evidence suggestive of persistent, undetected sylvatic circulation. The Panama OROV sequence shows marked amino acid divergence from the ancestral BeAn19991 strain, especially in the L and M segments, and fewer differences relative to strains currently circulating in Brazil and South America, which have been reported since 2022 (*5*). Those changes are similar to mutations reported in recent studies (G.C.

Table 1. Signs and symptoms found in symptomatic contacts of case-patient with Oropouche virus from study of detection of Oropouche and Punta Toro virus infections by enhanced surveillance, Panama, 2023–2024

Sign/symptom	No. (%) contacts, n = 12
Fever >38°C	8 (67)
Severe headache	8 (67)
Intense chills	7 (58)
Retro-orbital pain	4 (33)
Conjunctivitis	2 (17)
Body pain	1 (8)

Table 2. Sequence analysis results from a study of detection of Oropouche and Punta Toro virus infections by enhanced surveillance, Panama, 2023–2024*

Organism and segment	GenBank accession no.	Start position	End position	No. reads	Base coverage	Coverage, %	Mean depth of segment, reads, n	Mean base quality, %	Mean mapped read quality, %
Oropouche virus sample A003066									
M	PP154171	1	4371	6,387	4,364	99.4	162.4	37.5	41.3
S	PP154170	1	944	3,411	846	89.6	405.13	37	45.5
L	PP154172	1	6814	14,128	6,814	100	239.7	37.5	46.2
Punta Toro virus sample A3416V2									
S	KP272018	1	1899	217,265	1,899	100	18.609	37	48.2
M	KP272017	1	4340	280,677	4,340	100	10.978	37	50.3
L	KP272016	1	6407	877,321	6,407	100	23.679	37	51.2

*L, large; M, medium; S, small.

Scachetti et al., unpub. data, http://dx.doi.org/10.1101/2024.07.27.24310296). The differences between the Panama strain and newly described OROV reassortants suggests ongoing adaptive processes, driven potentially by local selective pressures or prolonged cryptic circulation in Panama. Sporadic retrospective OROV detections in Brazil from dengue surveillance samples mirror this context (*12*).

PTV, causing undifferentiated febrile illness (*10*), is an arbovirus that appears to be underreported in Panama, which complicates clinical suspicion required for an accurate diagnosis. Our sequenced sample revealed appreciable genetic variability compared with the reference strain but fewer differences relative to a more recent sequence, suggesting both divergence from the original reference and ongoing viral evolution.

Conclusions

Both of the case-patients we describe had worked in areas of mature broadleaf forest, suggesting those locations as the sites of infection and indicating possible simultaneous, cryptic circulation of different arboviruses. The enhanced arboviral surveillance described in our study, which involved testing across multiple viral genera, broadened the analysis of dengue-negative samples, enabling the detection of other arboviruses. Of note, the OROV and PTV strains in our study showed greater genetic similarity among recent strains, pointing to ongoing evolution, while divergence from older strains reflects accumulation of mutations over time. Together, those findings underscore the complexity and dynamic nature of arbovirus evolution and highlight the crucial need to enhance and expand arboviral surveillance frameworks

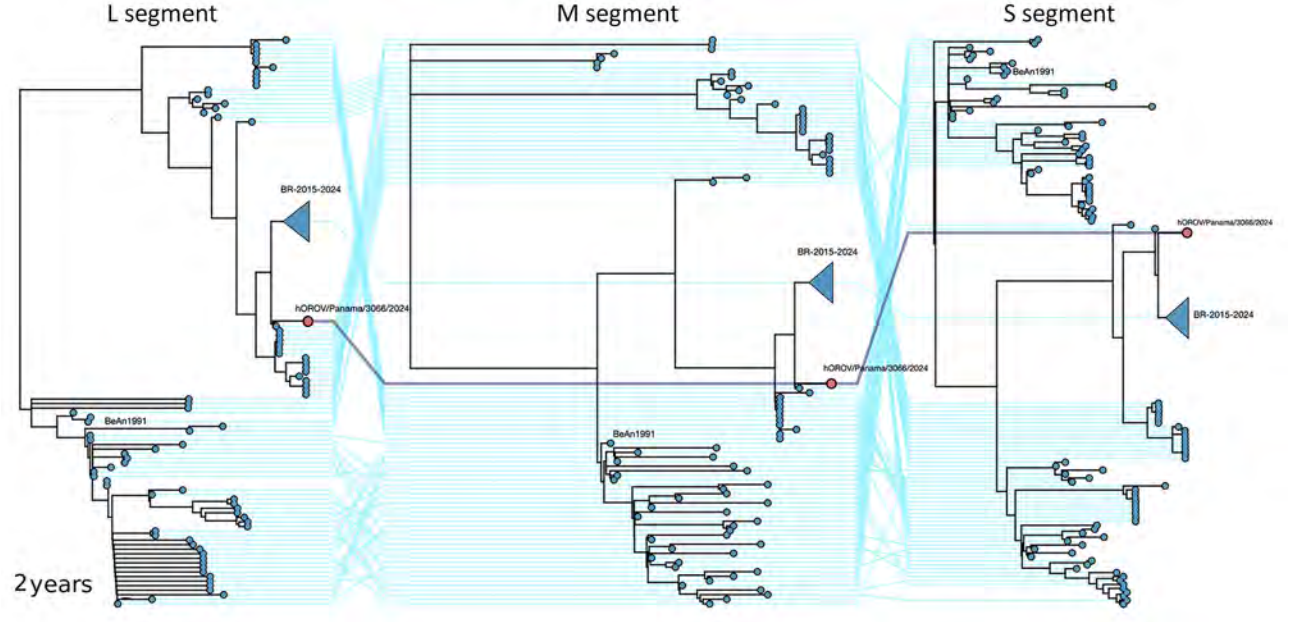

Figure. Concatenated maximum likelihood phylogenetic tree of 3 OROV segments from a patient found in study of detection of OROV and Punta Toro virus infections by enhanced surveillance, Panama, 2023–2024. The Panama sample is labeled as hOROV/Panama/3066/2024. Also shown in the tree are the prototype reference strain BeAn19991 and the Brazil outbreak clade BR-2015-2024, collapsed for better visualization. L, large; m, medium; OROV, Oropouche virus; s, small.

beyond the routine detection of dengue to encompass the full spectrum of circulating arboviruses and their potential effect on public health.

Acknowledgments

We thank Jairo Mendez and Lionel Gresh; the Pan American Health Organization, Health Emergency Department, Infectious Hazard Management Unit, Washington, DC; and PAHOGen, the PAHO Genomic Surveillance Regional Network, for support. We also thank Felipe Naveca and Tiago Gräf for the shared dataset for phylogenetic characterization. We also acknowledge the contributions of Yiseila Franco, Guillermo Alain, Carlos Yanguez, and Yanibeth Guevara.

This study has been registered in the RESEGIS platform from DIGESA from the Ministry of Health, Panama, under number 2652 and approved by the Bioethics Committee of Gorgas Memorial Institute for Health Studies Nº038/CBI/ICGES/25

About the Author

Ms. Chen-Germán is a medical technologist at the Gorgas Memorial Institute, where she specializes in arboviruses.

References

1. Sakkas H, Bozidis P, Franks A, Papadopoulou C. Oropouche fever: a review. Viruses. 2018;10:175. https://doi.org/10.3390/v10040175
2. US Centers for Disease Control and Prevention. Arthropod-borne virus information exchange: outbreak of Oropouche fever in Panama since August, 1989. CDC Stacks. 1989:70. https://stacks.cdc.gov/view/cdc/59573
3. Oropouche virus disease—Region of the Americas [cited 2025 Apr 11]. https://www.who.int/emergencies/disease-outbreak-news/item/2024-DON530
4. Schwartz DA, Dashraath P, Baud D. Oropouche virus (OROV) in pregnancy: an emerging cause of placental and fetal infection associated with stillbirth and microcephaly following vertical transmission. Viruses. 2024;16:1435.
5. Naveca FG, Almeida TAP, Souza V, Nascimento V, Silva D, Nascimento F, et al. Human outbreaks of a novel reassortant Oropouche virus in the Brazilian Amazon region. Nat Med. 2024;30:3509–21.
6. Sasaya T, Palacios G, Briese T, Di Serio F, Groschup MH, Neriya Y, et al. ICTV virus taxonomy profile: Phenuiviridae 2023. J Gen Virol. 2023;104:001893. https://doi.org/10.1099/jgv.0.001893
7. Keskek Turk Y, Ergunay K, Kohl A, Hughes J, McKimmie CS. Toscana virus—an emerging Mediterranean arbovirus transmitted by sand flies. J Gen Virol. 2024;105:002045. https://doi.org/10.1099/jgv.0.002045
8. Palacios G, Tesh R, Travassos da Rosa A, Savji N, Sze W, Jain K, et al. Characterization of the Candiru antigenic complex (*Bunyaviridae: Phlebovirus*), a highly diverse and reassorting group of viruses affecting humans in tropical America. J Virol. 2011;85:3811–20.
9. López Y, Miranda J, Mattar S, Gonzalez M, Rovnak J. First report of Lihan Tick virus (*Phlebovirus*, *Phenuiviridae*) in ticks, Colombia. Virol J. 2020;17:63.
10. Gundacker ND, Carrera JP, Castillo M, Díaz Y, Valenzuela J, Tamhane A, et al. Clinical manifestations of Punta Toro virus species complex infections, Panama, 2009. Emerg Infect Dis. 2017;23:872–4.
11. Naveca FG, Nascimento VAD, Souza VC, Nunes BTD, Rodrigues DSG, Vasconcelos PFDC. Multiplexed reverse transcription real-time polymerase chain reaction for simultaneous detection of Mayaro, Oropouche, and Oropouche-like viruses. Mem Inst Oswaldo Cruz. 2017;112:510–3.
12. Bernardes-Terzian AC, de-Moraes-Bronzoni RV, Drumond BP, Da Silva-Nunes M, da-Silva NS, Urbano-Ferreira M, et al. Sporadic oropouche virus infection, acre, Brazil. Emerg Infect Dis. 2009;15:348–50.

Address for correspondence: Brechla Moreno, Diagnostic and Surveillance Unit of the Virology Department, Gorgas Memorial Institute for Health Studies, 36th St and Justo Arosemena Ave, Panama City, Panama; bmoreno@gorgas.gob.pa

Sphingobacterium hotanense Infections in Immunocompromised Patients, United States

Khalid Abu-Zeinah, Benjamin D. Lueck, Shane A. Fuentes, Emily Puumala, Omar M. Abu Saleh

Sphingobacterium hotanense is a gram-negative bacillus identified in 2013 from soil samples that rarely causes infection in humans. We describe 2 cases of *S. hotanense* bacteremia secondary to skin and soft tissue infection in immunocompromised patients in Minnesota, USA, highlighting *S. hotanense* as a potential pathogen in immunocompromised hosts with environmental exposure.

Sphingobacterium hotanense is a strictly aerobic, gram-negative bacillus first isolated in 2013 from soil in China (*1*). The *Sphingobacterium* genus includes >50 species typically found in soil, compost, and aquatic habitats (*2*,*3*). Documented infections with *Sphingobacterium* spp. in humans are rare (*2*,*3*), manifesting mostly as skin and soft tissue infections (SSTI) in immunocompromised patients (*3*); we found limited reports of *S. hotanense* infections in the literature (*2*). We describe 2 cases of *S. hotanense* bacteremia secondary to SSTIs in Minnesota, USA.

The Mayo Clinic Institutional Review Board (IRB) acknowledged that based on the responses submitted for our activity through the Mayo Clinic Human Subjects Research Wizard tool, and in accordance with the Code of Federal Regulations, 45 CFR 46.102, this study did not require IRB review.

The Study

Case 1 was in a 78-year-old man who sought care for acute right lower extremity pain. His medical history included ulcerative colitis treated with mesalamine, cirrhosis from primary sclerosing cholangitis, and iron deficiency anemia from bleeding portal gastropathy. Five days earlier, the patient went fishing in Montana, USA, where he walked barefoot on riverbeds and fell in soil. No other travel history or animal exposure was reported. The patient was febrile (38.6°C); examination revealed erythematous right lower extremity (Figure 1) and abdominal tenderness. HIV test was negative. Computed tomography (CT) imaging of the abdomen demonstrated moderate ascites. Medical staff administered intravenous ceftriaxone to treat cellulitis and possible spontaneous bacterial peritonitis (SBP); however, subsequent diagnostic paracentesis was not suggestive of SBP.

Blood cultures grew gram-negative rods within 12 hours, and antimicrobial drugs were switched to intravenous piperacillin/tazobactam. After 18 hours, speciation identified *S. hotanense* (Figure 2) in 2 of 3 aerobic culture bottles of 2 sets, with antimicrobial susceptibilities (Table). Bacteremia was attributed to SSTI. The patient remained on intravenous piperacillin/tazobactam for 72 hours and then was discharged on a 7-day course of oral levofloxacin; outpatient follow-up visit showed resolution of cellulitis.

Case 2 was in a 75-year-old man who sought care for acute right lower extremity pain; his lethargic state limited the ability to obtain a detailed medical history. His medical history included HIV infection managed with abacavir/dolutegravir/lamivudine; viral load was undetectable but CD4 count low (93/μL), attributed to concomitant myelodysplastic syndrome. He had a previous diagnosis of remitting seronegative systemic synovitis managed with chronic prednisone (5 mg/d), and had lower extremity stasis dermatitis with chronic open wounds. He was afebrile but hypotensive (91/60 mm Hg). Examination revealed erythematous right lower extremity (Figure 3). Laboratory studies revealed elevated lactate (5.6 mmol/L). CT imaging of the right leg demonstrated subcutaneous edema without abscesses or gas. He was admitted to the intensive care unit for vasopressor treatment and received intravenous vancomycin, ceftriaxone, and clindamycin.

Blood cultures grew gram-negative bacilli after 12 hours, which was attributed to SSTI in his right leg. The antimicrobial regimen was narrowed to intravenous ceftriaxone and metronidazole. After 24 hours,

Author affiliation: Mayo Clinic, Rochester, Minnesota, USA

DOI: https://doi.org/10.3201/eid3201.251290

Figure 1. Lower extremities of patient in case 1 in report of *Sphingobacterium hotanense* infections in immunocompromised patients with skin and soft tissue infections, Minnesota, USA. Erythema and swelling of the right lower leg and foot are shown. No overt signs of abscess, necrosis, or purulence were noted at the time of examination.

S. hotanense was identified in 2 of 3 aerobic culture bottles from 1 set and in 1 bottle from a second set. Antimicrobial susceptibility was similar to that of case 1 (Table); intravenous ciprofloxacin was added to his regimen. Forty-eight hours after admission, his pain progressed, and operative debridement revealed extensive myonecrosis, necessitating above-knee amputation. Postoperative antimicrobial treatment was intravenous cefepime for 7 days. Intraoperative tissue cultures grew *Enterococcus faecalis* and *Enterobacter cloacae*; no additional antimicrobials were initiated because infection source was adequately controlled. Repeat blood cultures after the 7-day course of treatment indicated resolution of bacteremia. However, the patient then experienced acute pancreatitis, pulmonary embolism, candidemia, and pulmonary aspergillosis and died.

Blood cultures tested positive by BD BACTEC (Becton Dickinson, https://www.bd.com); we identified *S. hotanense* in our laboratory after subculture on standard growth media at 35°C with 5%–7% CO_2 (Appendix Figure, https://wwwnc.cdc.gov/EID/article/32/1/25-1290-App1.pdf). *Sphingobacterium* spp. are not detected by rapid syndromic assays, including commercial multiplex PCR panels; the optimal method of species-level identification is diagnostic mass spectrometry or sequencing of the variable regions of the 16S rRNA gene. We identified isolates from case 1 and case 2 using matrix-assisted laser desorption/ionization time-of-flight mass spectrometry (Bruker Daltonics, https://www.bruker.com) based on Biotyper numeric score of 2.00–3.00 with ≥10% score separation from the next best score. Given the rarity of *Sphingobacterium* organisms in human infections, data on performance of commercial automated identification systems remain limited. In smaller or resource-limited laboratories, phenotypic identification may be guided by the biochemical profile of *Sphingobacterium* spp. (*4*).

We performed drug susceptibility testing using the agar dilution method to determine the MIC of antimicrobial drugs. We used reporting guidelines and breakpoints for gram-negative bacilli that are non-Enterobacterales, nonfastidious, and nonfermentative according to Clinical and Laboratory Standards Institute guidelines (*5*) to determine *S. hotanense* susceptibility. On retrospective evaluation, we identified 10 *S. hotanense* isolates referred from external institutions during July 2020–July 2025 (Appendix).

Sphingobacterium spp. are rarely implicated in human infections, typically affecting elderly or immunocompromised hosts (*3*). Reported infections typically involve SSTI with or without bacteremia (*3*); however, acute cholangitis (*6*), respiratory tract infections (*7*), septic arthritis (*8*), and meningitis have also been reported (*9*).

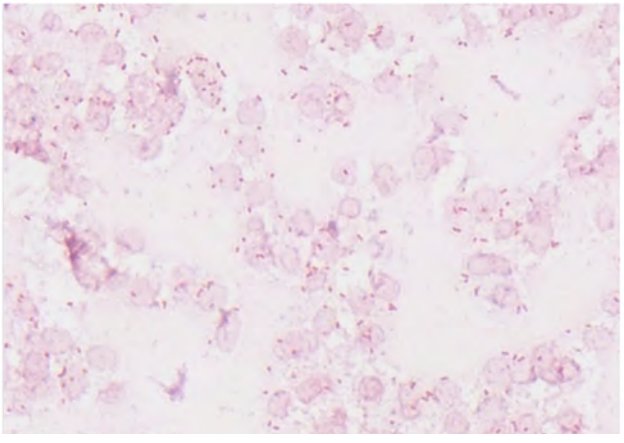

Figure 2. Gram stain of positive blood culture from patient in case 1 in report of *Sphingobacterium hotanense* infections in immunocompromised patients, Minnesota, USA. Numerous gram-negative bacilli are shown (pink rods), representing *S. hotanense* infection. Scale bar indicates 20 μm.

Table. Antimicrobial susceptibility profile of isolates from blood cultures of 2 patients in report of *Sphingobacterium hotanense* infection in immunocompromised patients, Minnesota, USA

Antimicrobial drug	MIC, μg/mL	Susceptibility
Amikacin	>32	Resistant
Aztreonam	16	Intermediate
Cefepime	≤2	Susceptible
Ceftazidime	≤4	Susceptible
Ciprofloxacin	≤0.25	Susceptible
Gentamicin	>8	Resistant
Levofloxacin	≤0.5	Susceptible
Meropenem	≤0.12	Susceptible
Piperacillin/tazobactam	≤8/4	Susceptible
Tobramycin	>8	Resistant
Trimethoprim/sulfamethoxazole	≤0.5/9.5	Susceptible

One documented case report from Europe described *S. hotanense* bacteremia secondary to cellulitis after a rooster scratch (*2*). Here, we report 2 additional cases of *S. hotanense* bacteremia from SSTI in immunocompromised hosts, consistent with previous reports. Case 1 involved a cirrhotic patient who had likely cirrhosis-associated immune dysfunction (*10*); exposure to river water and soil likely served as the source of inoculation (*1*). Case 2 involved a patient who had multiple immunocompromising conditions, including HIV, myelodysplastic syndrome, and corticosteroid use; lower-extremity wounds likely served as the port of entry.

The patient in case 1 had uncomplicated recovery after antimicrobial drug treatment. The patient in case 2 experienced a more severe course requiring above-knee amputation for necrotizing SSTI. In case 2, intraoperative tissue cultures grew *Enterococcus faecalis* and *Enterobacter cloacae*, consistent with the usual polymicrobial nature of necrotizing SSTI (*11*). The absence of *S. hotanense* from tissue cultures may reflect preoperative antimicrobial exposure affecting culture yield, given that no other source of bacteremia was identified.

Figure 3. Right lower leg of patient in case 2 in report of *Sphingobacterium hotanense* infection in immunocompromised patients, Minnesota, USA, demonstrating extensive skin discoloration with surrounding erythema and increased drainage from wound (not visible).

When *S. hotanense* was isolated in 2013, antimicrobial susceptibility testing revealed resistance to ampicillin and tetracycline but susceptibility to ceftazidime (*1*). In subsequent reports, the organism demonstrated susceptibility to β-lactams, fluoroquinolones, and trimethoprim/sulfamethoxazole and resistance to aminoglycosides (*2*). The susceptibility patterns of the *S. hotanense* isolates in the cases we describe were similar to those previously reported, including sensitivity to broad-spectrum β-lactams such as ceftazidime, cefepime, piperacillin/tazobactam, and carbapenems as well as to fluoroquinolones and trimethoprim/sulfamethoxazole. Given the rarity of *S. hotanense* infections, antimicrobial selection should be guided by in vitro susceptibility results; piperacillin/tazobactam or cefepime are reasonable empiric choices and fluoroquinolones appropriate oral step-down options. Additional considerations include underlying conditions, drug allergies, and concern for polymicrobial infection.

Identification of *S. hotanense* in both cases we report was possible because we obtained blood cultures. Blood culture yield in cellulitis is generally low (<5%); cultures are therefore reserved for patients with high-risk features, such as sepsis, necrotization, immunosuppression, immersion injuries, or animal bites (*12*). Because cellulitis is often treated empirically without obtaining blood cultures, it might be that *S. hotanense* SSTI is more common than currently recognized but underdiagnosed because of infrequent microbiologic testing.

Conclusions

S. hotanense is a rare cause of SSTI. Given its environmental reservoir, clinicians should maintain suspicion for *S. hotanense* in immunocompromised patients experiencing SSTI, especially with recent environmental exposure. More frequent microbiologic testing in select high-risk cases could reveal this organism as an underrecognized cause of infection.

All authors contributed to the writing and revision of this manuscript.

About the Author

Dr. Abu-Zeinah is an internal medicine resident physician at the Mayo Clinic in Rochester, Minnesota. His research interests include infections in immunocompromised and transplant patients.

References

1. Xiao T, He X, Cheng G, Kuang H, Ma X, Yusup K, et al. *Sphingobacterium hotanense* sp. nov., isolated from soil of a *Populus euphratica* forest, and emended descriptions of *Sphingobacterium daejeonense* and *Sphingobacterium shayense*. Int J Syst Evol Microbiol. 2013;63:815–20. https://doi.org/10.1099/ijs.0.030155-0
2. Kroumova V, Rossati A, Bargiacchi O, Garavelli PL, Camaggi A, Caroppo S, et al. From soil to blood: first human case of *Sphingobacterium hotanense* bacteraemia. Infez Med. 2017;25:75–6.
3. Nemoto D, Hitomi S, Moriyama Y, Iwamoto K, Saito K. Cellulitis complicated with bacteremia due to *Sphingobacterium* species: a report of two cases and a literature review. Intern Med. 2019;58:2573–6. https://doi.org/10.2169/internalmedicine.2178-18
4. Cools P, Nemec A, Abeele A-Mvd, Kämpfer P. *Acinetobacter*, *Chryseobacterium*, *Moraxella*, *Branhamella* and other nonfermentative gram-negative rods. In: Carroll KC, Pfaller MA, editors. Manual of clinical microbiology, 13th edition. Washington: John Wiley & Sons, Inc; 2023. p. 1–33.
5. Clinical and Laboratory Standards Institute. Performance standards for antimicrobial susceptibility testing, 35th edition. Supplement M100. Wayne (PA): The Institute; 2025.
6. Akazawa N, Itoh N, Morioka H, Ogata T, Ishibana Y, Murakami H, et al. Cholangitis with *Sphingobacterium multivorum* and *Acinetobacter junii* bacteremia in a patient with gastric cancer: a case report. J Infect Chemother. 2022;28:1419–23. https://doi.org/10.1016/j.jiac.2022.06.005
7. Lambiase A, Rossano F, Del Pezzo M, Raia V, Sepe A, de Gregorio F, et al. *Sphingobacterium* respiratory tract infection in patients with cystic fibrosis. BMC Res Notes. 2009;2:262. https://doi.org/10.1186/1756-0500-2-262
8. Mendes MD, Cavallo RR, Carvalhaes CH, Ferrarini MA. Septic arthritis by *Sphingobacterium multivorum* in imunocompromised pediatric patient. Rev Paul Pediatr. 2016;34:379–83. https://doi.org/10.1016/j.rpped.2015.12.001
9. Abro AH, Rahimi Shahmirzadi MR, Jasim LM, Badreddine S, Al Deesi Z. *Sphingobacterium multivorum* bacteremia and acute meningitis in an immunocompetent adult patient: a case report. Iran Red Crescent Med J. 2016;18:e38750. https://doi.org/10.5812/ircmj.38750
10. Rodriguez-Negrete EV, Galvez-Martinez M, Sanchez-Reyes K, Fajardo-Felix CF, Perez-Resendiz KE, Madrigal-Santillan EO, et al. Liver cirrhosis: the immunocompromised state. J Clin Med. 2024;13.https://doi.org/10.3390/jcm13185582
11. Dhanasekara CS, Marschke B, Morris E, Kahathuduwa CN, Dissanaike S. Global patterns of necrotizing soft tissue infections: a systematic review and meta-analysis. Surgery. 2021;170:1718–26. https://doi.org/10.1016/j.surg.2021.06.036
12. Stevens DL, Bisno AL, Chambers HF, Dellinger EP, Goldstein EJ, Gorbach SL, et al.; Infectious Diseases Society of America. Practice guidelines for the diagnosis and management of skin and soft tissue infections: 2014 update by the Infectious Diseases Society of America. Clin Infect Dis. 2014;59:147–59. https://doi.org/10.1093/cid/ciu444

Address for correspondence: Khalid Abu-Zeinah, Mayo Clinic, 200 1st St SW, Rochester, MN 55905, USA; email: abu-zeinah.khalid@mayo.edu

etymologia revisited

Petri Dish
[pe'tre 'dish]

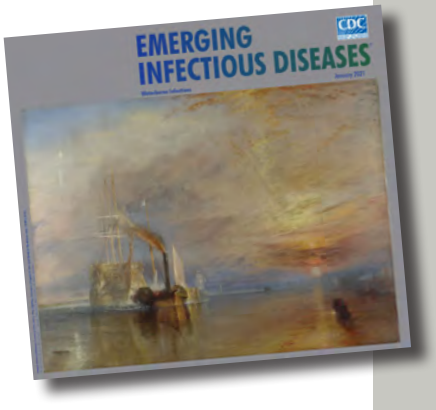

Originally published in January 2021

The Petri dish is named after the German inventor and bacteriologist Julius Richard Petri (1852–1921). In 1887, as an assistant to fellow German physician and pioneering microbiologist Robert Koch (1843–1910), Petri published a paper titled "A minor modification of the plating technique of Koch." This seemingly modest improvement (a slightly larger glass lid), Petri explained, reduced contamination from airborne germs in comparison with Koch's bell jar.

References

1 Central Sheet for Bacteriology and Parasite Science [in German]. Biodiversity Heritage Library. Volume 1, 1887 [cited 2020 Aug 25]. https://www.biodiversitylibrary.org/item/210666#page/313/mode/1up
2. Petri JR. A minor modification of the plating technique of Koch [in German]. Cent für Bacteriol und Parasitenkd. 1887;1:279–80.
3. Shama G. The "Petri" dish: a case of simultaneous invention in bacteriology. Endeavour. 2019;43:11–6.
4. The big story: the Petri dish. The Biomedical Scientist. Institute of Biomedical Science [cited 2020 Aug 25]. https://thebiomedicalscientist.net/science/big-story-petri-dish

https://wwwnc.cdc.gov/eid/article/27/1/et-2701_article

Dermacentor occidentalis Ticks and Link to *Rickettsia lanei* Infections, California, USA

Will S. Probert, Chantha Kath, Naomi Putirka, Megan E.M. Saunders, Brenda Bermudez, Matthew I. Cazas, Alex Espinosa, Hannah Romo, Jill K. Hacker

Rickettsia lanei is a newly recognized spotted fever group rickettsial species that causes severe Rocky Mountain spotted fever–like illness. We used genome sequencing, enabled by hybridization capture-based target enrichment, to establish *Dermacentor occidentalis* ticks as the likely source of a human infection with *R. lanei* in California, USA.

Spotted fever group (SFG) rickettsioses are acute undifferentiated febrile illnesses caused by tickborne transmission of intracellular gram-negative bacteria belonging to SFG *Rickettsia*. Rocky Mountain spotted fever (RMSF) is caused by *R. rickettsii* subspecies *rickettsii* and Pacific Coast tick fever by *R. rickettsii* subsp. *californica*; those 2 SFG rickettsioses are the most frequently reported in California, USA (*1*,*2*). We recently described 2 cases, 1 with disease onset in 2023 and 1 identified retrospectively with onset in 2004, of severe RMSF-like illness in northern California caused by a newly recognized SFG rickettsial pathogen, *Rickettsia* sp. CA6269 (*3*). This novel rickettsial genotype was first identified in *Haemaphysalis leporispalustris* ticks in Sonoma County, California, and, more recently in *H. leporispalustris* ticks in Maine, USA (*4*,*5*). Subsequently, whole-genome sequencing of rickettsial strain HLP 7421, isolated in 1961 from a pool of *H. leporispalustris* ticks collected in Montana, USA, supported classification of the *Rickettsia* sp. CA6269 genotype as a new species, *R. lanei* (*6*). In this study, we report on the detection of *R. lanei* in *Dermacentor occidentalis* and *H. leporispalustris* ticks collected at or near locations of exposure for the 2004 and 2023 cases.

Author affiliations: California Department of Public Health, Richmond, California, USA (W.S. Probert, C. Kath, M.E.M Saunders, B. Bermudez, M.I. Cazas, A. Espinosa, H. Romo, J.K. Hacker); San Francisco State University, San Francisco, California, USA (N. Putirka)

DOI: https://doi.org/10.3201/eid3201.251261

The Study

The California Department of Public Health monitors prevalence of SFG *Rickettsia* annually by collecting and testing *Dermacentor* spp. ticks (*3*,*7*). In 2024, SFG *Rickettsia* surveillance was enhanced to include collection of *H. leporispalustris* and additional *Dermacentor* spp. ticks from areas associated with exposures for the 2004 (Marin and San Mateo Counties) and 2023 (Alameda and Contra Costa Counties) cases. In addition, *H. leporispalustris* ticks were collected from an area in Sonoma County where *R. lanei*–positive ticks were originally described (*4*). In 2024, a total of 3,607 adult and nymphal ticks were tested for SFG *Rickettsia*: 2,872 *D. occidentalis* ticks collected from 34 of the 58 California counties and 69 *D. similis* and 666 *H. leporispalustris* ticks collected from 6 counties (Figure; Appendix, https://wwwnc.cdc.gov/EID/article/32/1/25-1261-App1.pdf).

We extracted and purified tick nucleic acids and screened for *Rickettsia* spp. using PanR8 real-time PCR (rPCR) (*3*,*8*). We tested all positive samples for *R. rickettsii* subsp. *californica* using the *nusG* rPCR and *R. rickettsii* subsp. *rickettsii*/*R. lanei* using RRi6 rPCR (*8*,*9*). We used a fourth rPCR to distinguish *R. lanei* from *R. rickettsii* subsp. *rickettsii* (*3*). We detected *Rickettsia* spp. in 14% of *D. occidentalis* ticks, 20.3% of *D. similis* ticks, and 3.5% of *H. leporispalustris* ticks (Table 1). We detected *R. rickettsii* subsp. *californica* only in *D. occidentalis* ticks (1.3%) and did not detect *R. rickettsii* subsp. *rickettsii* in any ticks. Two *H. leporispalustris* nymphs (24-5179 and 24-6522) collected 34 days apart from the same site in San Mateo County and 1 *D. occidentalis* adult female tick (24-7980) from Contra Costa County were positive for *R. lanei* by rPCR with cycle threshold values of 27.5 (24-5179; DNA diluted 1:20), 27.5 (24-6522; DNA diluted 1:20), and 18.4 (24-7980; DNA neat) (Figure). The overall prevalence of *R. lanei* was 0.3% in *H. leporispalustris* ticks and 0.03% in *D. occidentalis* ticks (Table 1).

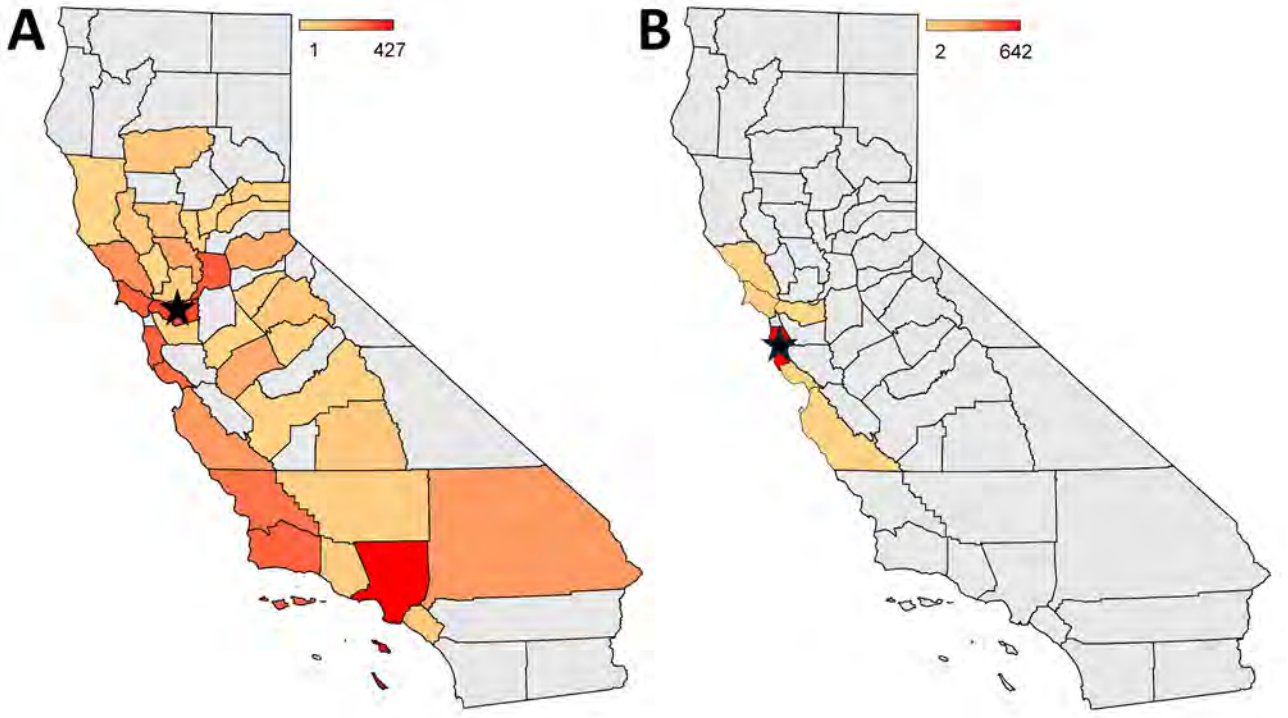

Figure. Heat maps displaying the number of *Dermacentor occidentalis* (A) and *Haemaphysalis leporispalustris* (B) ticks tested for spotted fever group *Rickettsia* in 2024, by county, in study of *D. occidentalis* ticks and link to *Rickettsia lanei* infections, California, USA. Color scale represents number of ticks. Black star represents the location of ticks testing positive by PCR for *R. lanei*: 1 *D. occidentalis* tick in Contra Costa County (A) and 2 *H. leporispalustris* ticks in San Mateo County (B). Gray shading indicates counties in which tick collection was not attempted or the tick species was not found.

We performed hybridization capture-based target enrichment sequencing to investigate genome relatedness of *R. lanei* strains from the 2023 case (strain CA23RL1) and ticks 24-5179, 24-6522, and 24-7980 (*10*). We amplified remnant nucleic acids from the plasma specimen collected on day 7 from the 2023 case using the REPLI-G whole genome amplification kit (QIAGEN, https://www.qiagen.com). Unfortunately, nucleic acids from the 2004 case had been depleted. We processed tick DNAs without whole-genome amplification. We performed DNA library preparation and hybridization capture-based target enrichment using a customized panel of ≈10,000 120-bp biotinylated oligonucleotides designed to span the genome of *R. rickettsii* subsp. *californica* (GenBank accession no. CP003308.1) end-to-end using the KAPA HyperCap workflow version 3 (Roche, https://www.roche.com). We sequenced enriched libraries on a MiSeq using reagent kit v2 (500 cycles) (Illumina, https://www.illumina.com).

We assembled a near whole-genome sequence of strain CA23RL1 from the 2023 case by mapping sequencing reads to the *R. lanei* type strain HLP 7421 genome (GenBank accession no. CP172233) using Geneious Prime v2022.0.2 (https://www.geneious.com). The percentage of CA23RL1 reads that mapped to HLP 7421 was 29.9%, providing 99.4% genome coverage with an average depth of 400 reads. We mapped unused reads to the genome of *R. rickettsii* subsp. *californica* and inserted the resultant mapped sequences into the CA23RL1 consensus sequence. We used Sanger sequencing to close genome sequence gaps and resolve repetitive regions, establishing a complete genome sequence of 1,270,942 bp for CA23RL1. Genome relatedness was 98.5%

Table 1. PCR detection of *Rickettsia* in *Dermacentor* and *Haemaphysalis* ticks collected in California, 2024

Tick species	No. ticks tested	No. PCR-positive ticks (%)			
		Rickettsia genus	*R. rickettsii* subspecies *rickettsii*	*R. rickettsii* subsp. *californica*	*R. lanei*
Dermacentor occidentalis	2,872	402 (14)	0	38 (1.32)	1 (0.03)
Dermacentor similis	69	14 (20.29)	0	0	0
Haemaphysalis leporispalustris	666	23 (3.45)	0	0	2 (0.3)

Table 2. Comparison of tick genome sequences to *Rickettsia lanei* strain CA23RL1 genome sequence in study of *Dermacentor occidentalis* ticks and link to *Rickettsia lanei* infections, California, USA

Tick identifier	Tick species	County of collection	Genome size, bp	Single-nucleotide polymorphisms	Insertions/deletions
24-5179	*Haemaphysalis leporispalustris*	San Mateo	1,270,870	19	4
24-6522	*H. leporispalustris*	San Mateo	1,270,870	19	4
24-7980	*Dermacentor occidentalis*	Contra Costa	1,270,942	0	0

between CA23RL1 and *R. rickettsii* subsp. *rickettsii*, 98.7% between CA23RL1 and *R. rickettsii* subsp. *californica*, and 99.7% between CA23RL1 and *R. lanei*, as determined by the orthologous average nucleotide identity algorithm (*11*).

We assembled genome sequences for the tick samples by mapping reads to the CA23RL1 genome. Genome coverage for the tick samples was ≥99.4%; average depth was >1,100 sequencing reads. We resolved repetitive regions and genome sequence gaps using Sanger sequencing and aligned complete genome sequences for the tick samples to the CA23RL1 genome using Mauve version 1.1.3 to determine genetic relatedness (*12*). The *D. occidentalis* 24-7980 genome sequence was identical to the CA23RL1 genome sequence, whereas those of the *H. leporispalustris* samples (24-5179 and 24-6522) were identical to one another but differed from the CA23RL1 and 24–7980 genome sequences by 19 nt polymorphisms and 4 insertions/deletions (Table 2).

Sequencing data are available in the National Center for Biotechnology Information BioProject database (accession no. PRJNA1261853). Limitations to our study are the lack of long-read next generation sequencing data to confirm lengthy repetitive DNA regions and the potential bias in using closely related reference sequences for guiding capture probe design and genome assembly.

Conclusions

We investigated the role of *Dermacentor* spp. and *H. leporispalustris* ticks as reservoirs and potential vectors of *R. lanei* in California and found a very low prevalence of infection. Ticks infected with *R. lanei* were only detected in counties identified as locations of exposure for the 2 cases: 2 *H. leporispalustris* nymphs collected in San Mateo County near a location of exposure for the 2004 case and 1 *D. occidentalis* adult tick collected in Contra Costa County at a site of exposure for the 2023 case. The positive *D. occidentalis* tick was collected at 1 of 5 golf courses visited by the case-patient within 14 days of illness onset (*3*). This ecoepidemiologic association and identical *R. lanei* genomic sequence match between the 2023 case and the *D. occidentalis* tick strongly implicate this tick species as the source of disease transmission. This conclusion is further supported by the observation that *D. occidentalis* ticks infest humans much more frequently than do *H. leporispalustris* ticks (*13*).

The *R. lanei* genome sequence from the *H. leporispalustris* ticks shared a high degree of sequence identity (orthologous average nucleotide identity >99.9%) with the sequence from the 2023 case and the *D. occidentalis* tick. Although it is unlikely that *H. leporispalustris* plays a role in the human transmission of *R. lanei* given both its preference for lagomorphs and the rarity of human infestations, this tick species may serve as a key vector for maintenance of *R. lanei* in nature, much as it does for *R. rickettsii* (*14*,*15*). Future studies are warranted to confirm vector competency of *D. occidentalis* and *H. leporispalustris* for *R. lanei* transmission. Acknowledging the severity of the 2 *R. lanei* infections and the broad distribution of the tick species, our results highlight the role of ecoepidemiologic investigations in identifying risk factors and guiding mitigation strategies for preventing vectorborne diseases.

Acknowledgments

We thank Mary Joyce Pakingan and Erin Belden for tick extractions and San Mateo County Mosquito and Vector Control District for tick collection.

This work was funded in part by the Centers for Disease Control and Prevention (CDC) Epidemiology and Laboratory Capacity for Infectious Diseases (grant no. 5 NU50CK000539). M.S. acknowledges support from the Pacific Southwest Center of Excellence in Vector-Borne Diseases, which has been funded by the cooperative agreement U01CK000649 (A. Swei, principal investigator) from the CDC. The findings and conclusions in this article are those of the authors and do not necessarily represent the views or opinions of the CDC, California Department of Public Health, or California Health and Human Services Agency.

About the Author

Dr. Probert is a research scientist with the Viral and Rickettsial Disease Laboratory of the California Department of Public Health, Center for Laboratory Sciences. He is interested in the development of molecular diagnostic assays for the detection and genotyping of microbial pathogens.

References

1. Kjemtrup AM, Padgett K, Paddock CD, Messenger S, Hacker JK, Feiszli T, et al. A forty-year review of Rocky Mountain spotted fever cases in California shows clinical and epidemiologic changes. PLoS Negl Trop Dis. 2022; 16:e0010738. https://doi.org/10.1371/journal.pntd.0010738
2. Paddock CD, Karpathy SE, Henry A, Ryle L, Hecht JA, Hacker JK, et al. *Rickettsia rickettsii* subsp *californica* subsp nov, the Etiologic Agent of Pacific Coast Tick Fever. J Infect Dis. 2025;231:849–58. https://doi.org/10.1093/infdis/jiae512
3. Probert WS, Haw MP, Nichol AC, Glaser CA, Park SY, Campbell LE, et al. Newly recognized spotted fever group *Rickettsia* as cause of severe Rocky Mountain spotted fever–like illness, northern California, USA. Emerg Infect Dis. 2024;30:1344–51. https://doi.org/10.3201/eid3007.231771
4. Eremeeva ME, Weiner LM, Zambrano ML, Dasch GA, Hu R, Vilcins I, et al. Detection and characterization of a novel spotted fever group *Rickettsia* genotype in *Haemaphysalis leporispalustris* from California, USA. Ticks Tick Borne Dis. 2018;9:814–8. https://doi.org/10.1016/j.ttbdis.2018.02.023
5. Xu G, Ballman E, Stamborski N, Siegel EL, Pearson P, Rich SM. A new spotted fever group *Rickettsia* genotype in *Haemaphysalis leporispalustris* from Maine, USA. Ticks Tick Borne Dis. 2025;16:102465. https://doi.org/10.1016/j.ttbdis.2025.102465
6. Paddock CD, Harris A, Clark TR, Bullock HA, Hecht JA, Ladner JT, et al. *Rickettsia lanei*, sp. nov. (Rickettsiales: Rickettsiaceae), a newly recognized pathogen of humans associated with the rabbit tick, *Haemaphysalis leporispalustris* (Acari: Ixodidae). Am J Trop Med Hyg. 2025;113:957–65. https://doi.org/10.4269/ajtmh.25-0134
7. California Department of Public Health. VBDS annual reports [cited 2025 May 26]. https://www.cdph.ca.gov/Programs/CID/DCDC/Pages/VBDSAnnualReports.aspx
8. Kato CY, Chung IH, Robinson LK, Austin AL, Dasch GA, Massung RF. Assessment of real-time PCR assay for detection of *Rickettsia* spp. and *Rickettsia rickettsii* in banked clinical samples. J Clin Microbiol. 2013;51:314–7. https://doi.org/10.1128/JCM.01723-12
9. Karpathy SE, Espinosa A, Yoshimizu MH, Hacker JK, Padgett KA, Paddock CD. A novel TaqMan assay for detection of *Rickettsia* 364D, the etiologic agent of Pacific Coast tick fever. J Clin Microbiol. 2019;58:e01106–19. https://doi.org/10.1128/JCM.01106-19
10. Jain K, Tagliafierro T, Marques A, Sanchez-Vicente S, Gokden A, Fallon B, et al. Development of a capture sequencing assay for enhanced detection and genotyping of tick-borne pathogens. Sci Rep. 2021;11:12384. https://doi.org/10.1038/s41598-021-91956-z
11. Lee I, Ouk Kim Y, Park SC, Chun J. OrthoANI: An improved algorithm and software for calculating average nucleotide identity. Int J Syst Evol Microbiol. 2016;66:1100–3. https://doi.org/10.1099/ijsem.0.000760
12. Darling AC, Mau B, Blattner FR, Perna NT. Mauve: multiple alignment of conserved genomic sequence with rearrangements. Genome Res. 2004;14:1394–403. https://doi.org/10.1101/gr.2289704
13. Eisen L. Tick species infesting humans in the United States. Ticks Tick Borne Dis. 2022;13:102025. https://doi.org/10.1016/j.ttbdis.2022.102025
14. Parker RR, Pickens EG, Lackman DB, Belle EJ, Thraikill FB. Isolation and characterization of Rocky Mountain spotted fever rickettsiae from the rabbit tick *Haemaphysalis leporis-palustris* Packard. Public Health Rep. 1951;66:455–63. https://doi.org/10.2307/4587691
15. Burgdorfer W. Ecology of tick vectors of American spotted fever. Bull World Health Organ. 1969;40:375–81.

Address for correspondence: Will Probert, California Department of Public Health, Center for Laboratory Sciences, Viral and Rickettsial Disease Laboratory, 850 Marina Bay Pkwy, Richmond, CA 94804, USA; email: will.probert@cdph.ca.gov

Disseminated *Nocardia ignorata* Infection with Splenic and Brain Involvement in Patient with Large B-Cell Lymphoma

Sherif Elbaz, Mahmoud Ismail, Seth Glassman, Asmaa Badr, Eric John Dove

A 79-year-old man in the United States with large B-cell lymphoma and chronic obstructive pulmonary disease had disseminated *Nocardia ignorata* infection involving the brain and spleen. Despite antimicrobial therapy, he died from complications. This rare manifestation highlights the need to consider *Nocardia* in immunocompromised patients with central nervous system and abdominal lesions.

Nocardia are filamentous, gram-positive, aerobic bacteria that infect immunocompromised hosts, causing pulmonary, cutaneous, or central nervous system disease (*1*–*4*). Dissemination to abdominal organs is rare (*5*). Among published cases, splenic involvement accounts for <10% of abdominal nocardiosis (*5*). We report disseminated *N. ignorata* infection with concurrent splenic and brain involvement in a patient in the United States who had large B-cell lymphoma.

The Study

A 79-year-old man with chronic obstructive pulmonary disease and large B-cell lymphoma had a new-onset seizure, left facial droop, and slurred speech. Computed tomography of the brain revealed multiple enhancing lesions with surrounding edema and mild herniation (Figure 1, panels A–E). Computed tomography of the abdominal pelvis (Figure 1, panel F, G) and chest showed a pulmonary nodule, a right renal lesion, and a 6.1-cm splenic mass.

Biopsy of the spleen demonstrated an extensively necrotic B-lymphocyte antigen cluster of differentiation 20–positive large B-cell lymphoma and limited viable tissue, explaining the negative primary stains we obtained (Figure 2). Cultures of splenic aspiration and brain biopsy grew filamentous branching *N. ignorata* (Figure 3). We used matrix-assisted laser desorption/ionization time-of-flight mass spectrometry for species-level identification. Blood culture results were negative. We used blood agar and chocolate agar for isolation. We extended the incubation period to accommodate slow growth.

We started the patient on antimicrobial therapy (intravenous imipenem and oral trimethoprim/sulfamethoxazole and linezolid) before susceptibility results were available. The patient's hospital course was complicated by upper gastrointestinal bleeding. He was transitioned to comfort care and subsequently died.

Conclusions

Disseminated nocardiosis frequently affects the lungs, brain, or skin, but splenic involvement is rare (*2*,*3*,*5*). Immunosuppression from malignancy predisposes patients to opportunistic infections such as those caused by *Nocardia* (*2*,*3*,*6*). This case highlights the diagnostic challenge posed by nonspecific clinical findings and the need for microbiologic confirmation, given that *Nocardia* species exhibit variable antimicrobial drug susceptibility (*1*,*3*). The observed pattern of simultaneous brain and splenic involvement in the setting of lymphoma underscores the need to consider the emergence of this disease in immunocompromised patients. Our findings also support early inclusion of nocardiosis in the differential diagnosis for patients with concurrent central nervous system and visceral lesions (*2*,*3*,*5*,*7*).

Author affiliations: University at Buffalo, Buffalo, New York, USA (S. Elbaz, M. Ismail, S. Glassman, E.J. Dove); The Ohio State University, Columbus, Ohio, USA (A. Badr)

DOI: https://doi.org/10.3201/eid3201.251546

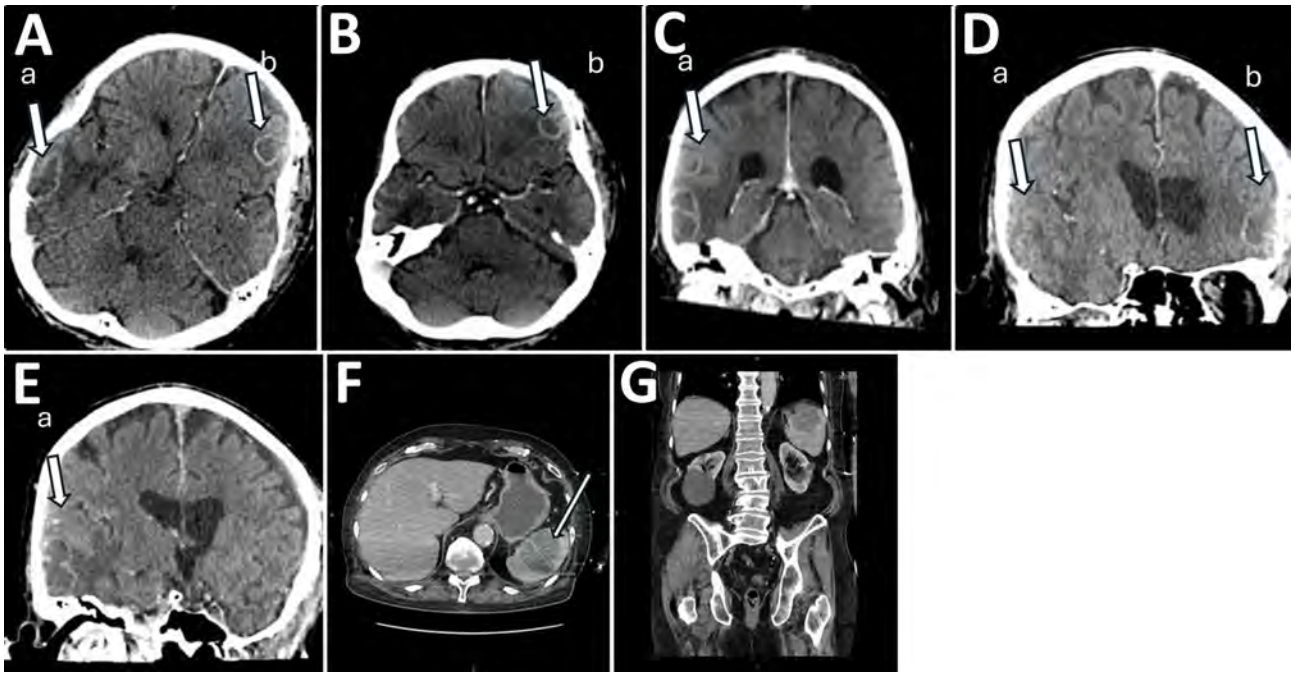

Figure 1. Computed tomography (CT) images of brain, abdomen, and spine of 79-year-old man with chronic obstructive pulmonary disease and large B-cell lymphoma who had disseminated *Nocardia ignorata* infection, United States. A–E) Brain CT with and without contrast showing multiple regular peripheral enhancing brain lesions (indicated by arrow and lowercase letters a and b) measuring 2.2 cm at the left frontal lobe (A) and 3.8 cm at the right (B); mildly lobulated at the right posterior lateral temporal lobe (C); and moderate edematous mass (D), resulting in mild brain herniation (E). F, G) CT images of abdomen (F) and pelvis (G). An indeterminate complex lesion measuring 6.1 cm is seen in the spleen (F, arrow).

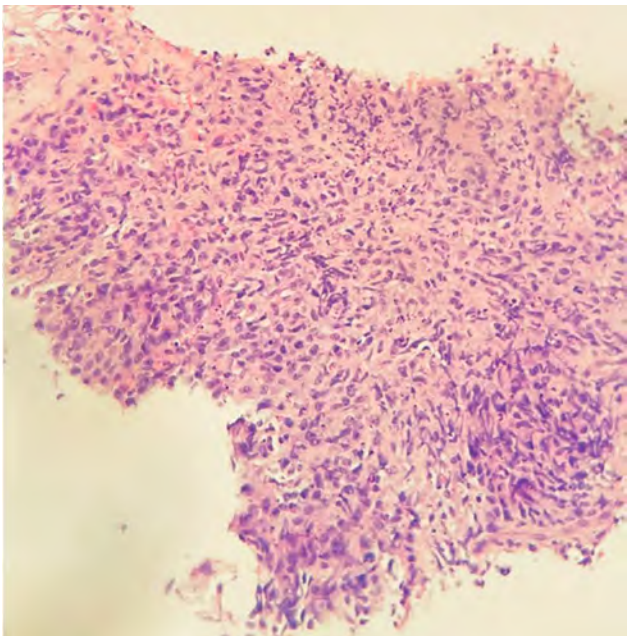

Figure 2. Ultrasound-guided biopsy image of spleen of 79-year-old man with chronic obstructive pulmonary disease and large B-cell lymphoma who had disseminated *Nocardia ignorata* infection, United States. Tissue fragment shows extensive necrosis with a small focus of large B-cell lymphoma. Neoplastic cells stain positively for CD20 antibody, paired box protein 5, and Bcell lymphoma 2, with 20% expression of myelocytomatosis oncogene, corroborating the diagnosis of disseminated *Nocardia ignorata* infection. Mindbomb1 antibody is positive in 90% of the cells. Acid-fast, Fite–Faraco, Gomori methenamine silver, and periodic acid–Schiff special stains do not demonstrate identifiable microorganisms or microbiota. Original magnification × 20.

About the Author

Dr. Elbaz is a physician and geriatrics fellow in the Division of Geriatrics, Department of Medicine, Jacobs School of Medicine and Biomedical Sciences, University at Buffalo, Buffalo, New York, USA. He is currently a second-year nephrology fellow at HCA Houston Kingwood's Tilman J. Fertitta Family College of Medicine, University of Houston, Houston, Texas, USA. His primary research interests include infectious diseases in older adults, immunocompromised host infections, geriatric nephrology, and onconephrology.

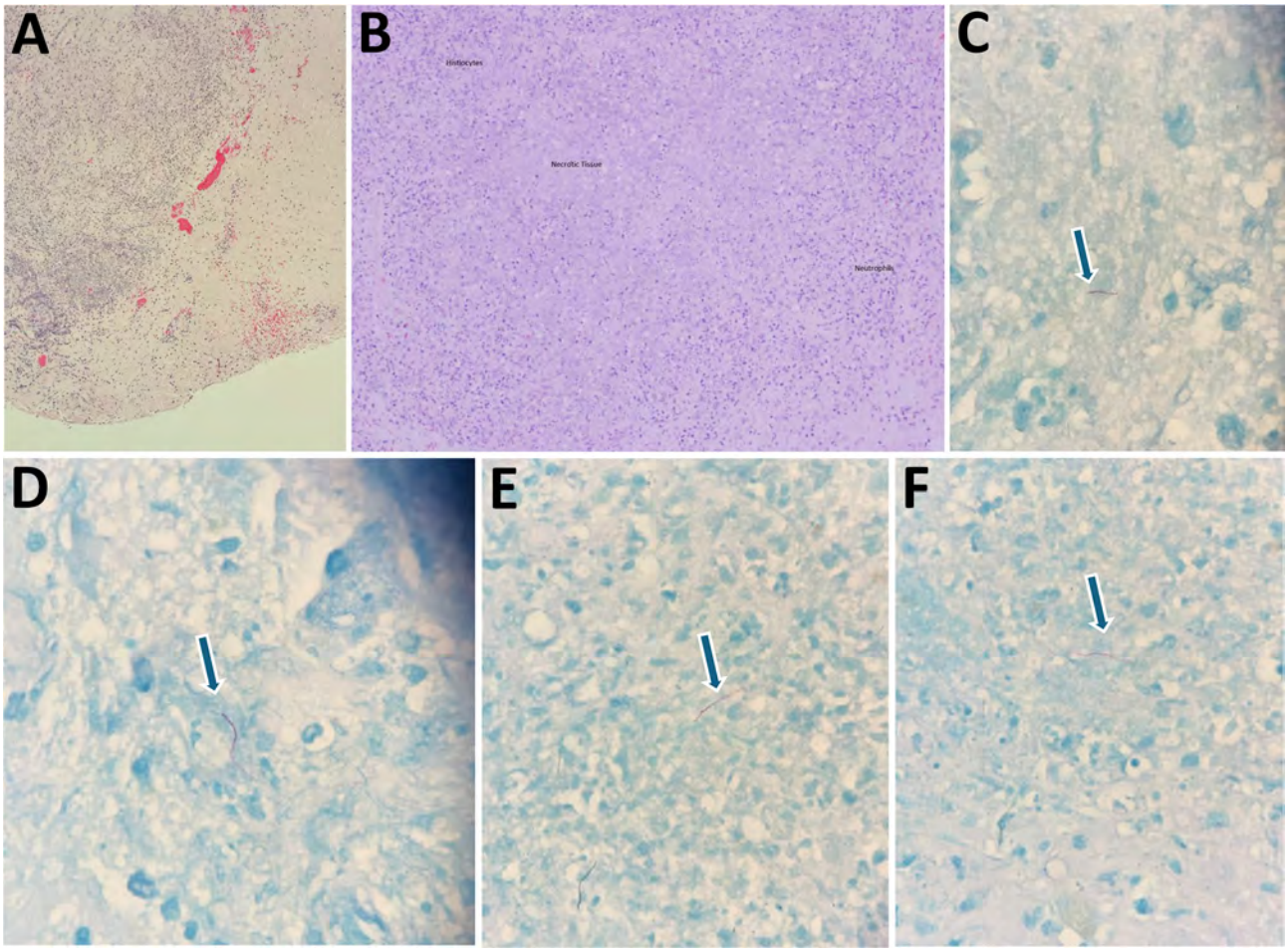

Figure 3. Brain tissue images from 79-year-old man with chronic obstructive pulmonary disease and large B-cell lymphoma who had disseminated *Nocardia ignorata* infection, United States. A, B) Parenchyma with identifiable granulation tissue, neutrophils, and histocytes and background hemorrhage and necrosis are seen. Hematoxylin and eosin stain; original magnification ×10. C–F) Thin, filamentous, partially acid-fast rods with a beaded appearance within the necrotic tissue background are visible. Branching within visualized organisms was not identified. Arrows indicate *N. ignorata* bacteria. Fite–Faraco stain; original magnification × 100.

References

1. Brown-Elliott BA, Brown JM, Conville PS, Wallace RJ Jr. Clinical and laboratory features of the *Nocardia* spp. based on current molecular taxonomy. Clin Microbiol Rev. 2006;19:259–82. https://doi.org/10.1128/CMR.19.2.259-282.2006
2. Minero MV, Marín M, Cercenado E, Rabadán PM, Bouza E, Muñoz P. Nocardiosis at the turn of the century. Medicine (Baltimore). 2009;88:250–61. https://doi.org/10.1097/MD.0b013e3181afa1c8
3. Lerner PI. Nocardiosis. Clin Infect Dis. 1996;22:891–903. https://doi.org/10.1093/clinids/22.6.891
4. Beaman BL, Beaman L. *Nocardia* species: host-parasite relationships. Clin Microbiol Rev. 1994;7:213–64. https://doi.org/10.1128/CMR.7.2.213
5. Tramèr L, Mertz KD, Huegli R, Hinic V, Jost L, Burkhalter F, et al. Intra-abdominal nocardiosis—case report and review of the literature. J Clin Med. 2020;9:2141. https://doi.org/10.3390/jcm9072141
6. Tajima K, Terada T, Okuyama S, Akaneya D, Hori R, Abe S, et al. *Nocardia otitidiscaviarum* meningitis in a diffuse large B-cell lymphoma patient with CD4-positive lymphocytopenia and persistent oligoclonal CD8-positive lymphocytes in the peripheral blood. Int J Clin Exp Pathol. 2018;11:455–61.
7. Patel H, Patel B, Jadeja S, Isache C. Central nervous system nocardiosis masquerading as metastatic brain lesions. IDCases. 2019;18:e00652. https://doi.org/10.1016/j.idcr.2019.e00652

Address for corresponding author: Mahmoud Ismail, Jacobs School of Medicine and Biomedical Sciences, University at Buffalo, 462 Grider St, Buffalo, NY 14215, USA; email: mahmoudi@buffalo.edu

Detection of Avian Influenza H5–Specific Antibodies by Chemiluminescent Assays

Ana Citlali Márquez, Saina Beitari, Tahereh Valadbeigy, Linda Hoang, Yohannes Berhane, Agatha N. Jassem

We evaluated 2 electrochemiluminescence serologic assays to detect avian influenza H5 antibodies. The assays identified H5 antibodies from both serum and dried blood spots and had strong specificity and minimal cross-reactivity in human and avian samples. Such assays can support populationwide serologic surveys aimed at assessing population-level immunity.

Since late 2021, highly pathogenic avian influenza virus (HPAIV) epizootic events in poultry have been reported worldwide, driven by HPAIV A(H5N1) clade 2.3.4.4b (*1*). Although wild birds are the natural reservoir for avian influenza viruses, H5N1 clade 2.3.4.4 has also infected wild mammals and, more recently, dairy cattle, raising concerns about viral adaptation to mammalian hosts, cross-species transmission, and increased risk for zoonotic spillover (*2*). Infections among agricultural workers have further amplified concern about possible human-to-human transmission and broader public health implications (*3*,*4*). Monitoring population-level exposure is critical for assessing susceptibility of human populations to H5N1 clade 2.3.4.4b infection and informing appropriate risk mitigation strategies.

Determination of HPAIV prevalence relies on passive surveillance from testing symptomatic persons through PCR and sequencing to detect active infections (*5*). However, HPAIV H5N1 can manifest as a mild infection and be underdetected and underreported (*6*). Serologic tools that detect virus-specific antibodies indicating prior exposures or infection can provide a more accurate estimate of infection prevalence at the population level. Serologic testing for HPAIV H5Nx subtype-specific antibodies has largely relied on hemagglutinin inhibition (HAI), neuraminidase inhibition, and microneutralization (MN) assays (*7*). HAI and MN are considered reference methods because of their high specificity and sensitivity and are often used in a complementary manner for influenza antibody characterization and quantitation. However, those assays are time-consuming and must be conducted primarily in a Biosafety Level 3 laboratory when performed with H5Nx viruses (*7*). Interpretation of such assays can be challenging, leading to undesired variability and lower sensitivity. We evaluated 2 assays from Meso Scale Discovery (MSD, https://www.mesoscale.com) for the detection of H5 antibodies to determine their feasibility and scalability for serosurveys.

The Study

The first of the 2 assays is a multiplex panel, the V-PLEX Respiratory Panel 7 (IgG) Kit, which includes antigens for SARS-CoV-2, respiratory syncytial virus, seasonal influenza, and avian influenza H5 (flu A/Ghana/39/2021 H5 clade 2.3.4.4b). The assay is designed to work only with human samples. The second assay, the Influenza H5 Bridging Serology Kit, uses a biotinylated H5 protein designed to detect H5 antibodies from multiple species, this antigen is the head fragment from the hemagglutinin of A/Ghana/AVL-763_21VIR750–39/2021 (H5N1 clade 2.3.4.4b). The second assay also includes an H1 cross-reactivity blocker to minimize nonspecific detection of H1 antibodies in human samples. We evaluated the assays only for influenza, not other respiratory pathogens.

For testing, we used residual serum samples previously submitted for clinical testing to the British Columbia Centre for Disease Control (Vancouver, BC, Canada). Positive samples (n = 6) were obtained from sequential serum samples collected

Author affiliations: British Columbia Centre for Disease Control, Vancouver, British Columbia, Canada (A.C. Márquez, S. Beitari, T. Valadbeigy, L. Hoang, A.N. Jassem); University of British Columbia, Vancouver (A.C. Márquez, L. Hoang, A.N. Jassem); Canadian Food Inspection Agency, Winnipeg, Manitoba, Canada (Y. Berhane); University of Manitoba, Winnipeg (Y. Berhane); University of Saskatchewan, Saskatoon, Saskatchewan, Canada (Y. Berhane)

DOI: https://doi.org/10.3201/eid3201.251117

12–22 days after onset from a patient infected with H5N1 clade 2.3.4.4b virus (*8*). Those serum samples were previously shown to be reactive for -H5 by HAI and MN assays at the National Microbiology Laboratory (Winnipeg, MN, Canada) (*9*). We also tested samples collected from close contacts (n = 8) of the infected patient that were determined to be negative for H5N1 by HAI and MN at the National Microbiology Laboratory. We used 23 residual antenatal serum samples submitted to the British Columbia Centre for Disease Control in 2022 for routine clinical testing as negative controls. To assess assay cross-reactivity, we tested residual samples from persons infected during the 2024–25 respiratory season with influenza A (H1, n = 15; H3, n = 6), confirmed by PCR.

In the multiplex assay (Figure, panel A), samples from the persons infected with H5N1 demonstrated the highest geometric mean concentration (GMC) to the H5 antigen (GMC = 630,877 arbitrary units [AU]/mL, 95% CI 622,836–639,021 AU/mL). Antenatal samples, H5N1 contact samples, and samples from those infected with H3 demonstrated low reactivity compared with samples from the infected patient (GMC <8,650 AU/mL). Samples from persons recently infected with influenza H1 exhibited some reactivity to the H5 antigen, suggesting cross-reactivity between H1 and H5 antibodies; however, the signal from H1-infected samples was significantly lower (GMC = 16,977 AU/mL, 95% CI = 4,412–65,320 AU/mL) than that of the confirmed H5N1 case (p<0.0001). Despite strong subtype-specific responses in H1- and H3-infected samples, the H5-infected samples demonstrated even higher signal intensity to both H1 and H3 antigens, suggesting the presence of antibodies to both H1 and H3 HA from past exposures (Appendix Figure, http://wwwnc.cdc.gov/EID/article/32/1/25-1117-App1.pdf). Cross-reactivity between H5 and H1 antibodies is expected because of the recognition of shared, conserved epitopes in the hemagglutinin stalk region. However, this cross-reactivity could only be assessed if acute and convalescent samples were available; in this case, only convalescent samples from the H5-infected patient were available (*10*).

The bridging serology assay functions on the basis of a biotinylated H5 antigen that binds to a streptavidin-coated plate, along with an H5-conjugated detection antigen. This setup forms a bridging complex in the presence of H5 antibodies, enabling their specific detection across species. We tested the same set of samples by using this assay (Figure, panel B).

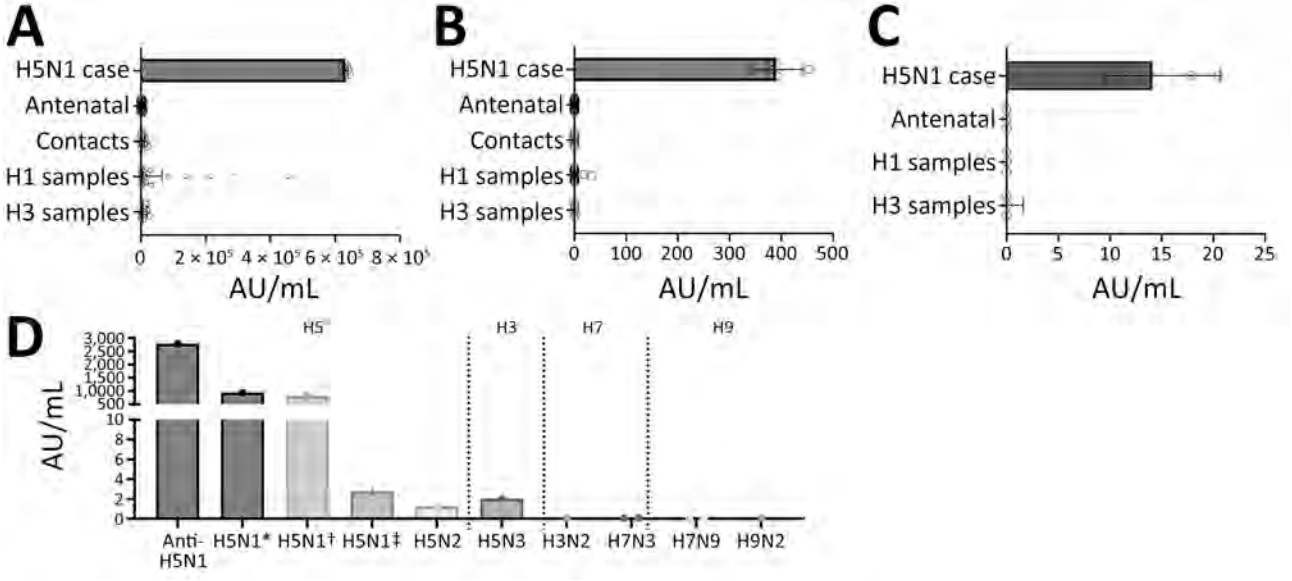

Figure. Specific detection of H5 antibodies in human and avian samples in a study on detection of avian influenza H5–specific antibodies by chemiluminescent assays. A) Results of human serum sample testing by using the MSD V-Plex Respiratory Panel 7 (IgG) kit (MSD, https://www.mesoscale.com), diluted 1:5,000 in the manufacturer-provided diluent. B) Results of human serum sample testing by using the MSD Influenza H5 Bridging Serology Assay (MSD, https://www.mesoscale.com), diluted 1:20 and prepared according to the manufacturer's instructions. C) Results of dried blood spot sample testing by using the MSD Influenza H5 Bridging Serology Assay at 1:10 dilution. D) H5 antibody polyclonal and avian sample results obtained from chickens inoculated with various influenza subtypes and tested on the MSD Influenza H5 Bridging Serology Assay according to the manufacturer's instructions. Antibody titer production was confirmed by hemagglutinin inhibition assay.*A/chicken/Vietnam/14/2005; †H5 DNA vaccinated with HA from A/mallard/BC/373/2005 (H5N2) and challenged with A/chicken/Vietnam/14/2005 (H5N1); ‡A/teal/Germany/Wv632/2005; AU, arbitrary units; MSD, Meso Scale Discovery.

Table. Viruses used to inoculate avian species for serum collection in a study on detection of avian influenza H5-specific antibodies by chemiluminescent assays*

Virus	Name	Lineage	Host	HAI titer†
Anti-H5N1	Anti-H5N1 polyclonal antibody‡	Clade 2.3.4.4b	Chicken	N/A
H5N1	A/chicken/Vietnam/14/2005	Clade 2.3.2	Chicken	256
H5N1	H5 DNA vaccinated with HA from A/mallard/BC/373/2005 (H5N2) and challenged with A/chicken/Vietnam/14/2005 (H5N1)	Vaccine: North American; challenge: Clade 2.3.2	Duck	1,024
H5N1	A/teal/Germany/Wv632/2005	Eurasian LPAI	Chicken	256
H5N2	A/turkey/Minn/3689-1551-1981	North American	Chicken	128
H3N2	A/DK/ON/05/2000	Triple reassortant North American	Chicken	128
H5N3	A/TY/CA/35621/1984	North American	Chicken	128
H7N3	A/chicken/BC/CN-7/2004	North American	Chicken	256
H7N9	A/Anhui/001/2013	East Asian	Chicken	128
H9N2	A/Ty/Mn/12877/1285/1981	North American	Chicken	128

*HA, hemagglutinin; HAI, hemagglutinin inhibition.
†Experimental serum generated at the National Centre for Foreign Animal Disease, Canadian Food Inspection Agency, where HAI testing was also performed.
‡Creative Diagnostics, https://www.creative-diagnostics.com.

Unlike the multiplex assay, background reactivity observed in H1-infected samples was largely eliminated (GMC = 0.18 AU/mL, 95% CI = 0.0066–4.88 AU/mL), and the assay specifically detected antibodies only in the samples from the H5N1-infected persons (GMC = 390.5 AU/mL, 95%CI = 344.5–442.7 AU/mL).

To assess the suitability of the assay across different sample types, we prepared contrived dried blood spot (DBS) samples by mixing packed red blood cells with either serum from antenatal testing or H5N1 cases. DBS samples from the H5N1 cases had detectable H5 antibodies, although the signal was lower than that observed in serum samples (GMC = 14.12 AU/mL, 95% CI = 9.627–20.7 AU/mL). We detected no cross-reactive background in the rest of the sample groups (Figure, panel C).

To evaluate the cross-species applicability of the assay, we tested a commercially available chicken H5 polyclonal antibody (Creative Diagnostics, https://www.creative-diagnostics.com) along with serum samples from chickens that were experimentally infected with low pathogenicity or inactivated highly pathogenic H5 influenza viruses, vaccinated with an H5N1 DNA vaccine, and subsequently challenged with inactivated H5N1 or exposed to other HA subtypes (Table). H5 antibodies were detectable in samples from animals infected with H5 viruses; the highest levels were observed in a vaccinated animal with H5 DNA vaccine and challenged with H5N1 (A/chicken/Vietnam/14/2005) and in a chicken infected with H5N1 (A/chicken/Vietnam/14/2005) (Figure, panel D). We observed no cross-reactivity in serum from animals infected with non-H5 subtypes.

Conclusions

Our results show that the V-PLEX Respiratory Panel 7 (IgG) and the H5 Bridging Serology serologic assays can specifically detect H5 antibodies in humans. In the V-PLEX panel, serum samples from H1 infected patients showed varied levels of cross-reactivity to the H5 antigen, whereas samples from H3 infected patients did not show cross-reactivity to the H5 antigen. The serology bridging assay shows a marked reduction in cross-reactivity with closely related hemagglutinin subtypes, such as H1 in humans. This assay is compatible with DBS and can detect antibodies from avian species.

This study is limited by the small number of H5N1-positive human samples available for testing and the absence of manufacturer-defined reactivity cutoffs. Additional samples from confirmed H5-infected patients with mild or moderate symptoms would enable determination of thresholds to distinguish between positive and negative results. For avian samples, the main limitation is that serum was obtained from experimentally inoculated animals; thus, the assay's performance in wild birds, or in other species, remains to be evaluated.

Although HAI and MN assays remain the reference methods for influenza subtyping, the assays we describe provide a versatile and scalable alternative. The assays have strong potential as screening tools for detecting anti-H5 in both humans and animals and for use in serologic surveys or contact tracing.

Acknowledgments

We would like to thank the British Columbia Centre for Disease Control Public Health Laboratory for supporting this work, in particular, Meghan McLennan, Branco Cheung, and Inaru Enriquez. We thank Meso Scale Discovery for generously providing the Influenza H5 Bridging Serology Kit for evaluation in this study.

About the Author

Dr. Márquez is a senior scientist at the British Columbia Centre for Disease Control Public Health Laboratory and a clinical assistant professor in the Department of Pathology and Laboratory Medicine at the University of British Columbia in Vancouver, Canada. Her research interests include seroepidemiology, immune correlates of protection, and the evaluation and implementation of serological assays to support infectious disease surveillance.

References

1. Webby RJ, Uyeki TM. An update on highly pathogenic avian influenza A(H5N1) virus, clade 2.3.4.4b. J Infect Dis. 2024;230:533–42.
2. Peacock TP, Moncla L, Dudas G, VanInsberghe D, Sukhova K, Lloyd-Smith JO, et al. The global H5N1 influenza panzootic in mammals. Nature. 2025;637:304–13.
3. Uyeki TM, Milton S, Abdul Hamid C, Reinoso Webb C, Presley SM, Shetty V, et al. Highly pathogenic avian influenza A(H5N1) virus infection in a dairy farm worker. N Engl J Med. 2024;390:2028–9.
4. Caserta LC, Frye EA, Butt SL, Laverack M, Nooruzzaman M, Covaleda LM, et al. Spillover of highly pathogenic avian influenza H5N1 virus to dairy cattle. Nature. 2024;634:669–76.
5. Government of Canada. Protocol for enhanced human surveillance of avian influenza A(H5N1) on farms in Canada. [cited 2025 Jun 25]. https://www.canada.ca/en/public-health/services/diseases/avian-influenza-h5n1/health-professionals/protocol-enhanced-human-surveillance-avian-influenza-farms-canada.html
6. Capelastegui F, Goldhill DH. H5N1 2.3.4.4b: a review of mammalian adaptations and risk of pandemic emergence. J Gen Virol. 2025;106:002109.
7. World Health Organization Global Influenza Surveillance Network. Manual for the laboratory diagnosis and virological surveillance of influenza [cited 2024 Jul 6]. https://www.who.int/influenza/gisrs_laboratory/manual_diagnosis_surveillance_influenza/en
8. Jassem AN, Roberts A, Tyson J, Zlosnik JEA, Russell SL, Caleta JM, et al. Critical illness in an adolescent with influenza A(H5N1) virus infection. N Engl J Med. 2025;392:927–9.
9. MacBain E, Znait A, Edwards L, Jassem A, Barakauskas VE, Harris KC, et al. Management of critical illness in an adolescent caused by highly pathogenic avian influenza A(H5N1) virus infection in British Columbia, Canada. Lancet Infect Dis. Epub 2026 Jan 20. https://doi.org/10.1016/S1473-3099(25)00773-X
10. Carreño JM, Strohmeier S, Kirkpatrick Roubidoux E, Hai R, Palese P, Krammer F. H1 hemagglutinin priming provides long-lasting heterosubtypic immunity against H5N1 challenge in the mouse model. mBio. 2020; 11:e02090–20.

Address for correspondence: Agatha N. Jassem, British Columbia Centre for Disease Control, 655 West 12th Ave, Vancouver, BC V5Z 4R4, Canada; email: agatha.jassem@bccdc.ca

etymologia revisited

Influenza

[in″floo-en′zə]

An acute viral infection of the respiratory tract. From Latin influentia, "to flow into"; in medieval times, intangible fluid given off by stars was believed to affect humans. The Italian influenza referred to any disease outbreak thought to be influenced by stars. In 1743, what Italians called an influenza di catarro ("epidemic of catarrh") spread across Europe, and the disease came to be known in English as simply "influenza."

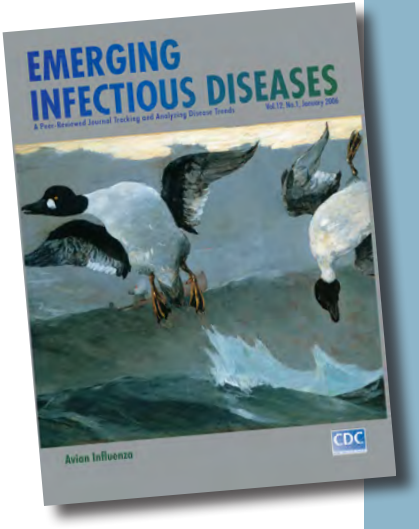

Originally published in January 2006

Reference

Dorland's illustrated medical dictionary. 30th ed. Philadelphia: Saunders; 2003 and Quinion M. World wide words. 1998 Jan 3 [cited 2005 Dec 5]. Available from http://www.worldwidewords.org/topicalwords/tw-inf1.htm

https://wwwnc.cdc.gov/eid/article/12/1/et-1201_article

Evidence of Rat Hepatitis E Virus Circulation through Wastewater Surveillance, Central Argentina

Bianca Filoni,[1] María Emilia Lucero,[1] Guadalupe Di Cola, Anabella Fantilli, Alfonsina Roccia, Paola Sicilia, Liliana Luque, Ariana Cachi, María de los Ángeles Marinzalda, Gonzalo Castro, Gisela Masachessi, Viviana Ré, María Belén Pisano

During 2023–2024, we detected rat hepatitis E virus in 67.7% of wastewater samples from central Argentina. This high level of detection opens new inquiries in the region, highlighting the need to investigate the virus in both animal reservoirs and humans, with a focus on hepatitis cases of unknown etiology.

Rat hepatitis E virus (R-HEV) (family Hepeviridae, species *Rocahepevirus ratti*) is an emerging cause of viral hepatitis in humans that belongs to the Hepeviridae family, the same family as hepatitis E virus (HEV) (species *Paslahepevirus balayani*), a major cause of hepatitis in humans (*1*). Rats are the primary reservoirs of R-HEV, and the virus has been detected in several countries, mainly in Europe, and in different species of rodents (*2*). Since the first reported human infection in a transplant patient in 2018 in Hong Kong, China, reports of human cases in immunosuppressed and immunocompetent patients from Asia, Europe, and North America have been increasing (*3*–*5*). Those cases highlight the zoonotic potential of R-HEV, positioning this agent as a growing concern for public health (*6*).

R-HEV and HEV are transmitted by the fecal–oral route. The virus is shed in the stool of infected humans and animals and subsequently discharged into wastewater. R-HEV can be studied under the One Health approach, enabling us to consider the interactions between environment, hosts, and the virus (*7*). Wastewater surveillance has proven to be effective in detecting the emergence of both well-known and little-studied enteric viruses in different regions and in tracking their spread and circulation within various communities (*1*,*8*). In South America, we found only 1 recent report of R-HEV detection from naturally growing mangrove bivalve mollusks collected for local sale in a touristic area of Brazil and demonstrating a low detection rate (2.2%) (*9*). Because of the scarce evidence of R-HEV circulation in South America, we aimed to assess the presence of R-HEV in wastewater from Córdoba, a central province of Argentina, as an indicator of viral circulation in the region.

The Study

During January 2023–December 2024, we collected sewage samples weekly (total n = 99: 2023, n = 49; 2024, n = 50) from the Bajo Grande wastewater treatment plant (BG-WWTP) of Córdoba city, the capital of the province of Córdoba, with 1,505,250 inhabitants (Figure 1, panel A). BG-WWTP receives the waste of ≈56.9% of the city's population (https://censo.gob.ar/index.php/mapa_desague_red_publica2). We concentrated each 500-mL sample 100 times by using the polyethylene glycol-6000 precipitation method, as described previously (*8*), and conducted RNA extraction by using the Nucleic Acid Extraction Versatile Spin Kit (Anatolia Geneworks, https://www.anatoliageneworks.com). We conducted molecular detection of the virus by using a real-time reverse transcription PCR (RT-PCR) targeting a 69-bp fragment of the open reading frame 1 genomic region, as described previously (*10*). We used the TaqMan Fast Virus 1-Step

Author affiliations: Instituto de Virología Dr. J.M. Vanella, Universidad Nacional de Córdoba, Córdoba, Argentina (B. Filoni, M.E. Lucero, G. Di Cola, A. Fantilli, A. Roccia, L. Luque, A. Cachi, M. de los Ángeles Marinzalda, G. Castro, G. Masachessi, V. Ré, M.B. Pisano); Consejo Nacional de Investigaciones Científicas y Técnicas, Buenos Aires, Argentina (G. Di Cola, G. Masachessi, V. Ré, M.B. Pisano); Ministerio de Salud de la Provincia de Córdoba, Córdoba (P. Sicilia, L. Luque, G. Castro); Instituto Nacional de Medicina Aeronáutica y Espacial, Facultad de la Fuerza Aérea, Facultad de la Fuerza Aérea, Universidad de la Defensa Nacional, Córdoba (A. Cachi, M. de los Ángeles Marinzalda).

DOI: https://doi.org/10.3201/eid3201.251218

[1]These authors contributed equally to this article.

master mix (Thermo Fisher Scientific, https://www.thermofisher.com), performed in a StepOne Real-Time PCR (Thermo Fisher Scientific). For positive controls we used synthetic oligonucleotide (Appendix, http://wwwnc.cdc.gov/EID/article/32/1/26-1218-App1.pdf), and for negative controls we used sterile water. We considered samples RNA R-HEV positive if we observed an S-shaped curve in the specific detection channel of each specimen and obtained a cycle threshold value ≤40 for viral specific target, as previously described (*1*,*8*). With the aim of genetic characterization of positive samples, we conducted heminested RT-PCR amplification of a 338-bp fragment within the open reading frame 1 genomic region of the Hepeviridae family (*11*). We purified PCR products by using the PureLink Quick Gel Extraction Kit (Invitrogen, https://www.invitrogen.com) and sequenced in both directions by using an Applied Biosystem 3500XL Genetic Analyzer (Thermo Fisher Scientific). We conducted phylogenetic analyses by using MEGA version11 (*12*), IQ-Tree (http://iqtree.cibiv.univie.ac.at), and FigTree (https://tree.bio.ed.ac.uk/software/figtree). In addition, we used a newly developed genotyping tool for R-HEV classification (*13*) and constructed an identity matrix to determine the similarity between the sequences obtained by using BioEdit software version 7.7.1 (https://bioedit.software.informer.com/Descargar-gratis).

Of the 99 samples analyzed, 67.7% (95% CI 58.5%–76.9%; n = 67) tested positive for R-HEV detection by RT-PCR (Appendix Table 1). By year, 77.6%; (95% CI 63.0%–87.8%; n = 38) of samples from 2023 were positive, and 58.0% (95% CI 43.3%–71.5%; n = 29) of samples from 2024 were positive (Figure 1, panel B). Of the 67 positive samples by real-time RT-PCR, 14 were positive by the heminested RT-PCR, and 10 were sequenced. The phylogenetic tree confirmed the virus species identity as *Rocahepevirus ratti* (GenBank accession nos. PX060496–504, PX060508) and showed grouping with sequences from sewage samples from Italy and rodents from Canada, within genotype C1 (Figure 2). The genotyping tool indicated that 9 sequences from this study belonged to the proposed clade I, subtype a. One sequence yielded an indeterminate result (Appendix Table 2). The similarity between the obtained sequences varied from 0.71 to 0.98 (Appendix Table 3).

Conclusions

This study revealed R-HEV circulation in Argentina, confirming the presence of emerging R-HEV in South America. R-HEV detection in wastewater samples

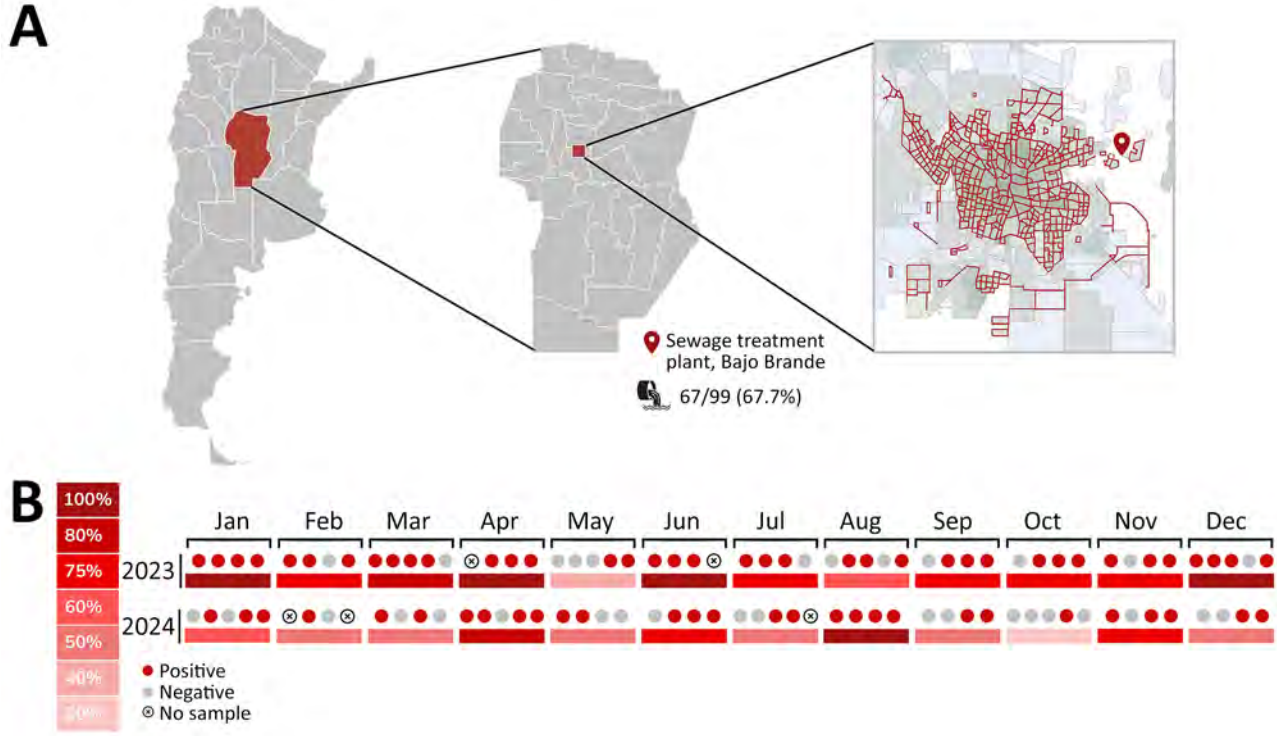

Figure 1. Emerging rat hepatitis E virus detection in Argentina, 2023–2024. A) Study area in the province of Córdoba (red shading), located in the central region of Argentina, and the location of Bajo Grande wastewater treatment plant in the city of Córdoba. Red lines indicate the sewage network, which covers 56.9% of the city's population. B) Frequency of detection of rat hepatitis E virus during 2023–2024, per month. The circles indicate detections per week sampled within each month.

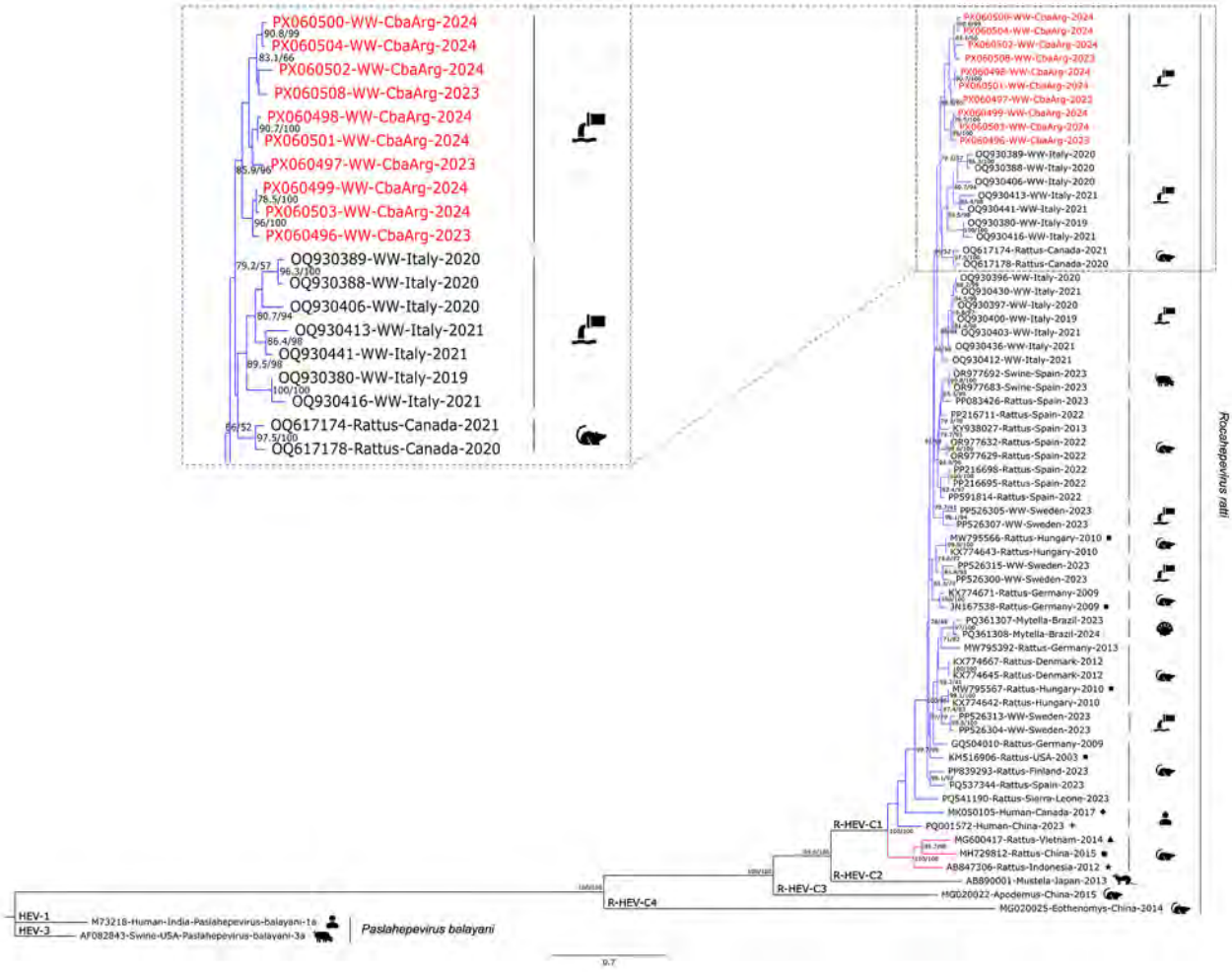

Figure 2. Maximum-likelihood phylogenetic tree on the basis of a 338 bp fragment of the open reading frame 1 genomic region of rat hepatitis E virus (R-HEV; *Rocahepevirus ratti*) from Argentina, 2023–2024. Red text indicates sequences obtained during this study. The tree includes representative sequences of each R-HEV genotype available in GenBank database, additional sequences of proposed clades (clade I in blue, clade II in pink) and subtypes a (square), b (circle), c (5-pointed star), d (4-pointed star), e (rhombus), and f (triangle) (*13*). Two hepatitis E virus (*Paslahepevirus balayani*) sequences (genotypes 1 and 3) were used as outgroups. Enlarged area shows sequences from this study and the first 10 most similar sequences from BLAST analysis (https://blast.ncbi.nlm.nih.gov). Statistical support values are indicated at nodes; only supports over 70/70 are shown. Scale bar represents the number of substitutions per site.

shows a high level of circulation (high detection rate) in the human environment from the central region of the country. The low number of sequenced samples could be explained by the dilution and degradation of viral RNA within the wastewater matrix, driven by factors such as pH fluctuations, temperature variation, and complex biochemical interactions. Those conditions might promote the formation of short, partially degraded RNA fragments that remain detectable by real-time RT-PCR but are insufficient for amplifying longer genomic regions required for conventional PCR and sequencing. Similar patterns were reported in previous wastewater studies (*8*). Contamination of wastewater by human waste is a possible source of the virus, although the involvement of rodents, the natural viral host, in sewers is the most likely scenario (*14*). To date, we have not found evidence of human or animal infections in Argentina; therefore, our results open new and unexplored fields for R-HEV research in South America. Studies from the past 2 years have demonstrated the presence of R-HEV RNA in wastewater from countries in Europe, underscoring the value of wastewater-based surveillance for detecting emerging viruses such as R-HEV (*1*,*8*). Concomitantly, studies were conducted to clarify the clinical implications of R-HEV in Europe. Those studies revealed that R-HEV could cause symptomatic disease in humans, both in immunosuppressed and immunocompetent patients, producing mild illness, severe hepatitis, and potentially death (*4*).

Phylogenetic analysis revealed that the sequences obtained in our study clustered together, although they were not identical (similarity 0.71–0.98). That clustering could suggest that the same strains circulated over the 2-year period. The sequences grouped close to strains previously detected in sewers in Italy and in rodents from Canada within genotype C1 (*1*,*15*). However, because of the limited available data—very few sequences of this virus are currently deposited in GenBank, and 3 are from South America—and because of the relatively short genomic fragment analyzed, definitive conclusions cannot be drawn. Recently published studies suggest our sequences would be assigned to clade I, subtype a (*13*).

In line with the One Health approach, our findings reinforce the need to further investigate R-HEV circulation in Argentina and South America. This effort should integrate environmental surveillance with clinical research, such as testing samples from symptomatic patients for R-HEV RNA and exploring potential viral reservoirs such as rats. In addition to rodents, attention should be given to other possible hosts, such as pigs, in which R-HEV infections have been documented (*6*).

Acknowledgments

We thank the staff of the Bajo Grande wastewater treatment plant for their collaboration in collecting water samples.

This study was supported by grants of the Secretary of Science and Technology of the National University of Córdoba (Secyt-UNC) and the Ministry of Science, Technology and Innovation of Argentina (Cofecyt, PFI-2022).

About the Author

Ms. Filoni is a doctoral student at the National University of Córdoba, Argentina, and recipient of the Secretary of Science and Technology doctoral scholarship. Her research interests include genomics and molecular biology of zoonotic emerging viruses.

References

1. Palombieri A, Di Profio F, Sarchese V, Fruci P, Suffredini E, Martella V, et al. Surveillance for rat hepatitis E in wastewater networks, Italy. Microbiol Spectr. 2023; 11:e0267523. https://doi.org/10.1128/spectrum.02675-23
2. Porea D, Raileanu C, Crivei LA, Gotu V, Savuta G, Pavio N. First detection of hepatitis E virus (*Rocahepevirus ratti* genotype C1) in synanthropic Norway rats (*Rattus norvegicus*) in Romania. Viruses. 2023;15:1337. https://doi.org/10.3390/v15061337
3. Rivero-Juarez A, Frias M, Perez AB, Pineda JA, Reina G, Fuentes-Lopez A, et al.; HEPAVIR and GEHEP-014 Study Groups. Orthohepevirus C infection as an emerging cause of acute hepatitis in Spain: first report in Europe. J Hepatol. 2022;77:326–31. https://doi.org/10.1016/j.jhep.2022.01.028
4. Caballero-Gómez J, Casares-Jiménez M, Gallo-Marín M, Pereira-Pardo S, Beato-Benítez A, Poyato A, et al.; GEHEP-014 Study Group. Rat hepatitis E virus as an etiological agent of acute hepatitis of unknown origin. J Hepatol. 2025;83:662–9. https://doi.org/10.1016/j.jhep.2025.02.027
5. Yadav KK, Boley PA, Lee CM, Khatiwada S, Jung K, Laocharoensuk T, et al. Rat hepatitis E virus cross-species infection and transmission in pigs. PNAS Nexus. 2024; 3:pgae259. https://doi.org/10.1093/pnasnexus/pgae259
6. Rios-Muñoz L, Gonzálvez M, Caballero-Gomez J, Castro-Scholten S, Casares-Jimenez M, Agulló-Ros I, et al. Detection of rat hepatitis E virus in pigs, Spain, 2023. Emerg Infect Dis. 2024;30:823–6. https://doi.org/10.3201/eid3004.231629
7. Velavan TP, Pallerla SR, Johne R, Todt D, Steinmann E, Schemmerer M, et al. Hepatitis E: an update on One Health and clinical medicine. Liver Int. 2021;41:1462–73. https://doi.org/10.1111/liv.14912
8. Fantilli AC, Masachessi G, Cola GD, Castro G, Sicilia P, Marinzalda MLA, et al. Integrated hepatitis E virus monitoring in central Argentina: a six-year analysis of clinical surveillance and wastewater-based epidemiology. Water Res. 2024; 261:122004. https://doi.org/10.1016/j.watres.2024.122004
9. Figueiredo AS, Negreiros IR, do Nascimento E Silva A, Salgado CRS, Dos Santos NL, Pinto MA, et al. Detection of *Rocahepevirus ratti* in bivalve mollusks from São Luís Island, Maranhão, Brazil: a potential transmission route of an emerging zoonotic pathogen? Food Environ Virol. 2025;17:11. https://doi.org/10.1007/s12560-024-09624-0
10. Sridhar S, Yip CCY, Wu S, Cai J, Zhang AJX, Leung KH, et al. Rat hepatitis E virus as cause of persistent hepatitis after liver transplant. Emerg Infect Dis. 2018;24:2241–50. https://doi.org/10.3201/eid2412.180937
11. Drexler JF, Seelen A, Corman VM, Fumie Tateno A, Cottontail V, Melim Zerbinati R, et al. Bats worldwide carry hepatitis E virus-related viruses that form a putative novel genus within the family *Hepeviridae*. J Virol. 2012;86:9134–47. https://doi.org/10.1128/JVI.00800-12
12. Tamura K, Stecher G, Kumar S. MEGA11: molecular evolutionary genetics analysis version 11. Mol Biol Evol. 2021;38:3022–7. https://doi.org/10.1093/molbev/msab120
13. Lo KH, Ho SS, Shun EH, Wu S, Yip CC, Situ J, et al. Enhanced surveillance, subtyping, and host adaptation analysis reveal genotype-wide zoonotic potential of rat hepatitis E virus. J Hepatol. 2026;84:51–61. https://doi.org/10.1016/j.jhep.2025.07.004
14. Rouba A, Ansmant T, Chaqroun A, Challant J, Josse T, Schvoerer E, et al. First detection of hepatitis E virus (*Rocahepevirus ratti*) in French urban wastewater: potential implications for human contamination. Sci Total Environ. 2024;954:176805. https://doi.org/10.1016/j.scitotenv.2024.176805
15. Robinson SJ, Borlang J, Himsworth CG, Pearl DL, Weese JS, Dibernardo A, et al. Rat hepatitis E virus in Norway rats, Ontario, Canada, 2018–2021. Emerg Infect Dis. 2023;29:1890–4. https://doi.org/10.3201/eid2909.230517

Address for correspondence: Bianca Filoni, Instituto de Virología Dr. J. M. Vanella, Facultad de Ciencias Médicas, Universidad Nacional de Córdoba, Enfermera Gordillo Gómez s/n, Ciudad Universitaria, Córdoba CP: 5016, Argentina; email: bianca.filoni@mi.unc.edu.ar

Presence or Emergence of Canine Leishmaniasis, Malawi

Boniface Chikufenji, Kyoko Hayashida, Yasuyuki Goto, Tatsuki Sugi, Chizu Sanjoba, Chrispin Njala, Inga McDermott, Frederic Lohr, Dagmar Mayer, Shohei Ogata, Masahiro Kajihara, Naganori Nao, Ryo Nakao, Laston Chimaliro, Donales Kapira, Janelisa Musaya, Junya Yamagishi, Elisha Chatanga

Canine leishmaniasis has long been thought to be absent in Malawi. However, our cross-sectional study in indigenous dogs showed a high prevalence of *Leishmania* infection in some areas, where seropositivity rates reached up to 7.0%. These findings suggest that this neglected zoonotic disease may already be endemic in Malawi.

Leishmaniasis is a neglected tropical diseases that is transmitted by female phlebotomine sandflies and affects ≥1 million persons annually (*1*). The disease manifests in 3 clinical forms, cutaneous, mucocutaneous, and visceral. Of those, human visceral leishmaniasis represents the most severe manifestation and is the second-leading cause of parasitic disease–related deaths in humans after malaria, causing ≥30,000 deaths annually (*1*). Infection with *Leishmania infantum* in humans causes severe systemic disease, with a higher risk for progression in infants and HIV-infected patients (*1*).

Dogs are the primary reservoirs of *L. infantum*, making them critical targets for surveillance and control to reduce the risk for zoonotic leishmaniasis. Although canine leishmaniasis, which is caused by *L. infantum*, has been widely reported in subtropical and tropical regions, including Asia, North Africa, Southern Europe, and the Americas (*2*), recent data from sub-Saharan Africa remain scarce. Human cutaneous leishmaniasis, which is caused by an unidentified *Leishmania* species, was reported in Malawi in 1993 (*3*), and 1 seropositive dog was reported in 2016 (*4*), but to our knowledge, no data regarding *Leishmania* infections in humans or animals have been reported since.

In Zambia, a neighboring country of Malawi, canine leishmaniasis was first reported in 1994 (*5*). Subsequently, no further cases were reported for nearly 30 years, until a 2021 study identified autochthonous infection cases of canine leishmaniasis in 3 dogs (*6*). Furthermore, a recent study conducted in 2022 revealed a high seroprevalence of *Leishmania* antibodies in dogs from 2 urban cities in Zambia (*7*). The reported high seroprevalence of *Leishmania* infection in Zambian dogs (≈17%) prompted us to investigate the presence of *Leishmania* infection in dogs in Malawi.

The Study

During 2023–2024, we collected 557 canine blood samples through convenience sampling during mass rabies vaccination campaigns, including 157 samples from Mchinji District, 100 from Nkhotakota District, and 300 from Zomba District (Table, Appendix 1 Figure 1, https://wwwnc.cdc.gov/EID/article/32/1/25-0855-App1.pdf). The areas of sampling were semiurban or rural, and all dogs were nonpedigreed, local, or mixed breeds based on visual observations. Most of the dogs were semi–free-ranging and lived outdoors. We took records and photographs for dogs showing alopecia, emaciation, or other abnormalities (Figure 1; Appendix 2, https://wwwnc.cdc.gov/EID/article/32/1/25-0855-App2.xlsx). We obtained blood from each dog into an EDTA tube and stored the samples in a DNA/RNA shield (Zymo Research, https://www.zymoresearch.com). We also obtained plasma from the remaining blood. The study protocol was approved by the Department

Author affiliations: Ministry of Agriculture, Lilongwe, Malawi (B. Chikufenji); Hokkaido University, Sapporo, Japan (B. Chikufenji, K. Hayashida, T. Sugi, S. Ogata, M. Kajihara, N. Nao, R. Nakao, L. Chimaliro, J. Yamagishi); University of Zambia, Lusaka, Zambia (K. Hayashida, S. Ogata, M. Kajihara); University of Tokyo, Tokyo, Japan (Y. Goto, C. Sanjoba); Mission Rabies Malawi, Blantyre, Malawi (C. Njala, I. McDermott, F. Lohr, D. Mayer); Malawi–Liverpool Wellcome Programme, Blantyre (D. Kapira, J. Musaya); Lilongwe University of Agriculture and Natural Resources, Lilongwe (E. Chatanga)

DOI: https://doi.org/10.3201/eid3201.250855

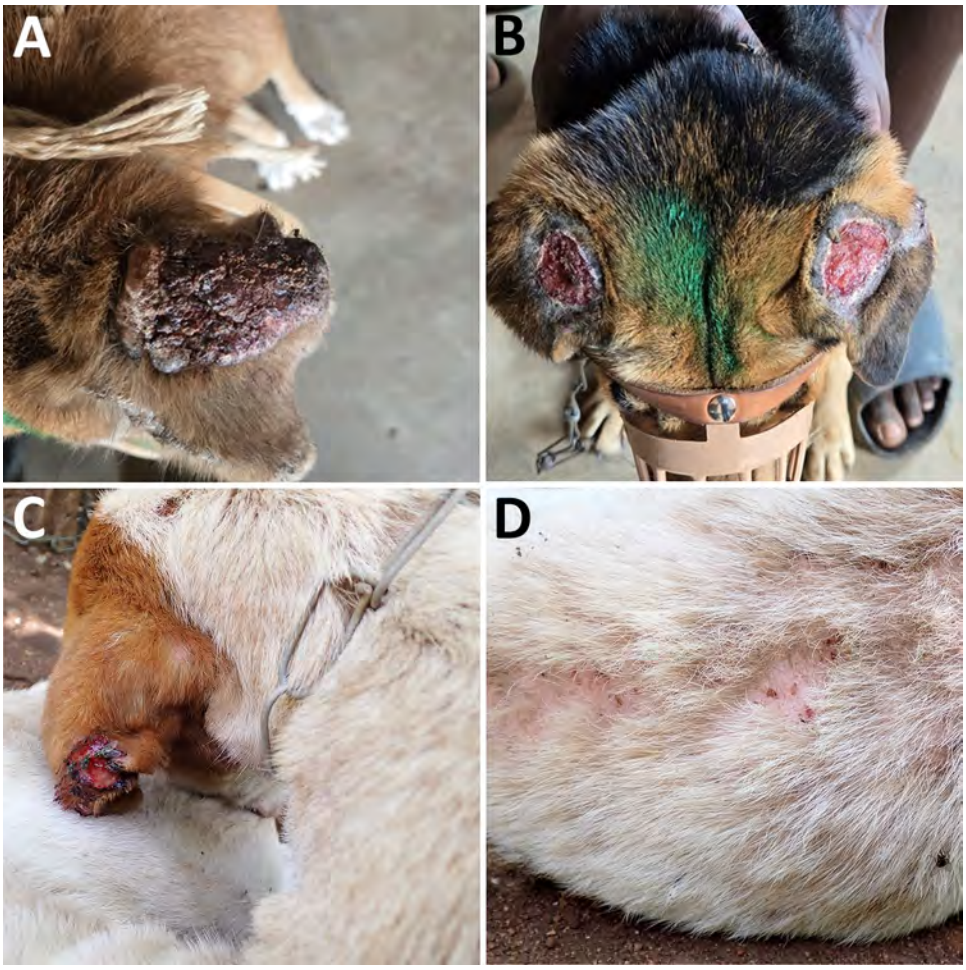

Figure 1. Clinical manifestations of *Leishmania infantum*–infected dogs in Mchinji, Nkhotakota, and Zomba districts in a study of canine leishmaniasis, Malawi. A) Severely crusted, thickened dark surface pinna (24MWD_C073). B) Bilateral ulcerative lesions on the ears with an exposed tissue (24MWD_C110). C, D) Unilateral ulcerative lesions on the ears and alopecia with severe thinning of the fur (24MWD_C040).

of Animal Health and Livestock Development in Malawi (approval no. DAHLD/AHC/07/2024/01).

We extracted DNA by using NucleoSpin DNA Blood Extraction Kit (Macherey-Nagel, https://www.mn-net.com) and amplified it by using conventional PCR targeting the small subunit RNA region (*8*) and internal transcribed spacer 2 region (*9*). We also tested DNA by using real-time PCR targeting kinetoplast DNA (*10*). The PCR detection targeting the small subunit region showed an overall detection rate of 7.9% (44/557) (Table). Similarly, PCR targeting the internal transcribed spacer 2 region identified an overall detection rate of 6.3% (35/557) (Table). Real-time PCR analysis demonstrated a detection rate of 4.7% (26/557) (Table). In total, 8.1% (45/557) of the samples showed ≥1 positive results in 3 PCR tests (Table). We sequenced positive samples from conventional PCR and confirmed that they were identical to the *L. infantum* reference genome (JPCM5 strain, GenBank accession no. GCF_000002875) (Appendix 2). In addition, we amplified the entire internal transcribed spacer region sequences (*11*) from the representative sequences in each district and compared them with global *L. infantum* sequences. As a result, all sequences from Malawi and most *L. infantum* sequence strains clustered together, corresponding to *L. infantum* zymodeme MON-1 (Appendix 1 Figure 2), the predominant zymodeme found worldwide in both humans and dogs, suggesting a shared ancestry of the parasite.

We also conducted ELISA for detecting IgG (*12*) by using *L. donovani* soluble lysate antigen from cultured promastigotes (LdSLA) and recombinant rK39r4 antigens. We used serum from clinically confirmed canine leishmaniasis dog (*6*) as a positive control, and we used healthy endemic dog control serum samples from 18 healthy confined breeding dogs in Malawi to determine the optimal cutoff value (mean ±5 SD). As a result, we observed a 3.0% (16/538) seropositivity for each antigen and an overall seroprevalence of 4.1% (22/538) (Table; Figure 2). The results of PCR and ELISA were not entirely concordant, and we found a large number of PCR-positive dogs to be seronegative (Figure 2). However, dogs exhibit-

Table. PCR and ELISA results for detecting *Leishmania* spp. in indigenous dogs from the Mchinji, Nkhotakota, and Zomba districts in a study of canine leishmaniasis, Malawi*

District	qPCR-positive†	SSU–cPCR-positive	ITS2–cPCR-positive	LdSLA-seropositive	rK39r4-seropositive	PCR-positive‡	Serologic test–positive§	Both PCR and serologic test–positive
Mchinji	12/157 (7.6)	17/157 (10.8)	13/157 (8.3)	0/140 (0)	1/140 (0.7)	17/157 (10.8)	1/140 (0.7)	0/140 (0)
Nkhotakota	5/100 (5.0)	5/100 (5.0)	5/100 (5.0)	0/98 (0)	0/98 (0)	5/100 (5.0)	0/98 (0)	0/98 (0)
Zomba	9/300 (3.0)	22/300 (7.3)	17/300 (5.7)	16/300 (5.3)	15/300 (5.0)	23/300 (7.7)	21/300 (7.0)	10/300 (3.3)
Total	26/557 (4.7)	44/557 (7.9)	35/557 (6.3)	16/538 (3.0)	16/538 (3.0)	45/557 (8.4)	22/538 (4.1)	10/538 (1.9)

*All values are no. (%). cPCR, conventional PCR; ITS2, internal transcribed spacer 2; LdSLA, *Leishmania donovani* soluble lysate antigen from cultured promastigotes; qPCR, real-time PCR; rK39r4, recombinant rK39r4 antigen; SSU, small subunit.
†Defined as cycle threshold value <35.
‡Defined as the count of the sample that showed positives in any of the 3 tests: qPCR, SSU-cPCR, or ITS2-cPCR.
§Defined as the count of the sample that showed positives in LdSLA, rK39r4 antigen, or both.

ing double seropositivity (i.e., positive on PCR and ELISA) for LdSLA and rK39r4 antigens were significantly more likely to be PCR-positive (odds ratio 57.1, 95% CI 13.7–387.4). In addition, dogs showing severe clinical signs were mostly positive by both PCR and ELISA (Figure 1, Figure 2).

After observing high seropositivity in Zomba District, we followed up on some of the seropositive dogs. We performed the original sample collection in September 2024 and revisited the area in March 2025. We found that 1 dog (24MWD_C040) was seriously ill (Figure 1), and we performed fine-needle biopsy on the enlarged superficial cervical lymph node. We cultured the collected fluid at room temperature in Novy-MacNeal-Nicolle medium overlaid with M199 media (*13*). Eleven days after inoculation, we observed a motile promastigote stage of the parasite and confirmed the internal transcribed spacer sequence to be *L. infantum*, further confirming the presence of the parasite (Figure 3; Appendix 1 Figure 2).

Conclusions

This study confirmed the presence and high endemicity of *L. infantum* in indigenous dogs in Malawi. Our study found that both symptomatic and asymptomatic dogs tested positive for *L. infantum* DNA. In addition, we successfully isolated the promastigote stage of the parasite from 1 dog, which showed severe clinical manifestations, was positive in all PCRs, and had high ELISA optical density values for LdSLA and rK39r4. This finding suggests that double positivity by PCR and ELISA is an indicator of disease progression, whereas PCR or ELISA single-positive dogs might still be asymptomatic carriers. As such, the strategic use of LdSLA and rK39r4 antigens in ELISA and PCR for

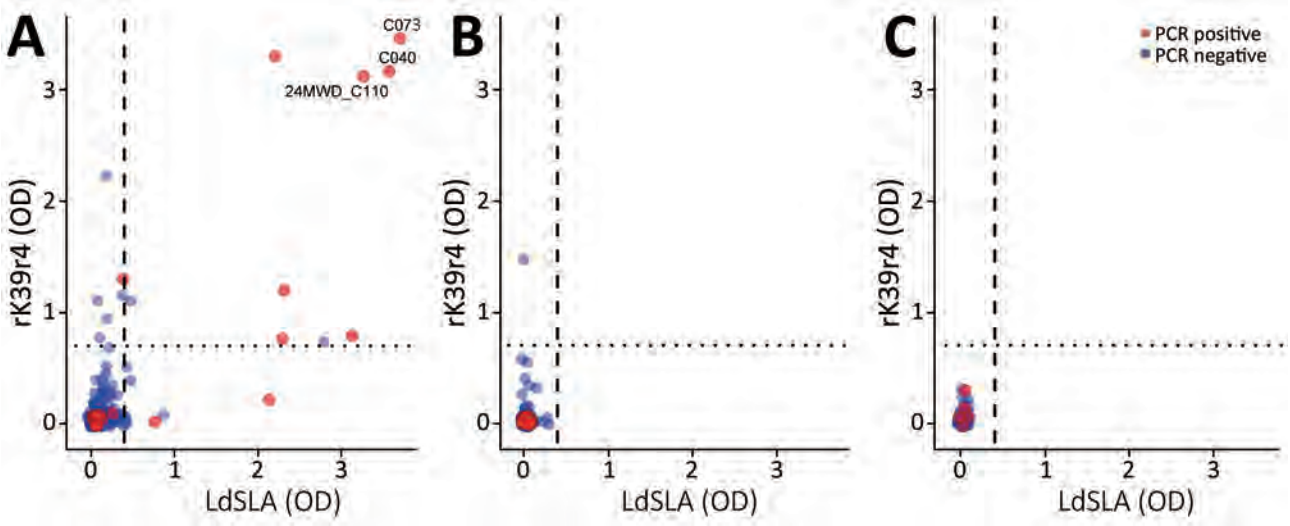

Figure 2. Scatterplots showing ELISA OD values for LdSLA and rK39r4 in indigenous dogs from Mchinji, Nkhotakota, and Zomba districts in a study of canine leishmaniasis, Malawi (Zomba, 300 samples; Mchinji, 140 samples; and Nkhotakota, 98 samples). Red indicates PCR-positive samples. Identification numbers of the dogs that exhibited clear clinical manifestations are also shown, corresponding to numbers in Figure 1. Plots were generated by using R studio software version 4.4.1 (https://rstudio.com/products/rstudio). Cutoff OD values (0.4 for LdSLA, vertical dashed line; 0.7 for rK39r4, horizontal dotted line) were determined as mean of the healthy endemic control dogs plus 5 SDs. LdSLA, *Leishmania donovani* soluble lysate antigen from cultured promastigotes; OD, optical density; rK39r4, recombinant rK39r4 antigen.

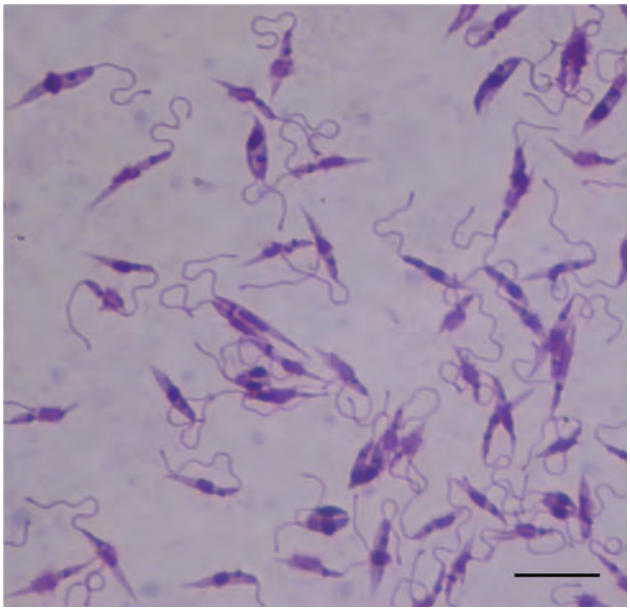

Figure 3. Promastigote stage of *Leishmania infantum* isolated from dog in Zomba District (24MWD_C040) cultured in Novy-MacNeal-Nicolle medium in a study of canine leishmaniasis, Malawi. The elongated, flagellated forms characteristic of extracellular stage observed under light microscopy. Giemsa stain. Oil immersion. Scale bar indicates 10 μm.

L. infantum testing will enhance diagnostic performance by increasing the tests' ability to correctly identify infected dogs.

Zomba District showed the highest disease prevalence in ELISA positives and PCR–ELISA double positives. Compared with the districts of Nkhotakota and Mchinji, Zomba can be characterized as urban, where higher dog-to-human population densities are observed. Because of the lack of information about vector sandfly distribution in Malawi, speculating on the possible risk factors explaining this prevalence difference by the region is difficult. Nevertheless, a higher prevalence in densely populated areas also has been reported in Zambia and Brazil (*7*,*14*). Canine leishmaniasis has been documented as a precursor to human outbreaks in other regions (*15*).

In summary, we report a high prevalence of *L. infantum* in dogs from 3 districts in Malawi, as detected by molecular methods and serologic assays. A live parasite also was confirmed and isolated from the lymph node biopsy fluid of 1 dog. Our findings indicate the possible emergence or reemergence of the disease in the country, highlighting the urgent need for broader disease surveillance of the disease in humans, dogs, and the sandfly vector. Our results underscore the role of dogs as reservoirs of *L. infantum* in Malawi, posing a zoonotic risk, and highlight the need for urgent public health interventions to prevent its spread.

Acknowledgments

We are grateful to Lemani Levi, Nathan Kamanga, Wanangwa Mhonjo, Dziko Muzungu, Praise Chilanga, Kumbukani Zinyawo, Mphatso Chibwana, William Mwamtoma, and all the staff at the Veterinary Office and Mission Rabies Malawi for supporting sampling during this study.

This research was supported by the Japan Agency for Medical Research and Development (grant nos. JP20wm0125008, 25wm0225052h0001, JP23wm0225034, and JP223fa627005) and the Japan Society for the Promotion of Science (grant nos. JPJSCCB20250010 and JPJSBP120259906).

About the Author

Dr. Chikufenji is a state veterinarian in Malawi and a PhD student at the Graduate School of Infectious Diseases, Hokkaido University. His research interests are dog-associated zoonotic diseases and tickborne pathogens.

References

1. World Health Organization. Leishmaniasis. 2023 Jan 12 [cited 2024 Oct 22]. https://www.who.int/news-room/fact-sheets/detail/leishmaniasis
2. Dantas-Torres F. Canine leishmaniasis in the Americas: etiology, distribution, and clinical and zoonotic importance. Parasit Vectors. 2024;17:198. https://doi.org/10.1186/s13071-024-06282-w
3. Pharoah PDP, Ponnighaus JM, Chavula D, Lucas SB. Two cases of cutaneous leishmaniasis in Malawi. Trans R Soc Trop Med Hyg. 1993;87:668–70. https://doi.org/10.1016/0035-9203(93)90282-U
4. Alvåsen K, Johansson SM, Höglund J, Ssuna R, Emanuelson U. A field survey on parasites and antibodies against selected pathogens in owned dogs in Lilongwe, Malawi. J S Afr Vet Assoc. 2016;87:e1–6. https://doi.org/10.4102/jsava.v87i1.1358
5. Matsukawa K, Chiti L, Yoshima M, Sayer PD. Canine visceral leishmaniosis: first case in Zambia. Onderstepoort J Vet Res. 1997;64:77–9.
6. Squarre D, Chambaro HM, Hayashida K, Moonga LC, Qiu Y, Goto Y, et al. Autochthonous *Leishmania infantum* in dogs, Zambia, 2021. Emerg Infect Dis. 2022;28:888–90. https://doi.org/10.3201/eid2804.212378
7. Chambaro HM, Hayashida K, Moonga LC, Shawa M, Muleya W, Chizimu J, et al. A high prevalence of dogs seropositive to *Leishmania* in Zambia. Parasitol Int. 2025;108:103081. https://doi.org/10.1016/j.parint.2025.103081
8. Meredith SE, Zijlstra EE, Schoone GJ, Kroon CC, van Eys GJ, Schaeffer KU, et al. Development and application of the polymerase chain reaction for the detection and identification of *Leishmania* parasites in clinical material. Arch Inst Pasteur Tunis. 1993;70:419–31.
9. Nateghi Rostami M, Darzi F, Farahmand M, Aghaei M, Parvizi P. Performance of a universal PCR assay to identify different *Leishmania* species causative of Old World cutaneous leishmaniasis. Parasit Vectors. 2020;13:431. https://doi.org/10.1186/s13071-020-04261-5

10. Lachaud L, Marchergui-Hammami S, Chabbert E, Dereure J, Dedet JP, Bastien P. Comparison of six PCR methods using peripheral blood for detection of canine visceral leishmaniasis. J Clin Microbiol. 2002;40:210–5. https://doi.org/10.1128/JCM.40.1.210-215.2002
11. Kuhls K, Mauricio IL, Pratlong F, Presber W, Schönian G. Analysis of ribosomal DNA internal transcribed spacer sequences of the *Leishmania donovani* complex. Microbes Infect. 2005;7:1224–34. https://doi.org/10.1016/j.micinf.2005.04.009
12. Goto Y, Carter D, Guderian J, Inoue N, Kawazu S, Reed SG. Upregulated expression of B-cell antigen family tandem repeat proteins by *Leishmania* amastigotes. Infect Immun. 2010;78:2138–45. https://doi.org/10.1128/IAI.01102-09
13. Zhang WW, Karmakar S, Gannavaram S, Dey R, Lypaczewski P, Ismail N, et al. A second generation l eishmanization vaccine with a markerless attenuated *Leishmania major* strain using CRISPR gene editing. Nat Commun. 2020;11:3461. https://doi.org/10.1038/s41467-020-17154-z
14. de Oliveira FVA, Garcia MSA, Rosa LB, Giorgio S, Miguel DC. An overview of *Leishmania* in vitro cultivation and implications for antileishmanial screenings against promastigotes. Parasitologia. 2024;4:305–18. https://doi.org/10.3390/parasitologia4040027
15. Morales-Yuste M, Martín-Sánchez J, Corpas-Lopez V. Canine leishmaniasis: update on epidemiology, diagnosis, treatment, and prevention. Vet Sci. 2022;9:387. https://doi.org/10.3390/vetsci9080387

Address for correspondence: Kyoko Hayashida, Division of Collaboration and Education, International Institute for Zoonosis Control, Hokkaido University, Kita-20, Nishi-10, Sapporo, Hokkaido, 001-0020, Japan; email: kyouko-h@czc.hokudai.ac.jp

Tularemia in New York, USA, 1993–2023

Dylan T. Gaber,[1] Melissa A. Prusinski,[1] Ashley Hodge, Alexis White, Michael P. Santoriello, Christopher L. Romano, Scott R. Campbell, Zahra LaTerra, Melissa D'Amico, Michael Perry, Jennifer L. White

During 1993–2023, health officials in New York, USA, received reports of 30 tularemia cases. Of those, 43% were from Suffolk County, 69% were diagnosed during 2014–2023, and 1 person died. Tick surveillance detected *Francisella tularensis* in 1 pool of nymphs from Suffolk County, indicating localized risk.

Francisella tularensis is a highly infectious, gram-negative bacterium that causes tularemia and may be transmitted through several pathways, including bites from infected ticks (primarily *Amblyomma americanum* and *Dermacentor variabilis* in the northeastern United States), deer flies (*Chrysops* species), contact with infected animals, ingestion of contaminated food or water, and inhalation of infectious aerosols (*1*). Clinical manifestations vary by route of exposure and consist of 6 primary forms, glandular, oculoglandular, oropharyngeal, pneumonic, typhoidal, and ulceroglandular; ulceroglandular is most common in the United States (*2*). Although treatable with antimicrobial drugs (*1*,*3*), case-fatality rates can reach 24% depending on clinical form and infecting subspecies (*4*,*5*).

The literature shows reports of tularemia from every US state except Hawaii; most historical cases have occurred in the south-central and Pacific Northwest regions (*6*). Incidence peaked in 1939, with 2,291 cases, and case rates remain highest during May–September, coinciding with periods of increased tick activity (*1*). Nationally, reported cases increased by 56% during 2011–2022 compared with 2001–2010, partly reflecting improved diagnostics (*7*). Incidence among American Indian and Alaska Native populations remains ≈5 times higher than among White persons, highlighting ongoing demographic disparities (*7*).

The state of New York, USA, recorded the first documented case of tularemia in 1927 and linked the transmission to rabbit consumption (*8*). Although tularemia remains rare, averaging <1 case/year in the state (*9*), recent reports show an increase in tularemia cases, particularly from Long Island, where Suffolk County sees >1 case/year (*9*). In response, the New York State Department of Health (NYSDOH) and the Suffolk County Department of Health Services initiated enhanced *F. tularensis* surveillance in ticks and conducted a retrospective analysis of human cases to better define tularemia epidemiology in this region.

The Study

We analyzed tularemia cases during 1993–2023 retrospectively for all New York counties, excluding New York City. As mandated by New York public health law, clinicians electronically reported provider-diagnosed tularemia cases and positive laboratory test results for *F. tularensis* to the NYSDOH (*10*,*11*), prompting their investigation by local health departments, who entered clinical and demographic information into the NYSDOH Communicable Disease Electronic Surveillance System (*11*). We classified reports based on the tularemia national surveillance case definition at the time of diagnosis (*7*). We included confirmed or probable cases in our study. We mapped cases in ArcGIS Pro 3.2 (Esri, https://www.esri.com) by county of residence, mapping Suffolk County cases also by residence postal (ZIP) code.

We analyzed data relevant to demographic and epidemiologic characteristics of tularemia cases (Table), revealing that cases were predominately among White men, with an average age of 40.7 years. Our case-fatality rate of 6.7% among cases with a known outcome (n = 15) was higher than the ≈2% previously

Author affiliations: New York State Department of Health, Albany, New York, USA (D.T. Gaber, M.A. Prusinski, A. Hodge, Z. LaTerra, M. D'Amico, M. Perry, J.L. White); Arthropod-Borne Disease Laboratory, Suffolk County Department of Health Services, Yaphank, New York, USA (A. White, M.P. Santoriello, C.L. Romano, S.R. Campbell)

DOI: http://doi.org/10.3201/eid3201.250854

[1]These first authors contributed equally to this article.

reported (*5*), although outcome was recorded in only 50% of our cases. We obtained sufficient clinical data to enable determination of disease form in 15 cases (50%): 10 case-patients had ulceroglandular/glandular tularemia, 3 had pneumonic tularemia, 1 had cellulitis, and 1 died as a result of sepsis and renal failure that developed in the setting of underlying chronic conditions. Half of cases (n = 15) were from counties on Long Island. Of those, 13 occurred in Suffolk County, representing 43% of the total reported cases during the study period, with 69% of all Suffolk County cases reported recently (2014–2023) (Figure). Reported cases of tularemia have emerged sporadically from across New York since 1993 at a rate of <1 case/year on average, but 50% of cases were reported during the last decade of the study: 67% from Long Island and 33% from elsewhere in the state (Figure).

We carried out standardized drag sampling of host-seeking *A. americanum* and *D. variabilis* ticks as previously described (*12*) during 2019–2023 at 21 surveillance sites across Suffolk County with suitable habitat for ticks and their vertebrate hosts or locations tied epidemiologically to tularemia cases. We collected a total of 27,158 ticks and pooled them by species, developmental stage, site, and collection date (up to 20 nymphs or 10 adult female or male ticks each) for nucleic acid extraction as previously described (*12*). We collected an additional 517 *D. variabilis* ticks from 57 locations in 18 other New York counties during the same timeframe. We screened the resulting 3,220 pools for *F. tularensis* using an in-house–validated real-time PCR targeting the Tul4 gene, capable of detecting multiple subspecies (*13*) (Appendix, https://wwwnc.cdc.gov/EID/article/32/1/25-0854-App1.pdf). We calculated measures of tick population density (ticks per 1,000 m^2 sampled) and minimum infection rate at the site level (*12*). We overlayed average tick density values on a map of Suffolk County tularemia cases using ArcGIS Pro.

Of 17,921 *A. americanum* nymphs collected, 1 pool tested positive for *F. tularensis*. Those ticks were collected on July 23, 2020, from Southampton Township, which had an *F. tularensis* minimum infection rate of 0.42% and the highest overall tick population density, averaging 266.8 ticks/1,000 m^2 sampled (Figure). Tularemia cases tended to be reported in residents of higher tick density regions of Suffolk County (Figure).

Conclusions

This study underscores the importance of ongoing human disease and vector surveillance, particularly in Suffolk County, where nearly half of New York tularemia case-patients resided during 1993–2023 and where we observed a recent increase in reported cases beginning in 2014. The demographics of New York tularemia cases resembled those observed nationally. Case-patients were predominantly White men, although the median age in New York (38.5 years) was lower than reported nationally (48 years) (*7*). The case-fatality rate of 6.7% in our study was higher than the ≈2% previously reported (*5*), but interpretation is limited because outcome was recorded in only 50% of the cases we report (n = 15). We did not observe increased incidence in American Indian or Alaskan Indigenous populations in New York; however, our data did not include race and ethnicity in nearly 27% of cases. Increased effort to improve the accuracy and completeness of communicable disease surveillance reporting data obtained from medical providers and patients during public health case investigations would enable better elucidation of epidemiologic risk factors associated with tularemia in New York.

Despite extensive sampling over 4 years, the prevalence of *F. tularensis* in ticks was low, highlighting the potential importance of other infection routes. The detection of *F. tularensis* in *A. americanum* nymphs from Southampton and the variability in tick densities across Suffolk County locations point to localized ecologic factors influencing tick distribution

Table. Demographic and epidemiological characteristics of confirmed and probable tularemia cases, New York, 1993–2023*

Demographics	No. (%) patients
Age, y	
0–9	3 (10)
10–19	2 (6.67)
20–29	4 (13.33)
30–39	6 (20)
40–49	3 (10)
50–59	4 (13.33)
60–69	5 (16.67)
70–79	3 (10)
≥80	0 (0)
Sex	
M	19 (63.33)
F	11 (36.67)
Race/ethnicity	
White	18 (60)
Black	2 (6.67)
Hispanic or Latino	2 (6.67)
Unknown	8 (26.67)
Outcome	
Alive	14 (46.67)
Dead	1 (3.33)
Unknown	15 (50)
Case status	
Confirmed	19 (63.33)
Probable	11 (36.67)

*Data represent cases reported to the New York State Department of Health; percentages calculated based on cases with available information. Mean age for case patients 40.7 (SD 21.97) years; median age 38.5 (range 2–78) years.

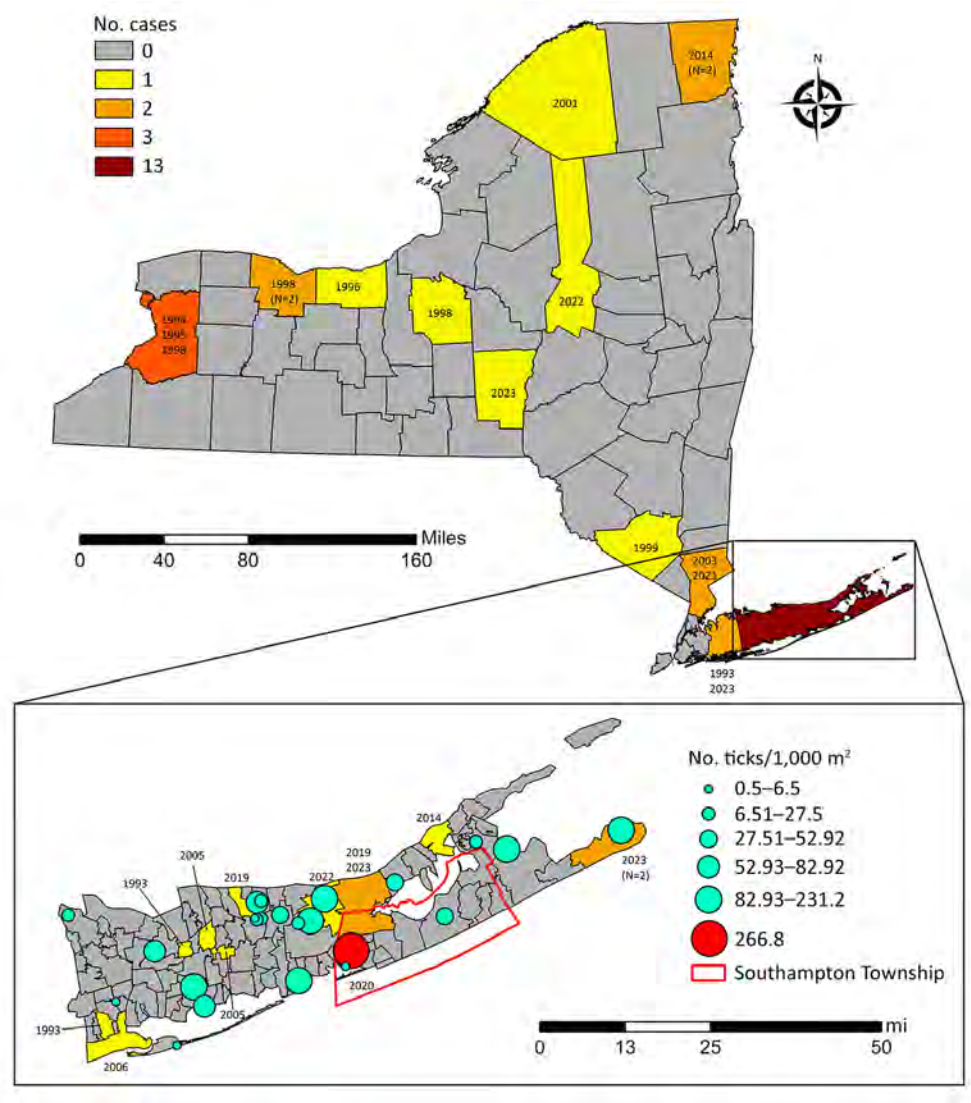

Figure. Human tularemia cases mapped by county of residence, New York, USA, 1993–2023. Year of case diagnosis shown. Inset displays tularemia cases by postal (ZIP) code tabulation area of residence, Suffolk County, New York, 1993–2023, overlaid with cumulative host-seeking tick density (2019–2023). Tick density expressed as ticks per 1,000 m^2 sampled (nymphs and adults combined), cumulative over the surveillance period. Red marker indicates location of the *Francisella tularensis*–positive tick pool.

and subsequent tick bite exposure risk. Tularemia cases tended to be reported in residents of higher tick density regions of Suffolk County, but averaging tick density values across sampling years and tick developmental stages limits temporal interpretability. Rising temperatures and changing precipitation patterns may lengthen the seasonal window of vector activity and alter host population dynamics and enzootic transmission cycles, ultimately affecting human exposure risk (*14*). This possibility is particularly relevant to coastal New York, where environmental changes could increase seasonal exposure risk (*15*), reinforcing the need for continued tick surveillance and targeted public health interventions.

Given tularemia's broad geographic distribution in the United States, prevention efforts should focus on increasing public and provider awareness, ensuring timely diagnosis, and promoting effective prevention strategies. Continued human and vector surveillance remains critical for early detection and risk assessment. However, the timeliness and completeness of epidemiologic data associated with human tularemia cases is paramount to gaining a better understanding of disease etiology.

Acknowledgements

The authors thank the following individuals: P. Egan, S. Yang, E. Daniel, J. Dwyer, J. Goldstein, S. Kutchava, T. Zembsch, L. Rose, A. Dupuis, J. Maffei, L. Tomaszek, C. Koetzner, J. Stout, A. Ciota, M. Meola, A. Chiefari, and C. Egan for their assistance with tick collections, tick identification, specimen accessioning, sample preparation, and pathogen testing. We also thank A. Kaufman for human case data compilation and exploratory analysis.

Funding was provided by the NYSDOH, the Wadsworth Center, and Association of Public Health Laboratories Internship Subaward Program to the NYSDOH Wadsworth Center from US Centers for Disease Control and Prevention (Cooperative Agreement #NU60OE000104).

About the Author

Mr. Gaber is a health science student at Boston University's Sargent College of Health and Rehabilitation Sciences and an intern with the Association of Public Health Laboratories at the Wadsworth Center, New York State Department of Health. His research interests focus on the epidemiology of tickborne pathogens, with a particular emphasis on the pathophysiology and etiology of human infections. Ms. Prusinski is a research scientist, laboratory supervisor, and Deputy Director of Vector Surveillance with the Vector Ecology Laboratory, Bureau of Communicable Disease Control, New York State Department of Health. Her research focuses on the ecology and epidemiology of tickborne and other arthropodborne diseases.

References

1. Francis E. Sources of infection and seasonal incidence of tularemia in man. Public Health Rep. 1937;52:103–13. https://doi.org/10.2307/4582067
2. Centers for Disease Control and Prevention. Tularemia: digns and symptoms of tularemia. May 17, 2024 [cited 2025 Oct 2]. https://www.cdc.gov/tularemia/signs-symptoms/index.html
3. Nelson CA, Winberg J, Bostic TD, Davis KM, Fleck-Derderian S. Systematic review: clinical features, antimicrobial treatment, and outcomes of human tularemia, 1993–2023. Clin Infect Dis. 2024;78(Suppl 1):S15–28. https://doi.org/10.1093/cid/ciad736
4. US Centers for Disease Control and Prevention (CDC). Tularemia—United States, 2001–2010. MMWR Morb Mortal Wkly Rep. 2013;62:963–6.
5. Kugeler KJ, Mead PS, Janusz AM, Staples JE, Kubota KA, Chalcraft LG, et al. Molecular epidemiology of *Francisella tularensis* in the United States. Clin Infect Dis. 2009;48:863–70. https://doi.org/10.1086/597261
6. Centers for Disease Control and Prevention. Tularemia data and statistics. May 20, 2024 [cited 2024 Sep 18]. https://www.cdc.gov/tularemia/data-research/index.html
7. Rich SN, Hinckley AF, Earley A, Petersen JM, Mead PS, Kugeler KJ. Tularemia—United States, 2011–2022. MMWR Morb Mortal Wkly Rep. 2025;73:1152–6. https://doi.org/10.15585/mmwr.mm735152a1
8. Gilbert R, Coleman MB. Incidence of tularemia in New York State. Am J Public Health Nations Health. 1932;22:1249–52. https://doi.org/10.2105/AJPH.22.12.1249
9. New York State Department of Health. Communicable disease in New York State—reported cases by disease and county: 1993–2023 [cited 2024 Sep 19]. https://www.health.ny.gov/statistics/diseases/communicable
10. New York State. Public Health Law Section 2102: communicable diseases; laboratory reports and records [cited 2024 Sep 19]. https://newyork.public.law/laws/n.y._public_health_law_section_2102r
11. New York State. 10 NYCRR 2.10: reporting cases or suspected cases or outbreaks of communicable disease by physicians. July 6, 2011 [cited 2024 Sep 19]. https://regs.health.ny.gov/content/section-210-reporting-cases-or-suspectedcases-or-outbreaks-communicable-disease-physicians
12. Dupuis AP II, Prusinski MA, O'Connor C, Maffei JG, Ngo KA, Koetzner CA, et al. Heartland virus transmission, Suffolk County, New York, USA. Emerg Infect Dis. 2021;27:3128–32. https://doi.org/10.3201/eid2712.211426
13. Forestal CA, Gil H, Monfett M, Noah CE, Platz GJ, Thanassi DG, et al. A conserved and immunodominant lipoprotein of *Francisella tularensis* is proinflammatory but not essential for virulence. Microb Pathog. 2008;44:512–23. https://doi.org/10.1016/j.micpath.2008.01.003
14. Rydén P, Sjöstedt A, Johansson A. Effects of climate change on tularaemia disease activity in Sweden. Glob Health Action. 2009;2:2063. https://doi.org/10.3402/gha.v2i0.2063
15. New York State Department of Environmental Conservation. Climate change effects and impacts in New York State [cited 2024 Sep 18]. https://dec.ny.gov/environmental-protection/climate-change/effects-impacts

Address for correspondence: Melissa Prusinski, Bureau of Communicable Disease Control–Vector Ecology Lab, New York State Department of Health, Wadsworth Center Biggs Laboratories C-456A, Empire State Plaza, Albany, NY 12237, USA; email: melissa.prusinski@health.ny.gov

Mycobacterium decipiens Infection in Patient Receiving Anti–TNF-α Therapy, France, 2024

Justin Charles-Antoine Destoop, Corentin Poignon, William Danjou, Alexandre Bleibtreu, Valerie Pourcher, Gentiane Monsel

Author affiliations: Pitié-Salpêtrière University Hospital, Paris, France (J.C.-A. Destoop, W. Danjou, A. Bleibtreu, V. Pourcher, G. Monsel); Dermatological Infectiology and Sexually Transmitted Infections Group of the French Society of Dermatology, Paris (J.C.-A. Destoop, G. Monsel); Sorbonne Université, Paris (C. Poignon); French National Institute of Health and Medical Research, Paris (C. Poignon, A. Bleibtreu, V. Pourcher)

DOI: http://doi.org/10.3201/eid3201.250518

Mycobacterium decipiens is a newly identified species with high genomic similarity to *M. tuberculosis*. We report a cutaneous *M. decipiens* infection in a patient in France who had inflammatory bowel disease being treated with anti–tumor necrosis factor-α therapy. The infection was successfully treated with an oral antimicrobial regimen.

Mycobacterium decipiens is a recently identified nontuberculous mycobacterium genetically closest to the *M. tuberculosis* complex but of low virulence. Since its description in 2018, the medical literature documents 2 human infections (*1*,*2*). We report a cutaneous case of *M. decipiens* in a 60-year-old man living in an area between Paris and Corsica, France.

The patient sought treatment for skin lesions on his anterior right knee evolving over 9 months. His medical history included irritable bowel disease treated with the anti–tumor necrosis factor-α monoclonal antibody adalimumab (80 mg subcutaneously on the abdomen every 2 wks) for 9 years. Two months after a 2-week trip to French Guiana, where he hiked in forests and swam in rivers and pools, he noticed an erythematous papule that progressively worsened. He reported no history of trauma, sick contacts, or animal exposure and no adalimumab injections during the trip. He did report multiple mosquito bites. The man's occupation involved building renovation and, on returning from French Guiana, he emptied stagnant swimming pool water in Corsica.

Clinical examination revealed an erythematous, exudative, budding lesion over the patella, with multiple satellite nodules (Figure, panel A). Ipsilateral inguinal lymphadenopathy was nontender and subcentimetric. The patient reported no fever or weight loss. Magnetic resonance imaging of the right knee revealed superficial prepatellar bursitis and tendinopathy of the patellar and pes anserinus tendons. Blood counts and protein electrophoresis were unremarkable; C-reactive protein was moderately elevated at 25.6 mg/L (normal <5 mg/L). HIV serology result was negative.

Histopathologic examination of a surgical biopsy showed epithelioid and giant cell granulomas without necrosis, along with superficial and deep lymphocytic inflammation around capillaries. Direct mycobacteriologic examination with auramine and Ziehl–Neelsen staining revealed 1–9 acid-fast bacilli per microscopic field. *M. tuberculosis* PCR (MDR/MTB ELITe MGB kit on ELITe InGenius platform; ELITechGroup; https://www.elitechgroup.com), targeting IS6110 and *rpoB*, produced negative results. Cultures produced dry, chamois-colored colonies on both liquid (mycobacteria growth indicator tube, modified 7H9) and solid (Coletsos) media. We observed growth after 24 days in the liquid medium and after 27 days on Coletsos medium at 30°C and 37°C; colonies were larger at 30°C. Commercial-line probe assays (GenoType CM and AS; Bruker; https://www.bruker.com) covering the most common and pathogenic nontuberculous mycobacterium as well as the *M. tuberculosis* complex failed to identify the isolate (*3*).

Sequencing of the 16S rRNA and *hsp65* genes showed 100% identity with *M. decipiens* (ATCC TSD-117; GenBank OY970459.1; TBL 1200985, Genbank

Figure. Cutaneous infection on the right knee before and after treatment from study of *Mycobacterium decipiens* infection in a patient treated with anti–tumor necrosis factor-α therapy, France, 2024. A) Before treatment: erythematous, exudative, budding lesion over the patella with multiple satellite nodules. B) After treatment: residual pigmented macular lesions, sometimes depressed, consistent with postinflammatory changes.

Table. Susceptibility of clinical isolates studied in prior reports and in our investigation of *Mycobacterium decipiens* infection in patient treated with anti–tumor necrosis factor-α therapy, France, 2024*

Antimicrobial drug	MIC of clinical isolates, μg/mL		
	Case 1 (*1*)	Case 2 (*2*)	Case 3 (this study)
Amikacin	≤1, S	4, S	1, S
Ciprofloxacin	4, R	1, S	4, R
Clarithromycin	4, S	0.25, S	8, S
Doxycycline	0.5, S	2, I	2, I
Ethambutol	4, I	8, R	4, I
Linezolid	≤1, S	≤1, S	1, S
Moxifloxacin	0.5, S	≤0.12, S	0.25, S
Rifabutin	≤0.25, S	≤0.25, S	<0.25, S
Rifampin	2, R	2, R	4, R
Trimethoprim/sulfamethoxazole	0.25/4.75, S	0.5/9.5, S	0.5/9.5, S

*The S/I/R breakpoints have been defined by analogy with the Clinical and Laboratory Standards Institute breakpoints for slowly growing mycobacteria other than *M. avium* and *M. kansasii* (*5*). I, intermediate; R, resistant; S, susceptible.

NR_178632.1 for 16S and GenBank KJ371035.1 for hsp65). The closest non–M. decipiens matches were M. tuberculosis strains LP-0106963-RM2 (GenBank CP194255.1) and RM1 (GenBank CP194256.1), which showed 99.4% identity for 16S, and *M. szulgai* (GenBank KC481265.1, 96.2%) and *M. intracellulare* subspecies. *yongonense* (GenBank OR672012.1, 95.7%) for *hsp65*. Whole-genome sequencing confirmed the identification; analysis with KRAKEN2 using a dedicated mycobacterial reference database identified the isolate as *M. decipiens*, with 92.8% of reads assigned (*4*). We deposited raw reads in the National Center for Biotechnology Information under BioProject PRJNA1308041 (accession no. SRR35034371).

We determined MICs for antimicrobial drugs potentially active against slow-growing mycobacteria using the SLOMYCO Sensititer system (Thermo Fisher Scientific; https://www.thermofisher.com) with Mueller–Hinton medium incubated at 30°C. MICs were readable after 10 days of incubation, and interpretation followed Clinical and Laboratory Standards Institute guidelines (*5*) for slowly growing mycobacteria other than *M. avium* and *M. kansasii*. The strain was susceptible to clarithromycin, rifabutin, moxifloxacin, amikacin, linezolid, and trimethoprim/sulfamethoxazole but resistant to rifampin.

The patient received empirical treatment with clarithromycin, ethambutol, and rifampin, resulting in poor response after 1 month. Once *M. decipiens* was identified, we replaced rifampin with moxifloxacin, leading to rapid clinical improvement within 4 weeks. We reduced adalimumab to 40 mg every 2 weeks. The patient continued on combination therapy for 2 additional months after complete remission. Reduction of adalimumab triggered an irritable bowel disease flare requiring corticosteroids and mesalazine enemas. Six months after discontinuation of antimicrobial drugs, only postinflammatory scarring remained (Figure, panel B).

M. decipiens is a slow-growing species, with optimal growth at 32°C–35°C. Colonies are rough, nonpigmented, and chamois-colored, resembling *M. tuberculosis*. Researchers have noted misidentification by rapid *M. tuberculosis* identification assays, complicating microbiologic diagnosis (*6*).

The reservoir of *M. decipiens* remains unknown. Reported cases of *M. decipiens* infection involved patients who had recently traveled to tropical regions (US Virgin Islands, Maldives, and French Guiana), suggesting a possible epidemiologic link (*1*,*2*). In this case, the patient reported river bathing in French Guiana and exposure to stagnant swimming pool water. In another case, the patient reported bathing in a tidal pool, raising the possibility of an aquatic reservoir (*1*). Reports have noted resistance of *M. decipiens* to first-line antituberculous drugs, including rifampin, isoniazid, and ethambutol (*6*). In our case, discontinuing rifampin and initiating moxifloxacin brought rapid clinical improvement. A prior reported case likewise involved administration of a macrolide-moxifloxacin combination with a third agent, which led to successful recovery (*1*).

In conclusion, clinical strains of *M. decipiens* in humans, as reported both here and in prior reports, appear to be susceptible to clarithromycin, moxifloxacin, linezolid, rifabutin, and trimethoprim/sulfamethoxazole (Table). Those agents should be considered in empirical regimens for possible *M. decipiens* infections, pending susceptibility results.

About the Author

Dr. Destoop is an infectious diseases and dermatology physician in the Infectious Diseases division of the Pitié-Salpêtrière University Hospital in Paris, France. His areas of clinical interest include emerging infectious diseases, infectious dermatology, and tropical medicine.

References

1. Simner PJ, Hyle EP, Buckwalter SP, Branda JA, Brown-Elliott BA, Franklin J, et al. Tenosynovitis caused by a novel nontuberculous *Mycobacterium* species initially misidentified as a member of the *Mycobacterium tuberculosis* complex. J Clin Microbiol. 2014;52:4414–8.
2. Brown-Elliott BA, Simmer PJ, Trovato A, Hyle EP, Droz S, Buckwalter SP, et al. *Mycobacterium decipiens* sp. nov., a new species closely related to the *Mycobacterium tuberculosis* complex. Int J Syst Evol Microbiol. 2018;68:3557–62.
3. Richter E, Rüsch-Gerdes S, Hillemann D. Evaluation of the GenoType Mycobacterium Assay for identification of mycobacterial species from cultures. J Clin Microbiol. 2006; 44:1769–75. https://doi.org/10.1128/JCM.44.5.1769-1775.2006
4. Hall MB. *Mycobacterium* representative Kraken2 database. Zenodo. 2023 [cited 2025 Aug 19]. https://zenodo.org/doi/10.5281/zenodo.8339821
5. Clinical and Laboratory Standards Institute. Performance Standards for Susceptibility Testing of Mycobacteria, Nocardia spp., and Other Aerobic Actinomycetes. 2nd edition. CLSI supplement M24S. Wayne (PA): The Institute; 2023.
6. Sous C, Frigui W, Pawlik A, Sayes F, Ma L, Cokelaer T, et al. Genomic and phenotypic characterization of *Mycobacterium tuberculosis'* closest-related non-tuberculous mycobacteria. Microbiol Spectr. 2024;12:e0412623.

Address for correspondence: Justin Charles-Antoine Destoop, Pitié-Salpêtrière University Hospital-Infectious Diseases, 83 bd de l'hopital Paris, Paris 75013, France; email: justin.destoop@gmail.com

Fatal *Ehrlichia muris eauclairensis* Infection in Liver Transplant Recipient, Minnesota, USA

Syeda Sahra, Supavit Chesdachai, Paschalis Vergidis, William Sanchez, Bobbi S. Pritt

Author affiliation: Mayo Clinic, Rochester, Minnesota, USA

DOI: https://doi.org/10.3201/eid3201.250893

Ehrlichia muris eauclairensis bacterial infections can manifest with atypical and severe symptoms in immunocompromised patients. We report a fatal case of severe ehrlichiosis caused by *E. muris eauclairensis* in a liver transplant recipient in Minnesota, USA. Healthcare providers must remain vigilant about tickborne infections in endemic regions, especially among immunocompromised patients.

Ehrlichiosis is a tickborne zoonosis caused by intracellular, *Rickettsia*-like *Ehrlichia* spp., which were first described in humans in 1987 (*1*). The primary human pathogens are *E. chaffeensis*, which causes human monocytic ehrlichiosis, and *E. ewingii* and *E. muris eauclairensis* (EME), which cause granulocytic ehrlichiosis. EME, identified in 2009 in Eau Claire, Wisconsin, USA, occurs mainly in the Upper Midwest, particularly Minnesota and Wisconsin (*2*). It is transmitted by the blacklegged tick (*Ixodes scapularis*), and incidence peaks in summer (*2*).

Clinically, ehrlichiosis manifests as an acute febrile illness, most often with fever (≈90%), headache, malaise, myalgia, and gastrointestinal symptoms (nausea, vomiting, diarrhea). Laboratory findings commonly include thrombocytopenia (≈76% of cases), leukopenia, lymphopenia, and elevated aspartate transferase (≈46% cases); rash occurs in ≈17% of cases (*3*). Neurologic symptoms such as confusion, amnesia, or seizures have been reported in ≈9% of cases, particularly in older or immunosuppressed patients, usually with unremarkable imaging (*4*). We report a fatal case of severe ehrlichiosis caused by *E. muris eauclairensis* in a liver transplant recipient in Minnesota.

In May 2025, a 52-year-old man from northern Minnesota who had liver cirrhosis and hepatocellular carcinoma underwent deceased-donor liver transplantation. Seven months later, he sought care for a 3-day history of headache, blurred vision, malaise, and throat congestion. His immunosuppression regimen included mycophenolate, sirolimus, cyclosporine, and prednisone. He had multiple episodes of glucocorticoid-resistant acute T-cell–mediated rejection treated with 4 doses of antithymocyte globulin, most recently 1 month earlier.

At the time of examination, the only notable finding was jaundice. The patient lived on a farm with tick exposure but denied known bites. Laboratory tests showed anemia, lymphopenia, thrombocytopenia, transaminitis, and hyperbilirubinemia (Table). A peripheral blood smear obtained at admission was negative for intracellular morulae. PCR tests for cytomegalovirus, Epstein-Barr virus, herpes simplex virus types 1 and 2, human herpesvirus 6, influenza, and SARS-CoV-2 were negative. Ferritin was elevated (331 μg/L). The patient was started on cefepime for neutropenic fever, but worsening headaches and confusion developed within 24 hours. Brain magnetic resonance imaging showed no acute infarcts. Empiric meningitis treatment was initiated (vancomycin, cefepime, and ampicillin). Lumbar puncture yielded clear yellow cerebrospinal fluid with 1 leukocyte, protein 17 mg/dL, and glucose 74 mg/dL. Results

of cerebrospinal fluid studies, including Gram stain, HSV PCR, and a meningitis-encephalitis panel, were negative. On hospitalization day 3, a tickborne disease panel was ordered, and doxycycline (100 mg intravenously every 12 h) was initiated. By day 4, acute hypoxic respiratory failure developed, requiring intubation and intensive care unit transfer.

On hospitalization day 5, results were received from the tickborne disease panel, a real-time PCR and DNA probe hybridization assay performed on whole blood at Mayo Clinic Laboratories (Rochester, MN, USA). The tests were negative for *Anaplasma phagocytophilum*, *E. chaffeensis*, *Babesia* spp., and *Borrelia miyamotoi* but positive for *E. muris eauclairensis*. Within 24 hours, the patient developed multiorgan failure and died.

Autopsy revealed patchy pulmonary edema, hemorrhage, hyaline membranes, and reactive pneumocytes in lung tissue (Figure, panel A). The liver showed extensive necrosis consistent with ischemic injury (Figure, panel B). Renal parenchyma demonstrated acute tubular injury with bile casts (Figure, panel C). The spleen was congested, and the heart exhibited moderate myocyte hypertrophy and mild perivascular fibrosis. No specific findings were reported from brain parenchymal tissue. Clinical findings supported severe ehrlichiosis manifesting with acute respiratory distress syndrome and multiorgan failure.

Diagnosis of EME relies on PCR, which is most sensitive during the first week of illness. Early serologic testing might be negative and cannot reliably differentiate EME from other species, and antibodies can persist for months to years; paired acute and convalescent serum sample testing is recommended. Treatment is doxycycline (100 mg orally or intravenously 2×/d for 7–14 days), guided by clinical response (*5*).

Table. Laboratory values at hospital admission for liver transplant recipient who later died of *Ehrlichia muris eauclairensis* infection, Minnesota, USA

Test (reference range)	Value
Hemoglobin, g/dL (13.2–16.6)	9.6
Platelets, × 10^9/L (135–317)	59
Leukocytes, × 10^9 cells/L (3.4–9.6)	1.2
Lymphocytes, × 10^9 cells/L (0.95–3.07)	0.04
Creatinine, mg/dL (0.74–1.35)	0.53
Alanine aminotransferase, U/L (7–55)	88
Aspartate aminotransferase, U/L (8–48)	142
Total bilirubin, mg/dL (0.0–12)	18.2

Immunosuppression impairs cell-mediated immunity and increases ehrlichiosis-related mortality, as demonstrated in animal models (*6*). High-risk groups include transplant recipients, asplenic patients, and patients with HIV, who can develop severe complications such as pancytopenia, renal failure, acute respiratory distress syndrome, shock, and neurologic dysfunction (*7*). In this patient, recent antithymocyte globulin therapy likely contributed to the poor outcome. That agent depletes T cells through complement-dependent lysis, activation, and apoptosis; induces B-cell apoptosis; alters leukocyte–endothelial interactions; disrupts endothelial function; and promotes regulatory and natural killer T cells (*8*).

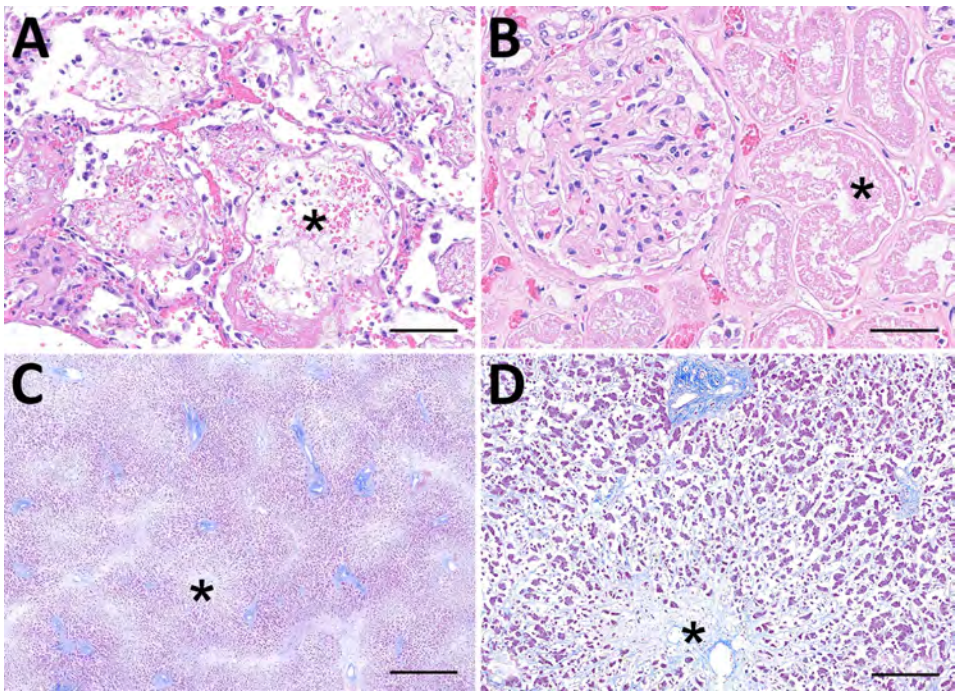

Figure. Microscopic findings from autopsy of liver transplant recipient with fatal *Ehrlichia muris eauclairensis* infection, Minnesota, USA. A) Hematoxylin and eosin stain of lung tissue shows acute diffuse alveolar damage with intraalveolar edema (asterisk) and focal hyaline membranes. Scale bar indicates 100 µm. B) Hematoxylin and eosin stain of kidney tissue shows acute tubular injury (asterisk). Scale bar indicates 50 µm. C) Masson's trichrome stain of the liver shows prominent zone 3 necrosis (asterisk) consistent with ischemic injury. Scale bar indicates 500 µm. D) Higher magnification of panel C shows the loss of hepatocytes (asterisk) near the central vein (zone 3). Scale bar indicates 100 µm.

Reported outcomes of ehrlichiosis in solid organ transplant recipients have generally been favorable; for example, 1 case of *E. chaffeensis* infection resolved despite multiorgan involvement (*9*). In a study of 75,077 US blood samples (2007–2013), EME was identified in 69 patients (0.1%), mostly in Minnesota and Wisconsin; 49 were immunocompromised, of which 13 (27%) were on immunosuppressive therapy, including 7 transplant recipients (*10*). All recovered, most after doxycycline treatment.

Clinicians should maintain a high index of suspicion for ehrlichiosis in febrile transplant recipients who have headache, altered mental status, thrombocytopenia, or transaminitis, particularly in those with tick exposure or residence in endemic areas. In this case, transaminitis and severe hyperbilirubinemia with liver allograft dysfunction complicated the diagnosis, underscoring the importance of timely tickborne disease testing. Early recognition and treatment are critical to preventing fatal outcomes.

About the Author

Dr. Sahra is a transplant infectious diseases fellow with academic appointment of assistant professor of medicine at the Mayo Clinic, Rochester, Minnesota, USA. Her research interests are fungal infections in heart transplant recipients and ventricular assist device infections.

References

1. Maeda K, Markowitz N, Hawley RC, Ristic M, Cox D, McDade JE. Human infection with *Ehrlichia canis*, a leukocytic rickettsia. N Engl J Med. 1987;316:853–6. https://doi.org/10.1056/NEJM198704023161406
2. Pritt BS, Sloan LM, Johnson DK, Munderloh UG, Paskewitz SM, McElroy KM, et al. Emergence of a new pathogenic *Ehrlichia* species, Wisconsin and Minnesota, 2009. N Engl J Med. 2011;365:422–9. https://doi.org/10.1056/NEJMoa1010493
3. Dumic I, Jevtic D, Veselinovic M, Nordstrom CW, Jovanovic M, Mogulla V, et al. Human granulocytic anaplasmosis—a systematic review of published cases. Microorganisms. 2022;10:1433. https://doi.org/10.3390/microorganisms10071433
4. Iyamu O, Ciccone EJ, Schulz A, Sung J, Abernathy H, Alejo A, et al. Neurological manifestations of ehrlichiosis among a cohort of patients: prevalence and clinical symptoms. BMC Infect Dis. 2024;24:701. https://doi.org/10.1186/s12879-024-09607-3
5. Biggs HM, Behravesh CB, Bradley KK, Dahlgren FS, Drexler NA, Dumler JS, et al. Diagnosis and management of tickborne rickettsial diseases: Rocky Mountain spotted fever and other spotted fever group rickettsioses, ehrlichioses, and anaplasmosis—United States. MMWR Recomm Rep. 2016;65(2):1–44. https://doi.org/10.15585/mmwr.rr6502a1
6. Winslow GM, Yager E, Shilo K, Collins DN, Chu FK. Infection of the laboratory mouse with the intracellular pathogen *Ehrlichia chaffeensis*. Infect Immun. 1998;66:3892–9. https://doi.org/10.1128/IAI.66.8.3892-3899.1998
7. Gygax L, Schudel S, Kositz C, Kuenzli E, Neumayr A. Human monocytotropic ehrlichiosis-A systematic review and analysis of the literature. PLoS Negl Trop Dis. 2024;18:e0012377. https://doi.org/10.1371/journal.pntd.0012377
8. Mohty M. Mechanisms of action of antithymocyte globulin: T-cell depletion and beyond. Leukemia. 2007;21:1387–94. https://doi.org/10.1038/sj.leu.2404683
9. Almajali F, Oleary C, Hallcox T, Lok J, Hermelin D, Guenette A, et al. Ehrlichiosis in a recent liver transplant recipient leading to multiorgan failure. Case Rep Transplant. 2022;2022:3062836. https://doi.org/10.1155/2022/3062836
10. Johnson DK, Schiffman EK, Davis JP, Neitzel DF, Sloan LM, Nicholson WL, et al. Human infection with *Ehrlichia muris*–like pathogen, United States, 2007–2013. Emerg Infect Dis. 2015;21:1794–9. https://doi.org/10.3201/eid2110.150143

Address for correspondence: Syeda Sahra, Mayo Clinic, Transplant Infectious Diseases, 200 1st St SW, Rochester, MN 55905, USA; email: sahra.syeda@mayo.edu

Molecular Analysis of Emerging MT27 Macrolide-Resistant *Bordetella pertussis*, Kobe, Japan, 2025

Shoko Komatsu, Noriko Nakanishi, Kousaku Matsubara, Yuui Inenaga, Masayuki Hori, Kiyo Shiotani, Rumi Morimoto, Chie Nantani, Yuki Muneta, Nobuya Kusunoki

Author affiliations: Kobe Institute of Health, Kobe, Japan (S. Komatsu, N. Nakanishi); Kobe City Nishi-Kobe Medical Center, Kobe (K. Matsubara, Y. Inenaga, M. Hori); Public Health Center of Kobe City, Kobe (K. Shiotani, R. Morimoto, C. Nantani, Y. Muneta, N. Kusunoki)

DOI: https://doi.org/10.3201/eid3201.250890

We report the emergence and spread of multilocus variable-number tandem-repeat analysis type 27 (MT-27) macrolide-resistant *Bordetella pertussis* (MRBP) in Kobe, Japan, in 2025. Whole-genome sequencing revealed that MT27-MRBP did not originate from the widely circulating MT27 macrolide-sensitive *B. pertussis* in Japan but was closely related to MRBP in China.

Table. Clinical features and microbiological profiles of 15 MT27-*Bordetella pertussis* isolates in Kobe, Japan, January 2013–March 2025*

Strain ID	Collection date	Patients		Macrolide susceptibility	Genotyping of virulence-related genes				
		Age/sex	Vaccination (no. doses)		*ptxP*	*ptxA*	*fhaB*	*fim3*	*prn*
KBP0005	2013 Mar 25	1 y/M	DPT (3)	Susceptible	3	1	1	1	2
KBP0006	2015 Apr 21	4 mo/F	NA	Susceptible	3	1	1	1	2
KBP0007	2016 Feb 25	8 mo/M	Unvaccinated	Susceptible	3	1	1	1	2
KBP0009	2019 Sep 24	1 mo/F	Unvaccinated	Susceptible	3	1	1	1	2
KBP0010	2024 Jun 24	1 mo/F	Unvaccinated	Susceptible	3	1	1	1	2
KBP0011	2024 Jun 24	35 y/M	DPT (4)	Susceptible	3	1	1	1	2
KBP0014	2025 Jan 25	8 y/F	DPT-IPV (4)	Susceptible	3	1	1	1	2
KBP0016	2025 Feb 3	10 y/F	DPT-IPV (4)	Resistant	3	1	1	1	150
KBP0017	2025 Feb 12	2 mo/M	DPT-IPV (1)	Resistant	3	1	1	1	150
KBP0018	2025 Feb 13	12 y/M	DPT-IPV (4)	Susceptible	3	1	1	1	2
KBP0019	2025 Feb 18	9 y/F	DPT-IPV (4)	Susceptible	3	1	1	1	2
KBP0020	2025 Feb 20	10 y/F	DPT-IPV (4)	Resistant	3	1	1	1	150
KBP0025	2025 Mar 7	12 y/F	DPT-IPV (4)	Susceptible	3	1	1	1	2
KBP0026	2025 Mar 7	12 y/F	NA	Resistant	3	1	1	1	150
KBP0028	2025 Mar 12	12 y/F	NA	Resistant	3	1	1	1	150

*DPT, diphtheria-pertussis-tetanus; IPV, inactivated polio vaccine; MT, multilocus variable-number tandem-repeat analysis type; NA, not available.

Bordetella pertussis, a gram-negative, pathogenic bacterium of the genus *Bordetella*, is the causative agent of contagious respiratory illness and whooping cough (pertussis). Diphtheria-pertussis-tetanus (DPT) combination vaccines have substantially reduced pertussis-related illness and deaths, especially among infants (*1*). Macrolides represent mostly natural polyketide-class products containing a large macrocyclic lactone ring with potential attachment groups (e.g., deoxy sugars), with antibiotic or antifungal activities. Macrolides are popular pharmaceutical drugs, frequently used for pertussis treatment and prevention. Macrolide-resistant *B. pertussis* (MRBP), characterized by the A2047G mutation in a region critical for macrolide binding to the 23S rRNA gene, has recently emerged and spread worldwide (*2*). In China, the predominant MRBP genetic lineage has shifted in the pertussis toxin promoter region (*ptxP*) allele type from *ptxP1* to *ptxP3*, and the prevalence of the *ptxP3*-carrying multilocus variable-number tandem-repeat analysis type (MT) 28 MRBP strain has increased rapidly (*3*).

In Japan, pertussis notifications, which decreased during the COVID-19 pandemic, have significantly increased since 2024 (*4*). MRBP was first documented in 2018 during the first isolation of *ptxP1*-MT195-MRBP (*5*). More recently, *ptxP3*-MRBP strains isolated from Tokyo and Okinawa have been described, demonstrating close genetic relation to the China strains (*6*,*7*).

MT27 is a single-locus MT28 variant, and this genotype, carrying the virulence-associated alleles *ptxP3*/*ptxA1*/*prn2*/*fim3-1*, became predominant among macrolide-susceptible *B. pertussis* (MSBP) strains in various countries, including Japan (*8*–*10*). In contrast, to date, just 1 MT27-MRBP strain has been reported in China in 2017 (*8*); no cases have been identified outside of China. In this study, we report 5 MT27-MRBP strains isolated during February–March 2025 from children with pertussis in 1 hospital and 2 private clinics in Kobe, Japan (Table). To investigate the molecular epidemiologic characteristics of these 5 MT27-MRBP isolates, we compared them to Japan MT27-MSBP strains isolated during 2010–2025, including 10 isolates from Kobe, and MRBP strains from China (*3*,*6*–*8*,*10*). This study was approved by the Kobe City Review Board (approval no. SenR3-10).

We collected 9 MT27 strains from patients 2 months through 12 years of age during January–March 2025 (Table). All 5 MT27-MRBP strains harbored the A2047G mutation in the 23S rRNA and exhibited MICs of >256 μg/mL for erythromycin, clarithromycin, and azithromycin. All MT27-MRBP–infected patients recovered without any sequelae. We used the BIGSdb-Pasteur platform (https://bigsdb.pasteur.fr/bordetella) to identify the MT27-MRBP virulence genotype, which yielded identical results for all strains: *ptxP3*/*ptxA1*/*fhaB1*/*fim3–1*/*prn150*. Among the 5 virulence-related genes, we observed a difference in the *prn* allele between the MT27-MSBP and MT27-MRBP strains isolated in Kobe (i.e., *prn2* in MSBP and *prn150* in MRBP) (Table). Of note, *prn150* was identical to the allele in the globally prevalent MT28-MRBP strains (*3*).

To determine genetic relatedness, we performed phylogenetic analyses using whole-genome sequences of 6 MT27-MSBP isolates obtained in Kobe since 2013 (Table) and other publicly available genomes (Appendix Table, https://wwwnc.cdc.gov/EID/article/32/1/25-0890-App1.xlsx). Our single-nucleotide variant–based phylogenetic analysis revealed that the 5 MT27-MRBP strains clustered within the *prn150* lineage, which is genetically closely related to the MRBP strain from

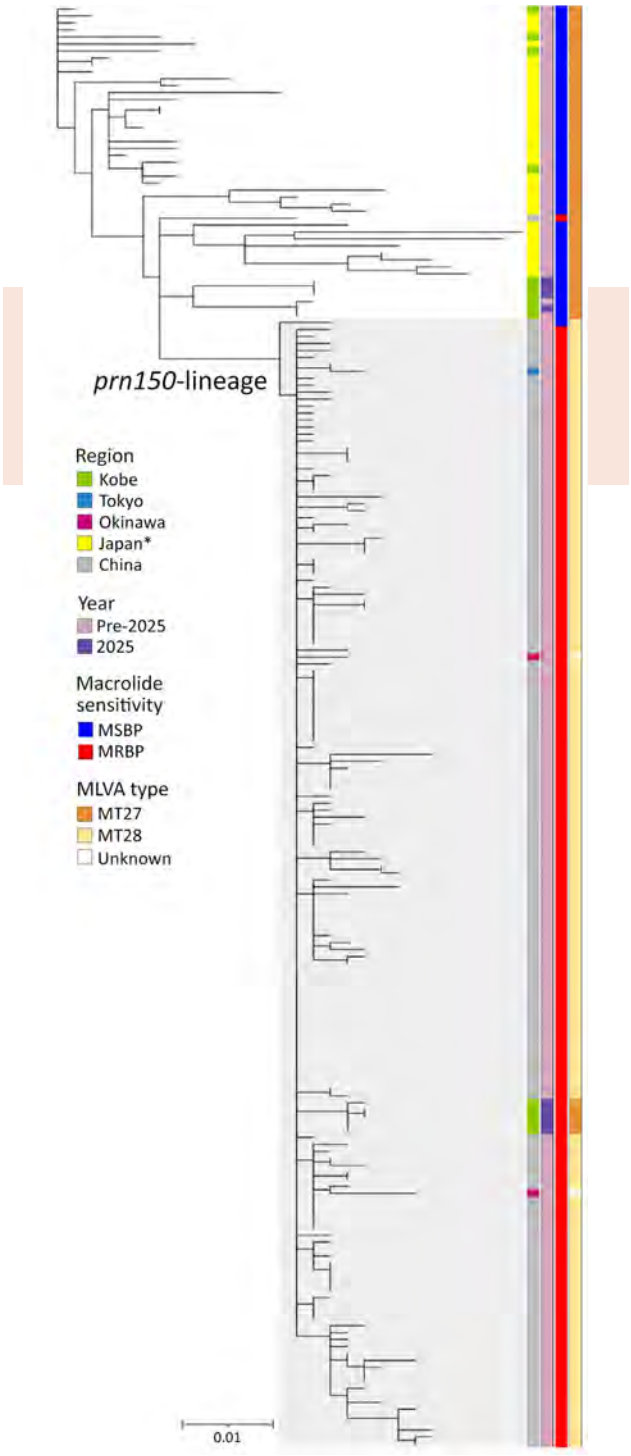

Figure. Phylogenetic tree based on single-nucleotide variants, showing 15 MT27 *Bordetella pertussis* strains isolated in Kobe (green); 37 strains from Japan (yellow), including Tokyo (blue) and Okinawa (magenta); and 155 strains from China (gray) in study of emerging MT27 MRBP, Kobe, Japan, 2025. Scale bar indicates number of substitutions per site. *Excluding regions previously listed. MRBP, macrolide-resistant *B. pertussis*; MSBP, macrolide-sensitive *B. pertussis*; MLVA, multilocus variable-number tandem-repeat analysis; MT, MLVA type.

China and that clonal population (Figure). Furthermore, MT27-MRBP strains in Kobe were genetically distinct from the China MT27-MRBP (GenBank accession no. SRR16306222), as well as from the Japan MRBP strains, BP636 (GenBank accession no. DRR631445) in Tokyo and OkiPb01308 and OkiPb01309 (National Center for Biotechnology Information BioProject accession no. PRJDB20292) in Okinawa (Figure). The identification of genetically divergent strains across 3 geographically separated regions of Japan suggests multiple, epidemiologically independent introductions. In contrast, MT27-MSBP strains KBP0014, KBP0018, KBP0019, and KBP0025, isolated in 2025, belonged to a clade of currently prevalent strains in Japan. Taken together, our results suggest that MT27-MRBP does not originate from the currently circulating MT27-MSBP in Japan but could have been potentially introduced from China. Finally, 5 MT27-MRBP–infected patients resided in 3 different wards with no apparent temporal links, suggesting that this newly emergent strain might be spreading latently in Kobe.

In conclusion, we identified distinct genetic differences between the MT27-MSBP and MT27-MRBP strains collected during January–March 2025 in Kobe. Our study suggests that MT27-MRBP strains closely related to the China MRBP strains have emerged and spread in Kobe, Japan.

Acknowledgments

We thank the medical institutions in Kobe for submitting specimens as part of the surveillance program.

Raw sequencing data for the isolates from Kobe have been deposited in DDBJ/EMBL/GenBank (DRA accession numbers DRR698592–606). GenBank accession numbers for all genome sequences used for phylogenetic analysis are listed in the Appendix Table.

This work was supported by JSPS KAKENHI (grant no. JP25K24232).

About the Author

Ms. Komatsu is a research scientist at the Kobe Institute of Health, Hyogo, Japan. Her primary research interests are molecular epidemiology of bacterial infections of the respiratory tract, such as *Bordetella pertussis* and *Legionella* spp.

References

1. Sheng Y, Ma S, Zhou Q, Xu J. Pertussis resurgence: epidemiological trends, pathogenic mechanisms, and preventive strategies. Front Immunol. 2025;16:1618883. https://doi.org/10.3389/fimmu.2025.1618883

2. Ivaska L, Barkoff AM, Mertsola J, He Q. Macrolide resistance in *Bordetella pertussis*: current situation and future challenges. Antibiotics (Basel). 2022;11:1570. https://doi.org/10.3390/antibiotics11111570
3. Fu P, Yan G, Li Y, Xie L, Ke Y, Qiu S, et al. Pertussis upsurge, age shift and vaccine escape post-COVID-19 caused by *ptxP3* macrolide-resistant *Bordetella pertussis* MT28 clone in China. Clin Microbiol Infect. 2024;30:1439–46. https://doi.org/10.1016/j.cmi.2024.08.016
4. Japan Institute for Health Security. Risk assessment: pertussis outbreak situation in Japan [cited May 18]. https://id-info.jihs.go.jp/diseases/ha/pertussis/020/250422_JIHS_Pertussis_en.pdf
5. Koide K, Uchitani Y, Yamaguchi T, Otsuka N, Goto M, Kenri T, et al. Whole-genome comparison of two same-genotype macrolide-resistant *Bordetella pertussis* isolates collected in Japan. PLoS One. 2024;19:e0298147. https://doi.org/10.1371/journal.pone.0298147
6. Iwasaki T, Koide K, Kido T, Nakagawa S, Goto M, Kenri T, et al. Fatal case of macrolide-resistant *Bordetella pertussis* infection, Japan, 2024. J Infect Chemother. 2025;31:102727. https://doi.org/10.1016/j.jiac.2025.102727
7. Tsukahara H, Araki K, Cho Y, Fujiwara N, Matsuoka T, Kakita T, et al. Severe macrolide-resistant *Bordetella pertussis* (ptxP3) infection in Japanese infants: first report of cases requiring intensive care. Int J Infect Dis. 2025;158:107960. https://doi.org/10.1016/j.ijid.2025.107960
8. Wu X, Du Q, Li D, Yuan L, Meng Q, Fu Z, et al. A cross-sectional study revealing the emergence of erythromycin-resistant *Bordetella pertussis* carrying *ptxP3* alleles in China. Front Microbiol. 2022;13:901617. https://doi.org/10.3389/fmicb.2022.901617
9. Koide K, Yao S, Chiang CS, Thuy PTB, Nga DTT, Huong DT, et al. Genotyping and macrolide-resistant mutation of *Bordetella pertussis* in East and South-East Asia. J Glob Antimicrob Resist. 2022;31:263–9. https://doi.org/10.1016/j.jgar.2022.10.007
10. Kamachi K, Koide K, Otsuka N, Goto M, Kenri T. Whole-genome analysis of *Bordetella pertussis* MT27 isolates from school-associated outbreaks: single-nucleotide polymorphism diversity and threshold of the outbreak strains. Microbiol Spectr. 2023;11:e0406522. https://doi.org/10.1128/spectrum.04065-22

Address for correspondence: Noriko Nakanishi, Health Research Department 2, Kobe Institute of Health, 4-6-5 Minatojima-nakamachi, Chuo-ku, Kobe, Hyogo 650-0046, Japan; email: noriko_nakanishi@city.kobe.lg.jp

Donor Screening Failure for *Strongyloides stercoralis* in Solid Organ Transplantation

Rocio Kohan, Helena Gil-Campesino, Inés O. García Rodríguez, Magdalena Lara

Author affiliations: Hospital Universitario de Canarias, San Cristóbal de La Laguna, Canary Islands, Spain (R. Kohan, I.O. García Rodríguez); Hospital Universitario Nuestra Señora de Candelaria, Santa Cruz de Tenerife, Canary Islands, Spain (H. Gil-Campesino, M. Lara).

DOI: https://doi.org/10.3201/eid3201.251483

We report 2 cases of donor-derived *Strongyloides stercoralis* infection in renal transplant recipients. Despite initial negative serologic testing in donor samples, retrospective testing confirmed transmission. This report underscores the limitations of serologic screening, the need for targeted protocols in endemic-risk populations, and the importance of close posttransplant surveillance.

Strongyloides stercoralis can persist for decades in humans (*1*). In immunocompromised patients, such as transplant recipients, *S. stercoralis* can cause disseminated infection or hyperinfection syndrome (*2*). Mortality exceeds 60% in immunosuppressed persons (*3*), reaching 87% if treatment is not initiated (*4*). We report 2 cases of strongyloidiasis in renal transplant recipients who shared the same donor.

The donor was a 72-year-old man who was born in Ghana and resided in Tenerife, Canary Islands, Spain, for 20 years. He died from subarachnoid hemorrhage after a traumatic brain injury. He had no known immunosuppressive condition, and his eosinophil count was unremarkable. Following National Transplant Organization guidelines on the selection criteria of donors in relation to infectious diseases (*5*), routine donor serologic screening was conducted. Testing for HIV, human T-lymphotropic virus 1 and 2, hepatitis C and B virus, syphilis, cytomegalovirus, Epstein-Barr virus, herpes simplex virus 1 and 2, and toxoplasmosis revealed no noteworthy findings except positive results for cytomegalovirus IgG and hepatitis B core antibody (hepatitis B surface antigen was negative). Because of the donor's geographic origin, Mantoux testing and testing for antibodies against *Coccidioides immitis*, *Histoplasma capsulatum*, *Plasmodium* spp., and *S. stercoralis* were conducted; all results were negative. The additional testing was conducted at an external reference laboratory (Reference Labo-

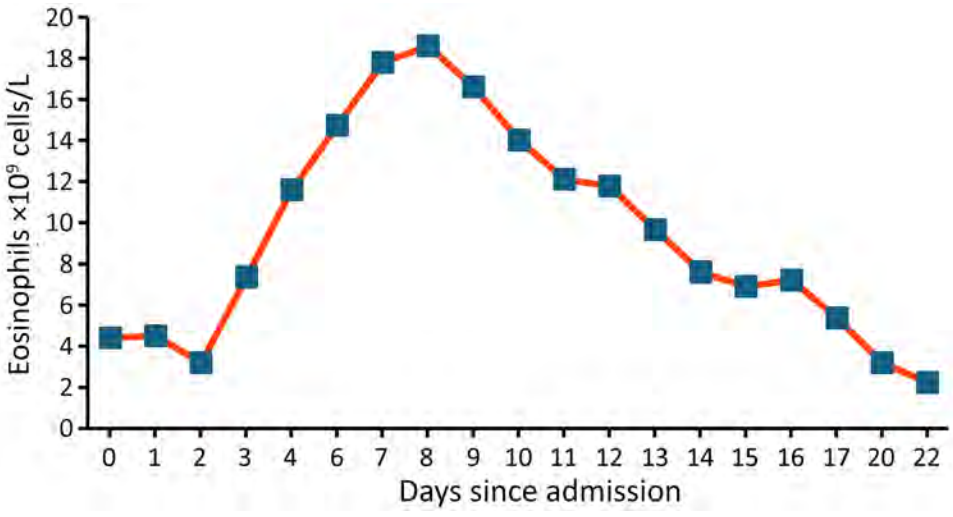

Figure 1. Eosinophil count evolution in recipient A during admission in a study of donor screening failure for *Strongyloides stercoralis* in solid organ transplantation.

ratory S.A., Barcelona, Spain), where *Strongyloides* serology was performed by using a crude-antigen enzyme-linked immunosorbent assay (SciMedx Corporation, https://www.scimedx.com), yielding an index value of <0.1 (>1 is considered positive). One kidney from the donor was transplanted into each of 2 recipients.

Figure 2. *Strongyloides stercoralis* L1 rhabditiform larva found in stool sample from recipient A in a study of donor screening failure for *Strongyloides stercoralis* in solid organ transplantation.

Recipient A was a 65-year-old man with diabetic nephropathy who was on continuous ambulatory peritoneal dialysis for 11 months before transplant. No complications were reported during the immediate posttransplant period. Approximately 2 months after transplant, a cough with sputum production developed; the patient was initially treated on an outpatient basis with oral amoxicillin/clavulanic acid (500 mg/8 h for 7 days). He then sought care at the local emergency department with severe epigastric pain and heartburn, asthenia, tendency toward hypotension, and persistence of mild respiratory symptoms. A computed tomography scan revealed gastric distension, mild small-bowel dilatation and thickening, minimal pelvic free fluid, and bilateral pleural and pericardial effusion. Laboratory findings included C-reactive protein of 114 mg/L (reference range <5 mg/L), increased leukocytes of 23 × 10^9 cells/L (reference 4–11 × 10^9 cells/L), serum IgE 1,664.9 IU/mL (reference <100 IU/mL), and marked hypereosinophilia, rising from 3.2 × 10^9 cells/L (reference <0.5× 10^9 cells/L) at admission to 18.7 × 10^9 cells/L on day 6 of hospitalization (Figure 1). We learned the patient had previously traveled by caravan across Spain's Mediterranean coast, an area described as endemic for strongyloidiasis (*6*). Formalin ethyl-acetate sedimentation concentration with subsequent microscopic examination of stool samples revealed *S. stercoralis* L1 rhabditiform larvae (Figure 2). Because of the donor's negative serology, we suspected endogenous reactivation. The patient received oral ivermectin (200 μg/kg/d for 25 days) and albendazole (400 mg 2×/d for 15 days), with progressive clinical improvement. Once the patient reached normalization of eosinophilia and preservation of graft function, he was discharged.

Recipient B was a 74-year-old man with diabetic nephropathy who was on hemodialysis for 20 months before transplantation; no complications were reported during the immediate posttransplant period. He had no known risk factors for *Strongyloides* infection. After the confirmed diagnosis in recipient A, we conducted targeted screening, revealing *S. stercoralis* L1 rhabditiform larvae in stool samples examined by direct microscopy by using the formalin ethyl-acetate sedimentation concentration technique. He did not show peripheral eosinophilia at any time and remained asymptomatic with unremarkable laboratory values throughout follow-up. We treated him with oral ivermectin (200 μg/kg/d for 2 days) and repeated treatment 2 weeks later. Both patients tested negative in follow-up stool examinations performed by using the same concentration and microscopy methods.

Because of the suspicion of a common transmission source, stored donor serum was sent for repeat *Strongyloides* serologic testing by using third-stage larvae antigen enzyme-linked immunosorbent assay for *Strongyloides* IgG (DRG Instrument Gmbh, https://www.drg-diagnostics.de). The sample tested positive with an index value of 1.61 (>1.1 is considered positive), confirming donor-derived transmission of the parasite.

This event highlights several clinically relevant considerations. First, the sensitivity of serologic assays varies widely (*7*,*8*); thus, active infection cannot be ruled out solely on the basis of a negative result in epidemiologically at-risk patients. This limitation is even more relevant for immunosuppressed patients, in whom serologic testing might yield false-negative results. Therefore, additional diagnostic methods, such as PCR, stool concentration techniques, or agar plate culture, should be considered to reliably exclude infection. Second, it underscores the need to reinforce targeted screening protocols in both donors and recipients with origin or prolonged residence in endemic areas, including national regions (*9*), which are often overlooked. Close monitoring of recipients from such donors remains essential, and the appearance of any new symptoms, such as mild respiratory symptoms seen in recipient A, should raise concern, even with negative donor serology, as in this case it might corresponded to Löffler syndrome. Finally, this report highlights the usefulness of storing serum from deceased donors for retrospective confirmation.

About the Author

Dr. Kohan is a pharmacist and currently works as a clinical microbiologist at the Hospital Universitario de Canarias in Tenerife, Spain. Her research interests include parasitic diseases and their diagnosis, management, and follow-up, and providing support to physicians in differential diagnosis.

References

1. Prendki V, Fenaux P, Durand R, Thellier M, Bouchaud O. Strongyloidiasis in man 75 years after initial exposure. Emerg Infect Dis. 2011;17:931–2.
2. Barkati S, Naeem F, Hales L, Quan C, Libman M. *Strongyloides stercoralis* prevalence in solid-organ and haematopoietic stem cell transplant candidates and recipients: a systematic review and meta-analysis protocol. BMJ Open. 2022;12:e057649.
3. Lo NC, Addiss DG, Buonfrate D, Amor A, Anegagrie M, Bisoffi Z, et al. Review of the World Health Organization guideline on preventive chemotherapy for public health control of strongyloidiasis. Lancet Infect Dis. 2025; 25:e146–52.
4. Lai C, Anderson M, Davis R, Anderson L, Wyburn K, Chadban S, et al. *Strongyloides* hyperinfection in an HIV-positive kidney transplant recipient: a case report. BMC Infect Dis. 2020;20:613.
5. Len O, Los-Arcos I, Aguado JM, Blanes M, Bodro M, Carratala J, et al. Consensus document of the Grupo de Estudio de la Infección en el Transplante of the Sociedad Española de Enfermedades Infecciosas y Microbiología Clínica and the Organización Nacional de Transplantes on the selection criteria of donors of solid organs in relation to infectious diseases. 2019 [cited 2025 Sep 7]. https://www.ont.es/wp-content/uploads/2023/06/Criteria-of-Donors-of-Solid-Organs-in-relation-to-Infectious-Diseases.-Year-2019.pdf
6. Barroso M, Salvador F, Sánchez-Montalvá A, Bosch-Nicolau P, Molina I. *Strongyloides stercoralis* infection: a systematic review of endemic cases in Spain. PLoS Negl Trop Dis. 2019;13:e0007230.
7. Bisoffi Z, Buonfrate D, Sequi M, Mejia R, Cimino RO, Krolewiecki AJ, et al. Diagnostic accuracy of five serologic tests for *Strongyloides stercoralis* infection. PLoS Negl Trop Dis. 2014;8:e2640.
8. Anderson NW, Klein DM, Dornink SM, Jespersen DJ, Kubofcik J, Nutman TB, et al. Comparison of three immunoassays for detection of antibodies to *Strongyloides stercoralis*. Clin Vaccine Immunol. 2014;21:732–6.
9. Rodríguez-Pérez M, Rivaya B, Vazquez F, Boga JA, Andrés-Galiana E, Cabo R, et al. First evidence of significant autochthonous transmission of strongyloidiasis in northern Spain: a retrospective study from Asturias, Spain. Travel Med Infect Dis. 2025;67:102900.

Address for correspondence: Rocio Kohan, Hospital Universitario de Canarias, Ctra. Ofra s/n, 38320 La Laguna, Santa Cruz de Tenerife, Spain; email: kohanrocio@gmail.com

Serologic Evidence of Exposure to *Burkholderia pseudomallei*, Nigeria

Jelmer Savelkoel,[1] Gabriel E. Wagner,[1] Chiedozie K. Ojide, Katrin Frankenfeld, Anne Rudloff, Susanna J. Dunachie, Michaela Lipp, W. Joost Wiersinga, Ivo Steinmetz,[2] Emma Birnie,[2] Rita O. Oladele[2]

Author affiliations: Amsterdam UMC location University of Amsterdam, Amsterdam, the Netherlands (J. Savelkoel, W.J. Wiersinga, E. Birnie); Medical University of Graz, Graz, Austria (G.E. Wagner, M. Lipp, I. Steinmetz); Ebonyi State University, Abakaliki, Nigeria (C.K. Ojide); Alex Ekwueme Federal University Teaching Hospital, Abakaliki (C.K. Ojide); Research Center for Medical Technology and Biotechnology, fzmb GmbH, Bad Langensalza, Germany (K. Frankenfeld, A. Rudloff); Mahidol-Oxford Tropical Medicine Research Unit, Mahidol University, Bangkok, Thailand (S.J. Dunachie); University of Oxford, Oxford, UK (S.J. Dunachie); College of Medicine University of Lagos, Lagos, Nigeria (R.O. Oladele); Lagos University Teaching Hospital, Lagos (R.O. Oladele)

DOI: https://doi.org/10.3201/eid3201.251113

Melioidosis is an underreported cause of community-acquired pneumonia and sepsis in Nigeria. We conducted a cross-sectional study using a *Burkholderia pseudomallei* protein microarray in 500 healthy participants from Nigeria. We observed a serologic response supportive of past exposure to the causative agent of melioidosis in 30% of study participants.

Melioidosis is a severely neglected tropical disease that is prevalent yet highly underreported in Africa (*1*,*2*). *Burkholderia pseudomallei*, as its causative agent, is a gram-negative environmental bacterium, and exposure can lead to pneumonia, sepsis, and abscess formation; mortality rates sometimes exceed 40% (*1*). Nigeria is a high-priority country for melioidosis surveillance efforts in Africa because the disease burden is thought to the highest on the continent (*2*–*4*). However, current epidemiologic estimates in Nigeria are derived solely from modeling (*3*,*4*). Environmental distribution of *B. pseudomallei* has been established in Nigeria; the highest soil positivity rate has been demonstrated in the southeastern state Ebonyi (*5*). We hypothesized that environmental exposure to *B. pseudomallei* would result in a serologic response among inhabitants of Ebonyi state. Thus, we performed a cross-sectional study to assess the extent of a serologic response to *B. pseudomallei* in this state.

We recruited healthy participants using a convenience sampling approach in communities and the blood bank of the Alex Ekwueme Federal University Teaching Hospital Abakaliki. Adult participants were only able to take part if they could provide consent and were without suspicion of acute disease or febrile illness. Every consecutive participant meeting those criteria was recruited using a 1:1 ratio between communities and the blood bank. We obtained serum samples, and participants completed a short survey with questions on demographics and risk factors related to *B. pseudomallei* exposure.

We tested serum at a 1:2,000 dilution for the presence of IgG against a panel of 4 *B. pseudomallei* antigens (BPSL2096, BPSL2697, BPSS0477, and BPSS1498) spotted at a concentration of 1 mg/mL on the INTER-ARRAY platform (fzmb GmbH, https://www.inter-array.com), and we applied a signal intensity threshold of 0.3 on the basis of previous studies (*6*,*7*) (Appendix, https://wwwnc.cdc.gov/EID/article/32/1/25-1113-App1.pdf). We verified array performance with buffer control and nonpooled positive (melioidosis, culture-confirmed) and negative (healthy, nonendemic) control samples in every run. We screened serum of healthy participants from the hyperendemic region of Ubon Ratchathani, Thailand, collected as part of a previous study, in parallel with the same assay and used it as a comparator (n = 50) (*6*,*8*).

Ethical approval for use of the Nigeria samples was obtained from the Research and Ethics Committee of Alex Ekwueme Federal University Teaching Hospital Abakaliki (ref. no. 10/06-2022-02/08/2022). Ethical approval for the use of the Thailand samples was obtained from the Faculty of Tropical Medicine, Mahidol University (ref. no. TMEC 12-014), Sappasitthiprasong Hospital, Ubon Ratchathani (ref. no. 018/2555), and the Oxford Tropical Research Ethics Committee (ref. no. 64-11); study details can be found elsewhere (*6*,*8*).

We recruited 500 participants in Nigeria, 60.6% men and 39.4% women, with a median age of 30 (interquartile range 23–38) years; most reported farming activities and soil exposure as risk factors for exposure to *B. pseudomallei* (Table). We observed 150 (30%) participants with a positive serologic response to ≥1 antigen of our panel, compared to 23 (46%) participants for the Thailand cohort (Figure). We observed positivity to BPSS1498, also known as hemolysin coregulated protein and considered to be the prime serodiagnostic target for *B. pseudomallei*

[1]These first authors contributed equally to this article

[2]These senior authors contributed equally to this article

and *B. mallei* (*7*), in 82 (16.4%) participants from Nigeria (Table; Figure, panel A). In Thailand, 20 (40%) participants had a positive response to BPSS1498 (Figure, panel B). No participants from Nigeria had a positive response to >3 antigens. We included the variables age, sex, smoking and alcohol use, soil exposure and farming activity, and sampling location (community vs. blood bank) in a logistic regression model. However, we excluded diabetes from this model because of the limited number of events, despite it being a known risk factor for melioidosis (*1*). Using the previously mentioned model, we found no significant predictors of a positive serologic response in participants from Nigeria when taking into account all pooled antigens.

Strengths of our study include the use of a multiplex assay that includes BPSS1498, which alone proves more sensitive as a serodiagnostic target than the indirect hemagglutination assay, the standard for melioidosis serodiagnosis (*9*,*10*). Of note, BPSL2096 showed a higher positivity in participants from Nigeria than BPSS1498 did, which might reflect differences in bacterial strains, host factors, or both. However, further studies are needed to elucidate this observation. Our positive results are strengthened by the fact that we tested serum from participants from regions in Nigeria in which the pathogen has been detected in the environment. Also, we compared our results to a selection of healthy serum samples from an endemic area in northeastern Thailand to contextualize our results. Limitations include possible underestimation of the seropositivity rate because of the use of a serodiagnostic cutoff value for signal intensity established in culture-confirmed melioidosis patients (*6*) or overestimation because of possible but considered limited cross-reactivity after exposure to other species (*9*,*10*).

Our seroepidemiologic panel should be further refined relating to cutoffs in ongoing surveillance efforts in Nigeria and other sub-Saharan countries to map the epidemiology of melioidosis. Our seropositivity estimates of exposure to *B. pseudomallei* among persons in Nigeria can be used to inform future serosurveillance and validation work.

Table. Demographic characteristics and serologic responses of 500 healthy participants in Ebonyi state, Nigeria, in study of serologic evidence of exposure to *Burkholderia pseudomallei**

Variable	Participants, n = 500
Sex	
M	303 (60.6)
F	197 (39.4)
Median age, y (IQR)	30.00 (23.00–38.00)
Farmer	370 (74.0)
Barefoot soil exposure	306 (61.2)
Smoking, current	32 (6.4)
Alcohol use, current	243 (48.6)
Diabetes	4 (0.8)
Serologic response	
BPSL2096	110 (22.0)
BPSL2697	2 (0.4)
BPSS0477	0
BPSS1498	82 (16.4)

*Values are no. (%) except as indicated. IQR, interquartile range.

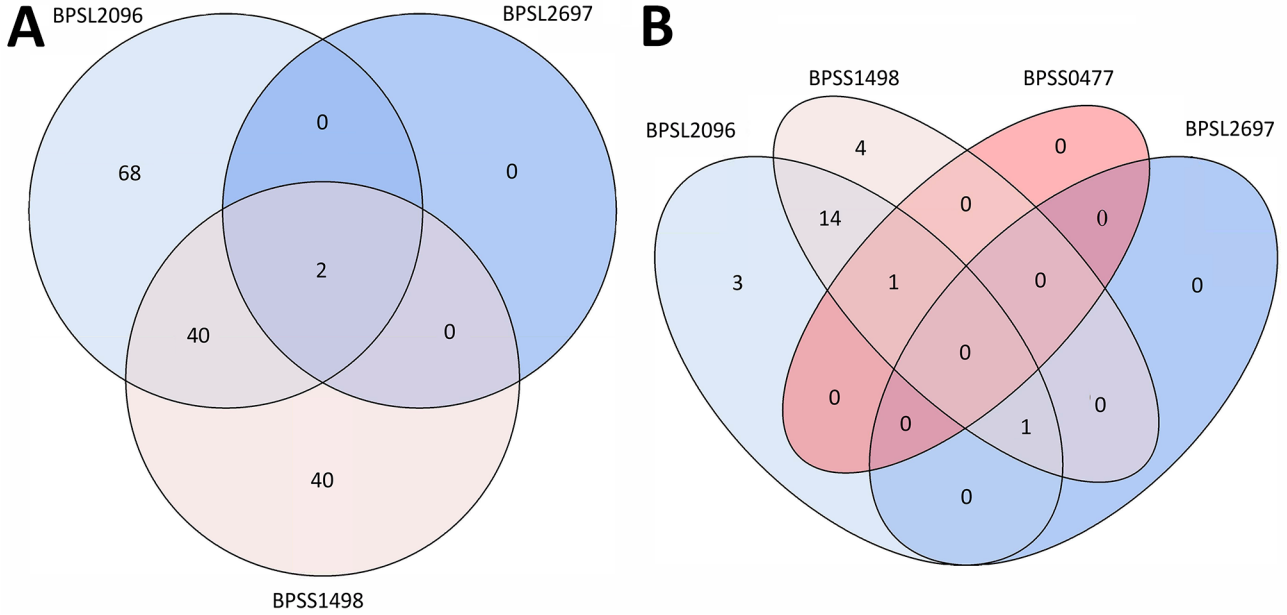

Figure. Venn diagrams displaying the serologic responses of participants from Nigeria (A) and Thailand (B) from study of serologic evidence of exposure to *Burkholderia pseudomallei*, Nigeria. The Venn diagram illustrates participants with a serologic response to ≥1 antigens (BPSL2096, BPSL2697, BPSS0477, and BPSS1498). Antigen BPSS0477 was excluded from the Nigeria Venn diagram because no participants displayed a positive response.

Acknowledgments

We thank everyone who helped with the collection, processing, and analysis of the research samples and all participants who took part in this study.

This work was financially supported by the Amsterdam University Fund, European Society of Clinical Microbiology and Infectious Diseases, and Federal Ministry for Economic Affairs and Climate Protection (ref. FKZ 49MF220067). The Thailand sample collection was financially supported by the Wellcome Trust (ref. 100174/Z/12/Z). We are thankful for the continued support of the Professor Faber Fund in advancing melioidosis research. Furthermore, J.S. was supported by an Amsterdam UMC PhD Scholarship, S.D. by a National Institute for Health and Care Research Global Health Research Professorship (ref. NIHR300791), and E.B. by a Veni grant from the Talent Programme of the Dutch Research Council (NWO-ZonMw ref. 09150162210184)

About the Author

Mr. Savelkoel is a researcher at the Center for Infection and Molecular Medicine of Amsterdam UMC. His research interests include the global distribution and global health aspects of melioidosis.

References

1. Meumann EM, Limmathurotsakul D, Dunachie SJ, Wiersinga WJ, Currie BJ. *Burkholderia pseudomallei* and melioidosis. Nat Rev Microbiol. 2024;22:155–69. https://doi.org/10.1038/s41579-023-00972-5
2. Birnie E, James A, Peters F, Olajumoke M, Traore T, Bertherat E, et al. Melioidosis in Africa: time to raise awareness and build capacity for its detection, diagnosis, and treatment. Am J Trop Med Hyg. 2022;106:394–7. https://doi.org/10.4269/ajtmh.21-0673
3. Birnie E, Virk HS, Savelkoel J, Spijker R, Bertherat E, Dance DAB, et al. Global burden of melioidosis in 2015: a systematic review and data synthesis. Lancet Infect Dis. 2019;19:892–902. https://doi.org/10.1016/S1473-3099(19)30157-4
4. Limmathurotsakul D, Golding N, Dance DA, Messina JP, Pigott DM, Moyes CL, et al. Predicted global distribution of *Burkholderia pseudomallei* and burden of melioidosis. Nat Microbiol. 2016;1:15008. https://doi.org/10.1038/nmicrobiol.2015.8
5. Savelkoel J, Oladele RO, Ojide CK, Peters RF, Notermans DW, Makinwa JO, et al. Presence of *Burkholderia pseudomallei* in soil, Nigeria, 2019. Emerg Infect Dis. 2023;29:1073–5. https://doi.org/10.3201/eid2905.221138
6. Kohler C, Dunachie SJ, Müller E, Kohler A, Jenjaroen K, Teparrukkul P, et al. Rapid and sensitive multiplex detection of *Burkholderia pseudomallei*–specific antibodies in melioidosis patients based on a protein microarray approach. PLoS Negl Trop Dis. 2016;10:e0004847. https://doi.org/10.1371/journal.pntd.0004847
7. Wagner GE, Berner A, Lipp M, Kohler C, Assig K, Lichtenegger S, et al. Protein microarray-guided development of a highly sensitive and specific dipstick assay for glanders serodiagnostics. J Clin Microbiol. 2023;61:e0123422. https://doi.org/10.1128/jcm.01234-22
8. Jenjaroen K, Chumseng S, Sumonwiriya M, Ariyaprasert P, Chantratita N, Sunyakumthorn P, et al. T-cell responses are associated with survival in acute melioidosis patients. PLoS Negl Trop Dis. 2015;9:e0004152. https://doi.org/10.1371/journal.pntd.0004152
9. Phokrai P, Karoonboonyanan W, Thanapattarapairoj N, Promkong C, Dulsuk A, Koosakulnirand S, et al. A rapid immunochromatography test based on Hcp1 is a potential point-of-care test for serological diagnosis of melioidosis. J Clin Microbiol. 2018;56:e00346–18. https://doi.org/10.1128/JCM.00346-18
10. Wagner GE, Föderl-Höbenreich E, Assig K, Lipp M, Berner A, Kohler C, et al. Melioidosis DS rapid test: a standardized serological dipstick assay with increased sensitivity and reliability due to multiplex detection. PLoS Negl Trop Dis. 2020;14:e0008452. https://doi.org/10.1371/journal.pntd.0008452

Address for correspondence: Jelmer Savelkoel, Amsterdam UMC location University of Amsterdam, Center for Infection and Molecular Medicine, Meibergdreef 9, 1105 AZ, Rm T1.0-234, Amsterdam, the Netherlands; email: j.savelkoel@amsterdamumc.nl

Localized Outbreak of Macrolide-Resistant Pertussis in Infants, Japan, March–May 2025

Takafumi Obara, Kyoko Kano, Takashi Yorifuji, Kohei Tsukahara, Naoki Yogo, Yuichiro Muto, Tetsuya Yumoto, Hiromichi Naito, Atsunori Nakao, Katsuki Hirai

Author affiliations: Japanese Red Cross Kumamoto Hospital, Kumamoto, Japan (T. Obara, K. Kano, N. Yogo, Y. Muto, K. Hirai); Okayama University, Okayama, Japan (T. Obara, T. Yorifuji, K. Tsukahara, T. Yumoto, H. Naito, A. Nakao)

DOI: http://doi.org/10.3201/eid3201.250824

A localized pertussis outbreak involving 10 unvaccinated infants occurred in Kumamoto, Japan, during March–May 2025. Nine infants were admitted to the pediatric intensive care unit, 6 of whom received a confirmed diagnosis of macrolide-resistant *Bordetella pertussis* infection. This outbreak highlights the importance of booster vaccinations and resistance surveillance.

Since the relaxation of COVID-19–related public health measures, health officials have observed increased pertussis notifications in some regions of Japan. By April 2025, reported cases had already exceeded the previous year's total. Alerts from the Japan Pediatric Society and the National Institute of Infectious Diseases have raised concerns about the rising incidence and spread of macrolide-resistant *Bordetella pertussis* (MRBP) (*1*,*2*), which has increased in East Asia, particularly in China, since around 2008 and more recently in Japan in 2024 (*3*,*4*). Nonetheless, clinical reports describing localized increases in pertussis incidence and the impact of MRBP on critical illness in infants remain scarce.

During late March through early May 2025, we identified an outbreak in Japan involving 10 unvaccinated infants < 2 months of age with PCR-confirmed pertussis. All infants were born at term and without perinatal complications. Nine required admission to the pediatric intensive care unit (PICU) for respiratory failure; 6 of those infants had confirmed MRBP infection. We conducted a retrospective descriptive analysis to characterize clinical features and examine potential association with regional pertussis trends.

Kumamoto Prefecture, in central Kyushu in western Japan, spans ≈7,400 km^2 and had a population of around 1,690,000 in fiscal year 2024, including 210,000 children (<15 years of age). The region has single PICU, an 8-bed general unit at the Japanese Red Cross Kumamoto Hospital, which provides emergency critical care for children. Since January 1, 2018, pertussis has been classified in Japan as a category V infectious disease, requiring physician reporting of confirmed cases. We diagnosed pertussis at admission using the BIOFIRE FILMARRAY Respiratory Panel (bioMérieux, https://www.biomerieux.com). We performed antimicrobial susceptibility test or 23S rRNA gene sequencing to estimate macrolide susceptibility of infected strains. We extracted data from medical records and conducted analysis with Stata 19 (StataCorp LLC, https://www.stata.com).

We investigated annual cumulative pertussis cases in Kumamoto Prefecture (all ages, since 2018) together with infant PICU admissions at Japanese Red Cross Kumamoto Hospital (Figure) (*5*). During the 2025 outbreak, both the number and proportion of PICU admissions were higher than in previous years. All 9 infants had identifiable sick contacts within their household, most frequently school-aged siblings (Table). Six patients received azithromycin (5-day oral treatment) before PICU admission. After the fourth PICU admission, we tested nasopharyngeal swab specimens from the subsequent 6 infants by using bacterial culture or genetic analysis. One sample tested positive for *B. pertussis* on culture, showing erythromycin resistance. The remaining 5 samples underwent direct DNA sequencing of the *B. pertussis* 23S rRNA gene, revealing the A2047G mutation in all cases. The remaining infant, not in PICU, had a macrolide-sensitive strain.

All PICU patients required intubation a median interval of 1 day after admission. The most frequent indications were paroxysmal coughing with desaturation and bradycardia. Most infants had persistent coughing and elevated airway resistance after intubation; 8 of 9 required continuous neuromuscular blockade. Six infants received oral trimethoprim/sulfamethoxazole for ≤14 days without adverse events, all from the fourth PICU case onward after MRBP identification. We did not give intravenous antibiot-

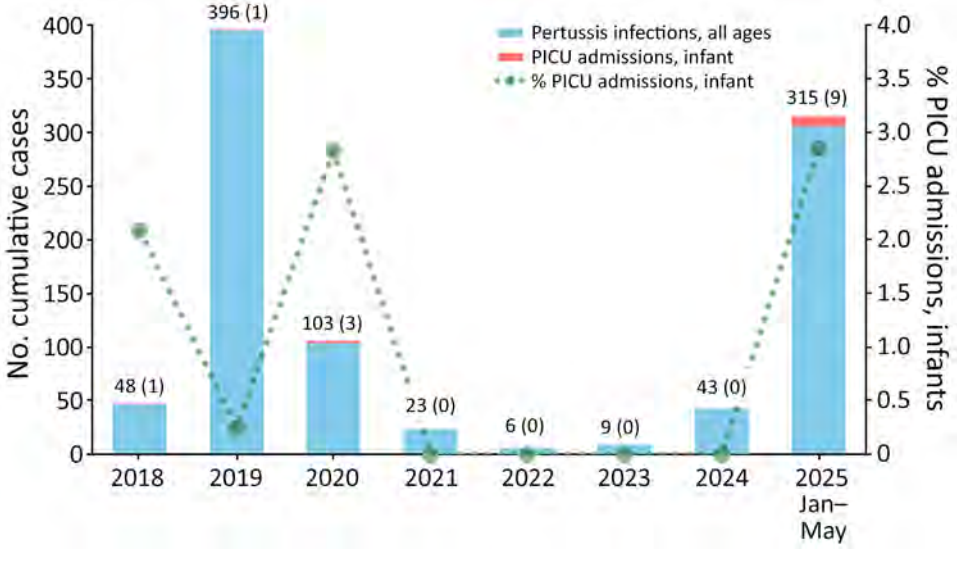

Figure. Cumulative reported pertussis cases (all ages) in Kumamoto Prefecture and infant PICU admissions at Kumamoto Red Cross Hospital, from study of a localized outbreak of macrolide-resistant pertussis in infants, Japan, March–May 2025. Reported pertussis cases are based on mandatory notifications (all ages) in Kumamoto Prefecture. PICU data represent infants admitted to the single regional PICU. Numbers above bars indicate total cases (PICU admissions). Data for 2025 are through May, and therefore interpretation of the proportion of PICU admissions relative to total cases should be made with caution. PICU, pediatric intensive care unit.

Table. Demographic information for 9 infants diagnosed with pertussis and admitted to the pediatric intensive care unit, Kumamoto, Japan, March–May 2025*

Variable	Value
Patient characteristics	
Median age, d (IQR)	44 (33–50)
Sex	
M	3 (33.3)
F	6 (66.7)
Median weight, g (IQR)	4,000 (3,600–4,266)
Median birthweight, g (IQR)	3,032 (2,560–3,190)
Median gestational age at birth, wk (IQR)	38 (37–39)
Underlying condition	0 (0.0)
Unvaccinated	9 (100)
Sick contact in family	9 (100)
Age group of symptomatic family members	
Siblings age 1–6 y	1 (11.1)
Siblings age 7–12 y	5 (55.6)
Parents age ≥18 y	3 (33.3)
Azithromycin use before PICU admission	6 (66.7)
MRBP confirmed†	6 (66.7)
Ventilator management	9 (100)
Nitric oxide therapy	1 (11.1)
Prone positioning	4 (44.4)
Rocuronium	8 (88.9)
Vasopressor	3 (33.3)
TMP/SMX use	6 (66.7)
Leukapheresis	3 (33.3)
Pulmonary hypertension diagnosis	2 (22.2)
Clinical course and outcomes	
Median days from symptom onset to PICU admission (IQR)	7 (7–12)
Median days from PICU admission to intubation days, d (IQR)	1 (0–1)
Median days of ventilator use, d (IQR)	8 (7–9)
Median PICU admission, d (IQR)	15 (14–19)
Median hospitalization, d (IQR)	23 (19–24)

*Values are no. (%) except as indicated. IQR, interquartile range; MRBP, macrolide-resistant *Bordetella pertussis*; PICU, pediatric intensive care unit; TMP/SMX, trimethoprim/sulfamethoxazole.
†Of 6 infants tested (MRBP undetermined in 3 infants).

ics prophylactically but initiated them after respiratory management for suspected secondary bacterial infection, including ventilator-associated pneumonia; 7 of 9 patients received ampicillin or ampicillin/sulbactam. Leukocytosis (>50,000 cells/μL) occurred in 3 infants, all treated with leukoreduction. Two patients developed pulmonary hypertension; 1 received inhaled nitric oxide. Median ventilation duration was 8 days and PICU stay 15 days for the PICU patients, longer than in our prior pertussis PICU cases (13 cases during 2012–2024). All patients survived without neurologic sequelae.

The temporal clustering of severe pertussis cases over a 2-month period suggests that increased community transmission contributed to the rise in critical cases. Although surveillance in Japan has reported sporadic MRBP cases, no prior studies have described a localized clinical outbreak. Despite the lack of prefectural-level susceptibility data, all 6 tested PICU cases were MRBP-positive, suggesting that a substantial proportion of circulating strains during this outbreak were resistant.

Pertussis most frequently affects children but also occurs in adults and adolescents. Outbreaks have been reported in fully vaccinated populations because of waning immunity, typically 5–10 years after vaccination (*6*,*7*). However, Japan does not currently require pertussis boosters beyond early childhood. From a public health perspective, a layered approach is essential: timely infant vaccination per the national schedule, booster doses for school-aged children to address waning immunity, and maternal tetanus-diphtheria-pertussis immunization during pregnancy to provide passive neonatal protection. Together, those strategies may help reduce secondary transmission within households and mitigate severe outcomes.

In severe infant pertussis, elevated leukocyte counts and pulmonary hypertension are associated with poor outcomes, underscoring the need for early monitoring and critical initiating of care-equipped setting (*8*–*10*). In the outbreak we describe, prolonged mechanical ventilation and extended PICU stays intermittently filled all PICU beds with MRBP-infected infant, placing a disproportionate burden on pediatric critical care capacity. This experience highlights how even localized outbreaks can strain systems in regions with only 1 PICU. In pertussis-endemic areas,

considering antimicrobial-resistant strains, including MRBP, may support timely treatment decisions and improved outcomes.

Acknowledgments

We thank the Laboratory of Pertussis Control, Department of Bacteriology II, National Institute of Infectious Diseases, Japan Institute for Health Security, and the infection control team at Kumamoto Red Cross Hospital for their support in the genetic characterization of the bacterial strains. We also thank Christine Burr for her assistance with editing.

The 23S rRNA gene sequences of *Bordetella pertussis*–infected strains described in this study have been deposited in the DNA Data Bank of Japan (accession nos. LC894622–LC894625 and LC894628), which is part of the International Nucleotide Sequence Database Collaboration.

This study was approved by the Kumamoto Red Cross Hospital Institutional Review Board (approval ID: 704).

About the Author

Dr. Obara is a pediatric emergency and critical care researcher at Okayama University, Japan. He is also clinically involved in the care of critically ill pediatric patients in Okayama and Kumamoto. His primary research interests include pediatric resuscitation, severe infectious diseases, neurocritical care, and end-of-life care, including organ donation.

References

1. The Japan Pediatric Society. Statement on the increase in pertussis cases and frequency of macrolide-resistant isolates. March 29, 2025 [in Japanese] [cited 2025 May 31]. https://www.jpeds.or.jp/uploads/files/20250402_hyakunitizeki1.pdf
2. National Institute of Infectious Diseases. Department of Bacteriology II, Applied Epidemiology Research Center, Field Epidemiology Specialist Training Course Infectious Disease Epidemiology Research Division, Infectious Disease Risk Management Research Center. Pertussis Outbreak Status. JIHS National Institute for Health Risk Management Infectious Disease Information website. April 22, 2025 [cited 2025 May 31]. https://id-info.jihs.go.jp/diseases/ha/pertussis/020/2504_pertussis_RA.html
3. Ivaska L, Barkoff AM, Mertsola J, He Q. Macrolide resistance in *Bordetella pertussis*: current situation and future challenges. Antibiotics (Basel). 2022;11:1570. https://doi.org/10.3390/antibiotics11111570
4. Koide K, Uchitani Y, Yamaguchi T, Otsuka N, Goto M, Kenri T, et al. Whole-genome comparison of two same-genotype macrolide-resistant *Bordetella pertussis* isolates collected in Japan. PLoS One. 2024;19:e0298147. https://doi.org/10.1371/journal.pone.0298147
5. Infectious Disease Outbreak Information (weekly report). Kumamoto Prefecture website in Japanese] [cited 2025 May 26]. https://www.pref.kumamoto.jp/soshiki/30/51400.html
6. Mattoo S, Cherry JD. Molecular pathogenesis, epidemiology, and clinical manifestations of respiratory infections due to *Bordetella pertussis* and other *Bordetella* subspecies. Clin Microbiol Rev. 2005;18:326–82. https://doi.org/10.1128/CMR.18.2.326-382.2005
7. Srugo I, Benilevi D, Madeb R, Shapiro S, Shohat T, Somekh E, et al. Pertussis infection in fully vaccinated children in day-care centers, Israel. Emerg Infect Dis. 2000;6:526–9. https://doi.org/10.3201/eid0605.000512
8. Akçay N, Tosun D, Bingöl İ, Bingöl İ, Çıtak A, Bayraktar S, et al. Severe pertussis infections in pediatric intensive care units: a multicenter study. Eur J Pediatr. 2025;184:138. https://doi.org/10.1007/s00431-025-05978-0
9. Guo S, Zhu Y, Guo Q, Wan C. Severe pertussis in infants: a scoping review. Ann Med. 2024;56:2352606. https://doi.org/10.1080/07853890.2024.2352606
10. Jayashree M, Kavitha TK. Critical pertussis: "prevention is better than cure". Pediatric Respirology and Critical Care Medicine. 2024;8:69–72. https://doi.org/10.4103/prcm.prcm_9_24

Address for correspondence: Takafumi Obara, Department of Emergency, Critical Care, and Disaster Medicine, Faculty of Medicine, Dentistry, and Pharmaceutical Sciences, Okayama University, 2-5-1 Shikata, Okayama 700-8558, Japan; email: tkfmobr16@okayama-u.ac.jp

Raffaello Sanzio da Urbino (Raphael), *Self-Portrait*, ca. 1504–1506 (detail). Oil on poplar. 47.3 cm × 34.8 cm (18.6 in × 13.7 in). The Uffizi, Florence, Italy.

Nocardia and the Death of Raphael (1520)

Philippe Charlier, Geneviève Héry-Arnaud, Kira Kofoed, Jean Armengaud

Raphael (Raffaello Sanzio da Urbino) was one of the greatest artists of the Italian Renaissance. Active in Perugia, Siena, Florence, Rome, and Urbino (his birthplace), he is responsible for numerous masterpieces of Western art, including the fresco of the School of Athens in the Vatican rooms and the painting of the Sistine Madonna accompanied by 2 cherubs (preserved in Dresden, Germany). He died at the age of 37 in Rome, Italy, on April 6, 1520, after a short chest infection with fever. Several hypotheses have been proposed to explain his premature death, including syphilis, typhoid, malaria, and even excessive bloodletting (*1*). The paleoproteomic study of his remains might be capable of revealing the exact cause of his death.

Raphael's body was placed in one of the walls of the Pantheon in Rome, where his remains are

Author affiliations: Laboratory Anthropology, Archaeology, Biology, UFR of Health Sciences Simone Veil, University of Versailles Saint-Quentin-en-Yvelines/Université Paris-Saclay, Paris, France (P. Charlier); University Hospital R. Poincaré (AP-HP), Garches, France (P. Charlier); Brest University Hospital, Brest, France (G. Héry-Arnaud); Brest University, INSERM, EFS, UMR 1078 Inserm Unit UMR1078 Genetics, Genomics and Biotechnology, Faculty of Medicine, Brest (G. Héry-Arnaud); Thorvaldsens Museum, Copenhagen, Denmark (Kira Kofoed); Université Paris-Saclay, CEA, INRAE, Bagnols-sur-Cèze, France (J. Armengaud)

DOI: https://doi.org/10.3201/eid3201.AC3201

entombed to this day. However, in 1833, an opening of the grave was carried out at the request of the Pope Gregory XVI to check the condition of the corpse and place it in a marble sarcophagus from the Vatican museums (Figure 1). On that occasion, casts of the skull and right hand were made, a piece of the heart was given to a Russian diplomat to the Holy See (*2*), and the Danish sculptor Bertel Thorvaldsen was given a fragment of the mortar hanging from the original coffin: he kept the fragment and later donated it to his Danish house servant (now at the Thorvaldsens Museum in Copenhagen, inv. no. N87). The French painter Jean-Auguste-Dominique Ingres, who was not present at the opening of the tomb, was given permission by the pope to have a piece of Raphael's bones (*3*). Keeping bone fragments as relics had been a practice for hundreds of years, especially when associated with religious figures. Raphael was highly venerated as an artist, to such an extent that he was considered almost a saint (*2*,*3*).

In the archives of Dominique Ingres, in Montauban (France), we found envelopes and a glass frame holding what were described by Ingres himself as "remains of the divine Raphael" (bone splinters and sediments; Figure 2). Because of the small amount of remaining bone material, no carbon-dating of the remains has been conducted to possibly confirm their authenticity. Apart from tradition (not questioned by art historians) and archives relating to the relics belonging to the Thorvaldsens Museum in Copenhagen (*4*), no conclusive evidence exists to confirm the authenticity of the Montauban's remains.

Nevertheless, the fragments were the subject of a sampling for a proteomic study, according to a now well-established paleopathological protocol (paleo-proteotyping) (*5*). The analysis revealed a significant proteomic signature for *Nocardia niigatensis* (50 peptides assigned, 11 of them species-specific peptides, and high redundancy of 91 spectra by tandem mass spectrometry), and the bacterium was detected only in the sample of bone marrow from a fragment of human rib. In contrast, several other bacteria, typically environmental, were detected in several of the other samples of the grave soil (*Pseudonocardia autotrophica*, *Nonomurae gerenzanensis*, *Streptomyces albireticuli*, *Hyphomicrobium* sp., *Paraburkholderia ribeironi*, *Lysobacter antibioticus*, *Blastocatella* sp., *Paenibacillus koleovorans*, *Arcicella rosea*, *Bacillus megaterium*, and *Rhizobium leguminosarum*). Finding *Nocardia* exclusively in the bone marrow supports a conclusion that *Nocardia* might have been a cause of death, especially since the dead body was placed in an above-ground niche within an ancient Roman monument that had been transformed into a church. No sign of embalming was found at the exhumation (*3*).

Figure 1. Francesco Diofebi, *The 1833 Opening of Raphael's Tomb in Pantheon*, 1836. Oil on canvas, 54.9 × 70 cm, Thorvaldsens Museum inv. no. B73. Photograph by Hans Petersen.

N. niigatensis is not part of the thanatomicrobiome (i.e., microbial communities residing in or moving on the surface of altered remains), so its presence cannot be explained by a process of decomposition/putrefaction (*6*). However, one may consider the possibility of a burial contamination by the waters of the Tiber during the numerous floods that occurred from the

Figure 2. General view of samples from Raphael's grave and cadaver analyzed for investigation of possible *Nocardia* infection. Ingres Museum, Montauban, France. Photograph by Philippe Charlier.

16th through the 19th Centuries (*7*). Indeed, the drawings (for example by Vincenzo Camuccini), paintings, and reports of the state of the skeleton during the exhumation of 1833 show a partially disarticulated skeleton, subsequently reassembled by the physician Antonio Trasmondo. The presence of slight deposits on Raphael's bones, potentially resulting from Tiber River flooding, were described by some witnesses in 1833 (*8*). However, the peptide signature of *N. niigatensis* was found only in the bone marrow sample of the rib segment and not in any other samples (e.g., soil, wall, dust), suggesting an intravitam origin for this infectious agent, rather than postmortem contamination by secondary deposition. The detection of environmental bacteria, the presence of deposits on bones attributed to flooding, and difficulty confirming that the bone fragments and sediments were from Raphael and his tomb exemplify some of the challenges to draw conclusions based on a full paleopathological study.

Nocardia spp. bacteria can infect bones through direct extension from a primary lung or skin lesion or via hematogenous dissemination from a pulmonary or soft tissue focus. The clinical manifestations of a *Nocardia* infection typically begin as a low-level, indolent infection, which then can progress to a febrile illness characterized by pulmonary abscesses, disseminated infection, or both, including osteomyelitis. That clinical course aligns with the symptoms reported for Raphael's last days of life and agony (*9*): we know from Vasari that Raphael's death was preceded by high fever; another source speaks of a 15-day illness (letter from Alf. Pauluzzi to Duke Alfonso d'Este, Rome, April 7, 1520) (*10*). Whatever the cause of the artist's death, the profound impact from his work remains for generations. As attributed to German Nazarene painter Johann Friedrich Overbeck, who was among those present in the Pantheon for the opening of Raphael's tomb, "Alas, the spirit of the great artist remains buried deeper than his bones."

Acknowledgments

The authors thank Laëtitia Vincent-Genod for the access granted to the remains and M. Adrien Goetz for putting us on this crucial trail.

References

1. Riva MA, Paladino ME, Motta M, Belingheri M. The death of Raphael: a reflection on bloodletting in the Renaissance. Intern Emerg Med. 2021;16:243–4.
2. Tiberia V. The collection of the Pontifical Insignia Academy of Fine Arts and Letters of the Virtuosi at the Pantheon: paintings and sculptures [in Italian]. Rome: Scripta Manent Editions; 2016.
3. Smithers T. The cults of Raphael and Michelangelo. Artistic sainthood and memorials as a second life. London & New York: Routledge; 2023. p. 220 and 232.
4. The Thorvaldsens Museum Archives. No.: 128. Kalk fra Raphaels Grav, skjænket til Undertegnede af Th: der modtog det som medlem af Accademiet S^{t} Lucca (1833)? da Raphaels Grav blev aabnet. [Mortar from the tomb of Raphael, given to the undersigned (Thorvaldsen's servant C.F. Wilckens who collected Thorvaldsen-souvenirs) by Thorvaldsen, who received it as a member of the Accademia di San Luca (1833?) when the tomb was opened] [cited 2025 Nov 26]. https://arkivet.thorvaldsens-museum.dk/documents/m34,nr.74
5. Charlier P, Armengaud J. Did Saint Leonard suffer from Madura foot at the time of death? Infectious disease diagnosis by paleo-proteotyping. J Infect. 2024;88:61–2.
6. Javan GT, Finley SJ, Can I, Wilkinson JE, Hanson JD, Tarone AM. Human thanatomicrobiome succession and time since death. Sci Rep. 2016;6:29598.
7. Camuffo D, Enzi S. The analysis of two bi-millenary series: Tiber and Po River Floods. In: Jones PD, Bradley RD, Jouzet J, editors. Climatic variations and forcing mechanisms of the last 2000 years. NATO ASI Subseries I: (ASII, vol. 41). Berlin: Springer; 1996. http://dx.doi.org/10.1007/978-3-642-61113-1_20
8. Nerlich F. La transfiguration de Raphaël. L'année 1833. Studiolo. 2020/2021;17:66–81.
9. Ozaras R, Mert A, Hakko E, Tabak F, Ozturk R. Pulmonary, cerebral, and soft tissue nocardiosis. Lancet Infect Dis. 2004;4:222.
10. Vasari G. Les vies des plus excellents: peintres sculpteurs, et architectes. Weiss C, translator. Paris: Dorbon-Aîné; 1903.

Address for correspondence: Philippe Charlier, Laboratory Anthropology, Archaeology, Biology (LAAB), UFR of Health Sciences Simone Veil (UVSQ/Paris-Saclay University), 2 avenue de la source de la Bièvre, 78180 Montigny-Le-Bretonneux, France; email: philippe.charlier@uvsq.fr

EMERGING INFECTIOUS DISEASES®

Upcoming Issue

- Life-threatening SARS-CoV-2-associated Encephalopathy with Fulminant Cerebral Edema, Shock, and Multiorgan Failure in Children, Asia and Oceania, 2022-2024
- Predictors of Fatal Outcomes among Hospitalized Pediatric Rocky Mountain Spotted Fever Patients, Sonora, Mexico, 2004–2024
- Assessing Dengue Transmission Risk in Travelers Using Routine Surveillance Data
- Pulmonary Complications in Fatal Yellow Fever Pathogenesis: An Autopsy Study from the 2017-2019 Epidemic
- *Leptotrombidium imphalum* as a Vector for Scrub Typhus in and Around Human Settlements in South India, 2022-2023
- Environmental and Phylogenetic Investigations of *Aspergillus flavus* Outbreak Linked to Contaminated Building Materials, Denmark, 2025
- Rethinking Leptospirosis Prevention in the Philippines: A Systems Thinking and Community-Led Approach
- Measles Outbreak Driven by Nosocomial Transmission, Armenia, February–July 2023
- Characteristics and Transmission Dynamics among Global Travel-Related Mpox Cases Caused by Clade Ib Monkeypox Virus
- Rabies Reemergence, Central Europe, 2022–2024
- Temporal Clustering of *Mycoplasma pneumoniae*-Associated Encephalitis and Stroke in South Korea, 2024
- Case of *Legionella pneumophila* Serogroup 1 Infection Linked to a Water Flosser
- Autochthonous *Angiostrongylus cantonensis* Infections in Accidental and Definitive Hosts in San Diego, California, USA
- Tracking *Neospora caninum* Infections in Marine Mammals Stranding in the Northeastern Pacific Ocean
- *Desulfovibrio Bacteremia* in Older Patients with Abdominal Infections, Japan, 2020–2025
- Genomic Analysis of Doxycycline Resistance-Associated 16S rRNA Mutations in Global and Canadian *Treponema pallidum* subsp. *pallidum*
- Donor-derived West Nile Virus Infection in Kidney Recipients, France.
- Avian Influenza A(H9N2) Transmission across Chicken Production and Distribution Networks, Viet Nam
- Effectiveness of RSV Vaccines against RSV-Associated Thromboembolic Events
- A Multiplex qPCR to Differentiate Monkeypox Virus Clades
- Retail Milk Monitoring of Influenza A(H5N1) in Dairy Cattle, United States, 2024–2025
- Severe Respiratory Diphtheria-Like Illness Caused by Toxigenic *Corynebacterium ulcerans*
- Primary Acute Severe Hepatitis B Virus Infection During Acalabrutinib Treatment, Despite Previous Effective Vaccination Against HBV.
- Detection of Vesicular Disease Cases Caused by Seneca Valley Virus (*Senecavirus valles*) in Pigs, England, 2022
- Detection of a Vaccine-like African Swine Fever Virus Strain with a Deletion of Six Genes in Domestic Pigs in Thailand
- Invasive Pneumococcal Disease among Pregnant, Postpartum, and Nonpregnant Childbearing-age Women, United States, 2007–2023
- Monkeypox virus neutralising antibodies detected against Clade Ib and Clade IIb in healthy individuals following vaccination with MVA-BN
- Airport Malaria Cluster in Certified Malaria-Free Country, Libya, 2024
- Serological Investigation of Influenza D Virus in Cats and Dogs in Europe

Complete list of articles in the February issue at https://wwwnc.cdc.gov/eid/#issue-329

Earning CME Credit

To obtain credit, you should first read the journal article. After reading the article, you should be able to answer the following, related, multiple-choice questions. To complete the questions (with a minimum 75% passing score) and earn continuing medical education (CME) credit, please go to http://www.medscape.org/journal/eid. Credit cannot be obtained for tests completed on paper, although you may use the worksheet below to keep a record of your answers.

You must be a registered user on http://www.medscape.org. If you are not registered on http://www.medscape.org, please click on the "Register" link on the right hand side of the website.

Only one answer is correct for each question. Once you successfully answer all post-test questions, you will be able to view and/or print your certificate. For questions regarding this activity, contact the accredited provider, CME@medscape.net. For technical assistance, contact CME@medscape.net. American Medical Association's Physician's Recognition Award (AMA PRA) credits are accepted in the US as evidence of participation in CME activities. For further information on this award, please go to https://www.ama-assn.org. The AMA has determined that physicians not licensed in the US who participate in this CME activity are eligible for AMA PRA Category 1 Credits™. Through agreements that the AMA has made with agencies in some countries, AMA PRA credit may be acceptable as evidence of participation in CME activities. If you are not licensed in the US, please complete the questions online, print the AMA PRA CME credit certificate, and present it to your national medical association for review.

Article Title

Retrospective Case Series of Ocular Lyme Disease, 1988–2025

CME Questions

1. Which of the following ocular complications was most common in the current case series of patients with presumed Lyme disease?

A. Uveitis
B. Conjunctivitis
C. Optic nerve palsy
D. Cranial nerve palsy

2. There were 38 cases of suspected Lyme disease associated with ocular complications in the current study. How many of these 38 cases included microbiological proof of Lyme disease?

A. 5
B. 16
C. 30
D. 36

3. Which of the following statements regarding ocular complications of Lyme disease in the current study is most accurate?

A. Half of cases included a history of tick bite on or around the eye
B. There were no cases of optic neuritis reported
C. There were no cases of retinal vasculitis reported
D. Many cases were associated with systemic or flu-like symptoms

Earning CME Credit

To obtain credit, you should first read the journal article. After reading the article, you should be able to answer the following, related, multiple-choice questions. To complete the questions (with a minimum 75% passing score) and earn continuing medical education (CME) credit, please go to http://www.medscape.org/journal/eid. Credit cannot be obtained for tests completed on paper, although you may use the worksheet below to keep a record of your answers.

You must be a registered user on http://www.medscape.org. If you are not registered on http://www.medscape.org, please click on the "Register" link on the right hand side of the website.

Only one answer is correct for each question. Once you successfully answer all post-test questions, you will be able to view and/or print your certificate. For questions regarding this activity, contact the accredited provider, CME@medscape.net. For technical assistance, contact CME@medscape.net. American Medical Association's Physician's Recognition Award (AMA PRA) credits are accepted in the US as evidence of participation in CME activities. For further information on this award, please go to https://www.ama-assn.org. The AMA has determined that physicians not licensed in the US who participate in this CME activity are eligible for AMA PRA Category 1 Credits™. Through agreements that the AMA has made with agencies in some countries, AMA PRA credit may be acceptable as evidence of participation in CME activities. If you are not licensed in the US, please complete the questions online, print the AMA PRA CME credit certificate, and present it to your national medical association for review.

Article Title

Group A *Streptococcus* Meningitis, United States, 1997–2022

CME Questions

1. What was the most significant difference in the demographic data among patients with meningitis and nonmeningitis invasive group A *Streptococcus* (iGAS) in the current study?

A. Patients with iGAS with meningitis were more likely to be male
B. Patients with iGAS with meningitis were younger
C. Patients with iGAS with meningitis were more likely to be Black
D. Patients with iGAS with meningitis were more likely to be Latino

2. What were the approximate rates of comorbid conditions among children and adults with group A streptococcal (GAS) meningitis in the current study?

A. Children: 95%. Adults: 92%
B. Children: 81%. Adults: 75%
C. Children: 52%: Adults: 85%
D. Children: 6%; Adults: 70%

3. Which of the following statements regarding clinical GAS syndromes among patients with GAS meningitis in the current study is most accurate?

A. Only 40% of patients had an additional GAS syndrome in addition to meningitis
B. Among children, otitis media was the most common additional GAS syndrome in addition to meningitis
C. Among adults, pneumonia was the most common additional GAS syndrome in addition to meningitis
D. Sepsis shock was the most common additional GAS syndrome in addition to meningitis among both children and adults

4. Antimicrobial resistance was highest for GAS meningitis against which of the following antibiotics in the current study?

A. Erythromycin
B. β-lactams
C. Vancomycin
D. Levofloxacin

Emerging Infectious Diseases

Spotlight Topics

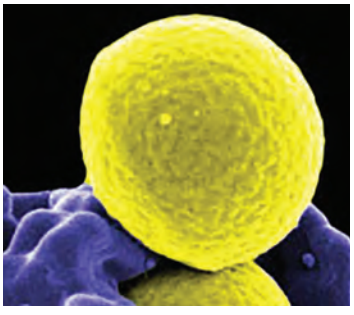


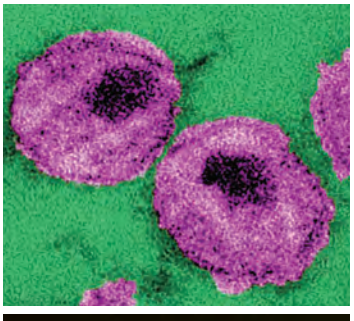

Antimicrobial resistance
Ebola • Etymologia
Food safety • HIV-AIDS
Influenza • Lyme disease
Malaria • MERS • Pneumonia •
Rabies • Ticks • Tuberculosis
Coronavirus • Zika • Monkeypox

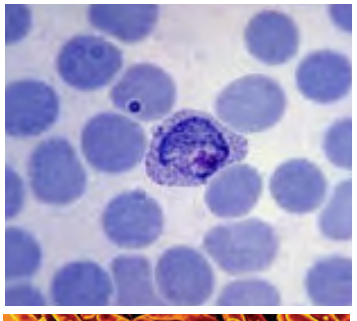
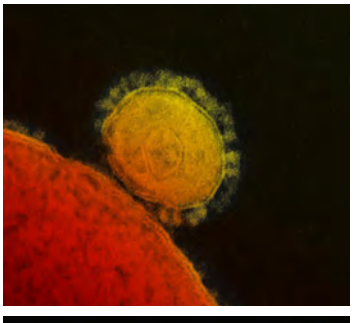
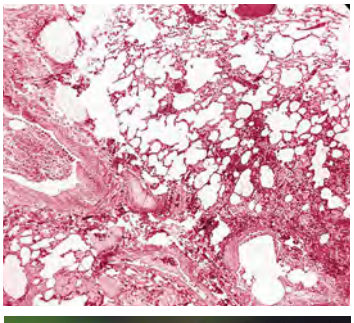
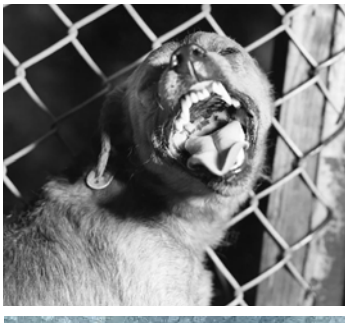




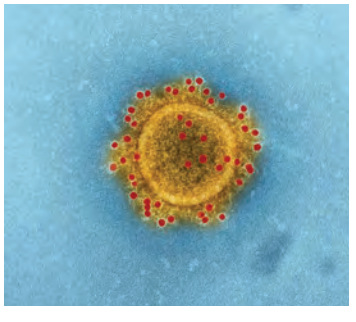

EID's spotlight topics highlight the latest articles and information on emerging infectious disease topics in our global community

https://wwwnc.cdc.gov/eid/page/spotlight-topics